
# Properties of Foamed Asphalt for Warm Mix Asphalt Applications

**DETAILS**

126 pages | 8.5 x 11 | PAPERBACK
ISBN 978-0-309-30866-3 | DOI 10.17226/22145



**AUTHORS**

Newcomb, David E.; Arambula, Edith; Yin, Fan; Zhang, Jun; Bhasin, Amit; Li, Wei; and Zelalem Arega

NATIONAL COOPERATIVE HIGHWAY RESEARCH PROGRAM

NCHRP REPORT 807

# Properties of Foamed Asphalt for Warm Mix Asphalt Applications

**David E. Newcomb**
**Edith Arambula**
**Fan Yin**
**Jun Zhang**
TEXAS A&M TRANSPORTATION INSTITUTE
TEXAS A&M UNIVERSITY
College Station, TX

**Amit Bhasin**
**Wei Li**
**Zelalem Arega**
CENTER FOR TRANSPORTATION RESEARCH
UNIVERSITY OF TEXAS
Austin, TX

*Subscriber Categories*
Construction • Materials • Pavements

Research sponsored by the American Association of State Highway and Transportation Officials
in cooperation with the Federal Highway Administration

TRANSPORTATION RESEARCH BOARD

WASHINGTON, D.C.
2015
www.TRB.org

## NATIONAL COOPERATIVE HIGHWAY RESEARCH PROGRAM

Systematic, well-designed research provides the most effective approach to the solution of many problems facing highway administrators and engineers. Often, highway problems are of local interest and can best be studied by highway departments individually or in cooperation with their state universities and others. However, the accelerating growth of highway transportation develops increasingly complex problems of wide interest to highway authorities. These problems are best studied through a coordinated program of cooperative research.

In recognition of these needs, the highway administrators of the American Association of State Highway and Transportation Officials initiated in 1962 an objective national highway research program employing modern scientific techniques. This program is supported on a continuing basis by funds from participating member states of the Association and it receives the full cooperation and support of the Federal Highway Administration, United States Department of Transportation.

The Transportation Research Board of the National Academies was requested by the Association to administer the research program because of the Board's recognized objectivity and understanding of modern research practices. The Board is uniquely suited for this purpose as it maintains an extensive committee structure from which authorities on any highway transportation subject may be drawn; it possesses avenues of communications and cooperation with federal, state and local governmental agencies, universities, and industry; its relationship to the National Research Council is an insurance of objectivity; it maintains a full-time research correlation staff of specialists in highway transportation matters to bring the findings of research directly to those who are in a position to use them.

The program is developed on the basis of research needs identified by chief administrators of the highway and transportation departments and by committees of AASHTO. Each year, specific areas of research needs to be included in the program are proposed to the National Research Council and the Board by the American Association of State Highway and Transportation Officials. Research projects to fulfill these needs are defined by the Board, and qualified research agencies are selected from those that have submitted proposals. Administration and surveillance of research contracts are the responsibilities of the National Research Council and the Transportation Research Board.

The needs for highway research are many, and the National Cooperative Highway Research Program can make significant contributions to the solution of highway transportation problems of mutual concern to many responsible groups. The program, however, is intended to complement rather than to substitute for or duplicate other highway research programs.

## NCHRP REPORT 807

Project 09-53
ISSN 0077-5614
ISBN 978-0-309-30866-3
Library of Congress Control Number 2015938508



### COPYRIGHT INFORMATION



### NOTICE

The project that is the subject of this report was a part of the National Cooperative Highway Research Program, conducted by the Transportation Research Board with the approval of the Governing Board of the National Research Council.

The members of the technical panel selected to monitor this project and to review this report were chosen for their special competencies and with regard for appropriate balance. The report was reviewed by the technical panel and accepted for publication according to procedures established and overseen by the Transportation Research Board and approved by the Governing Board of the National Research Council.

The opinions and conclusions expressed or implied in this report are those of the researchers who performed the research and are not necessarily those of the Transportation Research Board, the National Research Council, or the program sponsors.

The Transportation Research Board of the National Academies, the National Research Council, and the sponsors of the National Cooperative Highway Research Program do not endorse products or manufacturers. Trade or manufacturers' names appear herein solely because they are considered essential to the object of the report.

*Published reports of the*

**NATIONAL COOPERATIVE HIGHWAY RESEARCH PROGRAM**

*are available from:*

Transportation Research Board
Business Office
500 Fifth Street, NW
Washington, DC 20001

*and can be ordered through the Internet at:*

http://www.national-academies.org/trb/bookstore

Printed in the United States of America

THE NATIONAL ACADEMIES

*Advisers to the Nation on Science, Engineering, and Medicine*

The **National Academy of Sciences** is a private, nonprofit, self-perpetuating society of distinguished scholars engaged in scientific and engineering research, dedicated to the furtherance of science and technology and to their use for the general welfare. Upon the authority of the charter granted to it by the Congress in 1863, the Academy has a mandate that requires it to advise the federal government on scientific and technical matters. Dr. Ralph J. Cicerone is president of the National Academy of Sciences.

The **National Academy of Engineering** was established in 1964, under the charter of the National Academy of Sciences, as a parallel organization of outstanding engineers. It is autonomous in its administration and in the selection of its members, sharing with the National Academy of Sciences the responsibility for advising the federal government. The National Academy of Engineering also sponsors engineering programs aimed at meeting national needs, encourages education and research, and recognizes the superior achievements of engineers. Dr. C. D. Mote, Jr., is president of the National Academy of Engineering.

The **Institute of Medicine** was established in 1970 by the National Academy of Sciences to secure the services of eminent members of appropriate professions in the examination of policy matters pertaining to the health of the public. The Institute acts under the responsibility given to the National Academy of Sciences by its congressional charter to be an adviser to the federal government and, upon its own initiative, to identify issues of medical care, research, and education. Dr. Victor J. Dzau is president of the Institute of Medicine.

The **National Research Council** was organized by the National Academy of Sciences in 1916 to associate the broad community of science and technology with the Academy's purposes of furthering knowledge and advising the federal government. Functioning in accordance with general policies determined by the Academy, the Council has become the principal operating agency of both the National Academy of Sciences and the National Academy of Engineering in providing services to the government, the public, and the scientific and engineering communities. The Council is administered jointly by both Academies and the Institute of Medicine. Dr. Ralph J. Cicerone and Dr. C. D. Mote, Jr., are chair and vice chair, respectively, of the National Research Council.

The **Transportation Research Board** is one of six major divisions of the National Research Council. The mission of the Transportation Research Board is to provide leadership in transportation innovation and progress through research and information exchange, conducted within a setting that is objective, interdisciplinary, and multimodal. The Board's varied activities annually engage about 7,000 engineers, scientists, and other transportation researchers and practitioners from the public and private sectors and academia, all of whom contribute their expertise in the public interest. The program is supported by state transportation departments, federal agencies including the component administrations of the U.S. Department of Transportation, and other organizations and individuals interested in the development of transportation. **www.TRB.org**

**www.national-academies.org**

# COOPERATIVE RESEARCH PROGRAMS




## AUTHOR ACKNOWLEDGMENTS

The research reported herein was performed under NCHRP Project 09-53 by the Texas A&M Transportation Institute (TTI) as lead agency and the University of Texas at Austin (UT-Austin) as subcontractor. Dr. David E. Newcomb, senior research engineer at TTI, was the Principal Investigator. Other authors were Dr. Edith Arambula, associate research engineer at TTI; Mr. Fan Yin, graduate research assistant at TTI; Jun Zhang, graduate student at Texas A&M University; Dr. Amit Bhasin and Dr. Wei Li, associate professors at UT-Austin; and Dr. Zelalem Arega, researcher at UT-Austin.

The authors gratefully acknowledge Mr. Jean-Paul Fort of Colas, Inc., Barrett Paving of Ohio; Mr. Gene Smith from Pavers Supply Company of Conroe, Texas; and Mr. Mike Brown from the Oldcastle Materials Group, the Wheeler Companies, Austin, Texas, for allowing access to their personnel, plants, and facilities as well as their generous support during this study. The team is also very appreciative to Mr. Richard Steger and Dr. Todd Lynn from InVia Pavement Technologies, LLC, of Tulsa, Oklahoma, for their help and access to laboratory equipment. Sincere appreciation is also extended to the asphalt binder suppliers that provided materials for this study: Alon, Flint Hills, Holly, Marathon, NuStar (now Axeon), and Valero.

Gratitude is also extended to Mr. Rick Canatella, research technician at TTI, and Mr. Guillermo Gomez Salas and Mr. Adolfo Portilla, student workers at TTI, for their contributions in the laboratory.

# FOREWORD

By Edward T. Harrigan
Staff Officer
Transportation Research Board

This report presents proposed AASHTO standard test methods for measuring performance-related properties of foamed asphalts and designing foamed asphalt mixes with satisfactory aggregate coating and workability. Thus, the report will be of immediate interest to materials engineers in state highway agencies and the construction industry with responsibility for design and production of foamed asphalts and foamed asphalt mixes for warm mix asphalt (WMA) applications.

---

Several WMA technologies, including those using zeolites, direct-water injection, and residual aggregate moisture, use asphalt foaming to enhance coating and provide workability at lower production temperatures. When small amounts of water are added to hot asphalt binder, the water vaporizes and the vapor is temporarily encapsulated in the binder. This encapsulation produces a foaming action in the binder, temporarily increasing its volume and enhancing its coating ability and the workability of the asphalt mix.

The present understanding of the properties and performance of foamed asphalt is mainly based upon evaluation techniques developed in the 1970s for cold foamed asphalt for base stabilization, which is conducted with higher water dosage rates than WMA. With the wide variety of WMA foaming technologies and equipment now available and the dramatic increase in the use of foamed asphalt by paving contractors over the past several years, research was needed to understand foamed asphalt for WMA applications, the mechanisms of its production, and the properties of foamed asphalt needed for successful WMA design, production, and construction.

The objectives of NCHRP Project 9-53 were to determine key properties of foamed asphalt binders that significantly influence the performance of asphalt mixtures and develop laboratory protocols for foaming of asphalt binders and laboratory mixing procedures. The research was performed by the Texas A&M Transportation Institute, Texas A&M University, College Station, Texas, in conjunction with the Center for Transportation Research, University of Texas, Austin, Texas.

The production and performance-related properties of foamed asphalt were investigated through a series of laboratory and field experiments. A key finding of the research is that the foaming characteristics of an asphalt binder are primarily affected by its source (i.e., its crude oil slate), the production date for a given refinery and crude oil slate, and polymer modification. A laser-based method was developed to measure parameters associated with the expansion and collapse of foamed asphalt. A digital photographic approach was developed to characterize the size, distribution, and surface area of bubbles formed during production of foamed asphalt. Methods were also identified for determining a coatability index for foamed asphalt and the workability of mixes produced with foamed asphalt. A foamed

asphalt mixture design procedure was developed to identify the optimum water content for coating and workability. Finally, the utility and effectiveness of these various methods were verified through their application to foamed asphalt binder and mix produced in full-scale asphalt mix plants.

This report fully documents the research and includes the following four appendixes:

- Appendix A: Influence of Binder Properties on Binder Foam Expansion
- Appendix B: Draft Commentary on Guidelines Proposed for Revising Appendix to AASHTO R 35
- Appendix C: AASHTO Style Standards
- Appendix D: Field Foaming Data Acquisition Form

# CONTENTS


1 Summary

3 **Chapter 1** Background
3 A. Introduction
4 B. Foaming Theory and Applications
9 C. Binder Foaming Technology and Applications
11 D. Review of Past Work
12 E. Study Objectives
12 F. Study Scope
12 G. Report Organization

14 **Chapter 2** Research Approach
14 A. Test Methods and Metrics to Characterize Binder Foaming
20 B. Test Methods and Metrics to Characterize Foamed Mixtures
21 C. Initial Foamed Mix Design Approach

23 **Chapter 3** Findings and Applications: Laboratory Studies
23 A. Laboratory Binder Study
41 B. Laboratory Mixture Study
46 C. Validation of Proposed Mix Design Approach with Various Laboratory Foaming Units

53 **Chapter 4** Findings and Applications: Field Studies
53 A. Initial Trial
58 B. Comparison of Plant Foaming Units
64 C. Field Validation of Proposed Mix Design

74 **Chapter 5** Conclusions

78 References

81 Abbreviations, Acronyms, and Definitions

83 **Appendix A** Influence of Binder Properties on Binder Foam Expansion

89 **Appendix B** Draft Commentary on Guidelines Proposed for Revising Appendix to AASHTO R 35

104 **Appendix C** AASHTO Style Standards

122 **Appendix D** Field Foaming Data Acquisition Form

SUMMARY

# Properties of Foamed Asphalt for Warm Mix Asphalt Applications

Economic, environmental, and performance benefits have motivated the reduction of asphalt mixing and compaction temperatures to obtain decreased energy consumption, emissions, odors, and fumes at the plant and at the construction site; extended haul distances and a longer pavement construction season; and improved workability and compactability of the asphalt mixture. The use of warm mix asphalt (WMA) technology results in reduced production and paving temperatures without sacrificing the quality of the final product. There have been a number of products and processes introduced to produce WMA since 2005, including waxes, surfactants, mineral additives, and mechanical foaming processes. The work in this study focused on central plant–produced foamed WMA because foaming asphalt is currently the largest segment of the WMA market.

The objectives of this research study were to (1) determine the properties of foamed binders that relate to asphalt mixture performance and (2) develop laboratory foaming and mixing protocols that may be used to design asphalt mixtures. As part of this effort, foamed binder and mixture test methods and analysis procedures were developed. In addition, a mix design procedure was developed and validated with field and laboratory data.

The main accomplishments of this research effort are:

- An explanation of the fundamentals of foaming as they pertain to WMA.
- Development of a laser-based approach to measuring the expansion and collapse of foamed binder to characterize:
  - The maximum expansion ratio ($ER_{max}$) and expansion ratio (ER) with time.
  - The rate of collapse (*k*-value).
  - The foamability index (FI).
- Development of a photographic approach to characterize:
  - Bubble size distribution.
  - Bubble surface area index (SAI).
- Measurements of foamed binder characteristics using both of these methods in laboratory and field environments.
- Validation of compaction shear stress as a workability measure for foamed asphalt mixtures.
- Modification of an existing coating evaluation procedure to obtain a coatability index for foamed asphalt mixtures.
- Development of a foamed asphalt mixture design procedure to identify the optimum water content for coating and workability.

The main findings of this research effort are that:

- Binder foaming characteristics may vary according to:
  - Source.
  - Date of production.
  - Polymer modification.
- Binder foaming characteristics may be improved with the addition of certain additives.
- The three commercially available laboratory foamers produce different foaming characteristics.
- Increasing water content produces larger expansion ratios but a smaller *k*-value, FI, and SAI for most of the binders tested (i.e., faster collapse).
- The SAI served as an indicator of the quality and longevity of the foam, with larger values for binders that produced smaller-sized, longer-lasting, and better-distributed bubbles.
- Increasing water content does not result in improved workability and coatability.
- The lowest maximum shear stress (best workability) was identified and generally occurred between 1% and 2% moisture.
- Workability improves with higher mixing temperatures for foamed binder.
- The mix design procedure for optimum water content was validated through a laboratory study and field trial.
- The coatability of foamed mixtures at the optimum water content was better than the coatability of hot mix asphalt (HMA) mixtures.

CHAPTER 1

# Background

## A. Introduction

Hot mix asphalt (HMA) is a well-established paving material with over 100 years of proven performance. It has been used to pave 94% of the more than 2.5 million miles (4.0 million km) of hard-surfaced roads in the United States [FHWA 2008; National Asphalt Pavement Association (NAPA) 2010]. It is combined at an elevated temperature in either batch or drum mixing plants and then compacted at temperatures ranging from 250°F (121°C) to 325°F (163°C) (Kuennen 2004; Newcomb 2005a). High temperatures are necessary to ensure complete drying of the aggregate and subsequent bonding with the binder, coating of the aggregate by the binder, and workability for adequate handling and compaction. All of these processes contribute to good pavement performance in terms of durability and resistance to permanent deformation and cracking.

In the past few decades, advances in asphalt technology such as polymer-modified binders and the use of angular aggregate that improve resistance to permanent deformation (stone matrix asphalt, for example), and an emphasis on compaction for quality assurance, have resulted in further increases in HMA mixing temperatures up to a limit of 350°F (177°C), where polymer breakdown in the binder may occur. These high temperatures are linked to increased emissions and fumes from HMA plants (Stroup-Gardiner et al. 2005). In addition, the HMA process consumes considerable energy in drying the aggregate and heating all materials prior to mixing and compacting. The use of warm mix asphalt (WMA) technology results in reduced production and paving temperatures without sacrificing the quality of the final product. This has led to a wider range of available production temperatures that may be employed by the contractor.

Economic, environmental, and possible performance benefits motivate the reduction of asphalt mixing and compaction temperatures. Past efforts that date back to the late 1950s include binder foaming processes (using either steam or water), binder emulsification, and incomplete aggregate drying (Kristjansdottir 2006; Zettler 2006). The latest technology is WMA, where temperatures range from 175°F (79°C) to 295°F (146°C), and for which the following benefits have been cited [Koenders et al. 2002; Jones 2004; National Center for Asphalt Technology (NCAT) 2005; Newcomb 2005b; McKenzie 2006; Button et al. 2007]:

- Decreased energy consumption of up to 30% to 40% (Jenkins et al. 2002; Kuennen 2004; Prowell et al. 2011a).
- Reduced emissions and odors at the plant [30% reduction in carbon dioxide ($CO_2$)] (Kuennen 2004; Prowell et al. 2011a).
- Reduced fumes and improved working conditions at the construction site (fumes below detection limits) (Newcomb 2005b; Prowell et al. 2011a).
- Decreased plant wear and costs.
- Extended haul distances, a longer pavement construction season, and a longer construction day than if produced at typical HMA temperatures (NCAT 2005; Kristjansdottir 2006; Ursich 2008; Prowell et al. 2011b).
- Reduced construction time for pavements with multiple lifts (Kuennen 2004).
- Improved workability and compactability (Bistor 2008; Prowell et al. 2011a, 2011b).
- Reduced initial costs in some cases.
- Reduced aging and subsequent susceptibility to cracking and raveling.
- Decreased life-cycle costs in some cases.

There have been a number of products and processes introduced to the marketplace to produce WMA over the last several years (Prowell et al. 2011a). These include waxes, surfactants, mineral additives, and mechanical foaming processes. Waxes, such as those from the Fischer-Tropsch process, montan, and polyolefin, are high–melt-point materials that become fluid at mixing and placement temperatures and then harden at service temperatures. Surfactants reduce the surface tension of the liquid binder, allowing it to better coat

the aggregate at low temperatures and to remain workable at reduced placement temperatures.

WMA production in the United States has increased exponentially in recent years, from 19.2 million tons [17.4 million metric tons (mt)] in 2009 to 86.7 million tons (78.7 million mt) in 2012, an increase of more than 400% in only 3 years (Hansen and Copeland 2013). The work in this research study focused on central plant–produced foamed WMA because foaming asphalt is the largest segment of the WMA market. According to a survey done by NAPA (Hansen and Copeland 2013), mechanical foaming units were responsible for about 88% of all WMA produced in 2012.

Binder foaming has become the process of choice for most contractors using WMA. There are different techniques used in the production of plant-produced foamed asphalt mixtures, including the use of zeolite, wet sand, and mechanical foaming units. Zeolite, a mineral additive, has a small amount of water contained in its interstices that is released in the form of steam when the material is exposed to the hot asphalt mixture. The steam then foams the liquid binder, increasing its volume and allowing it to coat the aggregate at a lower temperature. The warm asphalt mixture (WAM) foam process used in Norway consists of pre-coating the aggregate with low-viscosity binder and then adding a foamed hard binder to provide cohesion to the mixture. In the low-emission asphalt (LEA) process used by McConnaughy in New York, coarse aggregate is dried and coated with binder, after which wet sand and an additive are introduced to create foam with the already heated binder. In current mechanical plant foaming processes in the United States, cold water is injected into a hot binder stream that may be anywhere from 285°F to 340°F (140°C to 171°C). The cold water turns to steam when it comes in contact with the hot binder, and the water expands creating an increased volume of binder. The amount of water used in producing the foam has normally varied between 1.0% and 3.0% by weight of binder. Foaming works in two ways to promote mixing at lower temperatures: (1) it increases the volume of the binder, which makes it easier to coat particles, and (2) it reduces the overall viscosity of the binder through shear thinning, which makes the mix more workable (Fort et al. 2011). All of these processes and products work to allow asphalt mixing and placement temperatures to be reduced, but they introduce a new set of conditions that are not readily accounted for in the selection of materials and mixture design.

The changes brought about by WMA in mixture components, mix processing, and plant design have left many paving technologists questioning the validity of current mix design methods in adequately assessing the volumetric needs of asphalt mixtures and the physical characteristics required to meet performance expectations. While a variety of other NCHRP projects (9-43, 9-47A, 9-48, 9-49, 9-49A, and 9-52) attempted to address many of these issues, this study considered the impact of WMA foaming technology on the volumetric and performance characteristics of binders and mixtures.

While foaming is popular, there have been a number of questions surrounding the use of water in WMA. For instance:

- Will the presence of water in the mix have detrimental effects on performance in terms of its strength and durability?
- How long will the effect of the foam last?
- How can a distinction be made between the foaming abilities of different binders?
- How much mix production and paving temperature reduction may be realistically achieved by foaming?
- Will all foaming techniques produce the same quality and quantity of foam?
- How will the presence of additives in the liquid binder affect the ability of the binder to foam?
- How will polymer-modified binders behave in the presence of foaming?
- Will mix design and evaluation procedures need to be modified to accommodate foaming?

These questions were addressed during the course of this study.

## B. Foaming Theory and Applications

This section presents a review of foaming technology in both the asphalt mixture and other industries. This is an essential first step prior to researching and understanding the foaming characteristics of binders.

### B.1. Definitions

It is important to identify a few common terms used in the industry and literature to characterize foams. The term "foamability" is often used to describe the extent to which a liquid can be foamed, both in terms of volume and stability. Foamability is a property of the liquid, although it is governed by external factors such as gas concentration and temperature. There are types of foams prepared by processes not involving the direct dispersion of a gas in a liquid phase (Klempner et al. 2004). These may be prepared by the leaching of a fugitive phase such as a water-soluble salt, sintering small particles dispersed in a heat-stable matrix, fusing initially discrete polymer particles that initially entrap air or other gases, and forming a polymer matrix around hollow spheres. These processes do not follow the same steps of gas dispersion, bubble growth, and stabilization as are found in the binder foaming process and, thus, are not considered in this review.

The terms "foam" and "froth" are often used interchangeably. However, the term "foam" is used to describe a two-component

system composed of a gas and a liquid (typically), which when broken down leaves a homogenous liquid phase (Pugh 2005). In some cases, foam is also regarded as an emulsion of a liquid and a gas. The term "froth" is used to described a three-component system, typically a gas, a fluid, and a solid, which when broken down results in a two-component composite.

Not all foams are the same. Foams are typically classified and studied in two different categories (Adamson and Gast 1997; Pugh 2005):

- Polyederschaum (polyhedral foam): In this type of foam, the volume of gas is much larger as compared to the volume of the fluid. The fluid exists in the form of very thin films separating the gas, which are also referred to as lamella. The name is derived from the fact that the gas cells are polyhedral in shape (Adamson and Gast 1997).
- Kugelschaum (spheroidal foam): In this type of foam, the gas volume is relatively low compared to the polyederschaum. A relatively thicker film of the fluid separates the gas bubbles.

Figure 1-1 shows a schematic of the two types of foam. These two types of foam could coexist in the same material, given the highly dynamic process of foaming. Bubbles could start as isolated and then begin impinging on each other and form polyhedral foam as they grow. In the context of foamed asphalt mixtures, the latter (kugelschaum) type of foam appears to be more relevant as the bubbles would emerge to the surface and collapse before a thin wall between bubbles could be formed. This was substantiated by Hailisilassie et al. (2014) by means of X-rays of binder foam in a study conducted at the Swiss Federal Laboratories for Materials Science and Technology.

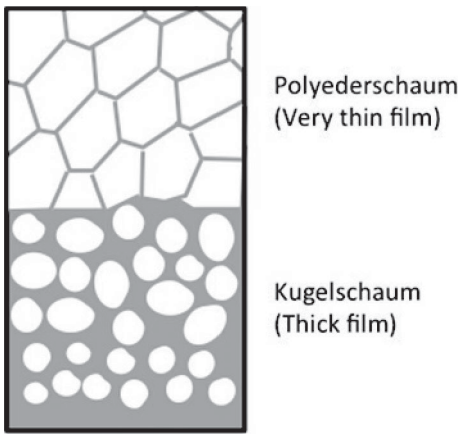


***Figure 1-1. Schematic to illustrate two types of foam (adapted from Pugh 2005).***

## B.2. Foaming in Other Industries

There are a number of industries that require the design and use of foamed materials. The applications range from food, pharmaceutical and health care products, polymers, and in some cases even metals (Koehler et al. 1998). Several different methods are used to produce foam in the food industry, including whipping, injection, sparging (bubbling a gas through a liquid), and shaking (German et al. 1985). The characteristics of the foam produced using each of these methods are different. There are several different variables associated with each of these four methods that can result in the production of foams with very different characteristics.

Arzhavitina and Steckel (2010) present a detailed review of the different types of foams typically used in the pharmaceutical sector. One of the types of foam that is commonly used is the pressurized aerosol foam. Aerosol foam is produced by using a propellant vapor to drive the liquid through a nozzle from a storage can.

In the packaging industry, foaming is typically achieved using a blowing agent, which upon controlled energy input (e.g., thermal) causes a desired level of foaming of a polymer. In a typical foaming process, the blowing agents gasify through chemical reaction or thermal decomposition under the foaming process conditions. The blowing agent is mixed with pelletized polymer and loaded into an extruder. It decomposes in the extruder barrel at an elevated temperature, resulting in gas formation in the polymer melt. The gas formed in the polymer melt leads to bubble nucleation and growth. On exiting the extruder, the polymer profile expands in volume because of the bubble growth. In addition to chemical reaction and thermal decomposition, gas can be delivered to the extruder through either pre-saturation of the polymer pellets or high-pressure injection right into the polymer melt inside the extruder. Foams produced in this way have a smaller bubble size and a more uniform foam structure.

## B.3. Metrics to Characterize Foam in Other Industries

The two most common attributes that are used to characterize foams across different industries are the volume and stability of the foam. In fact, as will be evident in the summary that follows, these two attributes and concomitant metrics are similar to what is currently being used to characterize binder foaming: expansion ratio (ER) and half-life (HL).

Foamability of wines is an important characteristic that is measured to select base wines for the production of sparkling wines. Over the past few years, researchers in this area have developed two different sets of parameters to characterize the foamability of different wines. The first set has three different parameters: (1) maximum height (HM) reached by the foam

after carbon dioxide injection for a specific interval of time; (2) foam stability height (HS) during carbon dioxide injection, which represents persistence of the foam; and (3) foam stability time (TS), identified as the time it takes for all the bubbles to collapse after carbon dioxide injection has stopped. The second set has two different parameters: (1) *E*, or foam expansion, which is very similar to the ER used to characterize expansion of binders; and (2) $L_f$, or foam stability, which is broadly defined as the area under the foam height versus time curve following the peak expansion divided by the maximum height of the foam. These two parameters are sometimes accompanied with a characteristic bubble size. Andrés-Lacueva et al. (1996) demonstrated that the first set of parameters, HM and HS, were strongly correlated, and therefore only HM and TS were adequate to describe the foamability of different wines. Gallart et al. (1997) compared the relative benefits between the two sets of parameters and reported that the precision of each set of parameters was dependent on the extent to which the wine foamed—the second set being more appropriate for low-foaming wines.

Food products are routinely characterized to determine the influence of factors such as production method and ingredients (proteins in particular) on their foaming characteristics. The two parameters that are often used in the food industry are (1) foam overrun and (2) foam stability. Foam overrun is roughly a measure of the volume of foam produced. For example, Phillips et al. (1987) defined it as the difference between the weights of 100 mL of protein and 100 mL of foam divided by the weight of 100 mL of the foam. The measurements were made at a specific time after foaming the subject material. Foam stability was defined as the ability of the foam to resist rupture or collapse under the influence of gravity. In more recent studies, Raymundo et al. (1998) tried to modify these two metrics to come up with a single parameter, referred to as the foaming index. In this case, overrun was measured not at a prespecified point in time but continually as a function of time using automated equipment. The integral of the overrun with respect to time was used as a single parameter (the foaming index). Raymundo et al. tried to demonstrate the sensitivity and advantages of using this single parameter to characterize the foam.

In pharmaceutical applications, two metrics that are used to describe the quality of the foam are foam density and breakability (Arzhavitina and Steckel 2010). Foam density is simply the relative density of the foam with respect to water. Stability of the foam is characterized in terms of three different types of breaking behavior: (1) quick-breaking foams, or foams that are thermally unstable and collapse on contact with skin; (2) lathers, or stable foams that demonstrate a tendency to increase in volume when subjected to shearing action; and (3) breakable foams, or foams that are stable at skin temperatures but collapse and spread easily upon application of shear forces. Other metrics and methods, similar to those used in the food sector, are also used to describe binder foam stability.

In addition to foam density and stability, the rheology of the foam is considered of importance in pharmaceutical applications. However, there are several challenges associated with measuring the rheological properties of foam, even when the foam is relatively stable compared to foamed binder. Kealy et al. (2008) conducted a detailed study on the methods that can be used to measure the rheological properties of several different types of pharmaceutical foams. They cited several difficulties associated with the use of standardized methods, such as use of the dynamic shear rheometer (DSR), to measure the rheological properties of the foam. For example, they report that the small gaps in typical test geometries [0.03 to 0.08 in. (1 to 2 mm) with parallel plates or a few micrometers with the cone and plate geometries] are inappropriate because of the presence of large bubbles in the foam. Even if the bubble sizes were small, there were problems associated with slippage between the foam and the end plates. In their study they tried to overcome these limitations by using larger gaps and serrated plates. They also used vane geometry to measure the rheological properties. They were able to measure the yield stress for the different foams by applying a monotonically increasing shear stress until the specimen failed or started to flow (Figure 1-2). They also measured the complex shear modulus of different foams in the frequency domain and demonstrated that at low frequencies the rheological properties measured using the vane geometry were similar to the properties measured using the serrated parallel plate. In the context of foamed binder, this is an important finding because it may be possible to use geometry similar to the vane (e.g., a portable paddle viscometer) to obtain real-time viscosity and rheological measurements of the foam as it collapses.

One other characterization procedure that is worth mentioning is foam drainage. Drainage tests are frequently conducted to evaluate the structure and stability of different kinds of foam (Pugh 2005). There are several different methods that are used to drain foams to determine their characteris-

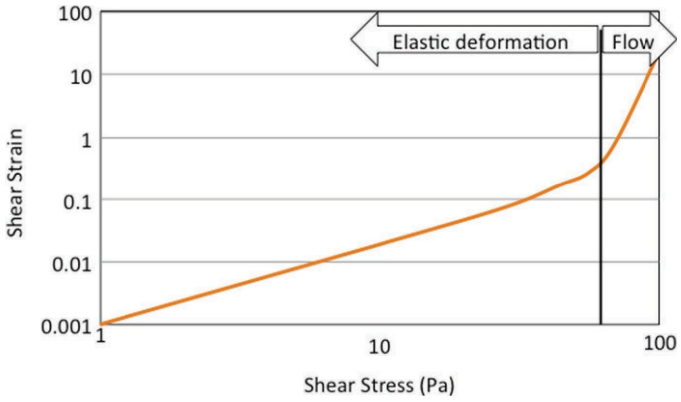


***Figure 1-2. Typical results for the yield strength of shaving foam (adapted from Kealy et al. 2008).***

tics. Koehler et al. (1998) identified four different methods of draining foams: (1) free drainage under gravity; (2) wetting of the foam by placing the foam in contact with a liquid bath; (3) forced drainage, where a constant liquid supply is pumped onto the top of the foam; and (4) response of the foam to an external pulse. Parameters that are measured in a foam drainage experiment may include the rate at which the liquid flows out of the foam and changes in pressure across the boundaries of the foam. Measurements are usually carried out using optical or electrical-based instrumentation attached to a column designed to create and drain foams (discussed in the following section). Koehler et al. (1998) present the analytical solutions that describe the rate at which foams drain as a function of the properties of the foam. However, based on the literature, it appears that the drainage method is more appropriate to characterize the polyederschaum category of foams (foams with very thin films of the fluid separating the gas).

## B.4. Mechanisms of Bubble Formation in Fluids

The mechanics of bubble formation in fluids have much to do with how gas is delivered in the fluid. Two different situations have been studied in the literature: (1) gas delivered in the fluid with the use of an orifice, nozzles, capillaries, and porous plates; and (2) gas dissolved in the fluid through diffusion. In the first case, the nozzle is submerged in the fluid, and the gas is blown into it. As the rate of gas flow is increased, three regions of bubble formation can be obtained. At very low rates of gas flow, bubble formation is almost a static problem. Bubble size is primarily determined by orifice diameter, surface tension, and the fluid density. Bubble formation under this condition is also the basis of the drop-volume method for measuring surface tension. At intermediate gas-flow rates, bubbles are formed at a constant frequency, and the bubble size is uniform, dependent on gas flow rate, orifice diameter, and the volume of the gas chamber upstream from the orifice. At high gas-flow rates, a normal distribution with respect to the logarithm of the bubble diameter is established for the turbulent flow of gas through the orifice. As turbulence becomes fully developed, a marked decrease in the bubble diameter occurs. For bottom entrance flow, the bubble diameter appears to be independent of the orifice diameter (Leibson et al. 1956). While bubble formation and detachment at low flow rates is well understood, the formation of a large quantity of fine bubbles at turbulent conditions appears to be due to the shattering of large bubbles by turbulent swirling discontinuous jets. It is also observed that, in general, lower surface tension helps create smaller bubbles.

The second case, where gas is delivered in fluid through diffusion, can be illustrated with the microcellular plastics injection molding process (Xu 2010). In the microcellular injection molding process, a gas-polymer solution is first created in an extruder barrel. The gas at the supercritical fluid state is metered and injected into the barrel and then dissolved into molten polymer. As the gas flows into molten polymer, it forms large gas droplets (bubbles) since it takes time for the gas to be dissolved. The large droplets of gas are sheared, elongated, and broken into smaller bubbles with the rotation of the extruder screw. Then the gas quickly diffuses into the molten polymer due to the increased polymer-gas interfacial area and the reduction of diffusion length. The gas dissolution process obviously depends on many factors, including gas pressure, temperature of the polymer melt, and diffusivity and solubility of the gas. It is possible that the gas is not completely dissolved in the polymer and small bubbles still exist during the gas-polymer mixing stage. These small bubbles will grow bigger in the next stage when the mixture is released through the exit of the extruder. Nucleation can also happen elsewhere in the mixture as long as the foaming condition is met. In the microcellular injection process, sudden release of pressure is the cause of bubble nucleation and subsequent bubble growth.

In addition to direct gas injection, foaming agents can be mixed with polymers as additives, which will then decompose and give off the needed gas inside the extruder barrel. This is how gas is delivered in regular foam extrusion processes that will yield larger bubble sizes than the microcellular injection molding process.

Bubble growth in polymer foaming with $CO_2$ has been explicitly modeled, and the significance of material properties has been demonstrated (Wang and Li 2008; Kim and Li 2011). In $CO_2$ polymer foaming, a small weight percent of $CO_2$ is injected into the polymer matrix. The bubble growth process is modeled as a quasi-static diffusion-driven pressure and momentum-balanced process in a viscoelastic fluid. Figure 1-3 shows a single bubble model for a polymer-gas system.

The foaming of liquid binder is a dynamic process where water is used as the foaming agent in the hot binder. As water

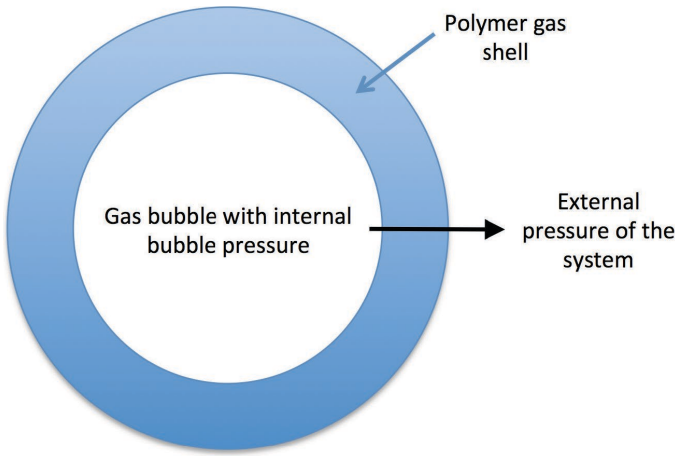


***Figure 1-3. Schematic of the single bubble model for polymer-gas systems.***

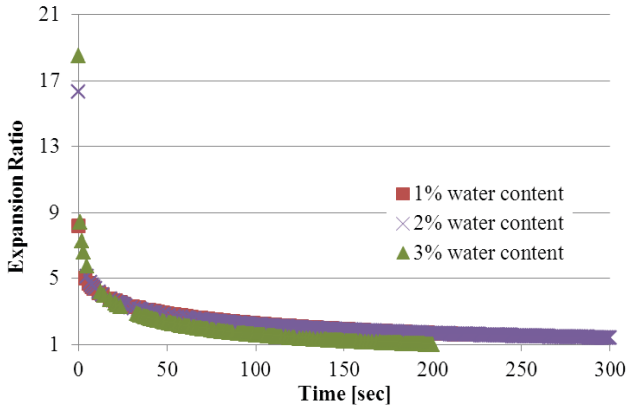


***Figure 1-4. Expansion ratio versus time curve of foamed binder.***

turns to steam in atmospheric pressure, it expands by a factor of about 1,600, but in binder the steam is confined by the pressure of the liquid and the size of the pipe or vessel in which the foaming is initiated. Once the foamed liquid is released in the asphalt mixing chamber (drum or pugmill), the expansion of the binder reaches its full potential as it is mixed with the aggregate. The degree of expansion of the binder is dependent on a number variables that will be discussed later, but the major factors are the temperature and viscosity of the binder as well as system characteristics such as the external pressure and rate of flow.

The dynamic nature of binder foaming is illustrated in Figure 1-4, where it can be seen that expansion of the binder on the order of about 18 times happens almost instantaneously, and its subsequent collapse to its HL (where the volume equals half its maximum expansion) occurs within the first few seconds. At the maximum expansion, the density of the binder is reduced from 0.96 g/cm$^3$ to about 0.05 g/cm$^3$, which places it generally between a liquid and a gas for most substances. This unstable state quickly moves toward liquid initially as the gas in the bubbles is released. The rate of dissipation slows considerably after the initial collapse of the foam and continues for minutes afterward. It is believed that this region of stable dissipation is critical in terms of providing coating and workability in foamed asphalt mixtures, as will be discussed later. At this point, a discussion of the theory of foaming provides the background needed to understand the mechanisms of binder foaming.

The momentum equation of the polymer shell surrounding the gas bubble can be expressed as:

$$P_{bubble} - P_{system} - \frac{2\gamma}{R} + 2\int_{R}^{Rshell} \frac{\tau_{rr} - \tau_{\theta\theta}}{r} dr = 0 \qquad (1\text{-}1)$$

Where:

$P_{bubble}$ = the gas pressure inside the bubble.
$P_{system}$ = the system pressure around the bubble.
$r$ = the radial distance from the center of the bubble.
$R$ = the bubble radius.
$R_{shell}$ = the bubble shell radius representing the polymer around the bubble.
$\gamma$ = the surface tension at the bubble surface.
$\tau_{rr}$ and $\tau_{\theta\theta}$ = the stress components in the shell along the $r$ and $\theta$ directions, respectively.

The viscoelastic rheology of the polymer-$CO_2$ system can be modeled as:

$$\frac{d\tau_{rr}}{dt} = -\left(\frac{1}{\lambda} + \frac{4R^2\dot{R}}{y+R^3}\right)\tau_{rr} - \frac{4\eta_o}{\lambda}\left(\frac{R^2\dot{R}}{y+R^3}\right)$$
$$\frac{d\tau_{\theta\theta}}{dt} = -\left(\frac{1}{\lambda} - \frac{2R^2\dot{R}}{y+R^3}\right)\tau_{\theta\theta} + \frac{2\eta_o}{\lambda}\left(\frac{R^2\dot{R}}{y+R^3}\right) \qquad (1\text{-}2)$$

Where:

$\lambda$ = the relaxation time of the polymer/gas solution.
$\eta_o$ = the zero-shear-rate viscosity of the polymer-gas system.
$y$ = the transformed Lagrangian coordinate, defined as:

$$y = r^3 - R^3 \qquad (1\text{-}3)$$

From these equations, the bubble pressure $P_{bubble}$ can be calculated by assuming a known bubble size at a given time step. On the other hand, it is clear that the bubble growth process is driven by gas diffusion into the bubble. The mass transfer equation can be modeled as:

$$\frac{\partial C}{\partial t} = \frac{D_G}{r^2}\frac{\partial}{\partial r}\left(r^2\frac{\partial C}{\partial r}\right) - \frac{\dot{R}R^2}{r^2}\frac{\partial C}{\partial r} \qquad (1\text{-}4)$$

Where:

$C$ = the local gas concentration in the polymer matrix.
$D_G$ = the gas diffusivity.

The law of conservation of mass requires that the rate of change of the mass in the gas bubble be equal to the mass of gas diffusing into the bubble through the bubble surface. Thus, the bubble pressure can be related to the concentration gradient at the bubble surface by:

$$\frac{d}{dt}\left(\frac{4\pi}{3}\frac{P_{bubble}R^3}{KT}\right) = 4\pi R^2 D\frac{\partial C}{\partial r}\bigg|_{r=R} \qquad (1\text{-}5)$$

Where:

$K$ = the universal gas constant.
$T$ = the temperature that is estimated from the heat transfer model for the current time step.

Using these two equations, the pressure inside the bubble $P_{bubble}$ can be related to the bubble size $r$ as well.

By comparing the bubble pressures $P_{bubble}$ calculated from both the momentum and diffusion equations, the bubble size $r$ at each time step can be determined using a recursive proce-

dure. Such a procedure relates the bubble growth process with the material properties such as surface tension, relaxation time, viscosity, and gas diffusivity, as well as process parameters such as temperature, gas concentration, and the system pressure.

The knowledge obtained from $CO_2$ gas foaming of polymers can be readily extended to better understand the factors that affect the characteristics of water foaming of binders. The amount of water carried by the binder depends on the pressure of water and binder within the nozzle as well as the diffusivity of water or steam in the binder. While the pressure within the nozzle varies with the type of nozzle, the ability of the water to diffuse within the binder depends on the type of binder. The type of nozzle may also determine the water droplet size, which in turn determines how fast water converts to steam and the size of the steam bubbles in the binder. The importance of these two variables (type of nozzle and binder) has been recognized in previous studies (Castedo and Wood 1983). Ozturk and Kutay (2014a; 2014b) concluded that water content and the driving pressure behind the foam have profound effects on bubble size, ER, and HL of the binder. They inferred the bubble size distribution through the application of Stokes' law. It is also expected that the size and life of the bubbles (related to ER and HL) within the binder coming out of the nozzle will depend on the type of the binder—more specifically, the surface tension of the binder surrounding the bubble and its viscosity.

This preliminary understanding of the relationship between material properties and foaming helps explain the findings from other previous studies. For example, Fu et al. (2011) demonstrated that binder grade is not related to its ability to foam. This is expected because the binder grade does not reflect the material properties such as viscosity and surface tension that are related to foaming. Another example is that the addition of liquid anti-strip agents improves the ability of the binder to foam (Abel and Hines 1979; Engelbrecht 1999; Fu et al. 2011). This is also expected because Bhasin et al. (2007) have demonstrated that the addition of liquid anti-strip agents reduces the surface tension of the binder. A more detailed explanation of the influence of binder properties on foam expansion and applied foaming theory to binder foaming is included in Appendix A.

### B.5. Summary

Based on the survey of literature on foaming in binder and other industries, it is expected that a number of factors influence binder foamability, including but not limited to:

- Surface tension of the binder (which is governed by the chemical composition of the crude oil and processing of the crude oil to produce the binder, including chemical and polymer modifications).
- Temperature of the binder.
- Viscosity of the binder (which is governed by the same factors as surface tension).
- Water content used to produce foam.
- Size and dispersion of the water droplets introduced in the binder (which is governed by the characteristics of the nozzle delivering the water).
- Quality of the water and the presence of any additives in the water that influence its surface tension.
- Presence of anti-foaming agents in the binder.
- Use of foam promoters or other additives in the binder and the concentration of such additives.
- Atmospheric conditions (humidity, air pressure).

## C. Binder Foaming Technology and Applications

Most of the available literature dealing with foamed binder concerns its application in the stabilization of soils or base materials, which began with Csanyi (1957). Although Csanyi used steam injected into the hot liquid binder, Mobil Oil Australia acquired the patent and modified it so that cold water was introduced into a stream of hot binder and then the foamed binder was mixed with cold, wet aggregate or soil (Muthen 1998). The desired outcome for stabilization was the coating of the fine particles by binder and the spot welding of the coarse aggregate to achieve some measure of cohesion. This type of stabilization is usually done in place but can also be accomplished through the use of a mixing plant (Muthen 1998). In recent years, this has been increasingly applied to in-situ recycling of pulverized asphalt pavements (Fu 2011).

Fortunately, the process for WMA foaming, regardless of whether it is done mechanically through a nozzle, by introducing wet sand, or by using zeolite, all amounts to adding a small quantity of water to the hot binder (1.0% to 3.0% by weight) (Fort et al. 2011) and allowing the generation of steam to expand the binder through the formation of voids. Thus, lessons learned in base and soil stabilization apply to WMA production using foam.

### C.1. Mechanical Foaming

There are a variety of methods to disperse a foaming agent such as water into a medium such as liquid binder. Water in a liquid state is introduced to the hot binder stream, wherein it turns to steam. Mechanical systems, which could be used for foaming and applied in the field, have been identified by the authors as mechanical mixing, Venturi mixing, expansion chamber, shear/colloid mill, air-atomized water, and high-pressure atomized water. In some instances, more than one mechanism may be employed, or the system actually uses a hybrid of methods. The commercially available laboratory

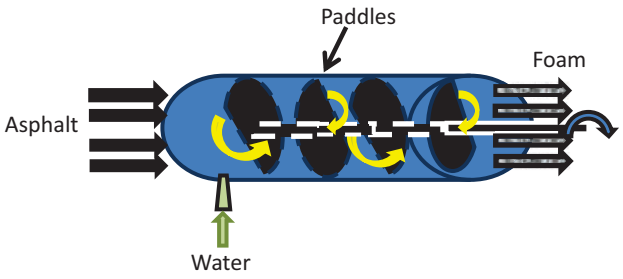


***Figure 1-5. Mechanical mixing.***

units use either air-atomized water or pressurized water in an expansion chamber.

### C.1.1. Mechanical Mixing

Systems using mechanical mixing (Figure 1-5) have an inlet port for introducing water into the binder stream. Downstream of the water introduction, the system may have paddles, baffles, or other means of mixing the water/binder mixture. In this approach, some dispersion of the water into the binder occurs as the cold water turns to steam and creates bubbles, followed by additional agitation that may serve to more finely divide the bubbles and enhance the foaming action.

### C.1.2. Venturi Mixing

Venturi mixing (Figure 1-6) is accomplished by introducing the water into the binder line ahead of a constriction in the pipe. This reduced cross-section increases the pressure in the line, which is released as the cross-section opens. This creates turbulence in the fluid, which acts to mix the steam and liquid binder.

### C.1.3. Expansion Chamber

In an expansion chamber (Figure 1-7), binder and water are introduced simultaneously. The cold water comes into contact with the hot binder and converts to steam, and expansion of the binder occurs. The foam is then forced out of a nozzle and into the mix. Expansion chambers can be configured in a manifold system where several are placed in parallel.

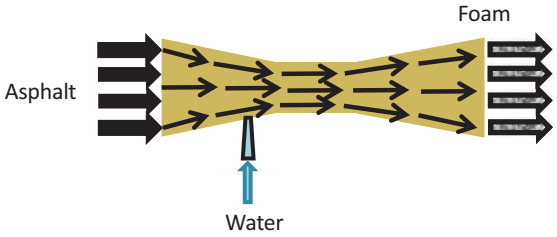


***Figure 1-6. Venturi mixing.***

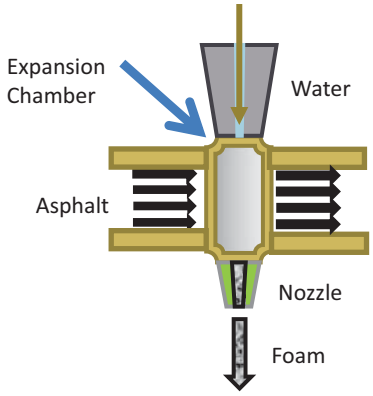


***Figure 1-7. Expansion chamber.***

### C.1.4. Shear/Colloid Mill

Shear/colloid mills (Figure 1-8) are used to mix substances such as binder and water. However, they are normally used to suspend binder in water for asphalt emulsions. In this case, cold water is introduced into a chamber with hot binder. The water turns to steam as it is forced with the binder through a very small opening between a rotor and a stator, which shears the water into very small particles. As the mixture exits the colloid mill, it expands and is introduced into the mix.

### C.1.5. Air-Atomized Water

The use of air-atomized water (Figure 1-9) is a variation on the expansion chamber discussed previously. In this case, a stream of air is forced into the stream of water to break it into finer droplets. This should disperse the moisture throughout the binder stream, and as the moisture comes into contact with the hot binder, it expands. The chamber allows for the expansion of the foamed binder, which is then forced out through a nozzle into the mixture.

### C.1.6. High-Pressure Atomized Water

In this type of system (Figure 1-10), water is forced through a very small orifice under very high pressure into the binder

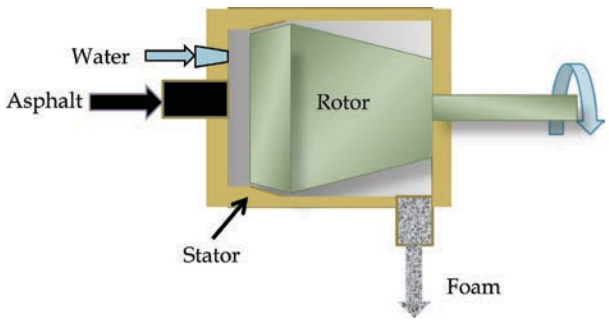


***Figure 1-8. Shear/colloid mill.***

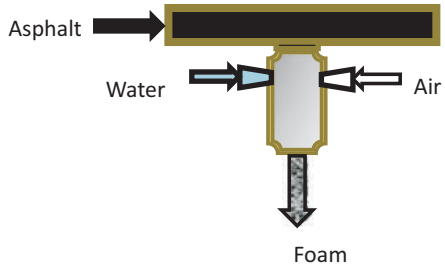


*Figure 1-9. Air-atomized water.*

line. At this point the binder line may be enlarged to accommodate the increased volume, or its cross-sectional area may remain the same, in which case the pressure is considerably increased.

A survey was sent to manufacturers of asphalt plant foaming equipment to gain an understanding of what types of systems exist and their operating characteristics. Of the seven manufacturers for which information was either found or who returned the survey, two used atomized water, one used an expansion chamber, one used multiple expansion chambers, one used mechanical mixing, one used a colloid mill, and one used a combination of mechanical mixing, Venturi mixing, and atomized water. The maximum water pressure varied from 60 to 2,000 psi (410 to 14,000 kPa), and only one manufacturer identified a maximum binder flow rate of 120 gal/min (450 L/min). Water meters varied, with Coriolis, orifice, Venturi, positive displacement pump, sparling magna flowmeter, and turbine systems being identified. None of the plant foaming manufacturers had laboratory-scale foaming units, and none had a procedure for identifying the optimum water content to use in their foaming process.

It is clear that plant foaming systems cover a span of relatively simple systems to complex systems, and thus the costs vary widely as well. The three laboratory foaming units investigated in this study use either an expansion chamber or air-atomized water to produce foaming. As will be shown later in this report, the optimum water content for foaming is relatively independent of the type of foaming unit used.

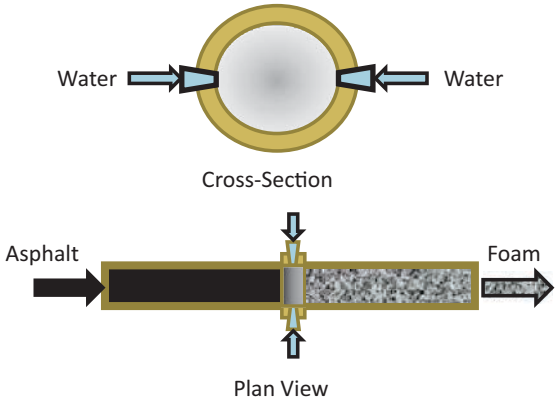


*Figure 1-10. High-pressure atomized water.*

### C.2. Zeolite

Zeolite is a mineral additive that has a small amount of water contained in its interstices that is released in the form of steam when the material comes in contact with the hot asphalt mix. It is introduced into the pugmill of a batch plant or the mixing zone of a drum plant as the binder and aggregate are being combined. The steam then foams the liquid binder, increasing its volume and allowing it to coat the aggregate at a lower temperature.

When an additive such as zeolite is used to provide moisture release, one must consider the potential residual impact of the additive once the moisture release has taken place. The release rates, moisture release quantities, and temperatures over which the moisture release takes place are important. There appears to be a gradual release of moisture that extends beyond the period required for improved workability during construction.

## D. Review of Past Work

There are numerous views on the importance of foamed binder properties on the final mixture properties and characteristics. Bowering and Martin (1976) maintained that the cohesion and compressive strength of foam-produced mixes were greater when the ER was on the order of 15:1. Fu et al. (2011) reported that small changes in binder temperature and foaming moisture could significantly change the characteristics of foamed binder while only having minimal effects on the final mixture properties. However, there was a correlation between the foaming characteristics and the dispersion of binder in mixtures.

The improved workability of foamed binder in WMA applications has been attributed to its shear-thinning characteristics by Fort et al. (2011). They claim this helps to maintain a greater film thickness without drain-down during storage and transport, yet helps the workability during paving and compaction. However, Clark and Rorrer (2011) noted that challenges with foamed binder included difficulty with handwork and temperature segregation, but that lower temperatures allowed for compaction of mixes sooner and for improved density.

Clark and Rorrer (2011) found that in Virginia, typical mixture temperature reductions achieved with foaming systems was between 25°F and 50°F (14°C and 28°C), but this depended on a number factors, including weather conditions, type of paving job, haul distance, and moisture content of the aggregate. It was common for the temperature of the mix to be increased if the paving required a significant amount of handwork, and for temperature segregation to be addressed by the use of a material transfer device. In the construction of I-55 and I-57 in Missouri, Fort et al. (2011) found that

the use of a polymer-modified binder (PG76-22) required that the average temperature of HMA production needed to be at 350°F (175°C) while the WMA average temperature was 293°F (145°C). The compaction temperature range was 320°F to 230°F (160°F to 110°C) and 275°F to 212°F (135°C to 100°C) for HMA and WMA, respectively, and the density of the final mat was 94% for both (Fort et al. 2011).

The formation of steam bubbles within the liquid binder increases the volume of binder, and foam reduces the mass viscosity from that of the liquid at the same temperature. External work in the form of shearing may destroy some or all of the bubbles. External work includes mixing; dropping into the slat conveyor, the silo, and the truck; dumping from the truck into the paver; and movement through the paver to the spreader auger, the spreader auger to screed, and finally to the compactor. At the same time, the mix is cooling, and as this progresses, the volume of steam contracts to the point of liquid, below the boiling point. Ideally, the mix would remain at a relatively constant level of workability up through its compaction, at which point the binder mat would assume its final density and stiffness.

Hajj et al. (2011) stated that Marshall mixture and volumetric properties for an asphalt mixture that contained an unmodified foamed binder were met if the lab compaction occurred within 4 hours of plant production. They also observed that the effect of foaming in a WMA project is lost somewhere between 4 and 15 hours after short-term oven aging at 250°F (121°C). They reported problems in meeting Marshall mix design requirements when polymer-modified foamed WMA was compacted in the laboratory at the project placement temperature of 255°F (124°C), and that these could only be obtained when the compaction temperature was raised to 305°F (152°C). The temperature observations agree with Fort et al. (2011), who suggested that polymer-modified binders may require an elevated temperature. However, the time that the foaming characteristics are reported to last in Hajj et al. (2011) and that was also noted by Prowell et al. (2011b) is far greater than the matter of minutes reported by Muthen (1998). The observations by Muthen (1998) are similar to the results obtained in the current effort.

For WMA applications, Allosta et al. (2011) and Abbas et al. (2013) found that the characteristics of asphalt mixtures produced by foaming were not very distinguishable from HMA. Nazzal et al. (2011) reported similar results for a foamed binder project in Ohio, except that the foamed mix seemed to have a greater tendency for rutting in the asphalt pavement analyzer. They speculated that the reason for the increased rutting may have been the presence of natural sand in the mix. This agrees with observations by Sakr and Manke (1985) and Abbas and Ali (2011). Fu et al. (2011) stated that binder temperature and foaming moisture could significantly change the foaming characteristics of the binder while only having minimal effects on the final mixture properties. However, they did find a correlation between the foaming characteristics and the dispersion of binder in mixtures.

## E. Study Objectives

The objectives of this study were to (1) determine the properties of foamed binders that relate to asphalt mixture performance and (2) develop laboratory foaming and mixing protocols that may be used to design asphalt mixtures. This report documents the selected test methods for determining properties of binder foaming and foamed asphalt mixtures as well as the laboratory and field results and analysis used to characterize the foamed binders and their relation to asphalt mixture characteristics.

When developing the testing protocols and equipment, the goals were to (1) minimize the complexity of any testing protocols and methods, (2) make any test applicable to both laboratory and field conditions, (3) simplify any testing equipment and design it to be as rugged as possible while being able to detect sensible differences in measurements, and (4) minimize, to the extent possible, the cost of the equipment and testing.

## F. Study Scope

In concert with the project panel, a decision was made to focus on mechanical foaming techniques and the use of zeolite for foaming. These approaches to foaming make up the vast majority of processes used by agencies and contractors in the United States. While the WAM-foam and LEA processes for foaming are both valid and have been successfully employed, they have not been used to a significant degree in this country. Readers who have an interest in WAM-foam are referred to Koenders et al. (2002) and D'Angelo et al. (2008). For those desiring more information on the LEA approach to WMA, Romier et al. (2006), Harder et al. (2008), and D'Angelo et al. (2008) are recommended.

## G. Report Organization

This report is composed of five chapters. Chapter 2 discusses the approach used in the laboratory binder foaming and foamed mixture studies. The test methods used to characterize binder foaming are discussed in addition to the laboratory mixture approach, including the development of measures for workability and coatability and the proposed foamed mix design procedure. Chapter 3 describes the results of the laboratory binder and mixture studies, including the

effect of selected variables on binder foaming characteristics (expansion/collapse, bubble size, and shear behavior), a comparison of laboratory foamers, and a description of the effects of foaming on workability and coatability of asphalt mixtures. The validation of the proposed mix design approach using various foaming units is also included in this chapter. Chapter 4 presents the results of foaming at field sites in Texas and Ohio, including an initial trial to explore the binder foaming and foamed mixture sampling and testing. A field comparison of plant foaming units is also discussed, along with a field evaluation of the proposed mix design approach. Performance test results using the Hamburg Wheel Track Test (HWTT), resilient modulus ($M_R$), and indirect tensile (IDT) strength are included for all mixtures. Conclusions stemming from the data generated in this study are reported in Chapter 5.

CHAPTER 2

# Research Approach

In order to use effectively foamed binder to produce WMA, it is important to understand the characteristics of the foamed binder that influence mixture workability and performance. The four broad steps to achieve this are:

1. Develop a method to precisely quantify the characteristics of the foamed binder.
2. Use this method to investigate the influence of factors such as binder source, water content, liquid additives, and shearing action on the foaming characteristics of binders.
3. Relate the binder foaming characteristics to foamed mixture coatability and workability.
4. Use the foamed mixture coatability and workability to estimate the optimum foamed water content and validate the performance of the foamed mixture.

## A. Test Methods and Metrics to Characterize Binder Foaming

This section presents a summary of the work done to achieve the first step (i.e., to develop a method and metrics by which to precisely quantify the characteristics of the foamed binder).

A review of the literature shows that a graduated dipstick is commonly used to characterize foamed binders for WMA and base stabilization applications (He and Wong 2006; Namutebi 2011). Most investigators have also regarded the maximum expansion ratio ($ER_{max}$) and HL of the foam as meaningful indicators for the quality of the foam (Abel 1978; Brennen et al. 1983; Jenkins 2000; Namutebi 2011; Namutebi et al. 2011). In fact, similar metrics (along with bubble size distribution, as discussed in Chapter 1, Section B) are typically used to characterize foam in other industries, such as the food and polymer industries (Huang et al. 1997; Phillips et al. 1987; Wilde 1996). Some of the limitations of using the dipstick method to measure HL and $ER_{max}$ are as follows:

- The method is highly dependent on the operator as it is based on manual observation of foam height and time.
- The approach is limited to only two points in describing the rate at which the foamed binder collapses.
- The idea of using HL to describe foaming characteristics of the binder implicitly assumes that the foam collapses following an exponential collapse.

Due to the limitations discussed here, the parameters $ER_{max}$ and HL measured using the dipstick method are not suitable to characterize foamed binder. Instead, three different approaches were considered and evaluated in this study: (1) two different noncontact methods to measure foam expansion and collapse over time, (2) an image-based method to characterize foam based on bubble size distribution, and (3) an in-situ density measurement method to characterize foam density over time. Results from these methods were used to develop metrics to characterize binder foam.

### A.1. Noncontact Measurement of Binder Foam Expansion and Collapse

Two different types of sensors were used to measure the change in height and corresponding change in volume of the foamed binder: (1) an ultrasonic sensor and (2) a laser-based sensor. The following sections briefly describe the use of the ultrasonic and the laser-based sensors to measure the change in the height and volume of the foamed binder.

The ultrasonic sensor comprises a transmitter and receiver to measure the distance from the sensor to a surface based on time-of-flight measurement. The laser-based sensor comprises an emitter and detector to measure the distance from the sensor to a reflecting surface based on the phase-shift principle. The main difference between the two methods is that the ultrasonic sensor measures the height of the surface by reflecting sound waves over a circular area of about 3.9 in. (100 mm) in diameter, whereas the laser sensor measures the height of the surface by reflecting light of different wavelengths over a very small circular spot of about 1 mm in

diameter. The ultrasonic sensor was able to collect data more frequently (about 10 points per second) but was susceptible to secondary sound reflections from the sidewalls of the container if not properly centered. The laser sensor collected data less frequently (about 1 point per second) but was more robust. Note that the limitation in the data collection rate for the laser sensor may be overcome using different hardware operating on the same principle.

The following method was used to measure the height and corresponding change in volume of the foam using the two aforementioned sensors. The two sensors were mounted on a tripod and aligned to point directly into a 1-gallon can of binder. The sensors were at least 1 m away from the surface of the can to avoid damage due to splatter from the hot foaming binder. A tube was used to enclose the ultrasonic sensor and prevent the sound waves from spreading to a larger area before reaching the container. No such arrangement was necessary for the laser sensor. The sensors were then connected to a computer using their respective data acquisition systems. The distance of each sensor from the bottom of the 1-gallon can was measured. Since the bottom of the 1-gallon can was not perfectly smooth but corrugated to improve stiffness, measurements were made to calibrate the weight and volume of the binder to the height of the binder in the can. In order to measure the collapse of the foamed binder, a sample was dispensed into a 1-gallon container. The container was immediately removed from underneath the foaming unit and placed under the sensors to measure the height of the foam as it collapsed over time. The ER was determined as the ratio of the volume of the foamed binder to the volume of the same mass of the binder without foaming. The volume of the foam (as a function of time) was calculated using the diameter of the can and height of the foam, which was measured using the sensors as it collapsed over time. The same weight of binder as used for foaming was placed into a similar can, and the height of the binder in the can was measured. The height of the binder and the diameter of the can were used to calculate the volume of the binder without foaming.

Figure 2-1 shows the setup of the sensors, and Figure 2-2 illustrates the ER for a typical foamed binder using both the ultrasonic and laser sensors. In Figure 2-2, the electrical noise resulting from the ultrasonic sensor measurement was filtered. Based on test results collected in this study, both methods were promising in terms of their ability to provide a detailed history of the change in the ER of the foamed binder. However, the method using the laser sensor was preferred for two reasons. First, it requires minimal hardware and software for setup and use. Second, the laser can be pointed into the sampling container without interference from other parts of the foaming unit. This allows measurement of foam formation and collapse as it is being dispensed into the sampling container.

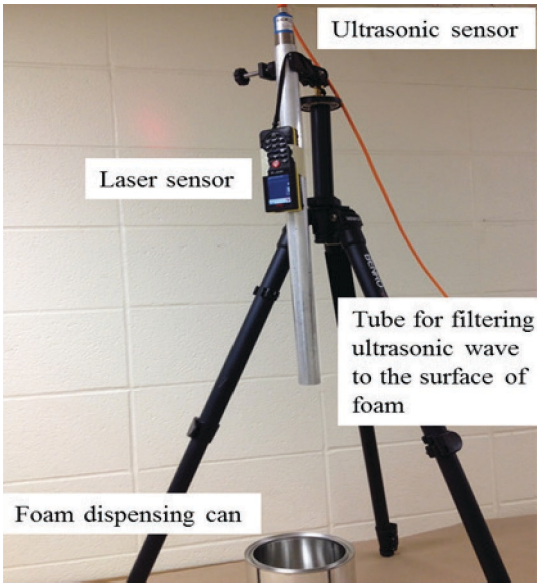


*Figure 2-1. Ultrasonic and laser sensor test setup.*

## A.2. Image-Based Method to Obtain Binder Foam Bubble Size

A preliminary method to obtain bubble size from digital images was developed. The methodology was subsequently revised, as will be discussed later. In the preliminary procedure, selected images of the foamed surface at different points in time were analyzed using an image processing and analysis program, ImageJ, to obtain the size and distribution of the bubble diameter on the surface. The following is a brief description of the preliminary method used to obtain this distribution.

A digital camera with a flash pointing directly into the foamed container was used to photograph periodically the

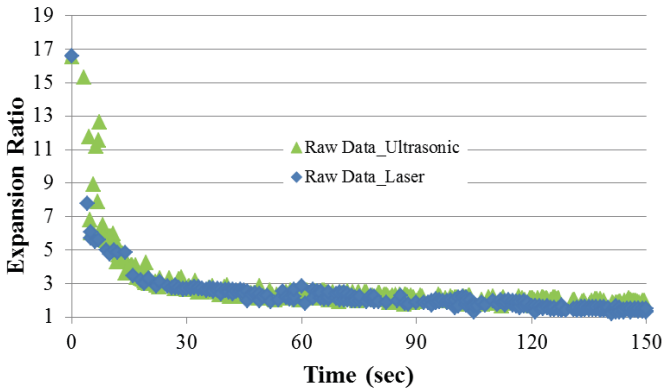


*Figure 2-2. Expansion ratio measurements using the two types of sensors.*

surface of the foamed binder. Due to the spherical nature of the bubbles, light from the flash was reflected strongly at the center of the bubble and along the edges of the bubble. The highlight at the center and edge combined with the low reflection of the curved surface (between the bubble center and edge) created a distinct high-contrast annular ring for each bubble. The outer circumference of this annular ring was used as a measure of the bubble diameter. The image analysis was achieved in three steps. The first step was to convert the image to a black-and-white image using ImageJ; this step demarcated the bubble boundaries from the center of the bubble. The second step was to identify individual bubble boundaries on the image. This was achieved using Hough transformation, which is an algorithm typically used to identify circular boundaries. The boundaries identified using this transformation were overlaid onto the image, manually compared, and corrected for any artifacts. The final step was to use the particle analysis feature in ImageJ to obtain the size (and location) of individual bubbles. Each image was calibrated with the known internal diameter of the container to convert the image dimensions from pixels to millimeters. This analysis could only be conducted on images obtained after approximately 15 s of foaming, when the large, unstable bubbles had collapsed and smaller semi-stable bubbles became clearly discernible.

An alternative method to obtain the bubble size distribution is by using 3D X-ray computed tomography (CT) scanning. However, unlike taking photographic images, CT scanning is a time-intensive technique. Depending on the resolution and specimen dimensions, it can take approximately 30 minutes or more to obtain a single 3D image. The previously described photographic method was preferred in lieu of CT scanning for the following reasons. In order to conduct CT scanning, the foamed binder must be cryogenically frozen immediately after foaming by immersing a sample container in a liquid nitrogen bath. However, in order to freeze the foam in the shortest time, the diameter of the container with the foam sample must be minimized. In other words, the foam inside a larger-diameter container takes several seconds to freeze to its core even when immersed in liquid nitrogen. In contrast, the foam inside a smaller-diameter container freezes to its core more rapidly. However, a container with a smaller diameter also influences the quality of the foam since the average size of the bubbles several seconds after dispensing the foam is still on the order of several millimeters, as will be shown in the results later. Considering these two factors, it was concluded that although CT scanning would provide some insights into the bubble size distribution (albeit at a compromise to the bubble structure itself), similar insights could also be gained by evaluating the bubble size distribution on the surface of the foam.

## A.3. Measurement of Binder Foam Density

In addition to the two methods described previously, the ultrasonic density method was considered for binder foam characterization. This method relies on the use of ultrasonic waves passing through a cross-section of the foamed binder to characterize the foam in real time. As the ultrasonic waves pass through the foam, the wave amplitude is damped. The magnitude of damping is directly proportional to the overall foam density (i.e., damping increases as the foam collapses over time). However, this approach was found to be very sensitive to changes in the viscosity of the binder due to small changes in temperature. Consequently, this approach was deemed appropriate when working with larger volumes of foamed sample under tightly temperature-controlled conditions that were less susceptible to temperature fluctuations. A picture of the ultrasonic density test setup is shown in Figure 2-3.

## A.4. Metrics to Characterize Binder Foam

The previous sections presented different methods by which different characteristics of the foam can be measured in real time. The next step is to use these methods to understand the process of foam expansion and collapse and to extract a metric or metrics from the measured properties to describe quantitatively the foamed binder.

In the case of foamed binder produced by water injection, a foaming unit homogenously combines very fine droplets of water with the binder at elevated temperatures. The water droplets turn into steam that expands and takes the form of bubbles within the binder, resulting in the formation of the foamed binder. The foamed binder has increased workability and aggregate coatability at temperatures lower than

*Figure 2-3. Ultrasonic density test setup.*

conventional HMA temperatures. The overall expanded volume and stability of the foam are important for WMA applications. It is hypothesized that foam with a higher expansion has a lower overall viscosity and easily coats aggregate particles. In addition, foam with a lower collapse rate has a longer effective time to coat the aggregate particles.

Jenkins (2000) also developed an exponential collapse model (Equation 2-1) for binder foam as a function of time, $ER_{max}$, and HL. This model was adapted from the isotope collapse model:

$$ER(t) = ER_{max} * e^{\frac{-\ln 2}{HL} * t} \quad (2\text{-}1)$$

Where:

$ER(t)$ = foam volume at time $t$ to the volume of the binder after the foam collapses.

$t$ = time starting from end of foam dispensing.

The parameters HL and $ER_{max}$ were measured using a dipstick. As noted before, the use of a dipstick to measure these parameters is highly dependent on the operator since it is based on manual observation of foam height and time. This approach is also limited to only two points in describing the rate at which the foamed binder collapses. Furthermore, observations made during this study show that HL is typically in the range of 1 to 4 s; consequently, manual measurements of HL are prone to high variability. Data collected in this study using the more precise and faster methods (as described in the previous sections) to measure expansion also indicate that the binder foam does not collapse following an exponential collapse form.

The following two mechanisms of bubble growth and collapse are proposed based on a review of such mechanisms for binder and other materials in the literature (Saye and Sethian 2013; Schick 2004; Schramm 1994; Sunarjono 2008) as well as observations made during this study.

### A.4.1. Unstable and Short-Life Bubbles

Initially, foamed binder consists of a cluster of bubbles separated by a thin layer of liquid binder (as shown in Figure 2-4), as confirmed by Hailisilassie et al. (2014). The thickness of the liquid binder layer is a function of $ER_{max}$. As $ER_{max}$ increases, the ratio of liquid to gas (steam) volume decreases, resulting in a decrease in the initial thickness of the binder film layer. Unstable bubbles cause a sharp decrease in the volume of the foam in a few seconds. The following are the possible mechanisms of collapse of the unstable bubbles:

1. *Liquid flow:* Immediately after the foam is dispensed into a can, the liquid binder flows down through the interconnected network of channels between the bubbles. At the same time, the bubbles also move up due to the buoyant force. As the liquid binder moves down and the bubbles move up, the film layer thins out, and finally the bubbles collapse. As the bubbles on the surface collapse, the liquid between these bubbles redistributes to the nearby bubbles.
2. *Excessive steam pressure:* In the case of larger water droplets (or coalescence of many fine droplets) that turn into steam, the vapor pressure inside the bubble causes the bubble diameter to grow rapidly to a point where the bubble becomes unstable and collapses.
3. *Drop in the temperature of steam:* For bubbles that are in direct contact with the atmosphere, the temperature of the steam may drop and cause the foam to collapse (implode).
4. *Rising velocity:* Larger bubbles rise to the surface at much higher speeds (proportional to the square of the diameter) and ultimately collapse. As will be shown later, this phenomenon explain why foams with higher water contents and higher expansion ratios are typically less stable than foams with lower water contents and expansion ratios.

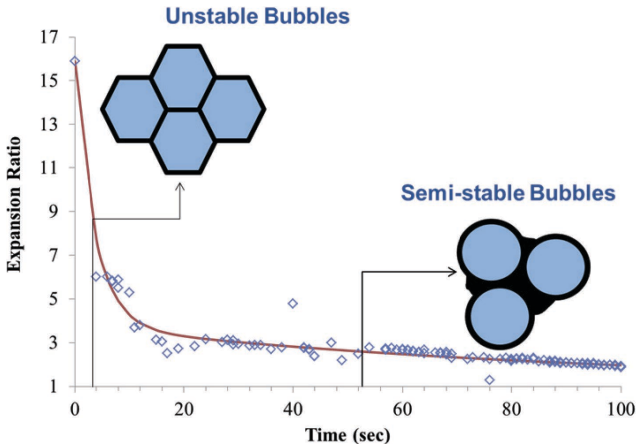


***Figure 2-4. Stability and shape of binder foam as function of time.***

### A.4.2. Semi-Stable and Long-Life Bubbles

As the unstable bubbles collapse over time, the volume of liquid binder that separates the bubbles from each other increases. The increase in liquid binder volume, by itself, increases the relative stability of the bubbles. In the case of smaller water droplets that turn into steam, the vapor pressure inside the bubble causes the bubble diameter to grow rapidly, as before. However, the bubble diameter reaches an equilibrium size since the surface forces of the bubble balance the internal pressure of the steam and allow the foam to remain stable for a finite amount of time. The equilibrium bubble diameter or radius was given by Laplace, as shown in Equation 2-2 (Pellicer et al. 2000). As before, such bubbles migrate toward the surface of the binder. However, the bubble velocity is much lower due to the smaller size, and the ratio

of liquid binder to air (steam) volume is higher, resulting in an increase in the shell thickness of the individual bubbles.

The relationship between bubble velocity and bubble diameter is given by Stokes' law in Equation 2-3 and clearly shows that the bubble velocity is directly proportional to the square of the bubble diameter and inversely proportional to the viscosity of the fluid. Finally, when such bubbles reach to the surface of the binder, the shell thickness decreases due to liquid binder flow, and the vapor pressure inside the bubbles reduces due to cooling, triggering an unstable reduction in the bubble diameter and collapse.

$$P_{bubble} - P_{atm} = \frac{2\gamma}{R} \quad (2\text{-}2)$$

Where:

$P_{bubble}$ = Pressure inside the bubble (Pa).
$P_{atm}$ = Atmospheric pressure (Pa).
$\gamma$ = Surface tension of the binder (N/m).
$R$ = Bubble radius (m).

$$D = \sqrt{\frac{18\mu V}{(\rho_f - \rho_b)g}} \quad (2\text{-}3)$$

Where:

$V$ = Rising velocity of the bubble (m/s).
$\rho$ = Density of the binder and the bubble ($\rho_f$, $\rho_b$) (Kg/m$^3$).
$\mu$ = Viscosity of the binder (Pa.s).

In summary, the largest bubbles that contribute most to the expansion of the binder are also the most unstable and short-lived. This effect was observed during the first few seconds as the foamed binder collapsed, and was exaggerated at higher water contents (i.e., higher air to liquid binder ratio) that are likely to result in larger water droplets and larger bubbles (see Figure 2-5). The collapse of the larger unstable bubbles was followed by a gradual rise and collapse of relatively less unstable or semi-stable smaller-diameter bubbles. This effect was relatively clear at lower water contents where bubbles continued to rise and collapse with the smaller bubbles taking the longest to rise and collapse (see Figure 2-6).

Based on the aforementioned understanding, the following approach was used to characterize the foamed binder. The exponential collapse model developed by Jenkins (2000) does not reflect the initial sudden collapse of foams in the first few seconds. Based on experimental observations, the following function was found to fit best the data obtained from testing the different binder, water content, and foaming equipment combinations:

$$ER(t) = 1 + ae^{-bt} + (ER_{max} - a - 1)e^{-ct} \quad (2\text{-}4)$$

Where:

$ER(t)$ = The expansion ratio at any time $t$,
$a$, $b$, and $c$ are constants.
$ER_{max}$ = The maximum expansion ratio that was directly measured during the foaming process.

Based on the form of this equation, it may be tempting to conclude that the overall collapse observed in the foam is the sum effect of two different collapse processes proceeding at different rates. However, Equation 2-4 was used only for data reduction purposes, and it is inappropriate to interpret the phenomenon purely based on this mathematical form. In fact, observations of the foam collapse process suggest that it may be more appropriate to model the collapse in the semi-stable foam after the first few seconds of foaming when the foam is in the semi-stable stage. This will be discussed in more detail.

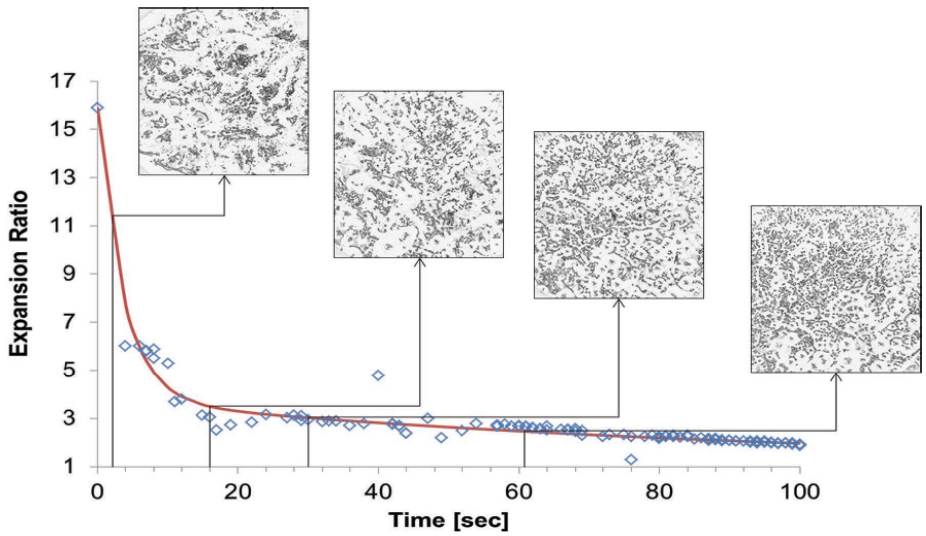


*Figure 2-5. Binder N6 with 3.0% water content.*

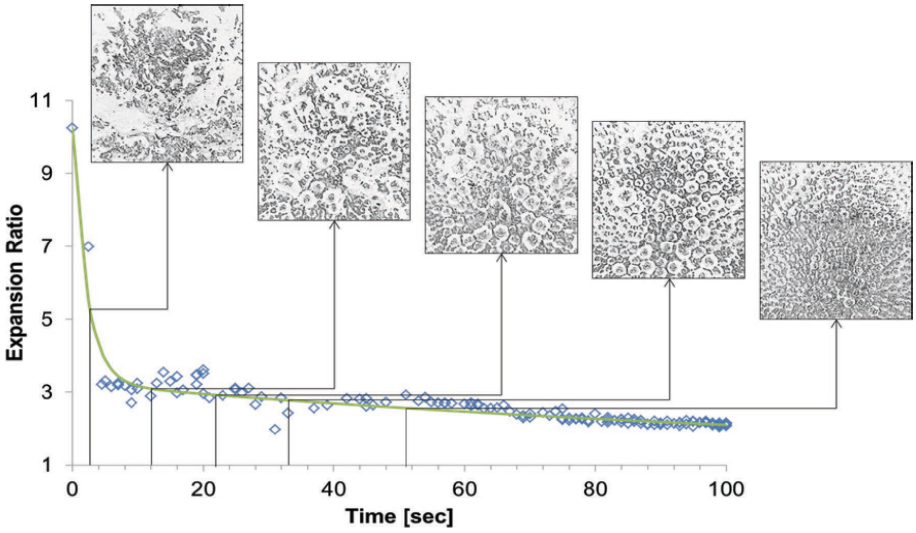


*Figure 2-6. Binder N6 with 1.0% water content.*

Figure 2-5 and Figure 2-6 illustrate typical ER measurements versus time for a particular binder (denoted as N6) with 1.0% and 3.0% water content. The discrete points illustrate the raw data, and the continuous line shows the fit. The expansion at the high water content shown in Figure 2-5 is extremely short-lived, and the collapse of foam is faster as compared to the lower water content presented in Figure 2-6, where the foam collapse is slower. The figures also illustrate a digitally inverted image of the surface of the foamed binder with bubbles at different points in time. (Bright annular bands indicate locations of bubbles.) As discussed before, the foamed binder with 3.0% water content initially expands much more than the foamed binder with 1.0% water content does. However, the foamed binder at the lower water content is more stable or semi-stable and clearly shows the migration and collapse of bubbles at the surface with the diameter of the bubbles decreasing with time.

Selected images of the foamed surface at different points in time were analyzed as explained in Section A.2 using an image processing and analysis program, ImageJ, to obtain the size and distribution of the bubble diameter on the surface. Figure 2-7 and Figure 2-8 show the size distribution of bubbles at three different points in time on the surface of the N6 binder foamed with 3.0% and 1.0% water content, respectively. The figures show that the bubble diameter at the surface becomes smaller as the foam continues to collapse

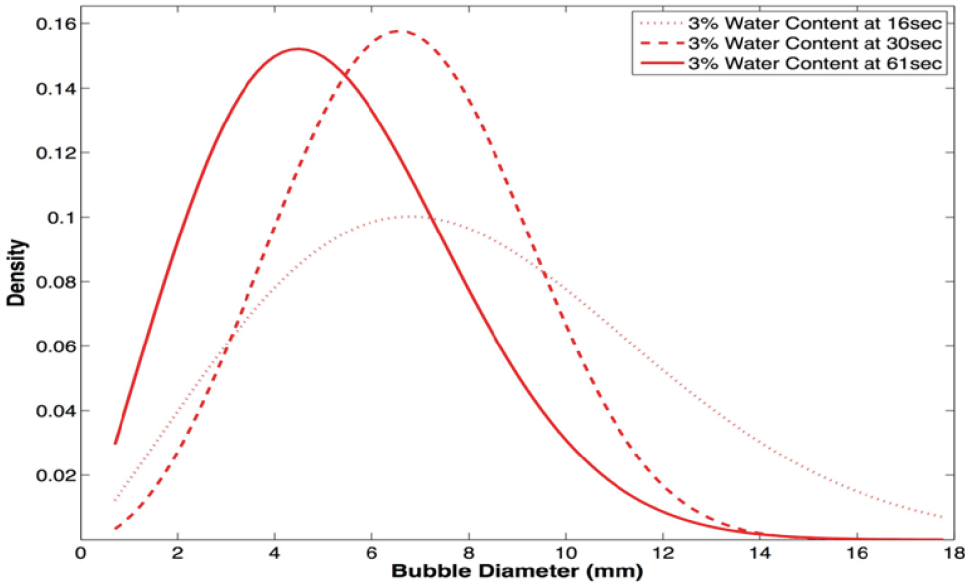


*Figure 2-7. Change of bubble size distribution with time for binder N6 with 3.0% water content.*

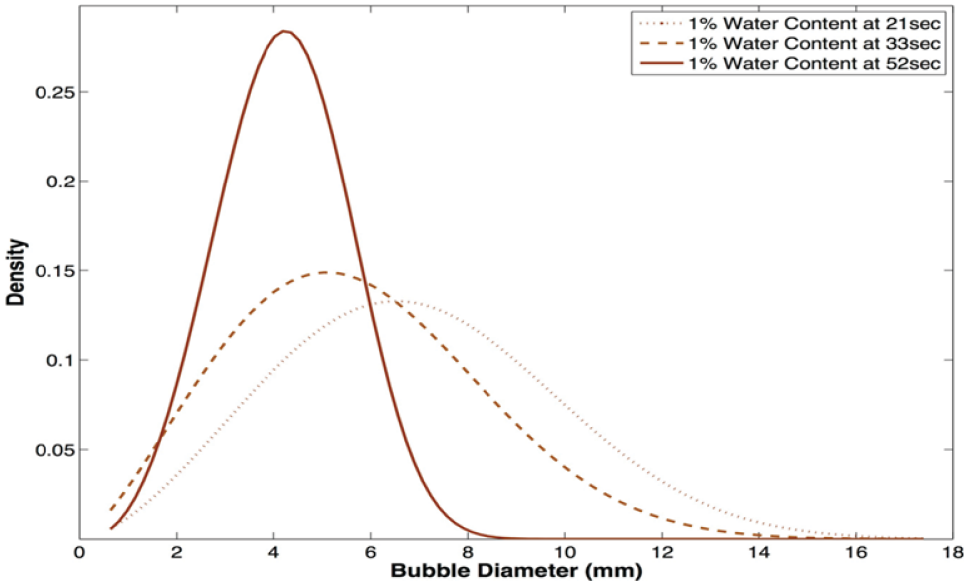


***Figure 2-8. Change of bubble size distribution with time for binder N6 with 1.0% water content.***

over time. This is consistent with what can be expected from Equation 2-3, in that the larger-diameter bubbles rise to the surface faster. In addition, the effect of water content and time on the mean diameter of the bubbles is clearly visible from the two figures. These observations substantiate conclusions made by Ozturk and Kutay (2014a, 2014b).

The proposed standard method for measuring expansion/collapse via laser-based sensor is presented in Appendix B. Based on preliminary results, the following metrics were considered to characterize foamed binders:

1. Maximum expansion ratio – $ER_{max}$: The ratio of the maximum volume occupied by the foamed binder to the volume occupied by the same mass of the binder without any water or foam in it.
2. Rate of collapse of semi-stable foam – *k*-value: Based on the results obtained thus far, a significant portion of the unstable bubbles collapsed during the first few seconds after foaming. The rate of collapse of the semi-stable foam was determined as the parameter *k* obtained by fitting the ER versus time to an exponential curve: $ER(t) = 1 + ce^{-kt}$. Note that the ER after 10 s of foaming was used to determine this parameter.
3. Foamability Index – FI: The area under the ER curve at selected times (Jenkins 2000).
4. Bubble size distribution: Bubble size distribution from digital image acquisition and analysis was also considered as an important metric to characterize binder foams. Bubble size distribution through image acquisition and analysis was used in some cases to better understand the mechanisms that drive foam expansion and collapse. A revised image-based method to obtain bubble size, including the ratio of the surface area of the foaming bubbles at selected times to the surface area of the binder without any water or foam in it, or SAI, is presented in Appendix B. A similar approach based on bubble size distribution calculated from Stokes' law was described by Ozturk and Kutay (2014b).

Note that the HL for most combinations of binder, water content, and foaming equipment was in the range of 1 to 4 s. This parameter was not very repeatable and was associated with the more turbulent collapse of larger unstable bubbles in the foamed binders. Consequently, this metric was not used to characterize foamed binders. The slope of the expansion ratio at selected times and the drop in expansion ratio between selected times were also explored as alternative metrics but did not provide meaningful trends.

The FI proved to be a good indicator of the differences in binder foaming characteristics, and SAI was able to provide a link between the bubble size distribution (obtained from digital image analysis) and the expansion ratio (obtained from laser measurement analysis) results. The applications of these two metrics are discussed in Chapters 3 and 4.

## B. Test Methods and Metrics to Characterize Foamed Mixtures

One of the major unknowns in the application of foamed binders for WMA is that, to date, there have been no established relationships between binder foam characteristics to mixture workability, coatability, or performance. Foaming is

intended to improve mixture workability and coatability from reduction in binder viscosity due to the binder volume expansion. Therefore, it was important to focus on the evaluation of workability and coatability of the foamed asphalt mixtures.

Most of the research conducted so far has been on binder foam characterization or mixture evaluation. As previously mentioned, Jenkins (2000) suggested using the area under the ER versus time curve to determine the optimum foaming water content. In this procedure, the optimum water content corresponds to the point where the area under the ER curve is at a maximum when plotted against water content. However, other studies found that the area under the ER curve versus water content did not have a maximum point for some binder foams (Sunarjono 2008). Also, the area under the ER curve was not compared to mixture workability or coatability. Consequently, the impact of change in binder foam characteristics on mixture workability and coatability has been unknown until this study.

Workability of asphalt mixtures is a property that describes the ease with which the mixture can be placed, worked by hand, and compacted. It is a function of temperature, binder properties (e.g., viscosity, grade, polymer modification), and aggregate properties (e.g., size, angularity), among other factors. Coatability of asphalt mixtures is defined as the degree of coating of the aggregates by the binder. This parameter is important to the performance of asphalt mixtures since well-coated aggregates are likely to have a stronger bond between the particle and the binder and, thus, a better resistance to moisture damage and other distresses.

The proposed method to evaluate workability of foamed WMA is based on the Superpave gyratory compactor (SGC) compaction data (i.e., shear stress versus number of gyrations). Densification of asphalt mixtures can be considered as a function of (1) reorientation of aggregate particles and (2) distortion due to the flow of the binder. Thus, resistance to shear in the asphalt mix is provided by the internal friction from a combination of the angularity and hardness of the aggregate and the cohesion provided by the asphalt binder (De Sombre et al. 1998). The maximum shear stress is proposed as a mixture workability parameter; mixtures with lower maximum shear stress are considered more workable. This method is based on work done at the University of Minnesota by De Sombre et al. (1998) in quantifying the workability of asphalt mixtures with various aggregate gradations and binders to define optimum compaction temperatures.

For coatability, an alternative method to AASHTO T 195 was explored. The AASHTO method is a very subjective approach to quantifying the asphalt coating of coarse aggregate. It relies on a visual assessment of the aggregate coating and may be subject to variability from a number of possible sources, including operator experience, aggregate coloring, and lighting. In this study, a modified procedure based on the aggregate absorption method originally developed by Velasquez et al. (2010) was used to measure mixture coatability. The method is based on the assumption that a completely coated aggregate submerged in water for a short period (i.e., 1 hour) cannot absorb water because water cannot penetrate through the binder film surrounding the aggregate surface. On the other hand, a partially coated aggregate is expected to have detectable water absorption since water is able to penetrate and be absorbed by the uncoated particle. The coatability index (CI) is proposed as the mixture coating parameter. The proposed protocols for workability and coatability are detailed in Appendix B.

## C. Initial Foamed Mix Design Approach

An initial foamed asphalt mix design method was developed to include the use of a laboratory unit to determine the foaming ability of the binder. As will be detailed later, laboratory foaming experiments indicate that certain binders have little foaming ability, possibly due to the presence of anti-foaming agents introduced during the crude refining or binder production process. Therefore, the development of a foamed asphalt mix design procedure that involves the validation of binder foaming ability was considered essential. As shown in Figure 2-9, after the binder foaming ability has been corroborated, a traditional hot mix design procedure (i.e., AASHTO R 35) is performed to determine the optimum binder content.

Afterward, the optimum foaming water content is established using the workability and coatability protocols described in the last section and Appendix B. Experimental results indicate that a considerable difference in foamed mixture workability and coatability can result from minor changes in the foaming water content (i.e., 0.5% by weight of the binder); thus, determination of the optimum foaming water content is essential. In the proposed procedure, the water content that yields the lowest maximum shear stress with a CI at least equivalent to the CI of HMA is considered the optimum.

The last step in the proposed mix design method is to evaluate the performance of the unfoamed and foamed asphalt mixtures at optimum water content. Standard tests, including $M_R$ per ASTM D7369, IDT strength per AASHTO T 283, and HWTT per AASHTO T 324, are suggested for performance evaluation. For HWTT, alternative parameters to the traditional rut depth at a specific number of load cycles are suggested, as detailed by Yin et al. (2014). If all performance parameters, namely wet IDT strength and tensile strength ratio (TSR), dry $M_R$, HWTT stripping number, HWTT remaining life, and HWTT viscoplastic strain at stripping number, comply with established specifications, the mixture is accepted. Otherwise, changes in material selection or other mixture components should be considered and the mixture retested.

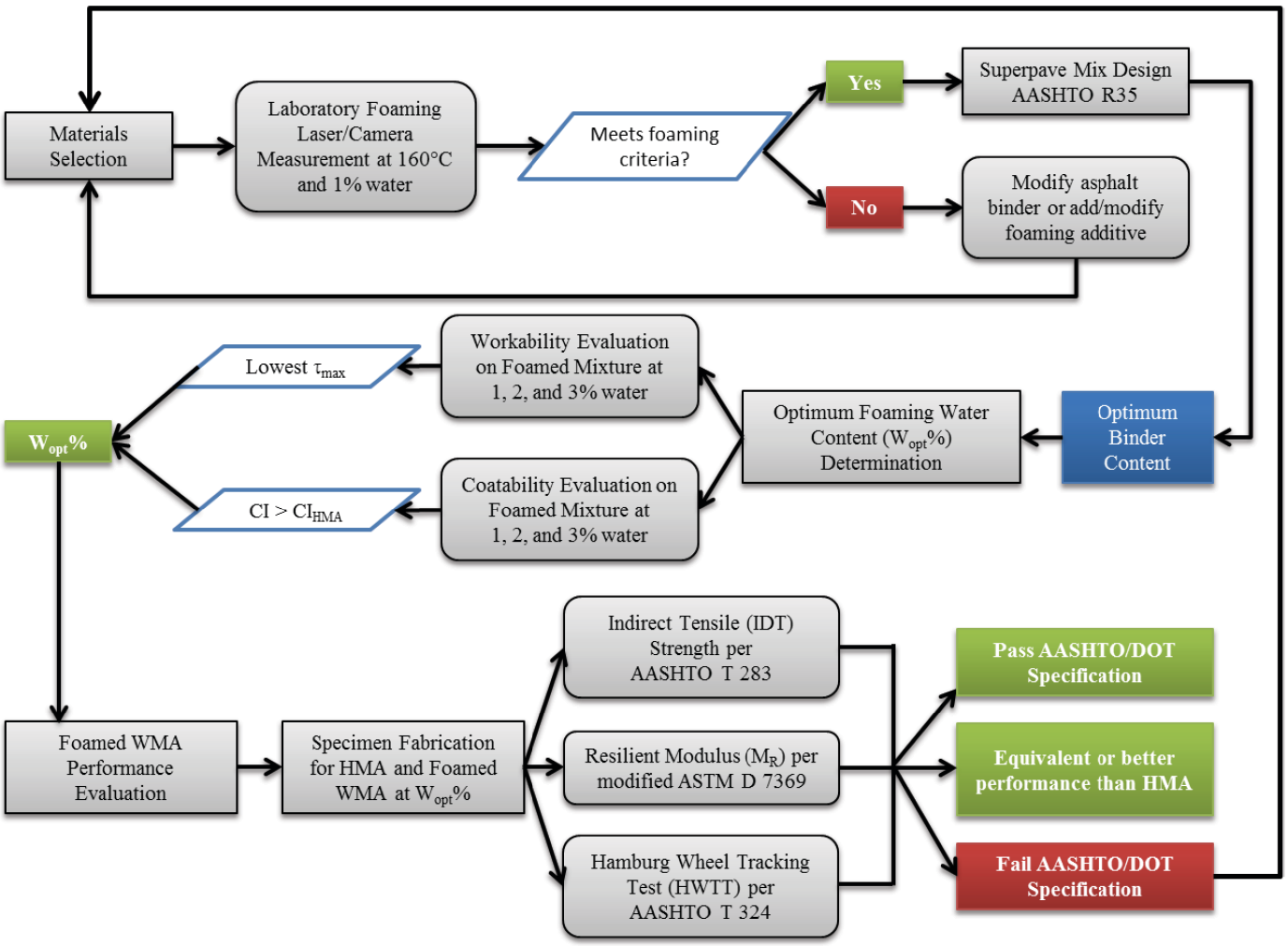


***Figure 2-9. Proposed foamed asphalt mix design method.***

CHAPTER 3

# Findings and Applications: Laboratory Studies

## A. Laboratory Binder Study

Several binders from six different producers and eight refinery locations were collected and used to investigate the influence of certain variables on their foaming characteristics using the test methods and metrics described in Chapter 2. The selected variables included binder source, water content, temperature, liquid additives, and shearing action. The list of binders is presented in Table 3-1. The asphalts graded as PG64-22 were neat binders, and those graded as PG70-22 were modified binders. A subset of these same binders was used in the laboratory mixture study that is described subsequently.

### A.1. Effect of Selected Variables on Binder Foam Characteristics

This section presents a summary of the work done to use the proposed methods and metrics to evaluate the influence of factors such as binder source, additive, and shearing action on the characteristics of the binder foam.

#### *A.1.1. Binder Source and Grade*

Eight binders from those listed in Table 3-1 were foamed at 160°C in the InstroTek Accufoamer at 2.0% water content and in the Wirtgen foamer at 1.0% and 3.0% water content and their foaming characteristics determined in terms of $ER_{max}$, *k*-value, FI, and bubble size distribution. Figure 3-1 through Figure 3-3 present a summary of results comparing binder source and water content. In the figures, each data point represents the average of two replicates.

In the Accufoamer with 2.0% water content, the $ER_{max}$ values were as low as 3.4 to as high as 13.0. The $ER_{max}$ values varied from 5.2 to 12.4 and from 8.1 to 24.7 with 1.0% and 3.0% water content in the Wirtgen foamer, respectively. When comparing different binders, there was no clear relationship between the maximum expansion of foamed binder and the stability of the foam. In other words, the $ER_{max}$ was not directly correlated to the foam stability (*k*-value). For example, in the Accufoamer Y6 had the lowest $ER_{max}$, and it was also the most unstable foam (highest *k*-value). However, for any given binder, an increase in water content resulted in an increase in expansion ratio and a decrease in the stability of the foam (or increase in *k*-value), as can be seen in the Wirtgen foamer results.

In addition, the ranking of the binders in terms of $ER_{max}$ and *k*-value was different in each case. For the Accufoamer, the N binders had the highest $ER_{max}$ values, while in the case of the Wirtgen foamer, O7 had the highest $ER_{max}$ values at both water contents. Also, Y6 had the highest *k*-value in the case of the Accufoamer but not in the case of the Wirtgen foamer. The rest of the *k*-values followed different trends in terms of ranking of the binders.

The $ER_{max}$ and FI of the binders foamed in the Wirtgen foamer at a selected time of 60 s after foaming are shown in Figure 3-3 for 1.0% and 3.0% water content. Ideally, binders with high $ER_{max}$ and high FI values are desirable since this indicates that the binder has a good initial expansion but is also stable after foaming. From Figure 3-3, it is apparent that higher water content generates binders with equivalent or larger FI values in most cases. Binders H6 and Y6 are exceptions because the binders were very unstable at 3.0% water content (i.e., large *k*-values as shown in Figure 3-2) and thus had smaller FI values than at 1.0% water content. It can be concluded that either $ER_{max}$ and *k*-value or $ER_{max}$ and FI can describe the binder foaming behavior and can be used to rank binders with respect to initial expansion and foam stability.

The SAI values at a selected time of 60 s for the eight binders foamed in the Wirtgen foamer are illustrated in Figure 3-4 along with the FI values at 60 s. Missing SAI values (such as O6 and O7 at 3.0% water content) indicate that the foamed binder did not generate bubbles or that the bubbles had dissipated at 60 s after foaming. The SAI could be considered a measure of the quality and longevity of the foam. The smaller, longer-lasting, and better-distributed the bubbles are in the foamed binder sample, the larger the SAI value will be. In general, for

**Table 3-1. Binders used in laboratory study.**

| Binder ID | Grade | Producer |
|---|---|---|
| N6 | 64-22 | A |
| N7 | 70-22 | |
| T6 | 64-22 | B |
| Y6 | 64-22 | C (1st shipment) |
| Y62 | 64-22 | (2nd shipment) |
| OM6 | 64-22 | D |
| M6 | 64-22 | |
| H6 | 64-22 | |
| AR6 | 64-22 | E |
| R6 | 64-22 | |
| R62 | 64-22 | |
| HO6 | 64-22 | F |
| O6 | 64-22 | |
| O7 | 70-22 | |

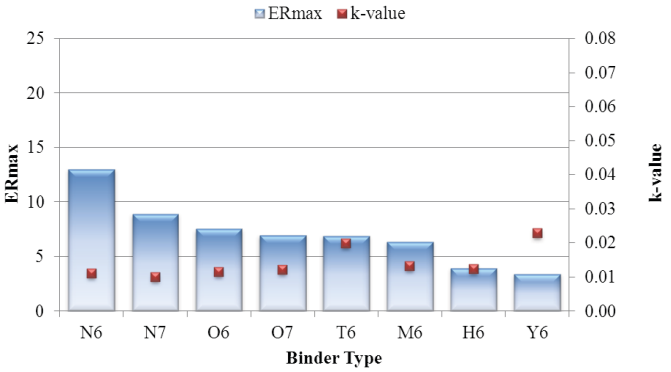


*Figure 3-1. $ER_{max}$ and k-value for various binders foamed in the Accufoamer at 2.0% water content.*

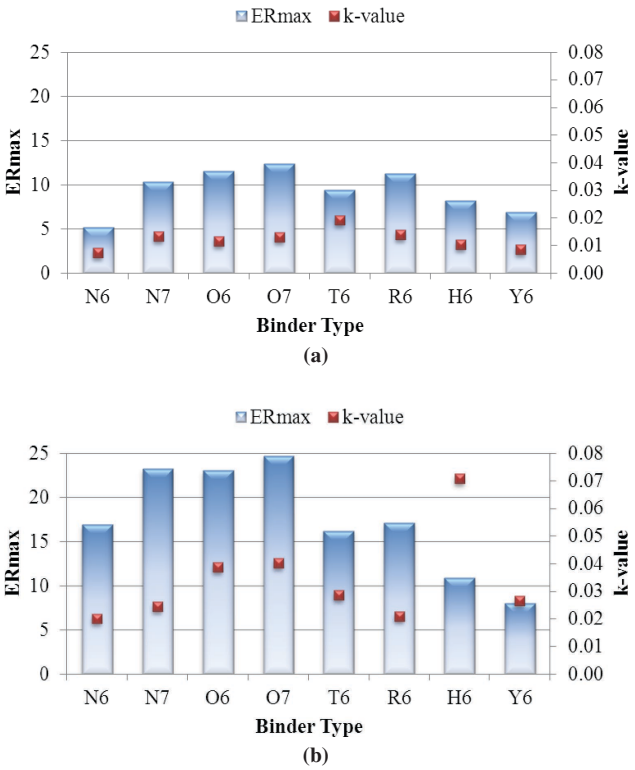


*Figure 3-2. $ER_{max}$ and k-value for various binders foamed in the Wirtgen foamer with (a) 1.0% water content, (b) 3.0% water content.*

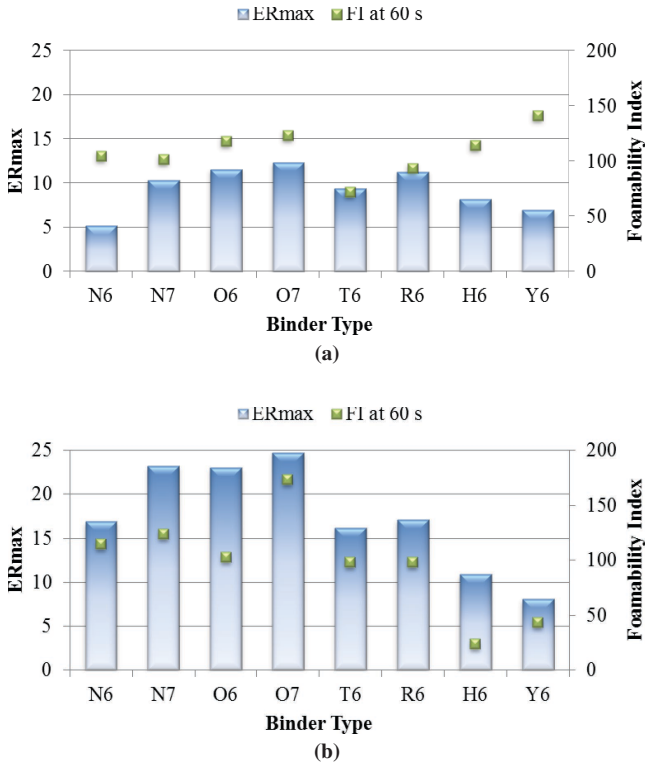


*Figure 3-3. $ER_{max}$ and FI for various binders foamed in the Wirtgen foamer with (a) 1.0% water content, (b) 3.0% water content.*

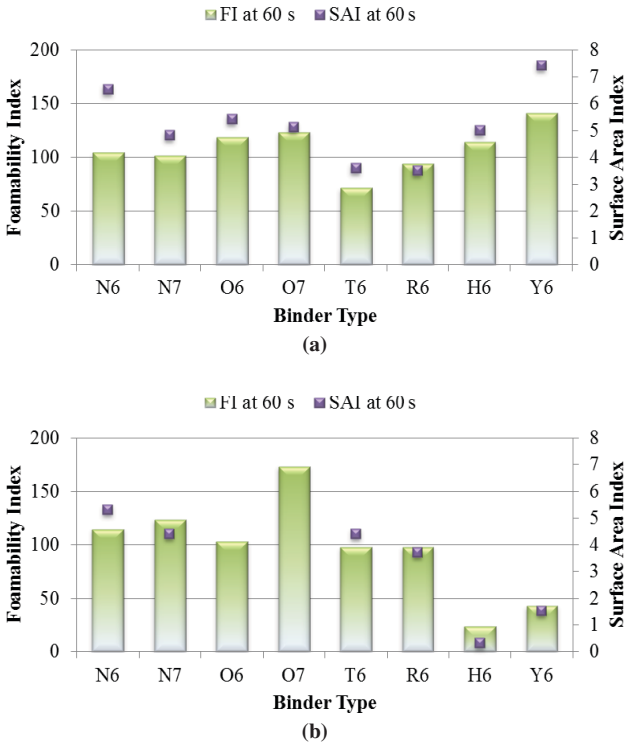


*Figure 3-4. SAI and FI values for various binders foamed in the Wirtgen foamer with (a) 1.0% water content, (b) 3.0% water content.*

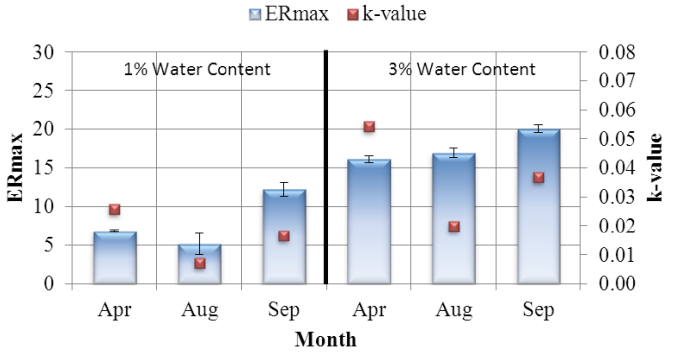


***Figure 3-5. $ER_{max}$ and k-value for binder N6 in the Wirtgen foamer at 1.0% and 3.0% water content.***

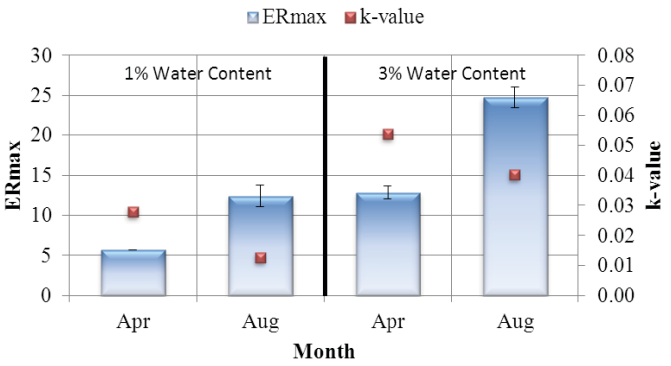


***Figure 3-7. $ER_{max}$ and k-value for binder O7 in the Wirtgen foamer with 1.0% and 3.0% water content.***

any given binder, the SAI values at 60 s are larger for the binders foamed at 1.0% water content, as expected. The most critical difference in SAI value between 1.0% and 3.0% water content is for binder H6, which, despite showing an acceptable $ER_{max}$ value, was very unstable when foamed at 3.0% water content and thus yielded very low FI and SAI values.

The elapsed time between measurements seemed to have an effect in the characteristics of the binder foamed in the Wirtgen foamer. In some instances, the changes could be due to modification in the crude streams at the refinery (i.e., when new samples of binder were obtained) or changes in the binder with time. Binders N6, N7, and O7 were measured on two to three separate occasions between the months of April and September in the Wirtgen foamer with 1.0% and 3.0% water content. Figure 3-5 through Figure 3-7 show the results. In the figures, each data point represents the average of two replicates, and the error bars span ±1 standard deviation from the $ER_{max}$ average value. Within the same measurement session, the majority of the replicate foaming measurements were highly repeatable.

As can be observed, the greatest differences in $ER_{max}$ were observed for binder O7, both at 1.0% and 3.0% water contents. This binder seemed to be particularly susceptible to the short elapsed time between measurements. The $ER_{max}$ measurements for N6 performed in September at both 1.0% and 3.0% water content seemed higher than the measurements from earlier in the year (i.e., April and August). The least affected binder by elapsed time seemed to be N7, especially when considering the variability in the replicate results with 3.0% water content. As before, *k*-value was not apparently correlated to $ER_{max}$.

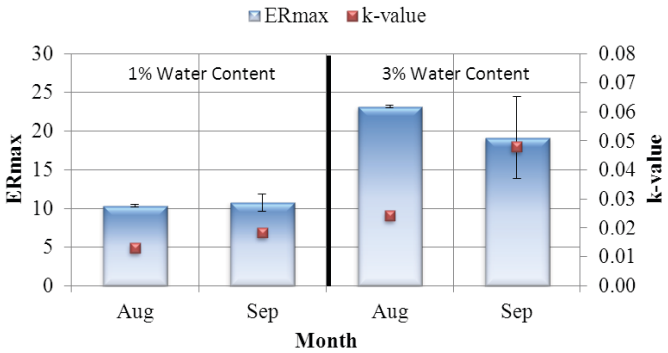


***Figure 3-6. $ER_{max}$ and k-value for binder N7 in the Wirtgen foamer at 1.0% and 3.0% water content.***

### *A.1.2. Water Content*

Three binders (N6, N7, and O7) from two sources were used to evaluate the influence of water content on foaming characteristics. Water content used for foaming was varied from 1.0 to 5.0%. The N6 and N7 binders were foamed at 1.0%, 3.0%, and 5.0% water contents, and the O7 binder was foamed at 1.0%, 2.0%, and 3.0% water content. All foamed binders were produced at a temperature of 160°C. Relatively lower water contents were used for the O7 binder because of its significantly higher ER compared to the other two binders. All three binders were foamed using both Wirtgen foamer and Accufoamer units. The quality of the foam was evaluated based on $ER_{max}$ and *k*-value for all binder–water content combinations produced using these two foaming units. Figure 3-8 compares $ER_{max}$ for the different binders at different water contents produced using the Accufoamer and Wirtgen foamer.

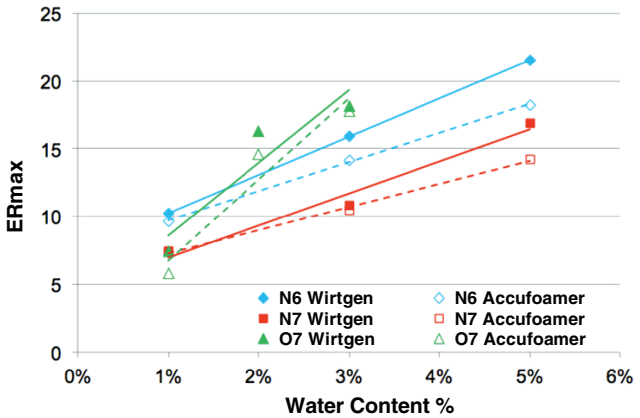


***Figure 3-8. Influence of water content and binder type on $ER_{max}$.***

The following observations can be made based on data presented in Figure 3-8:

- As discussed in the previous subsection, different binders clearly have different $ER_{max}$ values at the same water content. This finding was consistent with foams produced using both foaming units.
- For any given binder, $ER_{max}$ increased with an increase in the water content, and the relationship appears to be linear. This was consistent for data collected using both Wirtgen foamer and Accufoamer units and was noted by Ozturk and Kutay (2014b) for the Pavement Technology, Inc. (PTI) foamer. The trends for the water content versus $ER_{max}$ were similar for the two foaming units. However, the foams produced using the Accufoamer exhibited slightly lower $ER_{max}$ values. This can be attributed to the differences in the dispensing mechanisms between the two units; the Accufoamer creates the foam in a small enclosed chamber and dispenses it through a 0.25-in. (6.4-mm) diameter tube into the container, whereas the Wirtgen foamer creates the foam under atmospheric pressure, and it is dispensed directly into the container.
- The O7 binder was more sensitive to water content compared to the N6 and N7 binders. Also, both N6 and N7 binders had similar sensitivity to water content. These two binders were from the same producer and refinery location (Table 3-1).

The rate of collapse (*k*-value) of the semi-stable foam using the two different foaming units is presented in Figure 3-9. This parameter reflects the stability of the foam; higher values indicate lower stability and vice-versa. The following similarities and differences are observed in the rate of collapse of the foam:

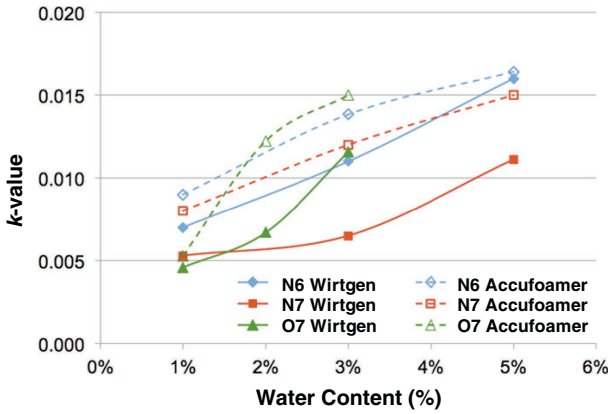


***Figure 3-9. Influence of water content and binder type on the rate of collapse of the semi-stable foam.***

- For both foaming units, an increase in the water content resulted in an increase in *k*-value. In other words, for a given binder, higher water content resulted in lower stability, and vice-versa. This is consistent with the hypothesized mechanism described earlier. Higher water content typically results in larger droplet sizes and larger bubbles, which in turn have a higher velocity to move to the surface (at a given temperature/viscosity) and collapse faster, and lower water contents produce smaller bubbles that take more time to come to the surface and collapse. This effect is also illustrated in Figure 3-10 and Figure 3-11, which

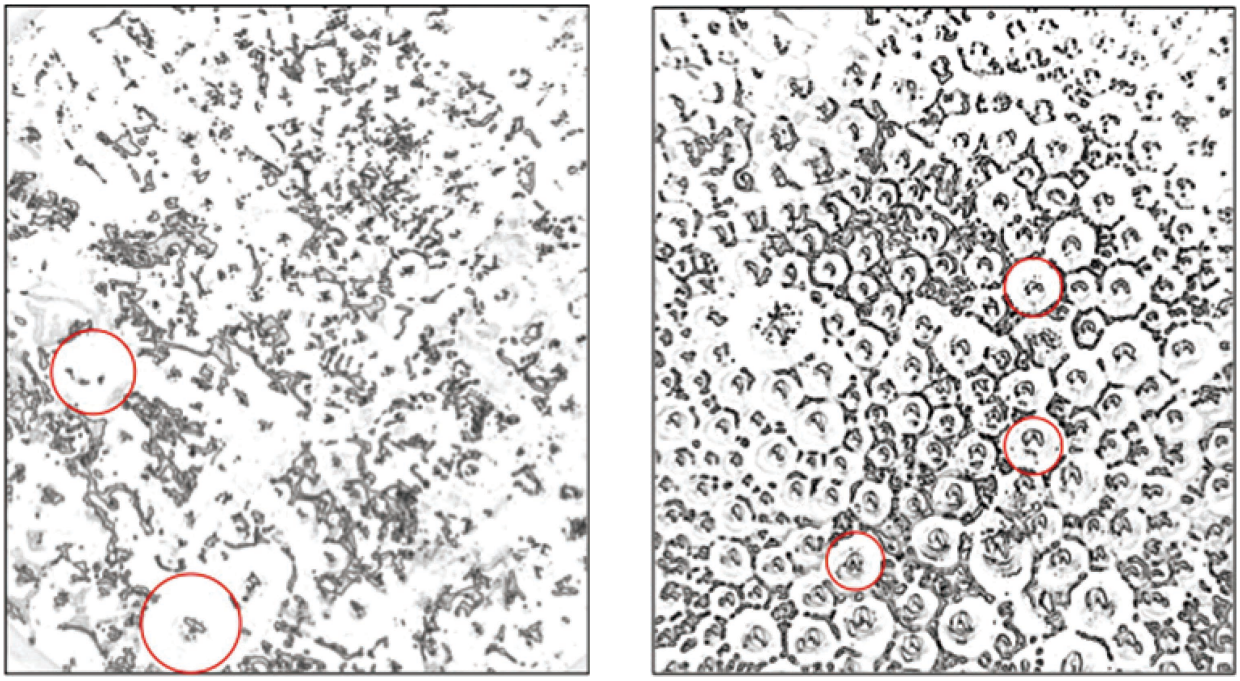

***Figure 3-10. Surface of binder A6 at approximately 30 s after foaming in the Wirtgen foamer with 3.0% (left) and 1.0% (right) water content.***

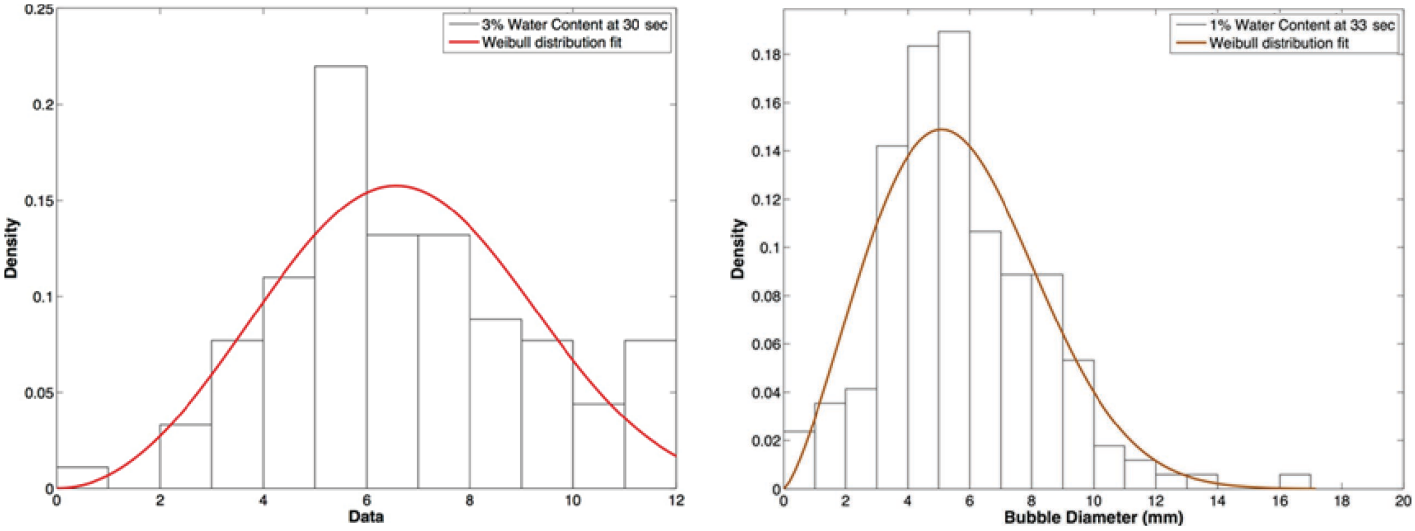


***Figure 3-11. Bubble size distribution of binder A6 foamed in the Wirtgen foamer with 3.0% (left) and 1.0% (right) water content.***

show the bubble size distribution of the surface of the binder at two different water contents after approximately 30 s of foaming.

- The rate of collapse from both foaming units was in the similar range or order of magnitude. Although the general trend for the rate of collapse with respect to increasing water content was similar for both foaming units, the rate of collapse of the semi-stable foam was typically higher for the Accufoamer compared to the Wirtgen foamer. This could be due to the differences in the delivery of the foamed binder between the two units (direct versus through a tube).

In summary, higher water contents result in higher $ER_{max}$ but also higher *k*-values (low stability) (see Figure 3-8 and Figure 3-9). An interesting consequence of the combination of these two effects is that a binder foamed with higher water content will start out with a higher ER compared to binders foamed with lower water contents. However, over time, binders foamed with lower water content will tend to be more stable and retain this expansion longer. This effect is illustrated in Figure 3-12 and Figure 3-13. Also, the almost instantaneous collapse of the foamed binder suggests that the HL of the foamed binder may not be of relevance in a real mixture production scenario at a hot mix plant. Of greater importance is the state of the foamed binder after it is exposed to the atmospheric pressure (as in a drum mix plant) for the few minutes during which the binder is mixed with the aggregates.

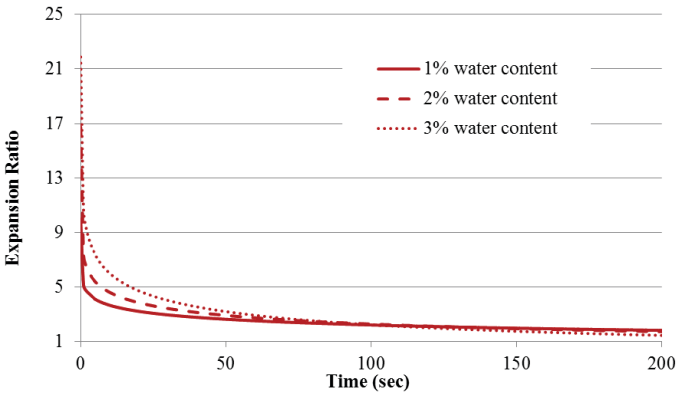


***Figure 3-12. Expansion ratio versus time for binder O7.***

### *A.1.3. Temperature*

In order to investigate the effect of temperature on the rate of collapse of the binder foam, the O6 binder was foamed at 1.0% and 3.0% water content in the Accufoamer and allowed to collapse at room temperature and at 160°C (foaming temperature). The elevated temperature of the foam was maintained by placing the collection can inside the heating mantle. The can was open to air on the top such that the heating mantle could only maintain the temperature of the wall and bottom of the can. Figure 3-14 and Figure 3-15 compare the results from the foam collapse when the collection can was at room temperature versus

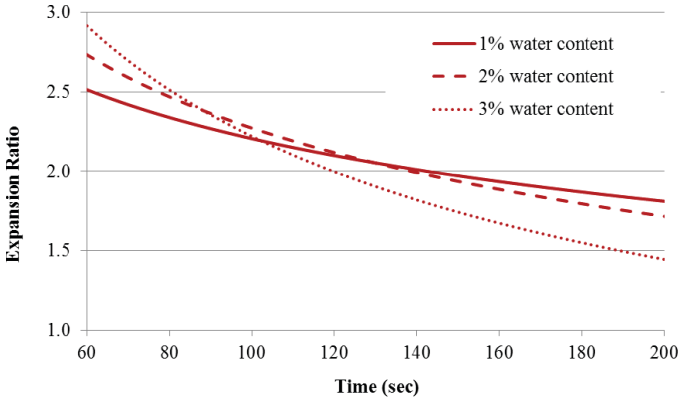


***Figure 3-13. Magnified view from 1 to 3 minutes of the expansion ratio versus time for binder O7.***

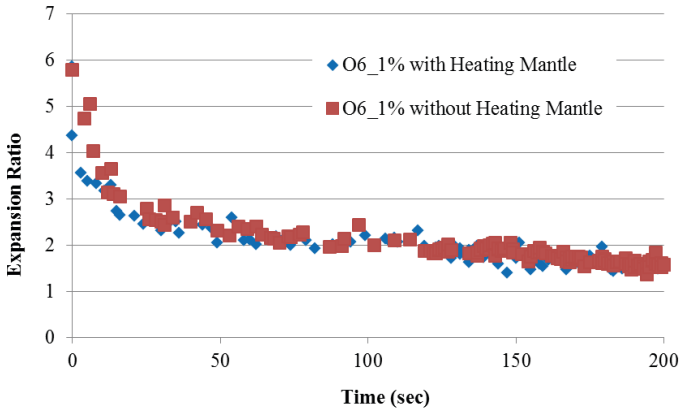


***Figure 3-14. Expansion ratio versus time for binder O6 with 1.0% water content in the Accufoamer with and without a heating mantle.***

foam collapse when the collection can was maintained at 160°C inside a heating mantle. These figures demonstrate that there is no noticeable influence of temperature on the measured foam properties. Similar results were obtained for a couple of other binders. Based on these results, the temperature of the collecting unit is not being considered as a factor to characterize binder foams. The temperature of the binder in the foaming unit was not reduced below 160°C because this would result in clogging of the pipes in the foaming unit.

### *A.1.4. Liquid Additives*

The influence of liquid additives on expansion and collapse characteristics of binders was evaluated using binder N7, two additives, and two water contents in the Accufoamer, and binders OM6, R62, Y6, and Y62, four additives, and two water contents in the Wirtgen foamer. The liquid foaming additives were received from two sources. Additive W1 was an amine surfactant commonly used in the production of WMA, and additives F1 through F3 were alkaline products manufactured with the specific objective of enhanced foaming. The additives were combined with heated binder to a temperature of 284°F to 320°F (140°C to 160°C) while using a rotating spindle for 1 minute, as shown in Figure 3-16, before being added to the foaming units. The additive dosage was selected according to the additive producer's recommendations. Table 3-2 presents a summary of the binders used for each type of additive and the dosage.

The $ER_{max}$ and *k*-value for binder N7 foamed in the Accufoamer with and without additives are presented in Figure 3-17 through Figure 3-19. The following similarities and differences are observed in the expansion and rate of collapse of the foams:

- Additive F1 significantly improved the $ER_{max}$ and *k*-value of binder N7.
- Additive W1 had a negligible impact on the $ER_{max}$ and *k*-value of the foam.
- As before, for any given binder or additive modified binder, $ER_{max}$ increased with an increase in the water content, the relationship was linear, and the stability decreased with an increase in the water content.
- The binder modified using additive F1 showed markedly different foam collapse. In particular, the sudden drop in volume of the foam during the first few seconds was not observed for the binder modified with additive F1. Instead, the foamed binder showed a gradual collapse over time (Figure 3-19).

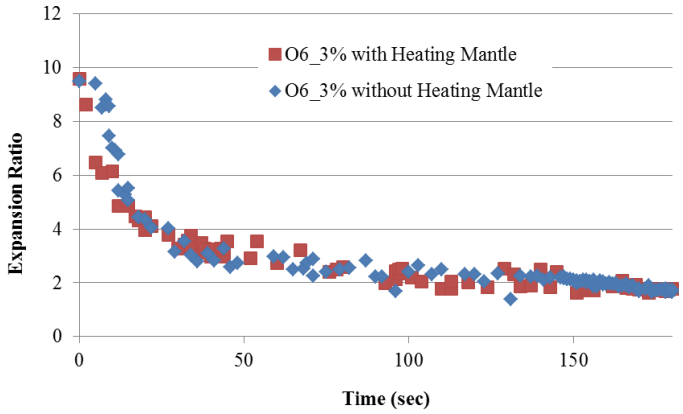


***Figure 3-15. Expansion ratio versus time for binder O6 with 3.0% water content in the Accufoamer with and without a heating mantle.***

***Figure 3-16. Additive blending.***

**Table 3-2. Additives used in laboratory study.**

| Additive | Binder ID | Foaming Unit | Additive Dosage by Weight of Binder (%) | Foaming Water Content (%) |
|---|---|---|---|---|
| W1 | N7 | Accufoamer | 0.5 | 1, 3 |
| | R62<br>OM6<br>Y62 | Wirtgen | | |
| F1 | N7 | Accufoamer | 0.5 | 1, 3 |
| | R62<br>OM6<br>Y6 | Wirtgen | | |
| F2 | R62<br>M6 | Wirtgen | 0.5 | 1, 3 |
| F3 | R62<br>OM6 | Wirtgen | 0.5 | 1, 3 |

Figure 3-20 presents a series of pictures of the surface of the Wirtgen foamed binder samples with and without additives after 5 s of being dispensed in a 1-gallon container. Both the foamed binder sample with W1 and the sample with no additive had clear, shaped bubbles on the surface, and the difference between these two samples was not significant. However, the samples with F1, F2, and F3 had no distinguishable bubbles on the surface. For W2, many tiny bubbles were observed, which lasted for a long time.

The results for the foamed binder in the Wirtgen foamer are presented in Figure 3-21. In most cases, additive W1 showed no significant effect on $ER_{max}$ as compared to the sample without additives, which was consistent with visual observations (Figure 3-20). As expected, the foaming-enhancing additives significantly increased $ER_{max}$ in most cases. R62 is an exception, which indicates that for some binders, even the addition of foaming-enhancing additives may not significantly improve the foaming characteristics. For any given binder with additive W1, higher water content corresponded to a higher *k*-value, which is consistent with the previous foamed binder trends without additives. In contrast, in most cases the samples with the foaming-enhancing additive had much lower *k*-values than the samples without additives.

The FI values along with $ER_{max}$ are presented in Figure 3-22. The results confirm that additive W1 had a negligible effect on the binder foaming metrics. For additives F1 through F3, there was a clear increase in the FI at 1.0% water content, but at 3.0% the trend was not consistent for all three additives. Even though binder R62 did not show clear differences in

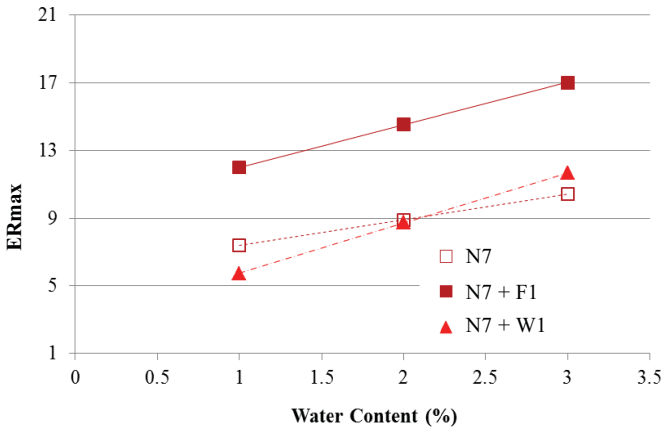


***Figure 3-17. Influence of liquid additives on $ER_{max}$ of binder N7.***

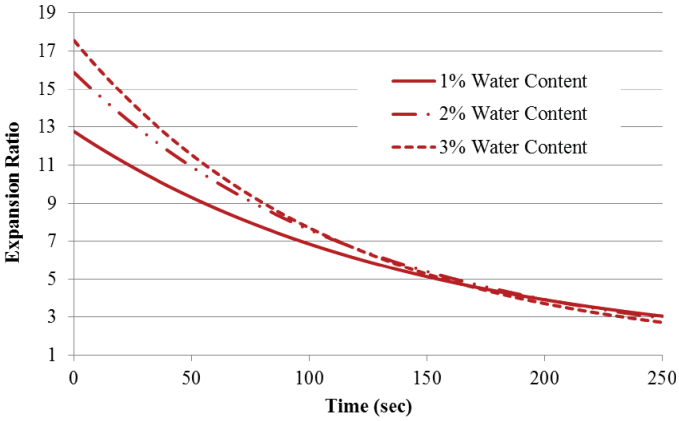


***Figure 3-18. Expansion ratio versus time of binder N7 with additive F1 foamed at various water contents in the Accufoamer.***

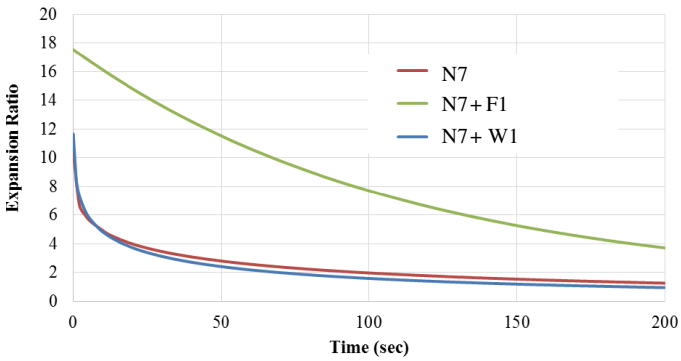


***Figure 3-19. Effect of modification on binder N7 foamed with 3.0% water content in the Accufoamer.***

*Figure 3-20. Surface of the foamed binder 5 s after foaming in the Wirtgen foamer: (a) without additive, (b) with additive F1, and (c) with additive W1.*

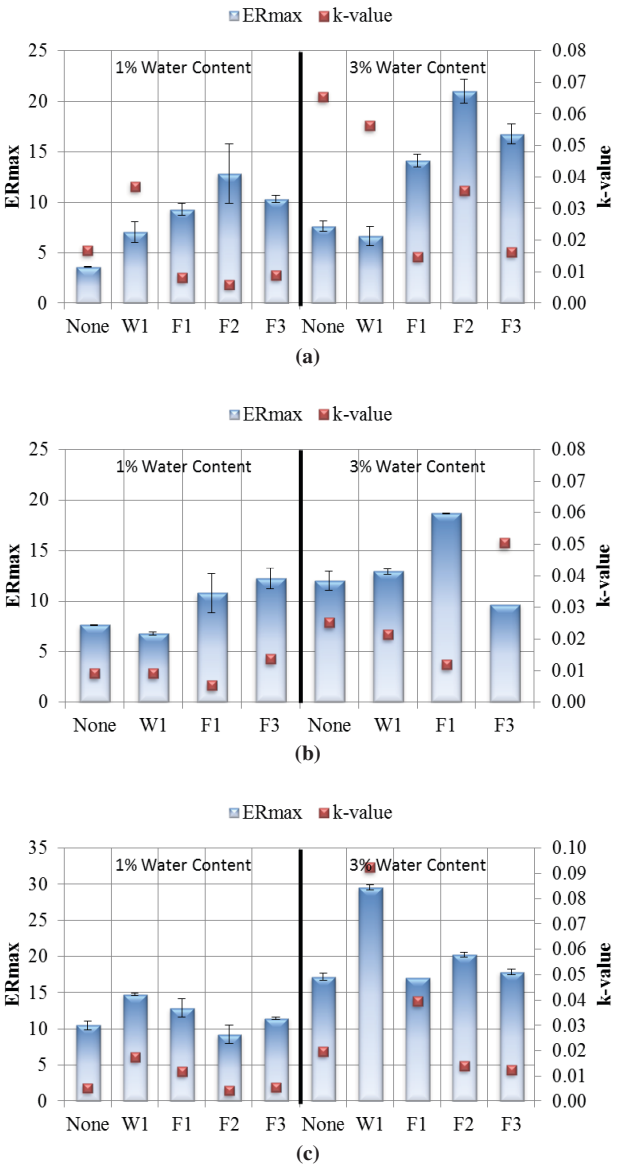


*Figure 3-21. $ER_{max}$ and k-value for foamed binders in the Wirtgen foamer at 1.0% and 3.0% water content with and without additives; (a) OM6, (b) Y62, and (c) R62.*

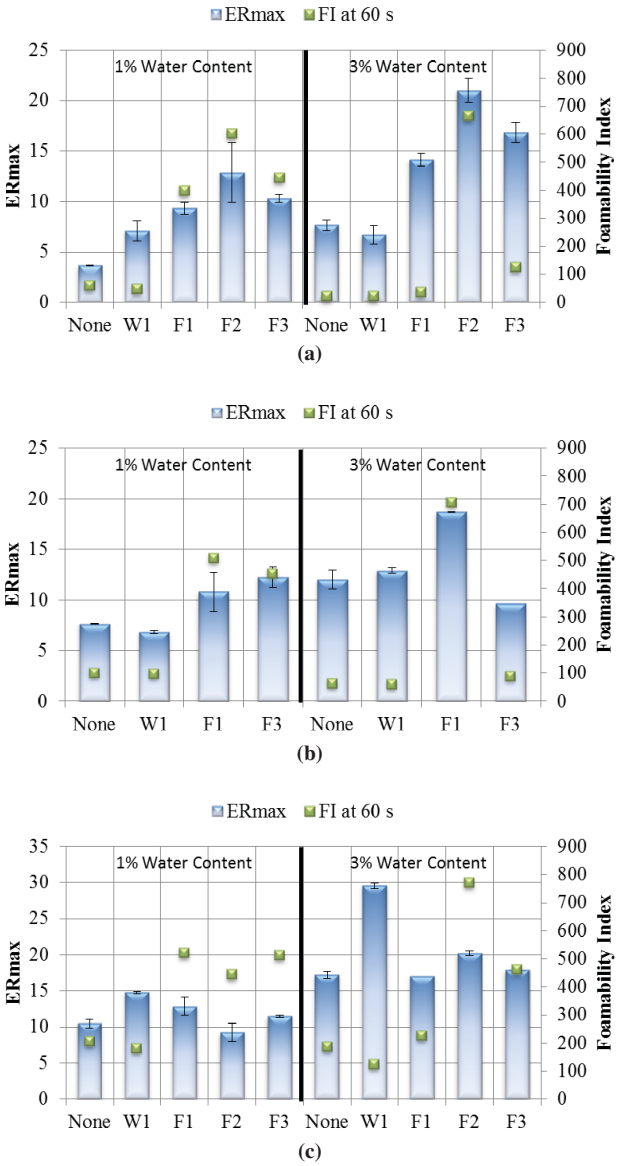


*Figure 3-22. $ER_{max}$ and FI for foamed binders in the Wirtgen foamer at 1.0% and 3.0% water content with and without additives; (a) OM6, (b) Y62, and (c) R62.*

$ER_{max}$ at 1.0% water content with and without additives, the FI values were distinctly larger than the ones obtained for the binder with no additives or the binder with additive W1.

The SAI and FI values at 60 s are illustrated in Figure 3-23. As before, missing values indicate that the images acquired of those samples were not able to be processed using the bubble size distribution procedure. In all cases where SAI data were available, higher SAI values also corresponded to higher FI values. This behavior is expected because higher FI values usually indicate more stable foam, which usually translated into longer-lasting and smaller-sized bubbles with elapsed time.

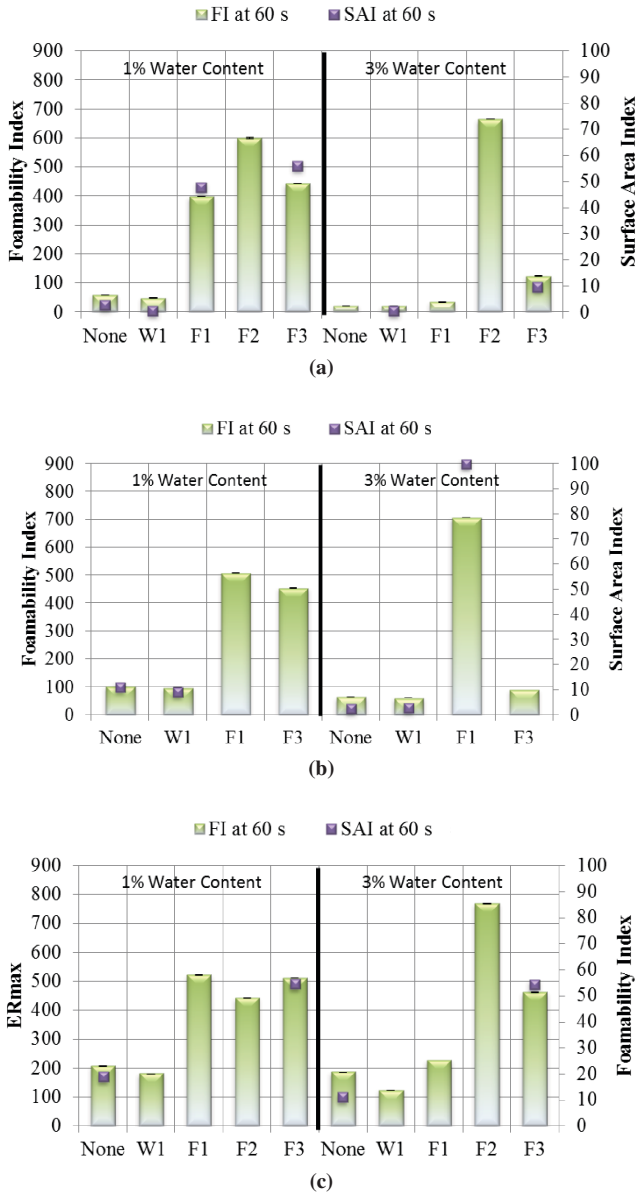


***Figure 3-23. FI and SAI for foamed binders in the Wirtgen foamer at 1.0% and 3.0% water content with and without additives; (a) binder OM6, (b) binder Y62, and (c) binder R62.***

### *A.1.5. Shearing Action*

ER is an indirect measure of workability (viscosity) of binder foams. However, it may sometimes give inconsistent results in terms of viscosity. For example, binders from different sources that have the same $ER_{max}$ may have different viscosities. Therefore, a direct measurement of viscosity of the foamed binders was undertaken. Note that viscosity measurement using a rotational viscometer also subjects the foam to a shearing action between the spindle and the walls of the container. Therefore, viscosity measurements of foamed binders reflect the combined effect of shearing action and foam collapse on workability.

The viscosity of binder foam was measured using a Brookfield rotational viscometer with a #27 spindle immediately after foaming. A sample of the foamed binder from the 1-gallon collection container was poured into the Brookfield sample holder. This process was accomplished within 2 minutes of dispensing the foam. Viscosity measurements were conducted at 275°F (135°C) and 20 rpm, and values were recorded after the reading stabilized (15 minutes after the foam was dispensed). The advantage of this approach is that it allows for a more sensitive measurement of binder viscosity. However, because of the time it takes to transfer a sample of the foamed binder from the 1-gallon container into the Brookfield sample holder, and because of the narrow gap between the spindle and the walls of the container, this method will only be effective for investigating whether the presence of any micro-bubbles during the latter stages of foaming affects the viscosity (and hence workability of the binder). Results for three binders (N6, N7, and O7) with 1.0%, 2.0%, and 3.0% water contents are presented in Figure 3-24. Results show that the foamed binders continue to have viscosities lower than the control even 15 minutes after foaming, although this effect was more prominent for two of the three binders. Foaming decreased the viscosity of N6, N7, and O7 on average by 7.0%, 23.0%, and 16.0% compared to their respective controls. The decrease was similar for all water contents.

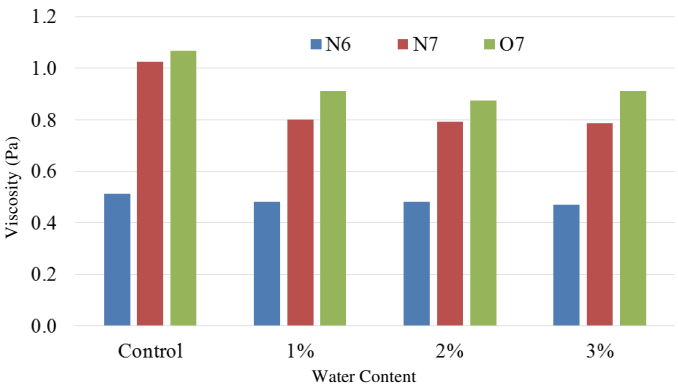


***Figure 3-24. Viscosity of foamed binders N6, N7, and O7.***

### *A.1.6. Water-Bearing Additives (Zeolite)*

In the case of binder combined using particulate additives such as zeolite, the additive is added to the binder (or mixture) typically at a rate of 5.0% by weight of the binder. These additives are hydrothermally crystalized silicates with large empty spaces in their structure that store up to 21% of water by weight of the additive (Hurley and Prowell 2005). When zeolites are mixed with hot binder, water is gradually released from their crystal structure to create a micro-foam, which is hypothesized to improve binder workability.

The typical dosage of 5.0% zeolite will result in approximately 1.0% water by weight of the binder being released (assuming all the water from the zeolite is released). However, unlike foaming by water injection, the rate of release of water with zeolite is much slower, resulting in the expansion and collapse of foam continuing over a much longer period. Consequently, $ER_{max}$ and the rate of decrease of the overall volume of the binder foamed using zeolite are very low. Due to the small size of bubbles, foams created using zeolite are also more stable (longer life) compared to foams produced using water injection.

Due to major differences in the foaming mechanisms of the two foaming methods, parameters developed to characterize foams by water injection may not be appropriate to characterize zeolite foams. In addition, zeolite particles left after foaming act as particulate fillers that can alter the rheological properties of the foamed binder residue.

Binder foams were produced for this study using zeolite (Advera). The typical recommended dosage for synthetic zeolite as a foaming agent is 0.25% by weight of the mix. Considering typical HMA with 5.0% binder content, this corresponds to approximately 5.0% zeolite by weight of the binder. Based on this, binders N7 and O7 were blended with 5.0% zeolite using a RW 20 digital overhead mixer equipped with a four-blade propeller. About 600 grams of the heated binder were poured into a quart can, and the can was inserted into a heating mantle to maintain the binder temperature at 160°C. The exact weight of the binder in the can was also determined. Zeolite (5.0% by weight of the binder) was then slowly added while the binder was stirred using the overhead mixer at a constant speed of 600 rpm. During blending of zeolite with the binder, micro-bubbles approximately 1 mm in diameter (shown in Figure 3-25) were visible on the surface.

A laser sensor was used to measure the change in height and corresponding volume of the foam. A schematic for the laser test setup is shown in Figure 3-26. Mixing and expansion had to be measured simultaneously due to the nature of the particulate additive. Since mixing of the binder creates a non-uniform surface profile, the measurement was carried out by pointing the laser at a location approximately at the midpoint between the center of the mixing container and its edge.

Figure 3-27 illustrates the change in height during mixing for the two blended binders normalized with the constant height

***Figure 3-25. Bubble size of foam produced using zeolite.***

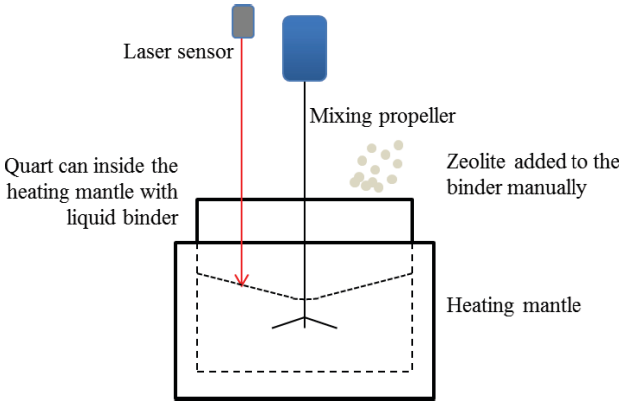


***Figure 3-26. Schematic of the zeolite modified binder foam test setup.***

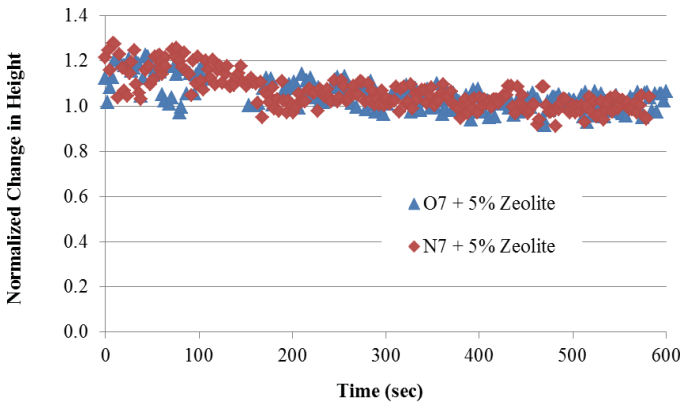


***Figure 3-27. Normalized change in height of binders N7 and O7 with zeolite.***

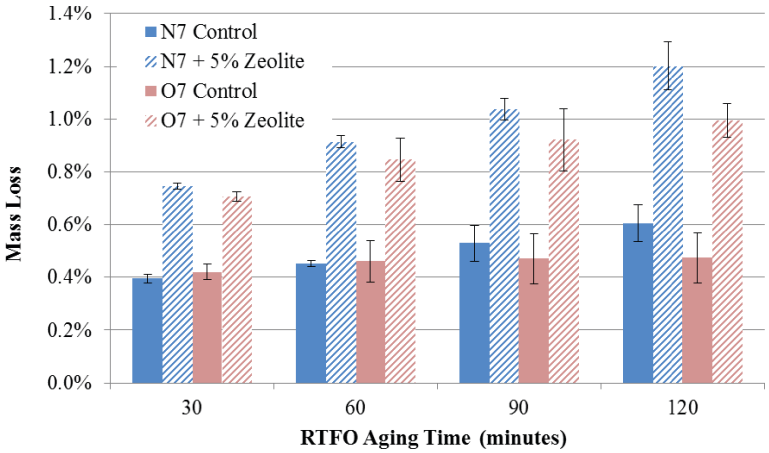


***Figure 3-28. Weight loss for control and zeolite-blended binders N7 and O7 during RTFO.***

that was observed approximately 10 to 15 minutes after starting to mix. This normalization also incorporates the increase in volume due to the addition of the zeolite particles, which was approximately 2.0%. Note that the normalized change in height is not the factor by which expansion occurs because of the non-uniform surface profile. Rather, this change is a qualitative indicator of the foam expansion and collapse characteristics. Similar results were observed when zeolite was mixed with binders OM6, R62, and Y62 using the procedure illustrated in Figure 3-16, where the additive was mixed for 1 minute before the laser measurements were performed. The modified binders did not expand, but many small bubbles were observed at the surface of the binder sample and lasted for a long time.

No noticeable change in the height of the binder occurred after 10 to 15 minutes from the start of blending. At this time, the blended binders were poured into rolling thin film oven (RTFO) bottles and aged at 290°F (143°C) for 120 minutes. A reduced temperature of 290°F (143°C) was used in lieu of the standard 325°F (163°C) to simulate a WMA aging condition. The weights of the control binder and the binders blended with zeolite were measured during the RTFO aging processes after 30, 60, 90, and 120 minutes. The average percent mass loss values are presented in Figure 3-28. Two replicate weight measurements were taken for both binders with/without zeolite, and the error bars indicate the minimum and maximum values. The results demonstrate that the weight loss in the binders with zeolite was significantly higher than that of the control binder, suggesting the presence and continued release of moisture from the blended binders.

## A.2. Effect of Foaming on the Properties of Binders

### *A.2.1. Residual Moisture*

One of the mechanisms associated with the collapse of the foamed binder is when the internal steam pressure causes the bubble diameter to increase to a point where the tensile stresses in the bubble film cause the bubble to collapse and the entrapped steam to escape. However, it is possible that not all the water used for foaming escapes as steam during this process. In fact, results from the Brookfield viscometer shown earlier suggest the possibility of residual micro-bubbles that influence the viscosity of the binder.

To investigate the possibility of residual water in the foamed binder, binder O7 was foamed in the Accufoamer at 2.0% water content, poured into RTFO bottles, and aged in the RTFO at 325°F (163°C). Weight measurements were taken for the foamed binder sample and the control binder at 0, 15, 30, 60, and 85 minutes of RTFO aging. Two replicates of each test were performed.

Figure 3-29 illustrates the weight loss during RTFO aging in the foamed and the control binder. Note that the weight loss in a typical binder, as in the case of the control, is associated with the loss of volatiles during short-term aging. Figure 3-29 clearly illustrates that the foamed binder had a greater weight loss compared to the control, suggesting the presence of residual

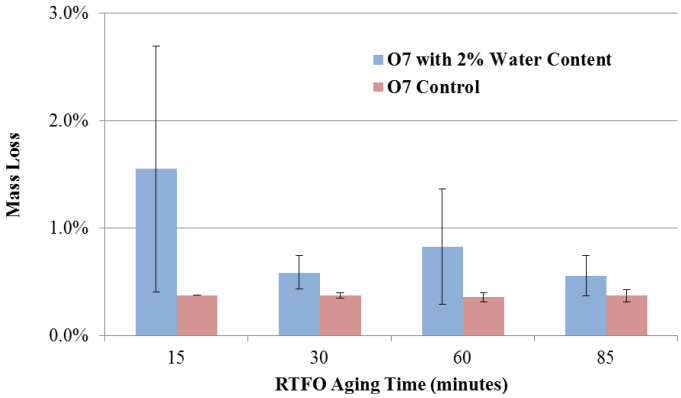


***Figure 3-29. Weight loss by foamed and control binder during RTFO.***

water from the foaming process. The error bars in this figure indicate the high and low values for the weight loss. The variability in weight loss for the foamed binder is significantly higher than the control. This is expected because any trapped moisture may not be homogenously distributed. Also, since the total initial water content was 2.0% by mass of the binder, even a small increase in percent points of weight loss indicates significant fraction of the residual water. The weight loss in the foamed binder slowly approached that of the control as it aged.

### *A.2.2. Rheological Properties of Foamed Residue*

The process of foaming was considered potentially able to alter the binder rheological properties. For example, the presence of highly polar water molecules during foaming and aging may alter the microstructure and, consequently, the rheological properties of the binder. Rheological tests were conducted on foamed binder residues using the DSR and bending beam rheometer (BBR) to verify whether these effects existed. The high-temperature grades of the control binders used for foaming were determined after RTFO aging in accordance with AASHTO M 320. Similarly, the residues of the foamed binders were RTFO aged and subsequently graded to determine the impact of foaming on the high-temperature performance grade (PG). Table 3-3 presents the results of the high-temperature performance grade for eight different binders after foaming with water content that varied from 1.0% to 5.0%.

There was a slight increase in the continuous high-temperature grade of the binders (based on RTFO-aged binder). Foaming increased the continuous high-temperature grade of O7 and N6 with 1.0% water content by 2.7°C and 1.2°C, respectively, compared to their respective controls. Foaming increased the continuous high-temperature grade of the other seven binders on average by less than 0.5°C. These results compare the foamed binder to the base (unfoamed) binder by aging the two different binders under the same conditions [325°F (163°C) for 85 minutes]. However, in practice, foamed binders will experience reduced short-term aging compared to conventional binders due to lower production temperatures. Hence, reduced short-term aging temperature may offset the slight increase in continuous high-temperature grade due to the foaming process.

The intermediate- and low-temperature performances of foamed binder residues were evaluated after pressure aging vessel (PAV) aging using the $G^*\sin\delta$ DSR and the $S$ and $m$-value BBR parameters. (Note: $G^*\sin\delta$ is an asphalt binder fatigue parameter, $G^*$ is the dynamic shear modulus of the asphalt, $\delta$ is the phase angle, $S$ is the low-temperature binder stiffness, and the $m$-value is the slope of the creep curve at low temperature.) The results presented in Table 3-4 clearly indicate that the $S$ and

**Table 3-3. DSR test results of RTFO-aged foamed binder residues.**

| Binder | Type | High PG Grade | Continuous Grade | $G^*/\sin\delta$ @ High PG Temp. (KPa) | Change in Continuous PG Grade | Normalized $G^*/\sin\delta$ |
|---|---|---|---|---|---|---|
| N6 | Control | PG64 | 66.5 | 3.08 | – | 1.00 |
| | 1.0% | | 67.7 | 3.78 | 1.2 | 1.23 |
| | 3.0% | | 67.0 | 3.31 | 0.5 | 1.07 |
| | 5.0% | | 67.0 | 3.12 | 0.5 | 1.01 |
| N7 | Control | PG70 | 74.2 | 3.36 | – | 1.00 |
| | 1.0% | | 74.7 | 3.54 | 0.5 | 1.05 |
| | 3.0% | | 74.3 | 3.45 | 0.1 | 1.03 |
| | 5.0% | | 74.5 | 3.52 | 0.3 | 1.05 |
| O6 | Control | PG64 | 69.7 | 4.54 | – | 1.00 |
| | 1.0% | | 70.1 | 4.81 | 0.4 | 1.06 |
| | 2.0% | | 70.2 | 4.89 | 0.5 | 1.08 |
| | 3.0% | | 69.3 | 4.31 | –0.4 | 0.95 |
| O7 | Control | PG70 | 72.0 | 2.75 | – | 1.00 |
| | 1.0% | | 74.7 | 3.66 | 2.7 | 1.33 |
| | 2.0% | | 74.8 | 3.71 | 2.8 | 1.35 |
| | 3.0% | | 74.7 | 3.64 | 2.7 | 1.32 |
| OM6 | Control | PG64 | 68.1 | 3.73 | – | 1.00 |
| | 2.0% | | 69.2 | 4.33 | 0.6 | 1.16 |
| H6 | Control | PG64 | 69.4 | 4.03 | – | 1.00 |
| | 2.0% | | 68.6 | 4.44 | 0.4 | 1.10 |
| M6 | Control | PG64 | 69.5 | 4.47 | – | 1.00 |
| | 2.0% | | 69.6 | 4.01 | –0.5 | 0.90 |
| Y6 | Control | PG64 | 67.6 | 3.51 | – | 1.00 |
| | 2.0% | | 68.3 | 3.84 | 0.3 | 1.09 |

**Table 3-4. DSR and BBR test results of PAV-aged foamed binder residues.**

| Binder | Type | DSR $G^*\sin\delta$ @ Intermediate Temp. (KPa) | Normalized $G^*\sin\delta$ (%) | BBR S @ -12°C (Mpa) | Normalized $S$ (%) | BBR $m$-value @ -12°C | Normalized $m$-value (%) |
|---|---|---|---|---|---|---|---|
| N6 | Control | 5,657 | 1.00 | 364 | 1.00 | 0.268 | 1.00 |
| | 1.0% | 5,849 | 1.03 | 378 | 1.04 | 0.269 | 1.00 |
| | 3.0% | 6,143 | 1.09 | 350 | 0.96 | 0.269 | 1.00 |
| | 5.0% | 5,341 | 0.94 | 386 | 1.06 | 0.266 | 0.99 |
| N7 | Control | 3,508 | 1.00 | 315 | 1.00 | 0.267 | 1.00 |
| | 1.0% | 3,521 | 1.00 | 312 | 0.99 | 0.270 | 1.01 |
| | 3.0% | 3,411 | 0.97 | 339 | 1.08 | 0.255 | 0.96 |
| | 5.0% | 3,172 | 0.90 | 317 | 1.01 | 0.269 | 1.01 |
| O6 | Control | 3,608 | 1.00 | 274 | 1.00 | 0.287 | 1.00 |
| | 1.0% | 4,384 | 1.22 | 275 | 1.00 | 0.280 | 0.98 |
| | 2.0% | 4,320 | 1.20 | 263 | 0.96 | 0.282 | 0.98 |
| | 3.0% | 3,925 | 1.09 | 230 | 0.84 | 0.298 | 1.04 |
| O7 | Control | 2,089 | 1.00 | 233 | 1.00 | 0.290 | 1.00 |
| | 1.0% | 2,256 | 1.08 | 234 | 1.00 | 0.264 | 0.91 |
| | 2.0% | 2,402 | 1.15 | 214 | 0.92 | 0.275 | 0.95 |
| | 3.0% | 2,171 | 1.04 | 231 | 0.99 | 0.278 | 0.96 |
| OM6 | Control | 5,133 | 1.00 | 227 | 1.00 | 0.30 | 1.00 |
| | 2.0% | 6,442 | 1.26 | 255 | 1.12 | 0.301 | 1.04 |
| H6 | Control | 4,345 | 1.00 | 215 | 1.00 | 0.284 | 1.00 |
| | 2.0% | 5,566 | 1.31 | 214 | 1.00 | 0.270 | 0.95 |
| M6 | Control | 4,189 | 1.00 | 193 | 1.00 | 0.301 | 1.00 |
| | 2.0% | 5,017 | 1.20 | 198 | 1.03 | 0.282 | 0.94 |
| Y6 | Control | 5,479 | 1.00 | 194 | 1.00 | 0.305 | 1.00 |
| | 2.0% | 5,747 | 1.05 | 175 | 0.90 | 0.302 | 0.99 |

*m*-value at low temperatures were similar to the *S* and *m*-value of base binders.

Most of the $G^*\sin\delta$ values for the foamed residues were slightly higher than those of their base binders. The slight increase in the $G^*\sin\delta$ values for the foamed residues, however, may be compensated for when the foamed binders are subjected to lower short-term aging temperatures in production. The DSR and BBR results demonstrate that foaming process may not have a significant influence on the short-term and long-term rheological properties of binders. This finding is substantiated by the observation that foaming does not result in a change in asphalt binder chemistry (Namutebi et al. 2011). The coefficient of variation for the data was less than 5.0%.

## A.3. Comparison of Laboratory Foamers

The objective of this section is to compare differences in laboratory foaming units and processes. The characteristics of foamed binders produced using three commercially available foamers (Wirtgen WLB 10S, InstroTek Accufoamer, and PTI foamer) were compared. The three units foam binders differently, likely resulting in different foam structures and properties. The following is a brief description of the working principles of the three foaming units.

### *A.3.1. Wirtgen WLB 10S*

The Wirtgen foamer is designed to regulate the amount of dispensed binder and water by mass flow meters. The binder is heated to 320°F (160°C) and circulated inside the unit. Then, the foamed binder is produced by combining specific quantities of water, compressed air, and heated binder inside an expansion chamber. During this process, the added water vaporizes and causes the binder to foam in the expansion chamber. The pressure at which the water and the air are injected in the expansion chamber is about 72 psi (500 kPa). After the binder is foamed, it is usually dispensed directly from the nozzle into the mixer, where it is combined with the heated aggregates. The unit can dispense about 0.4 lb (200 grams) of binder in 2 s due to the high pressure at which the water and air are injected. Figure 3-30 illustrates the equipment used in this study and a schematic of the foaming process.

### *A.3.2. InstroTek Accufoamer*

The Accufoamer is designed to deliver binder and the foaming agent (water) by regulating the overhead pressure that drives the flow of these liquids. The foaming unit is calibrated to determine the time taken to deliver a certain mass of binder at a fixed driving pressure and the time taken

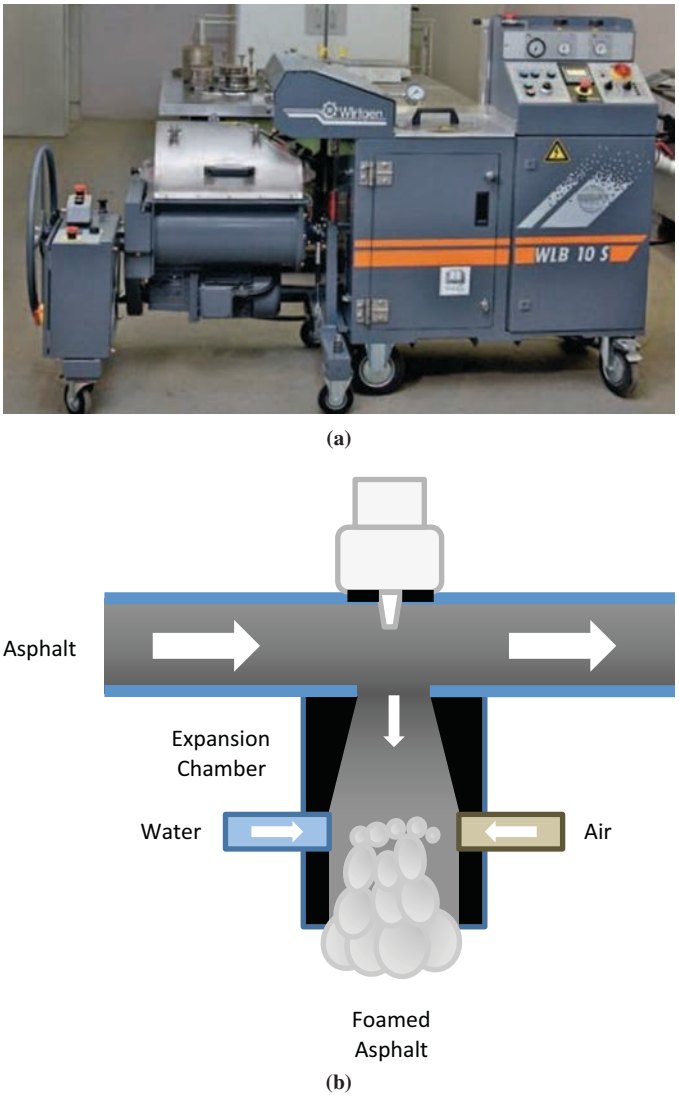


***Figure 3-30. Wirtgen WLB 10S; (a) foaming unit, (b) schematic of the foaming process.***

to deliver a certain mass of water at different pressures. In this study, the selected binder temperature and pressure were 320°F (160°C) and 30 psi (210 kPa). The unit comes with an Excel template programmed with the relationship between water content and pressure for a given binder flow rate. Once the calibration parameters are set in the template, it can be used to determine the flow time and water pressure that are required to produce the desired mass of foamed binder at any desired water content. Figure 3-31 presents a view of the unit used in this study and a schematic of the foaming process.

### *A.3.3. Pavement Technology Inc. (PTI) Foamer*

The PTI foaming unit regulates the mass of binder to dispense by load-cell scale. An air line with a minimum of 110 psi (760 kPa) is connected to the main regulator to actuate the unit. Air is used to charge a water reservoir and keep water at a regulated pressure. The pressure in the water tank is about 35 psi (240 kPa). A small amount of air is used to atomize the water to very fine droplets in order to achieve the largest binder expansion possible. The binder is discharged from the reservoir by actuating a pneumatic cylinder when the foam button is pressed. After the preset amount of binder is dispensed, the pneumatic cylinder closes, and the flow of binder is pinched. The binder discharge is by gravity and not through pressure. The unit is able to accommodate up to 14 lb (6.4 kg) of binder. In addition, the unit can raise or lower the chamber to meet the heights for various laboratory mixers. Figure 3-32 illustrates the PTI foamer unit used in this study and an overview of the foaming steps.

There are notable differences between the three foaming units. First, the nozzle types that spray the binder and the water are different. Second, the pressures at which the water, air, and binder are mixed in the expansion chamber are different. The Wirtgen foamer produces the foam by directing the two nozzles at each other. The resulting foam is dispensed into a container directly as it is being formed. The Accufoamer also produces the foam by directing the two nozzles at each other, but the foam is produced inside a small mixing chamber before being dispensed through a tube 0.25 in. (6.4 mm) in diameter to a container or mixer. The PTI unit dispenses the foamed binder by gravity. As a result, the Accufoamer dispenses about 0.4 lb (200 grams) of foamed binder in 10 to 12 s, the PTI dispenses 0.4 lb (200 grams) in 10 to 14 s, and the Wirtgen foamer dispenses about 0.4 lb (200 grams) of binder in about 2 s (see Table 3-5). In addition, the maximum expansion achieved by the Accufoamer and the PTI units is lower as compared to the Wirtgen foamer.

Since the expansion measurements could be taken directly during discharge from the Accufoamer, no foaming information was lost. The can needed to be moved from the foaming unit to a location where measurements could be taken for both the PTI and Wirtgen foamers. The time lost in moving the can from under the foamer's nozzle to the measurement area was approximately 3 s from discharge. For the Wirtgen foamer, a procedure was developed to extrapolate the expansion curve back to time zero. For the PTI foamer, no extrapolation was necessary as the foam volume change was extremely slow.

Table 3-5 summarizes the operation parameters and foaming process features of the three foaming units. Notwithstanding these differences, the goal of this exercise was to determine whether the characteristics of different foamed binders at various water contents were similar for the three foaming units.

The influence of the foaming equipment was evaluated using two different binders at two water contents. The metrics listed in Section 2.A.4 were used to compare the foaming

(a)

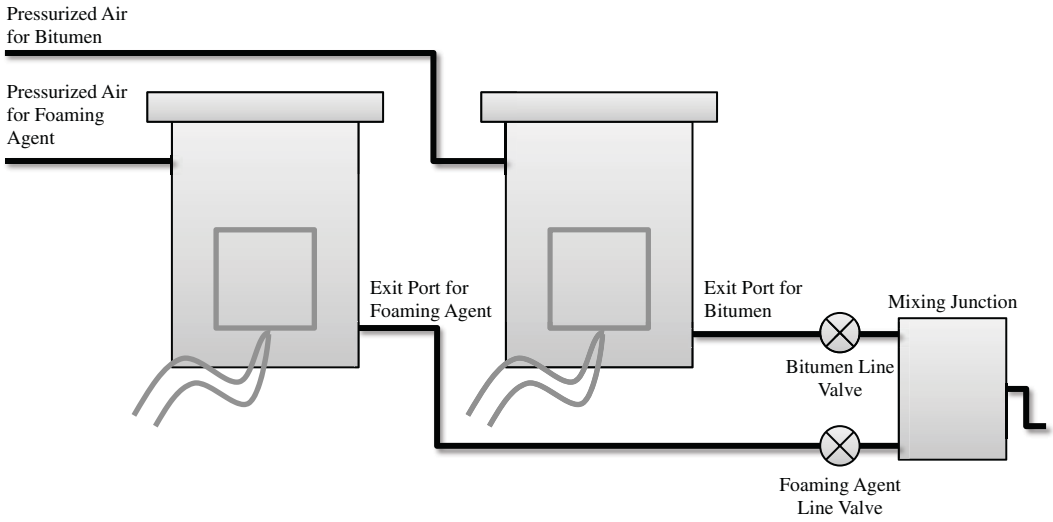


(b)

***Figure 3-31. InstroTek Accufoamer; (a) foaming unit, (b) schematic of the foaming process.***

**Table 3-5. Summary of characteristics of the foaming units.**

| Characteristic | Wirtgen WLB 10S | InstroTek Accufoamer | PTI foamer |
|---|---|---|---|
| Air flow pressure | Min. 15 psi (100 kPa) Max. 145 psi (1,000 kPa) | Min. 75 psi (517 kPa), Max. 150 psi (1,034 kPa) | Min. 80 psi (552 kPa) Max. 110 psi (758 kPa) |
| Water flow pressure | Max. 145 psi (1,000 kPa) | Max. 30 psi (207 kPa) | 33 psi (230 kPa) |
| Binder flow pressure | Max. 145 psi (1,000 kPa) | Max. 60 psi (413 kPa) | The binder is dispensed by gravity. |
| Reaction chamber | Water and compressed air are injected into the hot binder. | Pressurized binder and water meet at a single junction. | A small amount of air is used to atomize the water to a fine droplet. |
| Binder temperature | 284°F–392°F (140°C–200°C) | 320°F–390°F (160°C–200°C) | Max 350°F (177°C) |
| Discharge time | 100 g/s | 16–20 g/s | 14–20 g/s |
| Mass control | Mass flow control | Overhead pressure control | Scale control |
| Power requirement | Adaptable to various international supplies | 208–240 VAC, 220-volt, 30-amp circuit | 120 VAC, 20 amp |
| Binder chamber size | 5.3 gallon (20 L) | 0.3–15.0 lb (150 to 6,800 g) | 14 lb (6,350 g) |
| Foaming agent dosage (water content) | 0%–5% | 0%–9% | 1%–7% |
| Foaming agent temperature | No heat | Max. 180°F (82°C) | No heat |

VAC = volts alternating current.

(a)

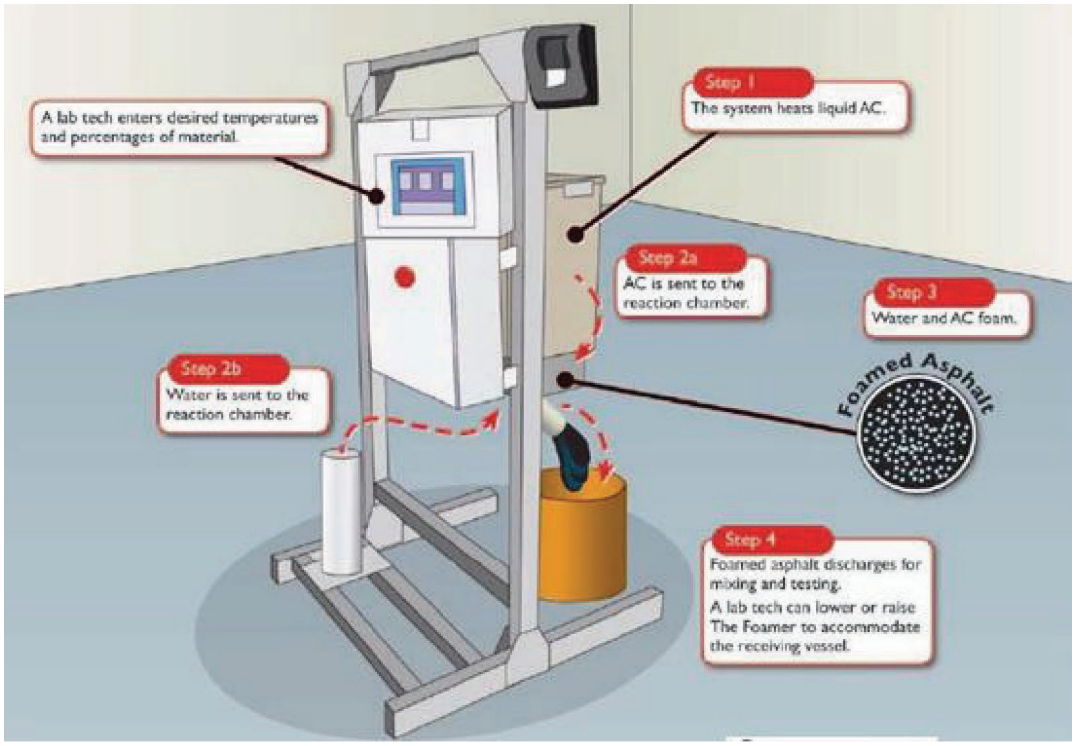


(b)

***Figure 3-32. PTI foamer; (a) laboratory unit, (b) foaming process (PTI Foamer Users' Guide, updated 11-20-12).***

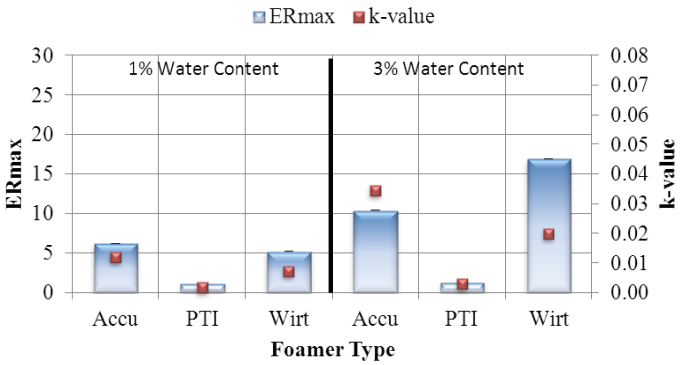


***Figure 3-33. $ER_{max}$ and k-value for binder N6 foamed in three different units with 1.0% and 3.0% water content.***

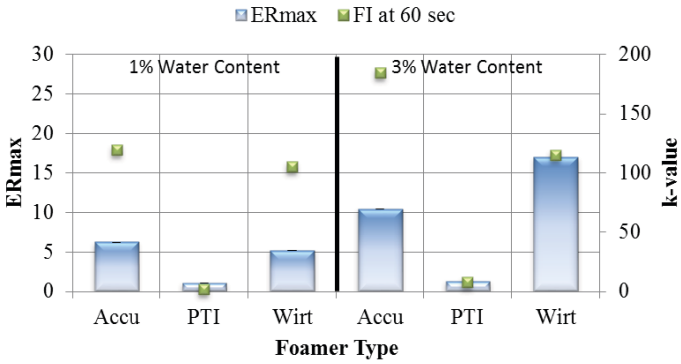


***Figure 3-35. Foamability index for binder N6 foamed in three different units at 1.0% and 3.0% water content.***

characteristics of N6 and O7 with 1.0% and 3.0% water contents from the three foaming units.

### *A.3.4. Binder Foaming Measurements*

To compare the foaming characteristics of the three units, the height of the foamed binder was measured using a laser sensor or laser distance meter (LDM) on two replicates. $ER_{max}$ and *k*-value are summarized in Figure 3-33 and Figure 3-34. The FI (i.e., area under the ER curve) is presented in Figure 3-35 and Figure 3-36 for binder N6 and O7, respectively.

The following observations can be made based on data presented in Figure 3-34 through Figure 3-36:

- $ER_{max}$ increased with increasing water content.
- In the majority of the cases (with the exception of N6 with 1.0% water content), the Wirtgen foamer had the largest $ER_{max}$ values, while the PTI foamer had the lowest $ER_{max}$ values in all cases.
- The PTI foamer showed very small expansion compared to the other two units (in the range of 1 to 1.5), which corresponds to observations made by Ozturk and Kutay (2014b).
- The *k*-value showed a similar trend to the one observed for $ER_{max}$: higher *k*-values correspond to higher $ER_{max}$ values (with the exception of O7 in the Accufoamer with 3.0% water content).
- For both water contents, N6 had lower or equivalent $ER_{max}$ values as compared to O7 in the Wirtgen and PTI foamers, but N6 had higher $ER_{max}$ values as compared to O7 in the Accufoamer.
- The FI at 60 s for both binders at 1.0% water content was very similar, while at 3.0% water content N6 in the Accufoamer seemed to have a larger FI than O7, but a lower FI in the Wirtgen foamer.

The procedure for determining the bubble size distribution of the foamed binder described in Appendix B was used to generate the following gamma function curves. The curves show the bubble size distribution at selected times for binders N6 and O7 foamed with 1.0% and 3.0% water content in the three foaming units. In Figure 3-37 and Figure 3-38, the solid and dashed lines represent 1.0% and 3.0% water content, respectively. The selected target times for the comparison were 30, 60, and 90 s (30 s was enough to avoid the turbulent phase shown in Figure 2-4 and any steam generated during foaming that could prevent photographing the surface of the binder). However, for the binders foamed in

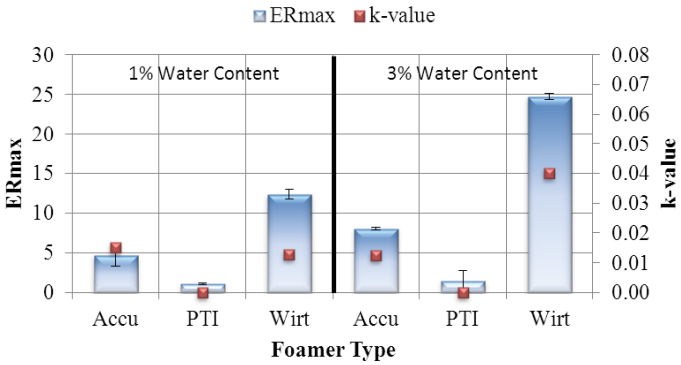


***Figure 3-34. $ER_{max}$ and k-value for binder O7 foamed in three different units at 1.0% and 3% water content.***

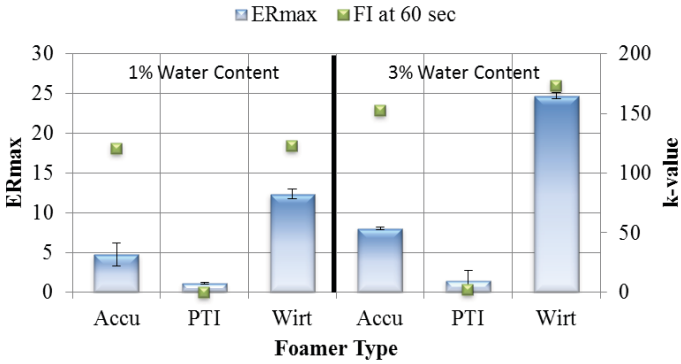


***Figure 3-36. Foamability index for binder O7 foamed in three different units at 1.0% and 3.0% water content.***

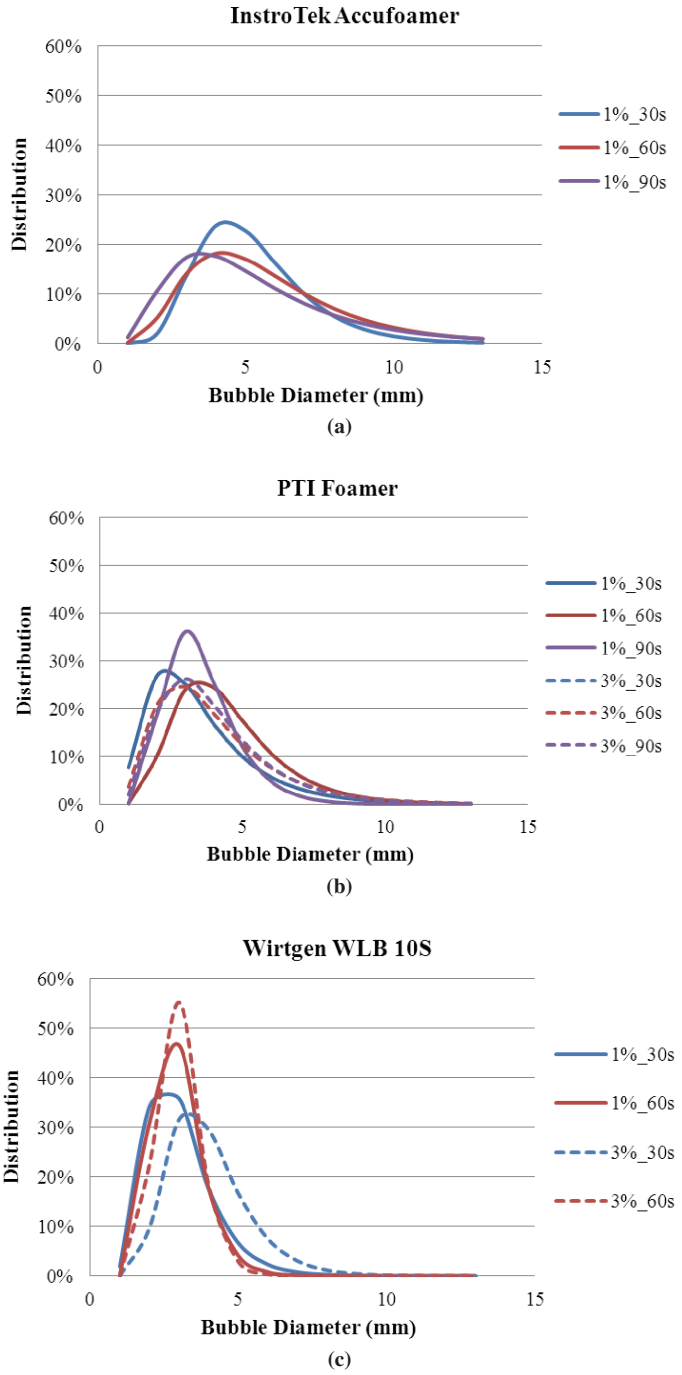


***Figure 3-37. Bubble size distribution for N6 with 1.0% and 3.0% water content.***

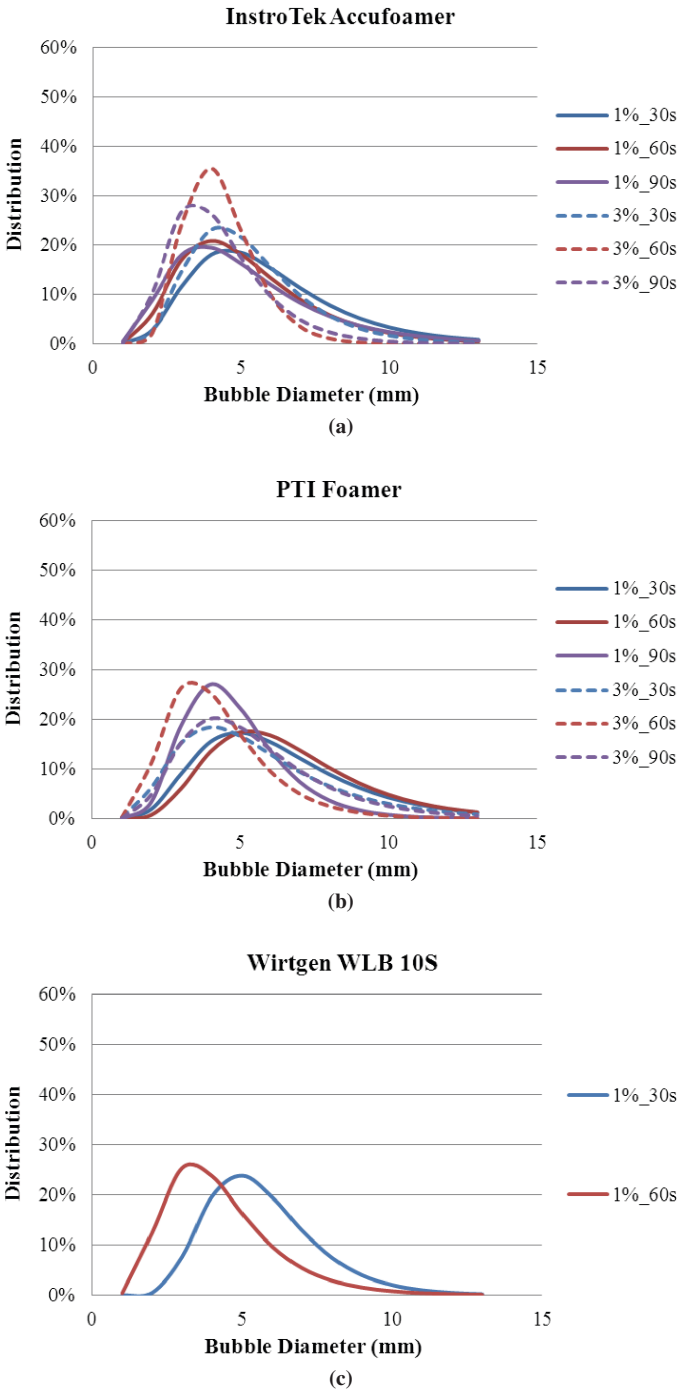


***Figure 3-38. Bubble size distribution for O7 with 1.0% and 3.0% water content.***

the Wirtgen foamer, only 30 and 60 s are reported because after 60 s the binders had very small and uniform bubble sizes. In addition, O7 with 3.0% water content in the Wirtgen foamer had a very turbulent expansion and collapse that did not form any distinguishable bubbles, and thus the results are not included in Figure 3-38. Binder N6 with 3.0% water content in the Accufoamer was not measured.

The following observations can be made based on the results:

1. In the majority of the cases, the foamed bubbles decreased in size with elapsed time and became more homogeneous (i.e., higher peak, more narrow spread, and shift to the left of the gamma function curves).

**Table 3-6. Experimental design for workability and coatability evaluation.**

| Binder Source | Mixture/Foaming Water Contents | | | | | | |
|---|---|---|---|---|---|---|---|
| | HMA/0% | Foamed WMA/1% | Foamed WMA/2% | Foamed WMA/3% | Foamed HMA/1% | Foamed HMA/2% | Foamed HMA/3% |
| N64-22 | X | X | X | X | X | X | X |
| O64-22 | X | X | X | X | X | X | X |
| Y64-22 | X | X | X | X | | | |
| N70-22 | | X | | | | | |
| O70-22 | | X | | | | | |

2. The difference in bubble size seemed to be more pronounced at 3.0% water content versus 1.0% water content.
3. The PTI foamer seemed to produce more stable bubbles regardless of the elapsed foaming time.
4. The minimum bubble size about 90 s after foaming seemed to be around 1.1 in. (2.8 mm), which is probably a result of the procedure used to determine the bubble size distribution as smaller bubbles were more difficult to identify.

## B. Laboratory Mixture Study

The objectives of this portion of the study were to (1) evaluate the effect of different binder types and foaming water contents on the workability and coatability of foamed asphalt mixtures and (2) compare the workability and coatability of foamed WMA versus HMA.

The experimental design for the initial workability and coatability evaluation is shown in Table 3-6. The aggregates used came from a field project located on I-25 in New Mexico. Three fractions of siliceous aggregates were combined following the mix design gradation shown in Figure 3-39. The optimum binder content by the weight of mix was 5.4%. For the coatability evaluation, the volumetrics for the coarse aggregate fraction were calculated based on the combined aggregate gradation and optimum binder contents from the mix design, as summarized in Table 3-7.

The Wirtgen foamer was used to produce foamed WMA and control HMA. The temperature of the binder chamber in the foaming unit was at 320°F (160°C), and the air and water pressure were set to 72 psi (500 kPa) per the manufacturer's recommendation. Foamed WMA using binders N6, O6, and Y6 was produced with three water contents, 1.0%, 2.0%, and 3.0%. To explore the foaming characteristics of polymer-modified binders versus neat binders, foamed WMA with binders N7 and O7 was also produced with 1.0% water content. The workability and coatability comparisons of those mixtures were used to validate the method listed in Section 2.B.

The control HMA using the neat binders was also included in the study and was produced by the same laboratory foaming unit with no foaming water. In addition, foamed HMA using neat binders with 1.0%, 2.0%, and 3.0% water contents was also produced and evaluated in the study. The production

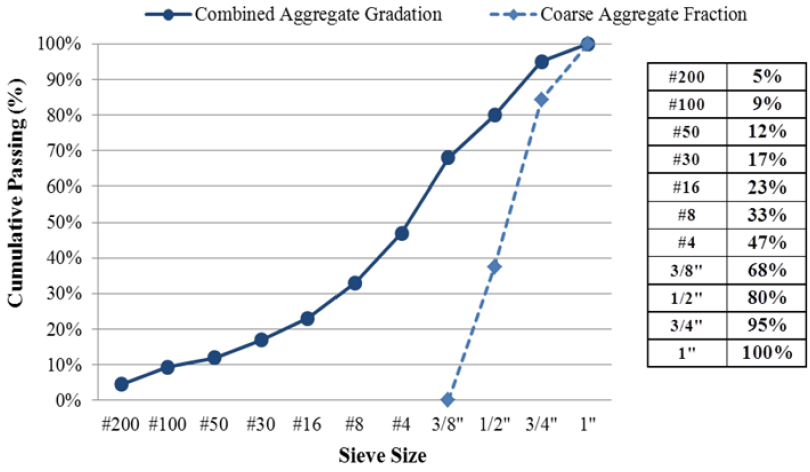


*Figure 3-39. Design aggregate gradation for the New Mexico field project.*

**Table 3-7. Volumetric calculation for the New Mexico coarse aggregate fraction.**

| Volumetrics | Values | Reference |
|---|---|---|
| $P_b$ | 5.4 (%) | Mix Design |
| SST | 5.093 ($m^2$/kg) | Mix Design and Kandhal et al. (1988) |
| $SA_{coarse}$ | 0.410 ($m^2$/kg) | Mix Design and Kandhal et al. (1988) |
| $W_b$ | 57 (g) | $W_b = 4{,}000 * \frac{P_b}{1 - P_b} * \frac{SA_{coarse}}{SST} * \frac{1}{P_{s-coarse}}$ |

**Table 3-8. Summary of production temperatures for foamed WMA and HMA and control HMA.**

| Foaming Water Contents | Mixing Temperature | Short-Term Aging Protocol | Compaction Temperature |
|---|---|---|---|
| 0.0% (Control HMA) | 290°F (143°C) | 2 hours at 275°F (135°C) | 275°F (135°C) |
| 1.0% (Foamed WMA) | 275°F (135°C) | 2 hours at 240°F (116°C) | 240°F (116°C) |
| 2.0% (Foamed WMA) | 275°F (135°C) | 2 hours at 240°F (116°C) | 240°F (116°C) |
| 3.0% (Foamed WMA) | 275°F (135°C) | 2 hours at 240°F (116°C) | 240°F (116°C) |
| 1.0% (Foamed HMA) | 290°F (143°C) | 2 hours at 275°F (135°C) | 275°F (135°C) |
| 2.0% (Foamed HMA) | 290°F (143°C) | 2 hours at 275°F (135°C) | 275°F (135°C) |
| 3.0% (Foamed HMA) | 290°F (143°C) | 2 hours at 275°F (135°C) | 275°F (135°C) |

temperatures for foamed WMA and HMA as well as the control HMA are summarized in Table 3-8. The comparison of workability and coatability by foamed WMA versus HMA was used to verify whether the foaming process produced WMA mixtures with better workability and coatability characteristics as compared to the control HMA. In addition, the comparison of foamed WMA versus foamed HMA helped evaluate the effect of production temperature on the foaming process.

## B.1. Effect of Foaming on Mixture Workability and Coatability

The workability and coatability results for the control HMA and the foamed WMA mixtures produced using three different neat binders with 1.0%, 2.0%, and 3.0% water contents are shown in Figure 3-40 and Figure 3-41. In these figures, the control HMA results are compared against the foamed WMA values within each binder source. Each bar in Figure 3-40(a) represents the average value of two replicates, and the error bars represent ±1 standard deviation from the average value. Based on the span of the error bars, good repeatability for the workability test method was achieved. The maximum shear stress and CI were normalized with respect to the control HMA value. Thus, in Figure 3-40(b), values equal to or less than 1.0 indicate equivalent or better workability than HMA, while in Figure 3-41(b), values equal to or greater than 1.0 indicate equivalent or better coatability than HMA.

A significant difference in workability (Figure 3-40) and coatability (Figure 3-41) was observed for the various foamed

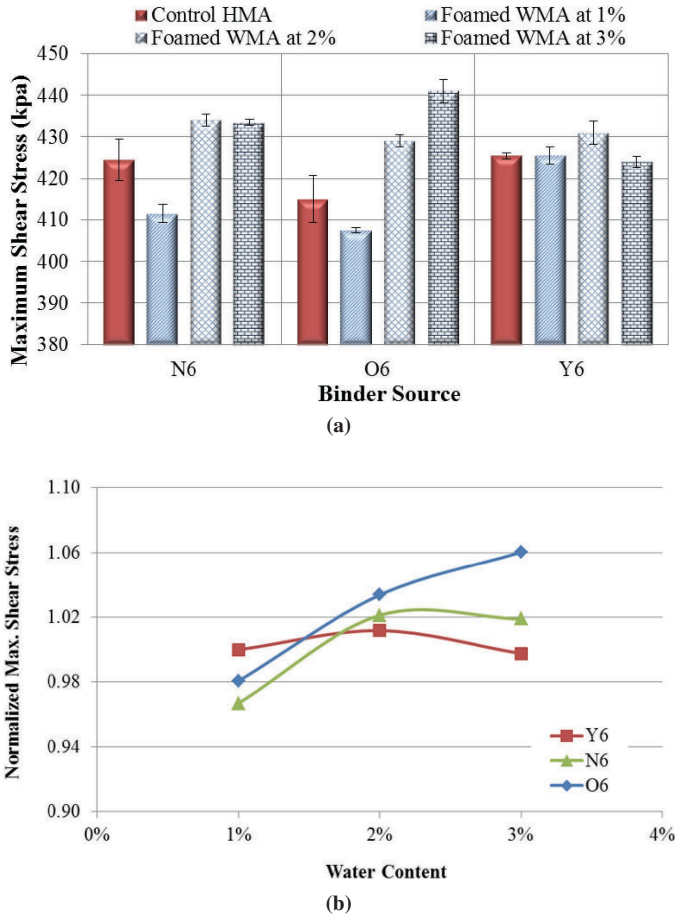


***Figure 3-40. Workability test results for foamed WMA versus HMA; (a) maximum shear stress, (b) normalized maximum shear stress.***

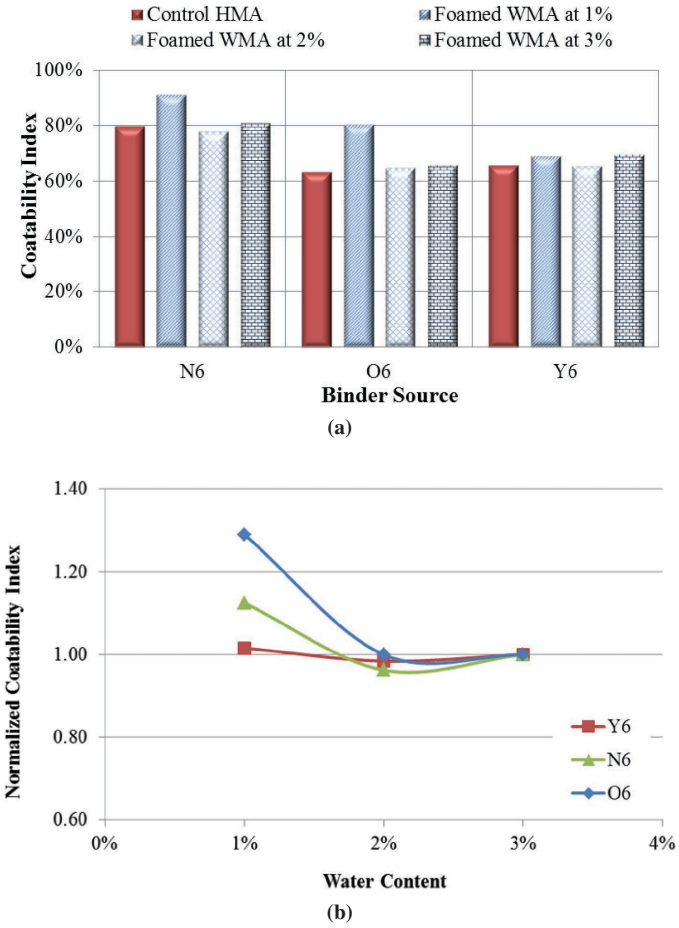


***Figure 3-41. Coatability test results for foamed WMA versus HMA; (a) coatability index, (b) normalized coatability index.***

WMA mixtures and as compared to the control HMA for binder N6 and O6. However, there was relatively little difference for binder Y6. Therefore, the workability and coatability test methods proposed in this study were validated as having the sensitivity to capture the characteristics of different mixtures, depending on the binder source.

As shown in Figure 3-40 and Figure 3-41, foamed WMA mixtures employing binders N6 and O6 with 1.0% water content had better workability and coatability characteristics (indicated by a lower maximum shear stress and a higher CI) as compared to both the WMA mixtures foamed at higher water contents and the control HMA. This was true despite the fact that the production temperature for the WMA mixtures was approximately 30°F (17°C) lower than the production temperature for HMA. Therefore, a water content of 1.0% was optimum for these WMA foamed mixtures. Contrary to expectations, however, WMA mixtures foamed with higher water contents (i.e., 2.0% and 3.0%) yielded mixtures with equivalent or worse workability and coatability characteristics as compared to the control HMA. This observation of decreased coating with increasing foaming water content was confirmed by Ozturk and Kutay (2014a).

A different workability and coatability trend was shown for mixtures employing binder Y6. These WMA mixtures had equivalent workability and coatability as compared to the control HMA despite the amount of water used during foaming. This binder did not appreciably foam at any water content (i.e., 1.0% to 5.0%). The reduced foaming abilities of binder Y6 could be due to the presence of an anti-foaming agent that is sometimes introduced during the crude refining or binder production process (Abel 1978; Fu 2011; Kekevi et al. 2012).

The following observations can be made from the normalized CI and normalized maximum shear stress values of the WMA for the mixes produced using binders N6, O6, and Y6 to that of their corresponding HMA values that were presented in Figure 3-40(b) and Figure 3-41(b):

- An increase in $ER_{max}$ did not necessarily translate into improvement in mixture workability or aggregate coatability of WMA mixtures.
- Lower water content values showed improvement in workability of WMA mixtures relative to HMA mixtures. However, an increase in water content did not appear to have an adverse effect on coatability relative to HMA.
- Workability and coatability typically improved compared to a similar HMA when the water content was between 1.0% and 2.0%.

The significance of change in foamed binder characteristics on mixture workability and coatability was further investigated by comparing ER (at 10 s) and *k*-value to the normalized maximum shear stress and CI as shown in Figure 3-42. The results for binder Y6 show less sensitivity to both *k*-value and ER. Increasing *k*-value decreased the workability and coatability of mixtures produced using binders N6 and O6. However, the coatability of the WMA mixtures performed as well as the HMA mixtures at higher *k*-values. Better coatability and workability was observed when the ER values of the mixtures were close to an ER value of 4, and a *k*-value of 0.01 seemed optimum for both the workability and coatability of the mixtures.

As foamed WMA using binders N6 and O6 with 1.0% foaming water content had the best workability and coatability, foamed WMA using the polymer-modified binders N7 and O7 was also produced at this water content. Workability and coatability results for foamed WMA using polymer-modified versus neat binders were compared and are summarized in Figure 3-43 and Figure 3-44, respectively.

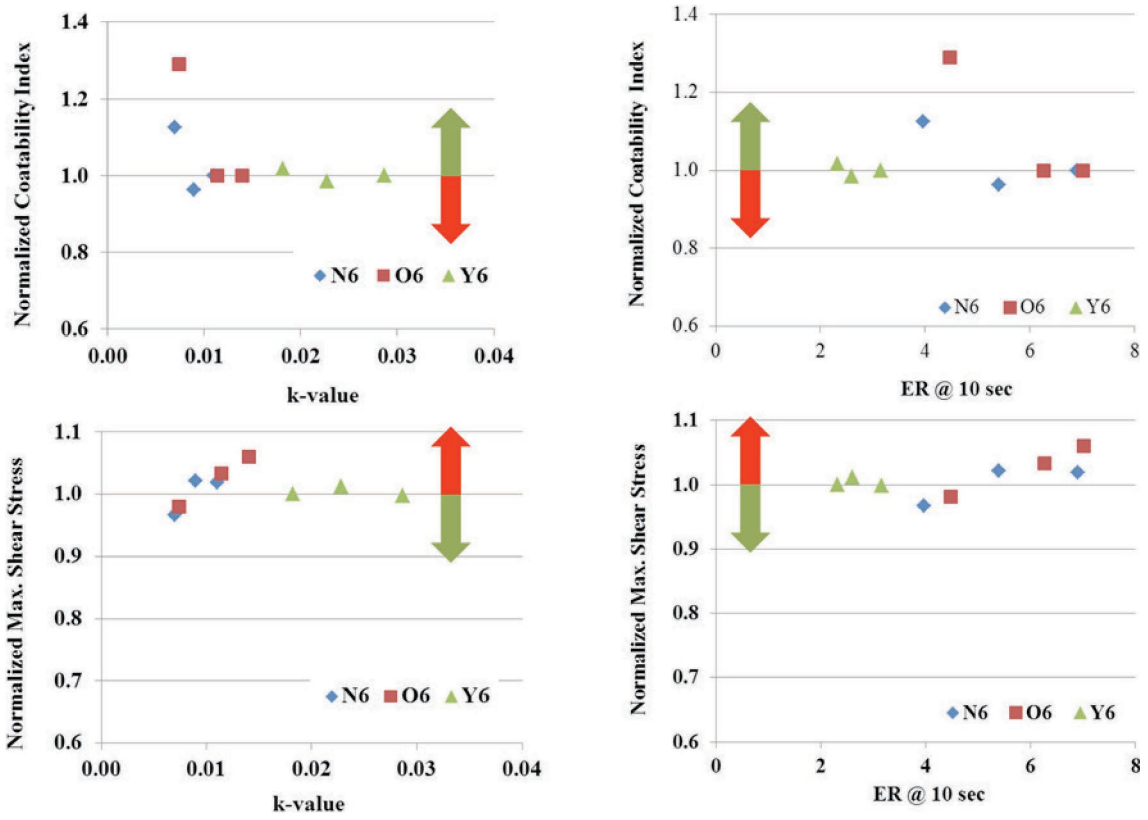


***Figure 3-42. Comparison of foamed binder parameters to mixture workability and coatability. (The green arrow indicates desirable range of coatability or shear stress compared to HMA.)***

As illustrated, better workability and coatability are shown for foamed WMA using neat binders than those using polymer-modified binders when produced at the same temperature. Adhering to the strict definition that WMA is produced at temperatures at or below 275°F (135°C), both mixtures prepared with PG64-22 and PG70-22 were mixed at the upper limit of the WMA conventional temperature range and conditioned for 2 hours at 240°F (116°C). The reduced properties of foamed WMA using polymer-modified binders are possibly attributed to the higher viscosity of the binder at the WMA production temperature, which was approximately 25°F lower than the recommended production temperature. Thus, it may be advantageous to increase the temperature for foaming polymer-modified binders. Additionally, the incorporation of polymer modifiers may have an effect on the binder foaming characteristics.

The effect of production temperature on the workability and coatability of foamed asphalt mixtures is illustrated in Figure 3-45 and Figure 3-46, respectively. In these figures, the properties of foamed WMA are compared to those of foamed

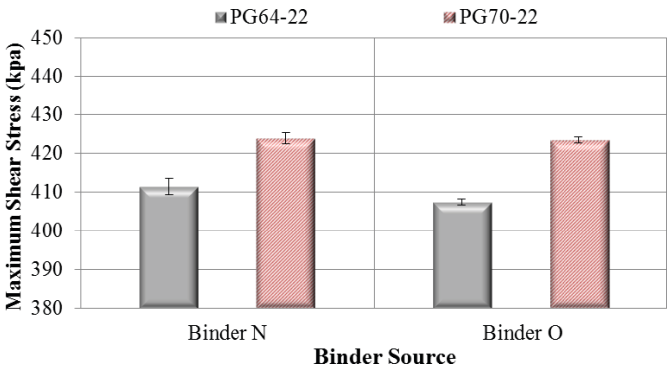


***Figure 3-43. Workability test results for foamed WMA with neat versus polymer-modified binder.***

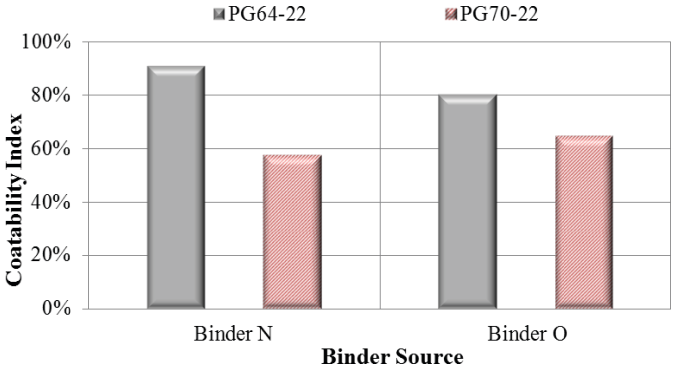


***Figure 3-44. Coatability test results for foamed WMA with neat versus polymer-modified binder.***

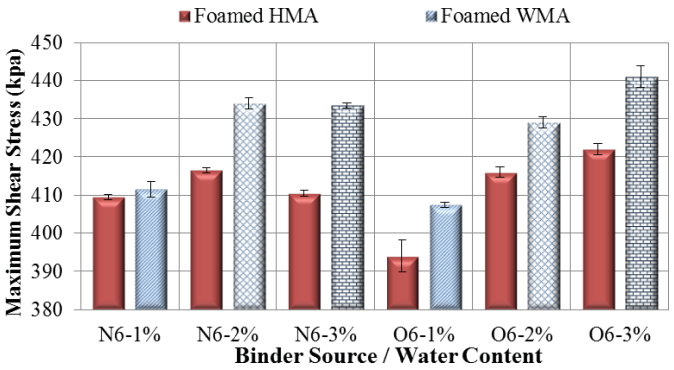


***Figure 3-45. Workability test results for foamed WMA versus foamed HMA.***

HMA for each foaming water content (i.e., 1.0%, 2.0%, and 3.0%). Binders N6 and O6 were used for this evaluation. As illustrated, better or equivalent workability and coatability (indicated by a lower maximum shear stress and a higher or equivalent CI) are shown for foamed HMA as compared to foamed WMA, for all three foaming water contents. Therefore, higher production temperature for the foaming process is able to produce foamed asphalt mixtures with better workability and coatability.

In summary, test methods for evaluating mixture workability and coatability were developed using SGC compaction data and a modified aggregate absorption method, respectively. The maximum shear stress and a CI were proposed as mixture workability and coatability parameters. For the coatability evaluation, only coarse aggregates retained on the ⅜-in. sieve were used. The relative difference in water absorption by the uncoated aggregates versus the loose mix was used to calculate the CI.

Foamed WMA using three binders with three foaming water contents was produced using the Wirtgen foamer. In addition, to validate the improved workability and coatability of foamed WMA, a control HMA mixture was also produced using the same laboratory foaming unit with no water content. The workability and coatability of the foamed WMA mixtures were compared against the characteristics of the HMA mixtures. In addition, the effect of binder source, binder grade, and foaming water contents on mixture workability and coatability was investigated. The following conclusions were made based on the results:

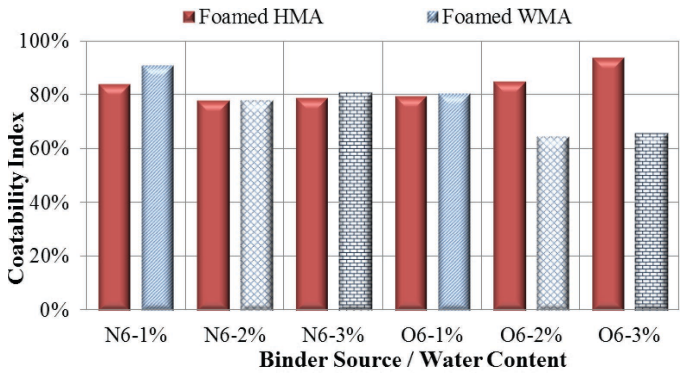


***Figure 3-46. Coatability test results for foamed WMA versus foamed HMA.***

1. Significant differences in the maximum shear stress and CI for foamed WMA mixtures versus the control HMA were observed for two of the three binders. Thus, the proposed test methods seem promising in evaluating the workability and coatability of asphalt mixtures.
2. Foamed WMA mixtures produced with binders N6 and O6 had better workability and coatability when 1.0% foaming water content was used as compared to higher foaming water contents (i.e., 2.0% and 3.0%). Thus, for these two binders, 1.0% was considered the optimum foaming water content. This trend is consistent with results from Abbas and Ali (2011). However, equivalent workability and coatability was observed for the WMA mixtures that employed binder Y6 as compared to the control HMA regardless of the foaming water content used.
3. Comparison of foamed WMA versus control HMA mixtures showed that WMA produced at 1.0% foaming water content had better workability and coatability characteristics, despite the fact that the WMA mixtures were produced at temperatures approximately 30°F (17°C) lower than the control HMA. However, the WMA mixtures foamed at higher foaming water contents (i.e., 2.0% and 3.0%) had equivalent or worse characteristics as compared to the control HMA. This finding highlights the importance of identifying the best materials and foaming conditions to maximize the workability and coatability of foamed mixtures.
4. At WMA production temperatures, foamed WMA employing binder N6 and O6 had better workability and coatability as compared to those mixtures with N7 and O7. The higher viscosity of polymer-modified binders is possibly causing the reduced mixture workability and coatability.
5. Comparison of foamed WMA versus foamed HMA showed that foamed HMA employing binders N6 and O6 had better or equivalent workability and coatability than the corresponding foamed WMA counterparts, for all three foaming water contents. Therefore, higher production temperature involved in the foaming process is able to produce foamed asphalt mixtures with better properties.

## B.2. Effect of Liquid Additives on Mixture Workability

The liquid additives used in the laboratory binder study (see Section A.1.4) were also employed to explore their influence on mixture workability. In this case, a local aggregate source from Huntsville, Texas (see Chapter 4, Section C.2 for details) was employed along with binders OM6 and Y62. These two binders were selected because they showed minimal

change in $ER_{max}$ with added water and were thus considered ideal candidates to assess changes in mixture workability after the inclusion of liquid additives.

Besides the additives listed in Table 3-2, a fourth additive was considered for this part of the study (henceforth labeled W2). Additive W2 consists of a synthetic zeolite that holds about 20% water within its crystalline structure. When combined with the binder or aggregate at temperatures ranging from 275°F (135°C) to 320°F (160°C), it releases the water, which foams the binder and reduces its viscosity. Additive W2 was incorporated in the mixture in two ways: (1) combining it with the binder at a dosage of 5.0% by weight of binder [labeled FWMA + W2 (binder)] before mixing (see Figure 3-16 for an illustration of the additive blending procedure), and (2) combining it with the aggregate at a dosage of 0.25% by weight of mixture [labeled FWMA + W2 (agg)] before mixing.

The binder for all mixtures was foamed in the Wirtgen foamer at 1.5% water content. The mixing temperatures for the HMA and foamed WMA (FWMA) were 290°F (143°C) and 275°F (135°C), respectively. The HMA was conditioned for 2 hours at 275°F (135°C) and compacted at the same temperature. The FWMA was conditioned for 2 hours at 240°F (116°C) and compacted at the same temperature. The maximum shear stress results for these mixtures are illustrated in Figure 3-47.

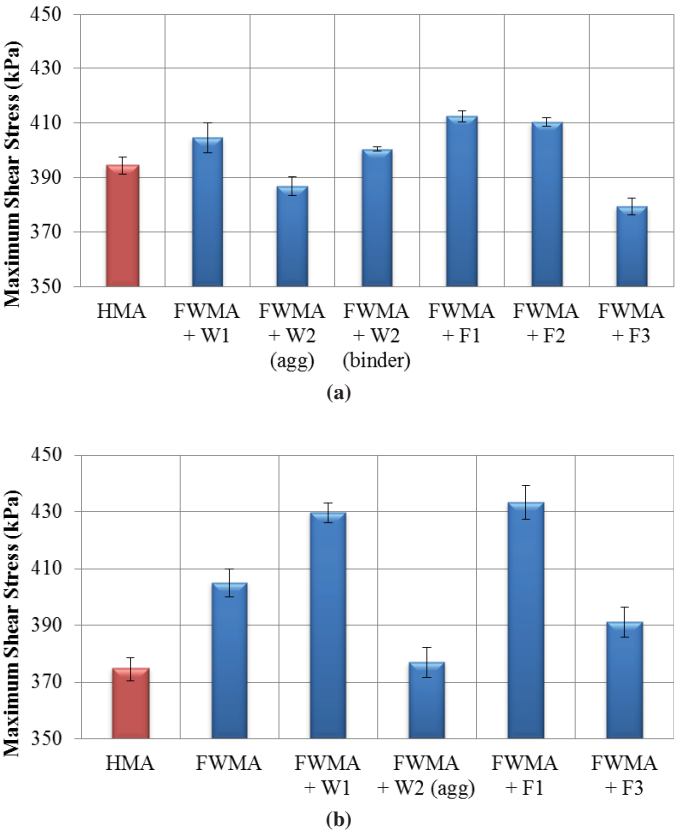


***Figure 3-47. Influence of various liquid additives on mixture workability for (a) binder OM6, (b) binder Y62.***

The lower $\tau_{max}$ for W2 (agg) as compared to W2 (binder) is possibly due to the fact that when additive W2 is combined with the aggregate, it does not start to release water until the mixing process, whereas when it is combined with the binder, the release of water starts well before the start of the mixing process. Thus, in the case of W2 (binder), some of the foamed binder bubbles may collapse between the additive blending and mixing processes and not be available to allow the binder to coat the aggregates to the same extent as the coating achieved by W2 (agg) during mixing.

For both binders, additives W2 (agg) and F3 yielded the best workability. Additives W1, W2 (binder), F1, and F2 had a neutral effect on the workability of the mixtures prepared with binder OM6. However, additives W1 and F1 had a negative impact on the mixtures prepared with Y62, yielding less workable mixtures than the HMA or FWMA without additives.

In the case of the binder, when foamed at 1.0% water content (see Section A.1.4), additive W1 had a negligible effect on the foaming metrics, and additives F1 and F3 had comparable $ER_{max}$ and *k*-values and the best impact on the foaming metrics for binders OM6 and Y62. In the case of the mixtures, W1 also had a negligible or even detrimental effect on workability, while additive F3 had a distinct improved workability as compared to mixtures with additive F1.

## C. Validation of Proposed Mix Design Approach with Various Laboratory Foaming Units

The foamed mix design approach described in Section 2.C was validated using the same laboratory foaming units included in the comparison of laboratory foamers: Wirtgen WLB 10S, InstroTek Accufoamer, and PTI foamer. The materials used for the validation and the results in terms of binder foaming characteristics, mixture workability, coatability, and performance are detailed next.

### C.1. Materials

The binder used for the validation was a Valero PG64-22. The optimum binder content was 4.7%. Details on the aggregate type, source, and gradation are presented in Table 3-9, Table 3-10, and Figure 3-48.

### C.2. Foaming Measurements

The $ER_{max}$ and *k*-value of the binder foaming measurements performed using the Accufoamer, the PTI foamer, and the Wirtgen foamer are illustrated in Figure 3-49. The bars and red squares represent the average $ER_{max}$ and *k*-value of three replicate measurements. The error bars span ±1 standard deviation from the average $ER_{max}$ value.

**Table 3-9. Aggregate source.**

| Aggregate Type | Bin No. 1 | Bin No. 2 | Bin No.3 | Bin No.4 |
|---|---|---|---|---|
| | C Rock | D/F Rock | Screenings | Washed Sand |
| Aggregate Pit | Marble Falls | Marble Falls | Marble Falls | Hallet |

**Table 3-10. Individual aggregate gradation.**

| Aggregate Type | Aggregate % | Sieve Analysis (Cum.% Passing) | | | | | | | |
|---|---|---|---|---|---|---|---|---|---|
| | | 1" | ¾" | 3/8" | #4 | #8 | #30 | #50 | #200 |
| C Rock | 25 | 100 | 99 | 22 | 4.3 | 2.0 | 1.1 | 0.8 | 0.1 |
| D/F Rock | 35 | 100 | 100 | 91 | 22 | 4.2 | 2.4 | 2.2 | 1.5 |
| Screenings | 25 | 100 | 100 | 100 | 99 | 80 | 39 | 25 | 4.2 |
| Washed Sand | 15 | 100 | 100 | 100 | 100 | 100 | 90 | 55 | 3.0 |

As was observed during the comparison of laboratory foamers (Section 3.A.3), binder foam produced in the Wirtgen foamer had the largest $ER_{max}$ values, while that produced in the PTI foamer had the lowest $ER_{max}$ values for three foaming water contents. The comparison in *k*-value showed a similar trend to the one observed for the $ER_{max}$ value. The increases in $ER_{max}$ values and *k*-values of binder foaming produced by the Accufoamer and the Wirtgen foamer are proportional to the water content. However, no significant effect from the water content on the binder foaming characteristics was observed for the binder foam produced in the PTI foamer.

The explanation for the differences in foaming characteristics between the three laboratory foaming units may lie in the way the foam is dispensed. In the Wirtgen foamer, the foam is expelled as soon as the water and binder are combined, whereas the Accufoamer forces the foam through a tube before it is dispensed, which restricts the flow. The PTI foamer allows the foamed binder to be drawn out of the expansion chamber by gravity, which produces an even slower flow of material as compared to the other two foamers, which use air pressure to expel the foamed binder. It appears that the slower the rate of flow, the lower the expansion of the foam.

Figure 3-50 presents the FI values of binder foaming at 1.0%, 2.0%, and 3.0% water contents produced by the Accufoamer and the Wirtgen foamer. The FI was not calculated for the PTI foamer since the binder did not expand and collapsed after foaming with this unit. As illustrated, similar tends in terms of FI values versus elapsed foaming time were observed for binder foaming produced by the Accufoamer and the Wirtgen foamer. In addition, higher FI values (indicating higher stability) for binder foaming produced by the Wirtgen foamer as compared to that produced by the Accufoamer were


***Figure 3-48. Combined aggregate gradation.***

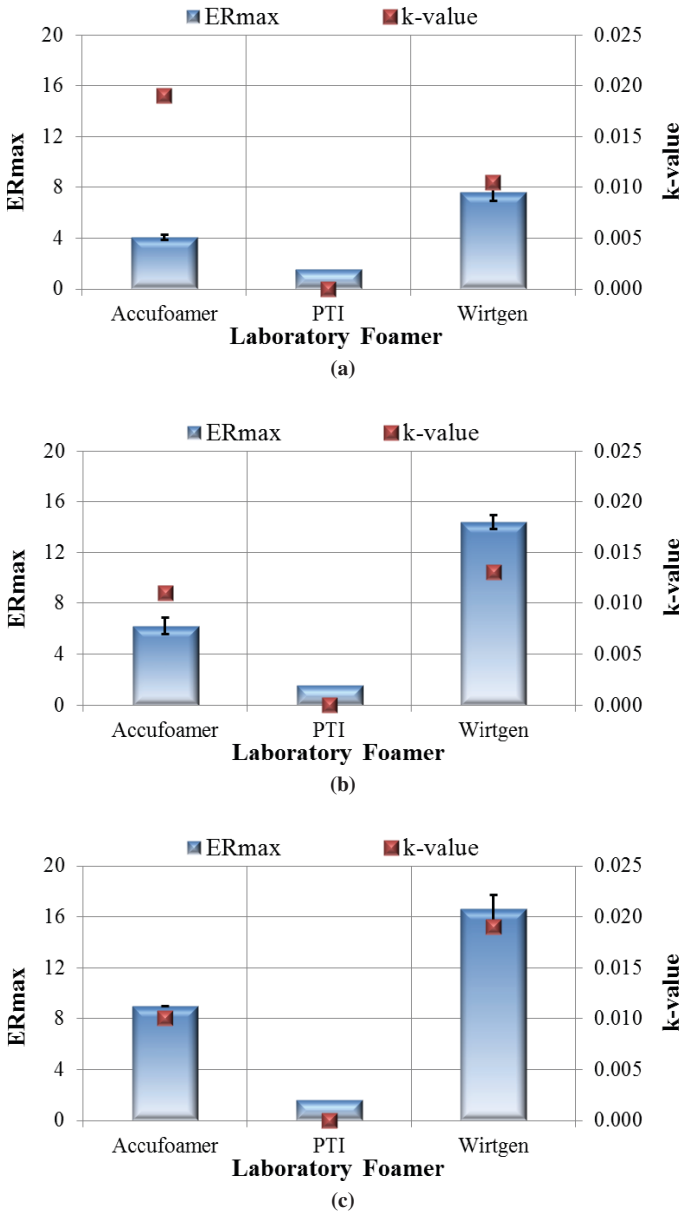


*Figure 3-49. $ER_{max}$ and k-value for various laboratory foaming units; (a) 1.0% water content, (b) 2.0% water content, and (c) 3.0% water content.*

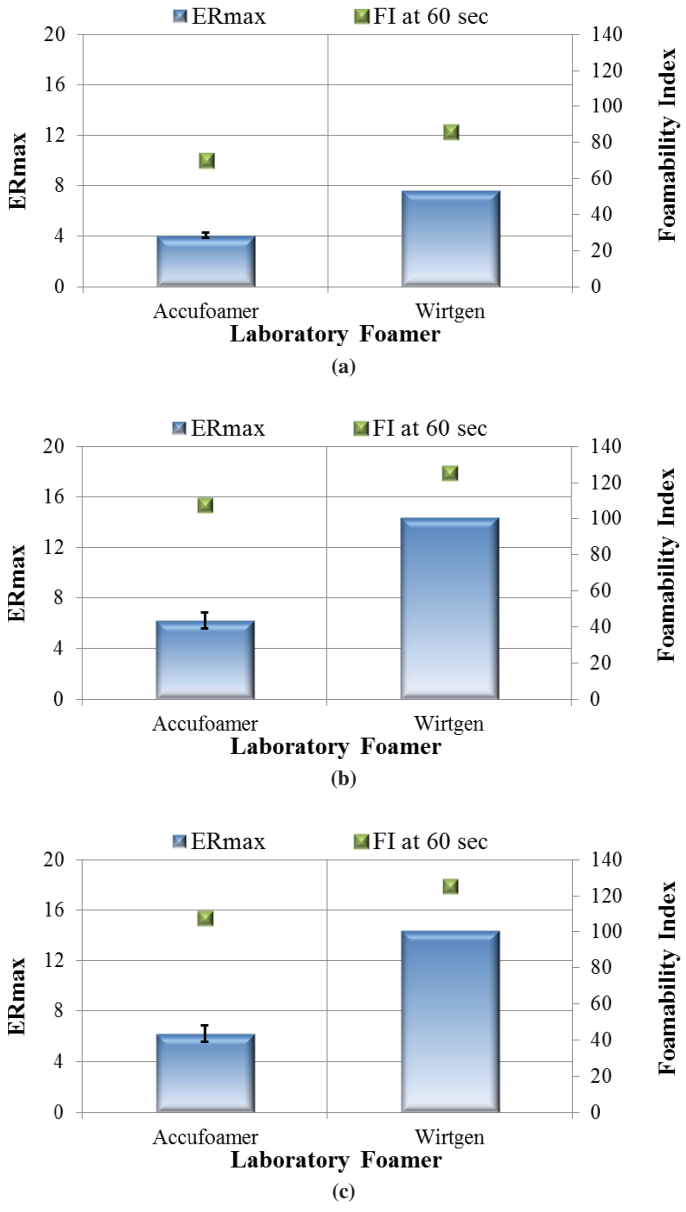


*Figure 3-50. $ER_{max}$ and FI for various laboratory foaming units; (a) 1.0% water content, (b) 2.0% water content, and (c) 3.0% water content.*

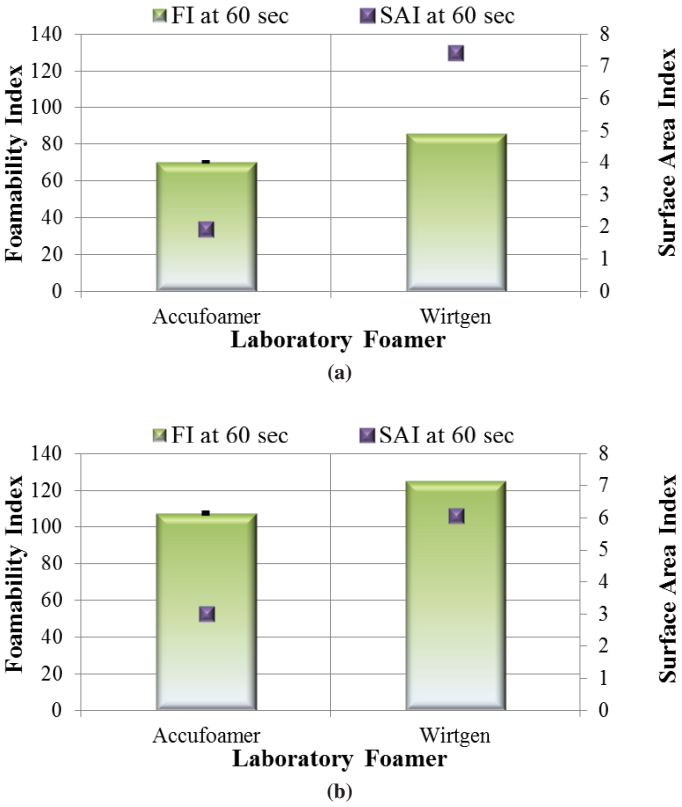


*Figure 3-51. FI and SAI for various foaming units; (a) 1.0% water content and (b) 2.0% water content.*

observed for 1.0% and 2.0% water contents, while the opposite trend was shown for 3.0% water content.

SAI values exhibited a gradual reduction with the elapsed foaming time, which was mainly attributed to the collapse of the binder foam. Figure 3-51 presents the SAI values at 60 s of binder foaming at 1.0% and 2.0% water contents produced by the Accufoamer and the Wirtgen foamer. The SAI values for binder foaming produced by the PTI foamer were not determined since no apparent foam bubbles were observed during the foaming process. Higher SAI at 60 s values were observed for binder foaming produced by the Wirtgen foamer as compared to those produced by the Accufoamer. Therefore, as compared to the Accufoamer, the Wirtgen foamer was able to produce more semi-stable foam bubbles, which were smaller in size but had larger surface area.

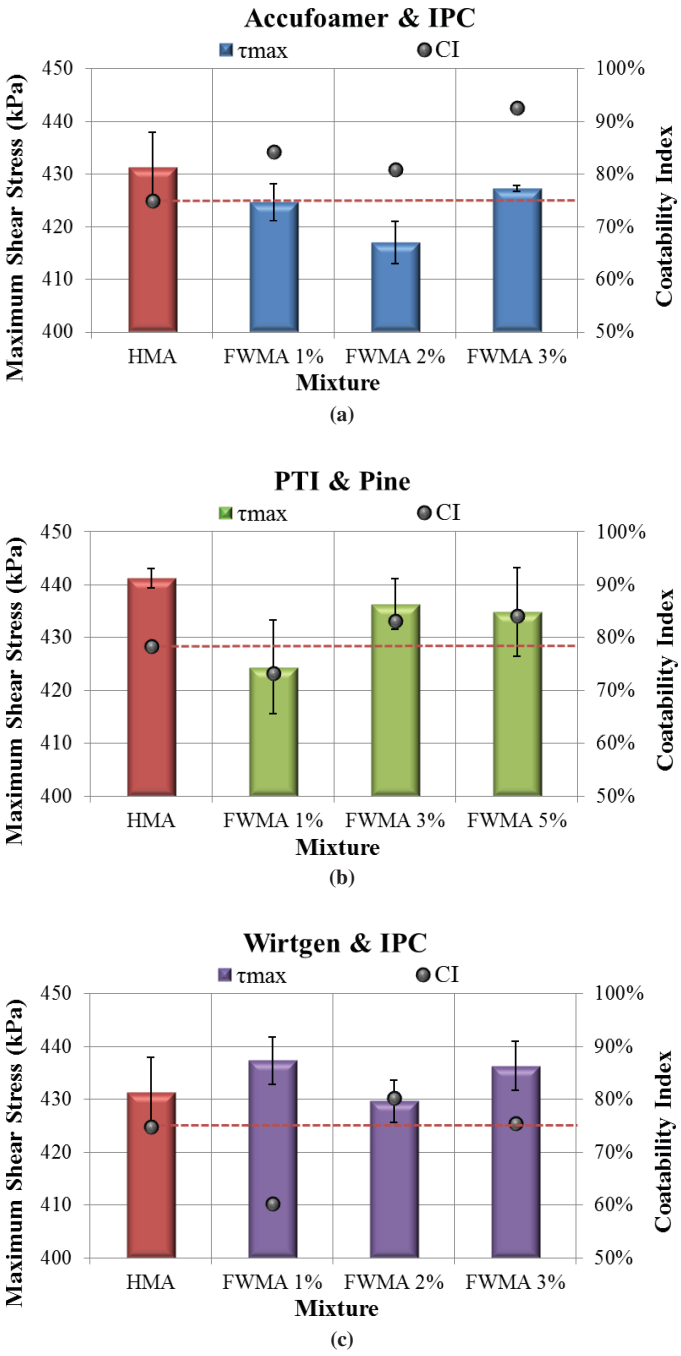


*Figure 3-52. Workability and coatability results for the control HMA and foamed mixture; (a) produced in the Accufoamer, (b) produced in the PTI foamer, and (c) produced in the Wirtgen foamer.*

## C.3. Mixture Workability and Coatability Measurements

The workability and coatability results for foamed laboratory-mixed, laboratory-compacted (LMLC) specimens fabricated using the Accufoamer, the PTI foamer, and the Wirtgen foamer are shown in Figure 3-52. The bars represent the average maximum shear stress of three replicate measurements, and the error bars span ±1 standard deviation from the average value. The dots represent the CI values of foamed mixtures at different water contents and the control HMA.

Figure 3-52(a) presents the workability and coatability results for the control HMA and the foamed mixture produced by the Accufoamer. The workability evaluation for these two mixtures was performed using an IPC SGC. As illustrated,

better mixture workability and coatability characteristics were shown for foamed mixtures at three different foaming water contents as compared to the control HMA, as indicated by lower maximum shear stress values and higher CI values. In addition, the selected optimum foaming water content for the foamed mixture produced in the Accufoamer was 2.0%, which was able to produce a foamed mixture with the best workability and coatability characteristics as compared to the HMA control.

Figure 3-52(b) presents the workability and coatability results for the control HMA and the foamed mixture produced by the PTI foamer. The workability evaluation for these two mixtures was performed using a Pine SGC. Mixture workability results shown in Figure 3-52(b) illustrate that foamed mixtures at 1.0%, 3.0%, and 5.0% had better or equivalent workability than the control HMA, as indicated by lower or equivalent maximum shear stress values. This trend was observed despite the PTI foamer resulting in practically null expansion, as shown in Figure 3-49. Therefore, binder foaming characteristics and foamed mixture properties may not have a direct relationship for all foaming units. A different trend was observed for coatability results, where higher CI values versus that of the control HMA were shown for foamed mixtures at 3.0% and 5.0% water contents, while the opposite trend was shown for foamed mixtures at 1.0% water content. According to the mix design approach described in Section 2.C, 5.0% was selected as optimum water content for the foamed mixture produced in the PTI foamer.

Figure 3-52(c) presents the workability and coatability results for the control HMA and the foamed mixture produced by the Wirtgen foamer. The workability evaluation for these two mixtures was performed using an IPC SGC at the Texas A&M Transportation Institute (TTI). As illustrated in Figure 3-52(c), equivalent or higher maximum shear stress values were achieved by foamed mixtures than by the control HMA, indicating equivalent or worse mixture workability characteristics. The coatability results in terms of CI values indicated that, as compared to the control HMA, equivalent or better mixture coatability was obtained by foamed mixtures at 2.0% and 3.0% water contents, while the opposite trend was shown for foamed mixture at 1.0% water content. Therefore, 2.0% was selected as the optimum foaming water content for the foamed mixture produced in the Wirtgen foamer.

## C.4. Performance Evaluation

To evaluate the performance of the foamed mixtures at their optimum foaming water contents, a new set of LMLC specimens were fabricated at 2.0%, 5.0%, and 2.0% water contents using the Accufoamer, the PTI foamer, and the Wirtgen foamer, respectively. In addition, a companion set of HMA LMLC specimens was produced. Foamed mixtures were mixed at 275°F (135°C) and then short-term aged for 2 hours at 240°F (116°C) prior to compaction. The control HMA was mixed at 290°F (143°C) and then short-term aged for 2 hours at 275°F (135°C). The compacted specimens were then tested to measure $M_R$, IDT strength, and HWTT. Testing parameters, including $M_R$ stiffness at 77°F (25°C), wet IDT strength and TSR at 77°F (25°C), HWTT load cycles to stripping number ($LC_{SN}$), load cycles to remaining life ($LC_{ST}$), and viscoplastic strain at $LC_{SN}$ ($\Delta\varepsilon_{SN}^{vp}$) at 122°F (50°C), were used to evaluate mixture stiffness, rutting resistance, and moisture susceptibility and to compare the performance of foamed mixtures to the control HMA.

$LC_{SN}$ represents the maximum number of load cycles that the asphalt mixture can resist in the HWTT before the adhesive fracture between the asphalt binder and the aggregate occurs; it is assessed by measuring the change in curvature from positive to negative of the rut depth versus the load-cycle curve. Mixtures that do not show a stripping phase in the HWTT are considered to have a robust resistance to moisture damage, with $LC_{SN}$ values larger than the number of load cycles applied during the test (e.g., 20,000). $LC_{ST}$ represents the number of additional load cycles after $LC_{SN}$ needed for the rut depth accumulated by the stripping strain to reach 0.5 in. (12.5 mm), which is the common HWTT failure criterion adopted by several agencies. $\Delta\varepsilon_{SN}^{vp}$ can be calculated as the ratio of the rut depth to the specimen thickness at any given number of load cycles up to $LC_{SN}$. A detailed description of the derivation and equations of the HWTT parameters can be found in Yin et al. (2014).

### C.4.1. Resilient Modulus Test

The results for $M_R$ stiffness at 77°F (25°C) for foamed mixtures at optimum foaming water contents produced by the Accufoamer, the PTI foamer, the Wirtgen foamer, and the control HMA are shown in Figure 3-53. Each bar represents

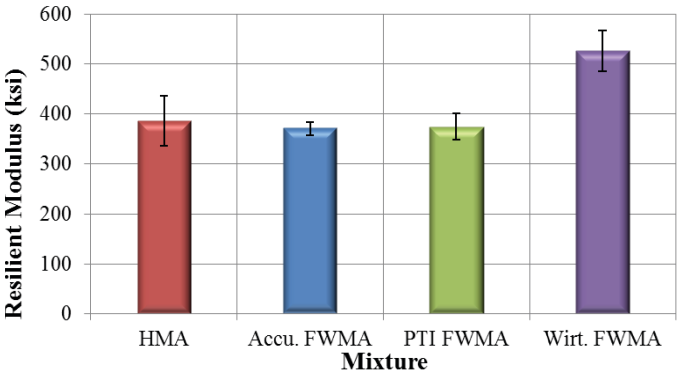


***Figure 3-53. $M_R$ at 77°F (25°C) test results for foamed mixtures produced in different laboratory foamers versus the control HMA.***

the average $M_R$ stiffness value of three replicates, and the error bars represent ±1 standard deviation from the average value.

As illustrated in Figure 3-53, equivalent $M_R$ stiffness was achieved by the control HMA, the foamed mixture produced by the Accufoamer (at 2.0% water content), and the foamed mixture produced by the PTI foamer (at 5.0% water content). In addition, a significantly higher $M_R$ stiffness was observed by the foamed mixture produced by the Wirtgen foamer. Therefore, inclusion of additional water and lower production and short-term aging temperature involved in the fabrication of foamed mixtures did not reduce the mixture stiffness.

### C.4.2. Indirect Tensile Strength Test

Three specimens were tested in a dry condition and three specimens after moisture conditioning following the procedure outlined by AASHTO T 283. The wet IDT strength and TSR value at 77°F (25°C) were considered as indicators of mixture moisture susceptibility. The IDT strength test results for foamed mixtures produced by three laboratory foamers and the control HMA are shown in Figure 3-54. The solid bar and pattern-filled bar represent the average dry and wet IDT strength, respectively. The error bars represent ±1 standard deviation from the average value. In addition, the TSR values are shown above the IDT strength bars.

Figure 3-54 illustrates that equivalent dry IDT strength at 77°F (25°C) was achieved by the three foamed mixtures and the control HMA. However, a significant reduction in IDT strength was observed for all mixtures after moisture conditioning per AASHTO T 283, which was likely due to the poor moisture resistance of the binder used in the mix. The comparison of wet IDT strength among foamed mixtures and the control HMA indicated that equivalent wet IDT strengths were achieved by the foamed mixtures produced in different laboratory foamers at their corresponding optimum water contents, which were significantly lower than the wet IDT strength for the HMA control. As a consequence, a higher TSR value was observed for the control HMA than the foamed mixtures, indicating better moisture resistance in the IDT strength test.

### C.4.3. Hamburg Wheel Tracking Test

The HWTT was performed at 122°F (50°C) following AASHTO T 324, and test parameters including $LC_{SN}$, $LC_{ST}$, and $\Delta\varepsilon_{SN}^{vp}$ were used to evaluate mixture moisture susceptibility and rutting resistance. HWTT results in terms of rut depth versus load cycle for foamed mixtures produced in the Accufoamer, the PTI foamer, the Wirtgen foamer, and the control HMA are shown in Figure 3-55.

As illustrated in Figure 3-55, both HMA and foamed mixtures did not pass the failure criteria of 20,000 load cycles with less than the 0.5-in. (12.5-mm) rut depth of Texas Department of Transportation (TxDOT) specifications. An equivalent creep slope was observed for all mixtures, while distinct differences in stripping slopes were shown, indicating different moisture susceptibility.

Figure 3-56 presents the $LC_{SN}$ and $LC_{ST}$ results of foamed mixtures produced in different laboratory foamers versus the control HMA. Test results shown in Figure 3-56 illustrate that HMA had better moisture susceptibility than the foamed mixtures, as indicated by higher $LC_{SN}$ and $LC_{ST}$ values. The reduced moisture resistance for the foamed mixture as compared to the control HMA could be attributed to the lower production and aging temperature involved in the mixture fabrication process.

The comparison of foamed mixtures illustrated that the foamed mixture produced in the Accufoamer at 2.0% water content had the best moisture susceptibility, followed by that produced in the Wirtgen foamer at 2.0% water content, and finally the mixture produced in the PTI foamer at 5.0% water content. Since the optimum water content for the mixture

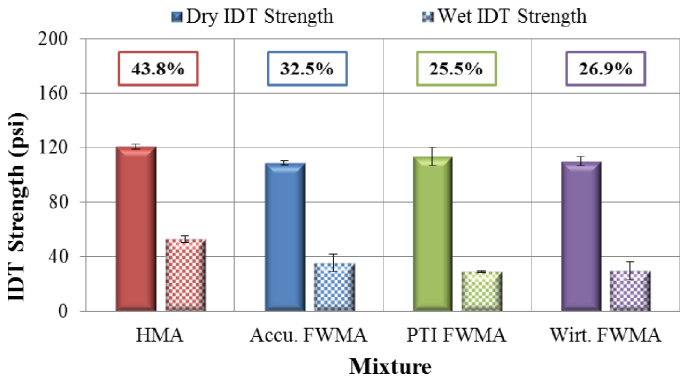


*Figure 3-54. IDT strength test results for foamed mixtures produced in different laboratory foamers versus the control HMA.*

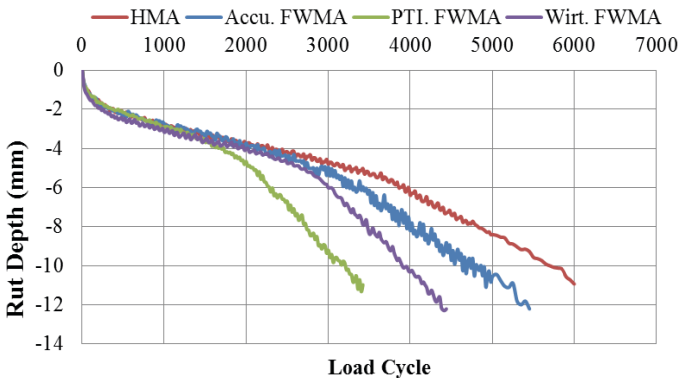


*Figure 3-55. HWTT rut depth versus load cycle for foamed mixtures produced in different laboratory foamers versus the control HMA.*

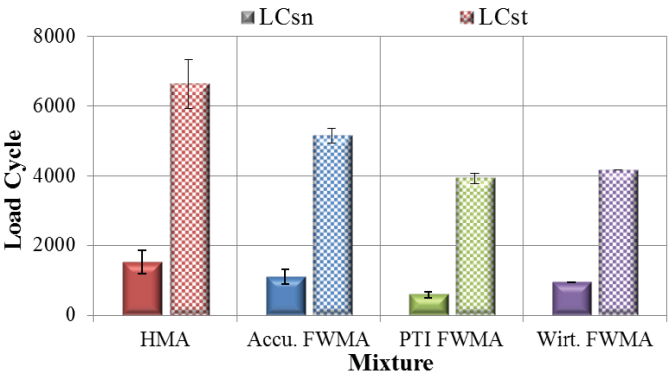


***Figure 3-56. HWTT $LC_{SN}$ and $LC_{ST}$ results for foamed mixtures produced in different laboratory foamers versus the control HMA.***

produced in the PTI foamer was established by comparing the CI of the foamed mixture against the CI of the HMA, a better approach would be to have a set CI threshold instead of comparing against the HMA value. Based on the results listed in Chapter 3, Section C.2, a CI threshold of 70% seems to be reasonable for all mixtures. If this new criterion was applied to the PTI foamer results, an optimum water content of 1.0% would have been selected instead of 5.0%.

The $LC_{SN}$ values for both HMA and foamed mixtures were less than 2,000 load cycles; therefore, all mixtures exhibited early stripping during the HWTT. As a consequence, the determination of the viscoplastic deformation and the rutting resistance parameter $\Delta\varepsilon_{SN}^{vp}$ was not possible due to the limited duration of the creep phase.

CHAPTER 4

# Findings and Applications: Field Studies

The test methods and metrics described in Chapter 2 were employed in various field settings to evaluate their applicability to on-site locations, their usefulness in describing the binder foaming characteristics of various plant foaming units, and their ability to differentiate specimens prepared in the laboratory and the field. In addition, the proposed foamed mix design was validated with plant data.

## A. Initial Trial

An initial plant field trial took place in Austin, Texas, on October 3, 2013. The template for field data acquisition shown in Appendix D was used to collect information about the plant characteristics. The plant type was a counterflow dryer drum (Figure 4-1) with a Maxam foaming unit installed in-line with an approximate 30-ft (9-m) run between the foamer and the inlet into the drum, an approximate 4- to 5-ft vertical rise, and extending into the drum about 8 ft. The pipeline was 4 in. in diameter and insulated. The day of the field test, conditions were fair and dry, temperatures were in the 70s, and a mild wind of 2 mph was blowing. The plant had a capacity of producing 300 tons of material each hour. The specific mix design being produced during the research team's visit is given in the following.

The foaming unit was suspended approximately 10 ft above ground level. In order to sample the material from the foaming unit, a ¾-in. pipe extension approximately 6 ft long was inserted into the sampling port (Figure 4-2). The moisture level in the foamed binder was supposed to be 2.5%. A small water leak was noted on the foaming unit during its normal operation prior to sampling. The effect of this leak on the water content of the foam is not known, although measurements on the foamed binder indicated that foaming had occurred. Control of the sampling valve required access with a ladder (Figure 4-2) while the sample was collected below.

In attempting to sample the foamed binder, it was found that the pipe extension caused the binder to cool and clog the line to the point that only a relatively thin stream of material flowed out of the pipe. After sampling in this manner, laser expansion and bubble size measurements were taken following the procedure detailed in Appendix B. Two replicate measurements were done using the extension pipe. Later, a sample was taken from the sampling port with no pipe extension. Although the foaming properties of this sample were more in line with what the team had seen in laboratory efforts (faster binder flow and better foaming), it was considered too dangerous to repeat sampling. Therefore, only one foaming measurement was done after the extension pipe was removed.

### A.1. Materials

The binder used in this plant was a PG64-22 by NuStar Logistics, L.P. The optimum binder content was 5.1%. Limestone was the primary aggregate type used in the mix design. Other aggregates such as field sand and fractioned reclaimed asphalt pavement (RAP) were used. Details on the aggregate type, source, and gradation are presented in Table 4-1, Table 4-2, and Figure 4-3.

### A.2. Foaming Measurements

#### *A.2.1. Effect of Container Size*

A 1-gallon metal can was employed during the laboratory studies to conduct all foamed binder measurements. Because of concerns of potential splash and binder overflow when sampling in the field, a 5-gallon bucket was preferred for all field studies. Ideally, the expansion ratio of the foamed binder should be independent of the size of the container and the amount of binder dispensed since these variables are taken into account when calculating ER (i.e., determination of $h_{final}$, using the density calculation method or the binder weight–height calibration). The effect of container size was evaluated to verify the equivalency of the measurements using binders from two sources.

*Figure 4-1. Counterflow drum plant, Austin, Texas.*

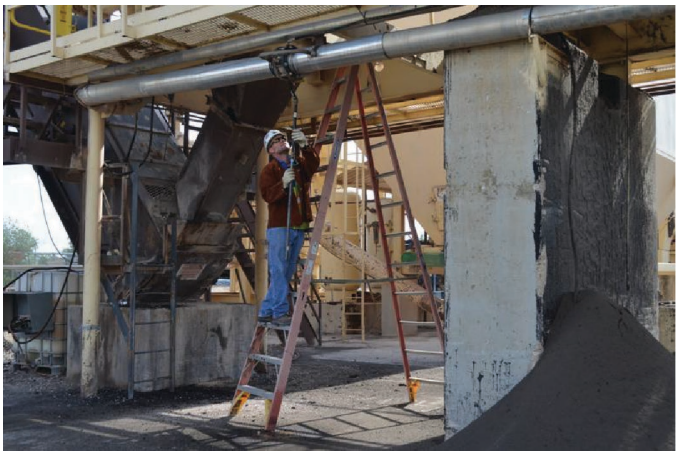

*Figure 4-2. Maxam Aquablack foam sampling port, Austin, Texas.*

**Table 4-1. Aggregate source, Austin, Texas.**

| | Bin No. 1 | Bin No. 2 | Bin No.3 | Bin No.4 | Bin No.5 |
|---|---|---|---|---|---|
| **Aggregate Type** | Limestone | Limestone | Limestone | Field Sand | Fractioned RAP |
| **Aggregate Pit** | Marble Falls | Marble Falls | Marble Falls | – | – |

**Table 4-2. Aggregate gradation, Austin, Texas.**

| | Sieve Analysis (Cum.% Passing) | | | | | | | | |
|---|---|---|---|---|---|---|---|---|---|
| **Aggregate Type** | **%** | **¾"** | **½"** | **⅜"** | **#4** | **#8** | **#30** | **#50** | **#200** |
| Limestone | 34.0 | 100 | 100 | 90.7 | 22.1 | 5.3 | 3.4 | 3.0 | 2.2 |
| Limestone | 11.0 | 100 | 100 | 100 | 69.1 | 7.1 | 2.1 | 1.7 | 1.1 |
| Limestone | 25.0 | 100 | 100 | 100 | 99.5 | 85.5 | 43.4 | 25.8 | 2.8 |
| Field Sand | 9.9 | 100 | 100 | 100 | 99.5 | 97.7 | 80.6 | 50.1 | 14.2 |
| Fractioned RAP | 20.1 | 100 | 100 | 94.0 | 68.1 | 49.3 | 31.5 | 23.2 | 7.1 |
| Combined Gradation | 100 | 100 | 100 | 95.6 | 63.5 | 43.5 | 26.5 | 17.3 | 4.4 |

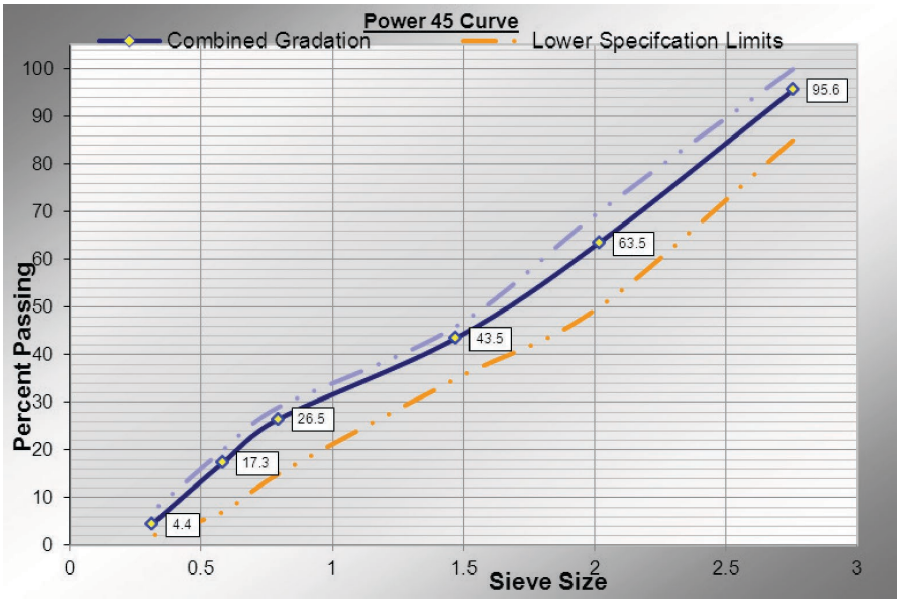


*Figure 4-3. Combined aggregate gradation, Austin, Texas.*
*Note: Dashed purple line is the upper specification limit.*

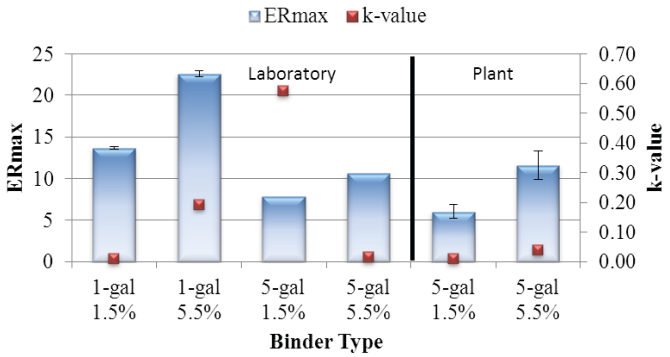


***Figure 4-4. Comparison of $ER_{max}$ and k-value for field and laboratory binder foam measurements using 1-gallon and 5-gallon containers.***

From the $ER_{max}$ and *k*-value results for the first binder that are presented in Figure 4-4, it is apparent that the container size did have an influence in the measurements, with higher ER and *k*-value for the 1-gallon can measurements versus the measurements performed in the 5-gallon bucket. This difference was more pronounced at higher water contents (i.e., 5.5%). The *k*-value for the laboratory measurements done in the 5-gallon container with 1.5% water content was considerably higher than any of the other measurements. The ratios between the 1-gallon and 5-gallon average $ER_{max}$ values measured in the laboratory were 1.7 and 2.1 for the 1.5% and 5.5% water contents, respectively. The difference between measurements using the 5-gallon container in the lab and in the plant was less pronounced. In this case, the largest difference in average $ER_{max}$ values was for the 1.5% water content with a 1-gallon to 5-gallon ratio of 1.3.

The second binder tested (i.e., binder R6 in Table 3-1) corroborated the observed differences in container size. $ER_{max}$ and *k*-value are illustrated in Figure 4-5. As in the case of the first binder, the 1-gallon container had larger values than the 5-gallon container did, and the difference was more pronounced at higher water contents. In this case, the ratios between the 1-gallon and 5-gallon average $ER_{max}$ values were 2.0 and 2.2 for the 1.0% and 3.0% water content, respectively.

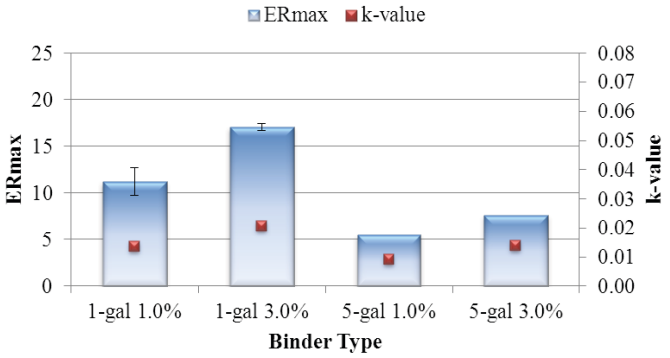


***Figure 4-5. Comparison of $ER_{max}$ and k-value for binder R6 using 1-gallon and 5-gallon containers.***

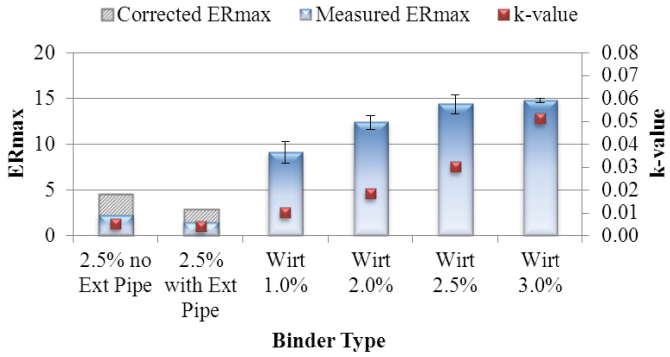


***Figure 4-6. On-site and laboratory $ER_{max}$ and k-value for the initial trial in Austin, Texas.***

When combined with the values of the first binder tested, an average ratio between the 1-gallon and 5-gallon $ER_{max}$ values of 2.0 was obtained.

From these observations, it is apparent that the size of the container used to conduct the foaming measurements had an impact on the results. The rest of the field $ER_{max}$ values collected in this study were corrected by a factor of 2.0 to make them comparable to the laboratory measurements. In addition, it is suggested to use the same size container when following the steps of the proposed mix design methodology or to compare the characteristics of different foamed binders.

### *A.2.2. On-Site and Laboratory Measurements*

The average of the two replicate measurements with the extension pipe and the single measurement collected when the extension pipe was removed is presented along with the average of two replicate measurements performed in the laboratory using the Wirtgen foamer. Figure 4-6 presents the $ER_{max}$ and *k*-value, while Figure 4-7 illustrates the FI obtained with the binder foam field and laboratory measurements. The corrected $ER_{max}$ values correspond to the modified field measurements after applying the container size correction

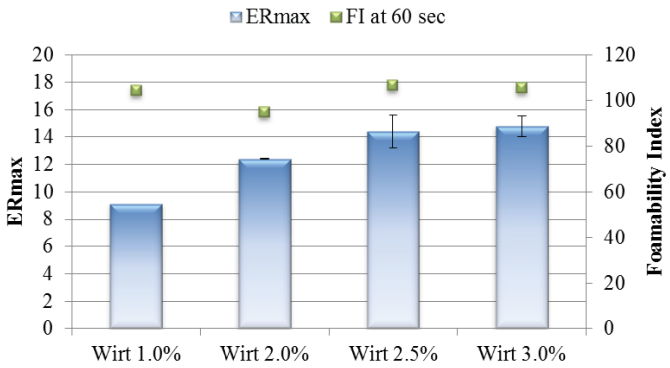


***Figure 4-7. $ER_{max}$ and FI for on-site and laboratory binder foam measurements for the initial trial in Austin, Texas.***

factor of 2.0. The error bars in Figure 4-6 span ±1 standard deviation from the average $ER_{max}$ value.

From Figure 4-6, it is apparent that the $ER_{max}$ of the field specimen without the extension pipe was only about 65% of the measurement obtained when the extension pipe was used. As mentioned before, the pipe extension likely caused the binder to cool and clog the line. Also, the $ER_{max}$ for both field measurements (with and without the extension pipe) was significantly lower than the $ER_{max}$ values obtained using the Wirtgen foamer, even after the container size correction factor was applied. As before, $ER_{max}$ and *k*-value had a direct correlation with the water content used to foam the binder; the higher the water content, the higher $ER_{max}$ and *k*-value (less stable foam).

The FI presented in Figure 4-7 illustrates the area under the ER curve at 60 s after foaming. Only the laboratory FI values are presented since the differences in container size yielded smaller field FI values that were not comparable on the same scale. The FI values were similar for all water contents.

The SAI is illustrated in Figure 4-8. Contrary to the FI trends that showed practically no difference between water contents, the SAI shows clear distinction between mixtures foamed with 1.0%, 2.0%, 2.5%, and 3.0% water content. The larger the water content, the smaller the SAI, which indicates that the binder is less stable after foaming, and fewer small-sized, long-lasting bubbles are formed.

## A.3. Mixture Workability Measurements

The workability results for plant-mix laboratory-compacted (PMLC) and LMLC specimens fabricated at 1.0%, 2.0%, 2.5%, and 3.0% foaming water contents are shown in Figure 4-9. Each bar in Figure 4-9 represents the average value of three replicates, and the error bars represent ±1 standard deviation from the average value.

As shown in Figure 4-9, a significantly lower maximum shear stress ($\tau_{max}$) value was shown for the PMLC specimen as compared to LMLC specimens at different foaming water contents,

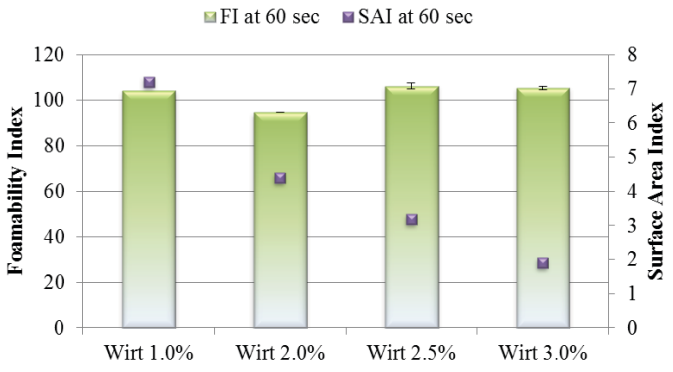


***Figure 4-8. FI and SAI for on-site and laboratory binder foam measurements for the initial trial in Austin, Texas.***

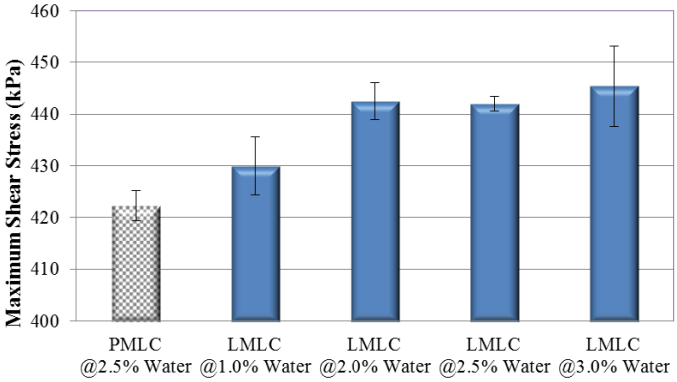


***Figure 4-9. Workability results for Austin mixtures.***

which indicated that the PMLC specimen had a better workability than the LMLC counterparts. The comparison in workability of LMLC specimens with different foaming water contents illustrated that the LMLC specimen at 1.0% foaming water content had better workability characteristics (indicated by a lower $\tau_{max}$ value) as compared to those foamed at higher water contents (i.e., 2.0%, 2.5%, and 3.0%). Therefore, 1.0% was the optimum foaming water content for this certain mixture.

## A.4. Performance Evaluation

To evaluate the performance of foamed mixtures at the optimum foaming water content, a new set of LMLC specimens were fabricated at 1.0% foaming water content using the Wirtgen foamer. In addition, another set of HMA LMLC specimens was also produced. Both the foamed mixture and the control HMA were mixed at 305°F (152°C) and then short-term aged for 2 hours at 275°F (135°C) prior to compaction. Then, the compacted specimens were tested for $M_R$, IDT strength test, and HWTT. Testing parameters, including $M_R$ stiffness, wet IDT strength, and TSR at 77°F (25°C), and HWTT $LC_{SN}$, $LC_{ST}$, and $\Delta\varepsilon_{SN}^{vp}$ at 122°F (50°C) and 104°F (40°C), were used to evaluate mixture stiffness, rutting resistance, and moisture susceptibility and to compare the performance of the foamed mixture versus the control HMA.

### *A.4.1. Resilient Modulus Test*

The $M_R$ stiffness results for the foamed mixture and the control HMA are shown in Figure 4-10. Each bar in Figure 4-10 represents the average $M_R$ stiffness value of three replicates, and the error bars represent ±1 standard deviation from the average value.

As illustrated in Figure 4-10, equivalent $M_R$ stiffness at 77°F (25°C) was achieved by the control HMA and the foamed mixture at 1.0% foaming water content. Thus, in this case the inclusion of water from the foaming process did not reduce the mixture stiffness.

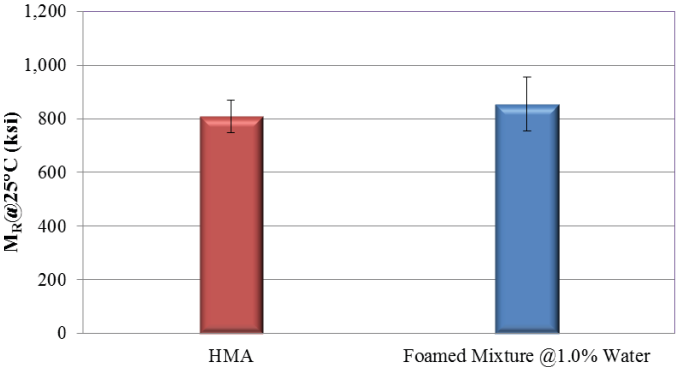


*Figure 4-10. $M_R$ test results for Austin mixtures.*

### A.4.2. Indirect Tensile Strength Test

Three specimens were tested in a dry condition and three specimens after moisture conditioning following the procedure outlined by AASHTO T 283. The wet IDT strength and TSR value at 77°F (25°C) were considered as indicators of mixture moisture susceptibility. The IDT strength test results for the foamed mixture and the control HMA are shown in Figure 4-11. The solid bar and pattern-filled bar represent the average dry and wet IDT strength, respectively. The error bars represent ±1 standard deviation from the average value. In addition, the TSR values are shown on top of the IDT strength bars.

As illustrated in Figure 4-11, equivalent dry IDT strength at 77°F (25°C) was achieved by the control HMA and the foamed mixture at 1.0% foaming water content. However, a significantly higher wet IDT strength and, subsequently, a higher TSR value, were shown by the foamed mixture as compared to the control HMA, which indicated that the foamed mixture produced at the optimum foaming water content had lower moisture susceptibility than the control HMA in the IDT strength test.

### A.4.3. Hamburg Wheel Tracking Test

The HWTT was performed at 122°F (50°C) following AASHTO T 324, and test parameters, including $LC_{SN}$, $LC_{ST}$, and

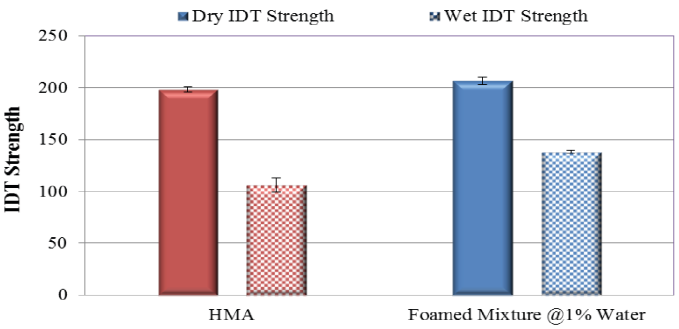


*Figure 4-11. IDT strength test results for Austin mixtures.*

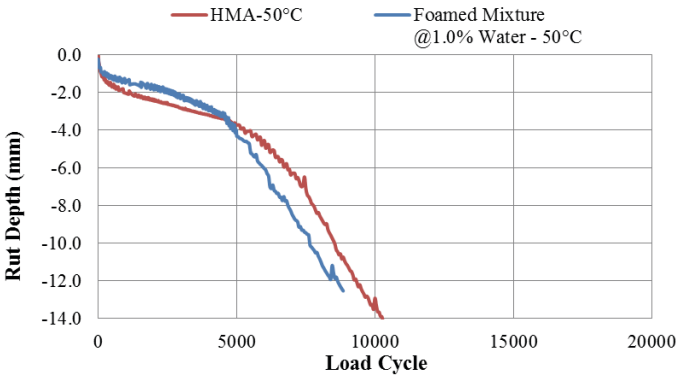


*Figure 4-12. HWTT rut depth versus load cycles at 122°F (50°C) for Austin mixtures.*

$\Delta\varepsilon_{SN}^{vp}$, were used to evaluate moisture susceptibility and rutting resistance. HWTT results for the control HMA and the foamed mixture at 1.0% foaming water content are shown in Figure 4-12.

As illustrated, the mixtures did not pass the failure criteria of 20,000 load cycles with less than 0.5-in. (12.5-mm) rut depth. Figure 4-13 shows the $LC_{SN}$, $LC_{ST}$, and $\Delta\varepsilon_{SN}^{vp}$ of the foamed

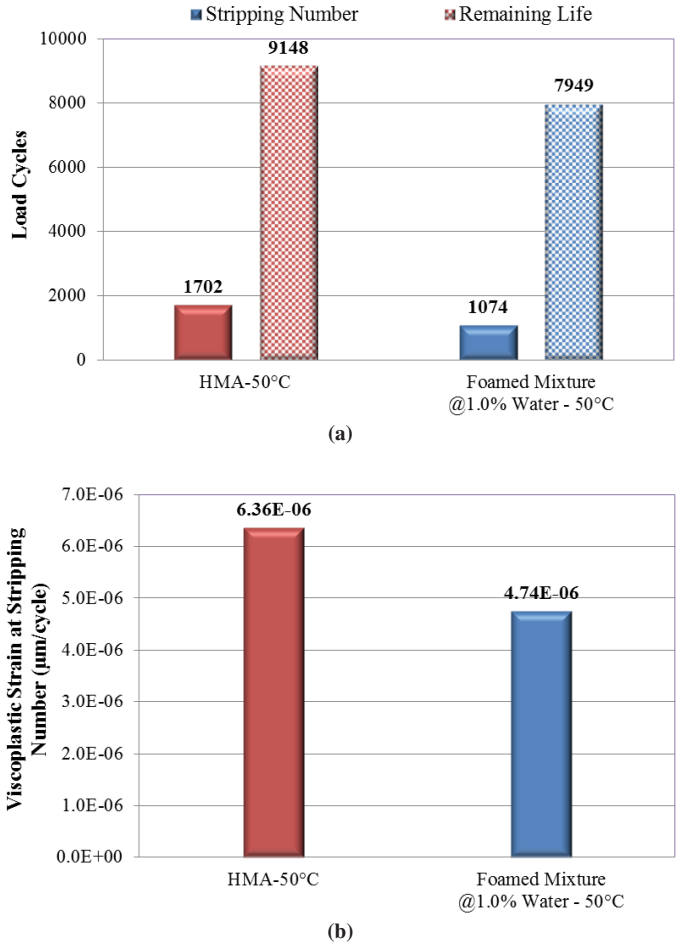


*Figure 4-13. HWTT results at 122°F (50°C) for Austin mixtures; (a) $LC_{SN}$ and $LC_{ST}$, and (b) $\Delta\varepsilon_{SN}^{vp}$.*

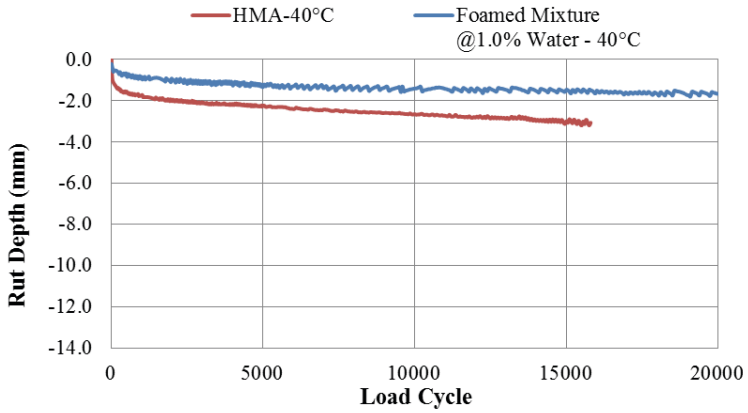


***Figure 4-14. HWTT rut depth versus load cycles at 104°F (40°C).***

mixture versus the control HMA at the test temperature of 122°F (50°C). As shown in Figure 4-13(a), slightly higher $LC_{SN}$ and $LC_{ST}$ values were shown for the control HMA as compared to the foamed mixture, indicating better moisture resistance. The $LC_{SN}$ values for both mixtures were less than 2,000 load cycles, and therefore, both mixtures experienced early stripping during the test at 122°F (50°C). Test results presented in Figure 4-13(b) illustrated that the control HMA had a $\Delta\varepsilon_{SN}^{vp}$ approximately 1.5 με/cycle (equivalent to rut depth of 0.09 mm per 1,000 load cycles) higher than the foamed mixture did. Thus, better rutting resistance was exhibited by the foamed mixture at 1.0% foaming water content than the control HMA in the HWTT at 122°F (50°C).

Laboratory experience with the HWTT shows that for an asphalt mixture exhibiting early stripping (i.e., $LC_{SN}$ less than 2,000 load cycles), the determination of the viscoplastic deformation and the rutting resistance parameter $\Delta\varepsilon_{SN}^{vp}$ is likely to be biased due to the limited duration of the creep phase. Therefore, to better evaluate the rutting resistance of the foamed mixture and the control HMA in the HWTT, the test was performed at a lower temperature [i.e., 102°F (40°C)], with HWTT results in terms of rut depth versus load cycle shown in Figure 4-14.

As illustrated, no stripping occurred for either mixture during the entire test ($LC_{SN}$ equaled 20,000 load cycles), and both mixtures passed the failure criteria of 20,000 load cycles with less than 0.5-in. (12.5-mm) rut depth. The $\Delta\varepsilon_{SN}^{vp}$ results at 102°F (40°C) for the foamed mixture and the control HMA are shown in Figure 4-15. As illustrated, both mixtures had insignificant viscoplastic deformation (indicated by $\Delta\varepsilon_{SN}^{vp}$ values lower than $10^{-6}$ με/cycle) due to the wheel load, and more specifically, a higher $\Delta\varepsilon_{SN}^{vp}$ value was shown for the control HMA as compared to the foamed mixture at 1.0% foaming water content. Thus, the foamed mixture at 1.0% foaming water content had better rutting resistance at 40°C in the HWTT than the control HMA, despite the inclusion of additional moisture involved in the foaming process.

## B. Comparison of Plant Foaming Units

Two plants in the Cincinnati, Ohio, area and operated by the same material supplier were visited by the research team on November 5 and 6, 2013, although originally three plants had been planned. The temperatures were falling at this point in time, and operations for this contractor were ending. Since the source of binder for the two plants was the same, this was seen as an opportunity to test two different plant foamers using the same binder. This trip was facilitated by the contractor's laboratory, which possessed SGCs with shear stress measuring capabilities. Thus, the research team was able to test PMLCs shortly after they were mixed.

### B.1. Description

#### *B.1.1. Plant 1*

This plant, located in Cleves, Ohio, was a counterflow plant with a continuous pugmill or coater box (Figure 4-16) to provide mixing. The plant had a capacity of 300 tons per hour

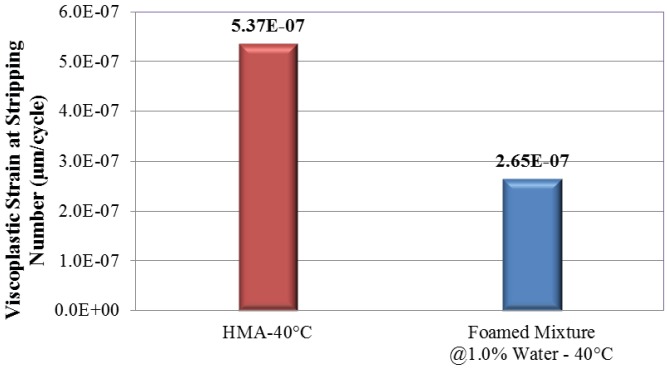


***Figure 4-15. HWTT $\Delta\varepsilon_{SN}^{vp}$ results at 104°F (40°C) for Austin mixtures.***

*Figure 4-16. Coater box, Plant 1, Cincinnati, Ohio.*

*Figure 4-18. Location of foam sampling port and heating to loosen valve, Plant 1, Cincinnati, Ohio.*

with a Gencor foamer (Figure 4-17), and the details of the mix being produced during the team's visit are given in the following. The foaming water content used during production was 1.5%. The foaming unit was located about 12 ft from the binder inlet to the coater box with a 3-ft drop and 5 ft to the sampling port. The binder line was 4 in. in diameter. Temperatures for that day were around 50°F, the skies were overcast, winds were calm, and rain was intermittent.

The sampling port for the foaming unit was about 3 ft away from the foaming unit itself, and although it was accessible from a platform, there was low overhead clearance (Figure 4-18). Because the sampling port had not been used before, it was necessary to heat the valve in order to turn it (Figure 4-18). Once the valve was loosened sufficiently to open it, the flow of the binder was restricted (Figure 4-19), possibly due to material being caked in the valve. Once the sample was taken, it needed to be handed down and to the testing area, which required the sampler handing the material to another member of the staff that carried it down a ladder to the testing area (Figure 4-20).

### *B.1.2. Plant 2*

The second plant tested in the Cincinnati area was a Terex counterflow plant (Figure 4-21) located in Fairborn, Ohio, with a 270-ton/hour capacity and a Terex foamer (Figure 4-22). The foaming water content used during production was 2.2%. The binder line was 4 in. in diameter. The distance from the foaming unit to the drum inlet was 10 ft, and the sampling port was located on the foaming unit. The

*Figure 4-17. Gencor foamer, Plant 1, Cincinnati, Ohio.*

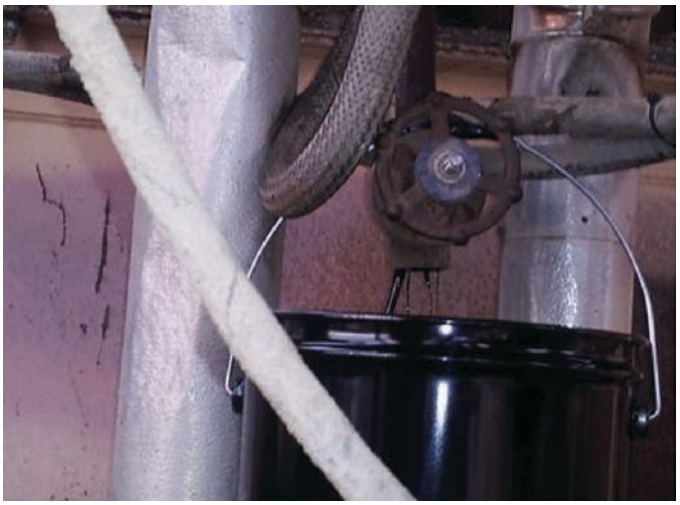

*Figure 4-19. Foamed binder flow from sampling port, Plant 1, Cincinnati, Ohio.*

*Figure 4-20. Overall picture of foam sampling area relative to testing area.*

line from the sampling port was 1 in. in diameter and 10 in. long (Figure 4-23).

## B.2. Materials

### *B.2.1. Plant 1*

The binder used in Plant 1 was a Marathon PG64-22, although the contractor later specified that the tank at the terminal had a blend of several sources. The binder content used in the mix design produced that day was 5.6%. Local gravel #8 was the primary aggregate used. Other aggregates, such as local natural sand and fractioned RAP, were also used. Details on the aggregate type, source, and gradation are presented in Table 4-3, Table 4-4, and Figure 4-24.


*Figure 4-21. Terex counterflow drum, Plant 2, Fairborn, Ohio.*


*Figure 4-22. Terex foamer, Plant 2, Fairborn, Ohio.*

### *B.2.2. Plant 2*

The same binder as used in Plant 1 was employed at this location. The binder content used in the mixture produced that day was 3.9%. Local stone, gravel, natural sand, and 40% crushed RAP were used in the mixture. Details on the aggregate type, source, and gradation are presented in Table 4-5, Table 4-6, and Figure 4-25.

*Figure 4-23. Foam sampling port, Plant 2, Fairborn, Ohio.*

**Table 4-3. Aggregate source, Plant 1, Cincinnati, Ohio.**

| | Bin No. 1 | Bin No. 2 | Bin No.3 |
|---|---|---|---|
| **Aggregate Source** | Gravel #8 | Natural Sand | RAP |
| **Aggregate Pit** | Martin Marietta/Fairfield, OH | Martin Marietta/E-Town, OH | Barrett/Cleves |

**Table 4-4. Aggregate gradation, Plant 1, Cincinnati, Ohio.**

| | Sieve Analysis (Cum.% Passing) | | | | | | | | |
|---|---|---|---|---|---|---|---|---|---|
| | ½" | ⅜" | #4 | #8 | #16 | #30 | #50 | #100 | #200 |
| **Combined Gradation** | 100 | 97.0 | 65.1 | 40.8 | 30.1 | 20.3 | 10.1 | 6.3 | 4.6 |

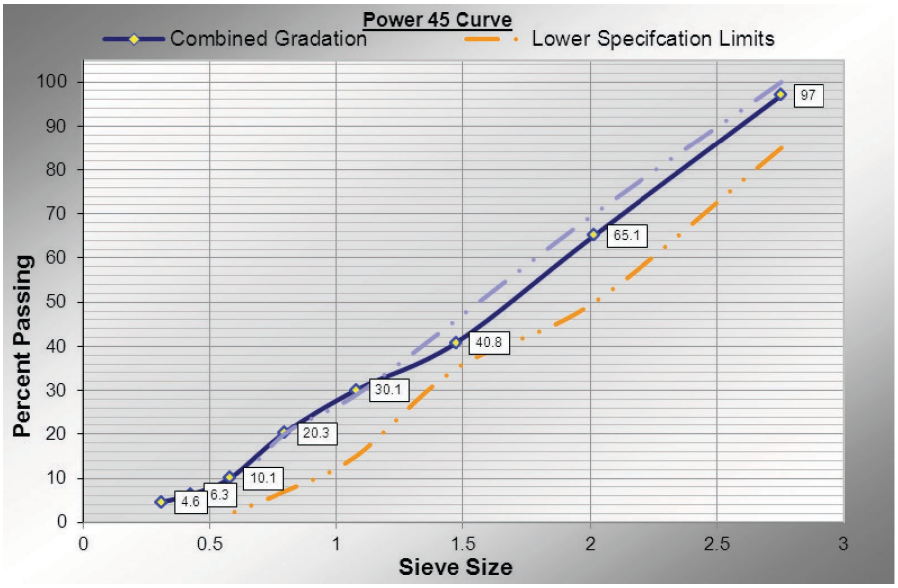


***Figure 4-24. Combined aggregate gradation, Plant 1, Cincinnati, Ohio. Note: Dashed purple line is the upper specification limit.***

**Table 4-5. Aggregate source, Plant 2, Fairborn, Ohio.**

| | Bin No. 1 | Bin No. 2 | Bin No. 3 | Bin No.4 |
|---|---|---|---|---|
| **Aggregate Source** | Stone | Gravel | Natural Sand | Crushed RAP |
| **Aggregate Pit** | Barrett Paving/Miami River Stone Quarry | Barrett Paving/Fairborn | Barrett Paving/ Fairborn | Barrett/ Fairborn |

**Table 4-6. Aggregate gradation, Plant 2, Fairborn, Ohio.**

| | Sieve Analysis (Cum.% Passing) | | | | | | | | | | | |
|---|---|---|---|---|---|---|---|---|---|---|---|---|
| | 1½" | 1" | ¾" | ½" | ⅜" | #4 | #8 | #16 | #30 | #50 | #100 | #200 |
| **Combined Gradation** | 100 | 86 | 70 | 60 | 52 | 40 | 31 | 22 | 15 | 9 | 5 | 4.2 |

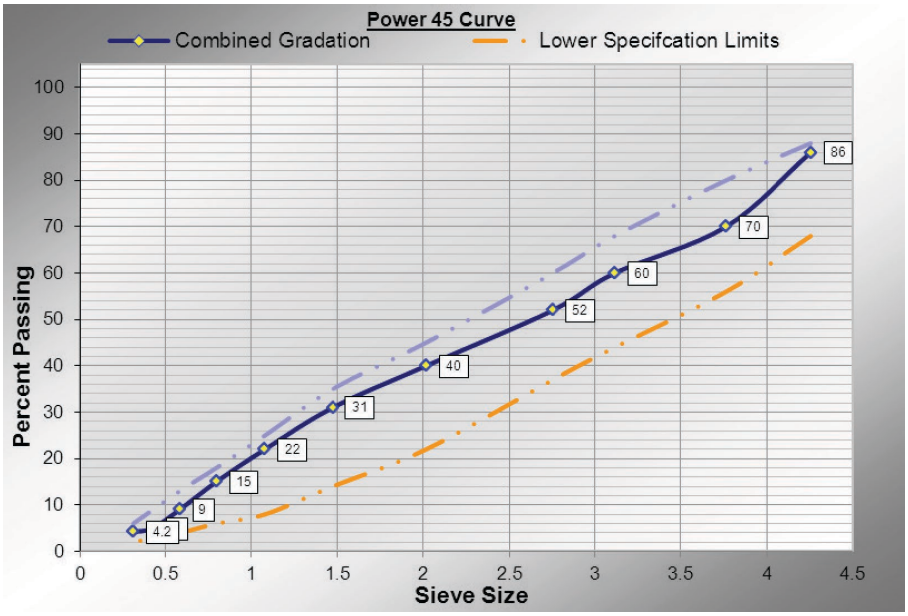


***Figure 4-25. Combined aggregate gradation, Plant 2, Fairborn, Ohio. Note: Dashed purple line is the upper specification limit.***

## B.3. Foaming Measurements

Average $ER_{max}$ and *k*-value of three replicate measurements performed on-site and two replicate measurements performed in the laboratory using the Wirtgen foamer are presented in Figure 4-26. The corrected $ER_{max}$ values correspond to the modified field measurements after applying the container size correction factor of 2.0. The error bars in Figure 4-26 span ±1 standard deviation from the average $ER_{max}$ value. From the figure, it is apparent that $ER_{max}$ and *k*-value for both field measurements were lower than the laboratory measurements, even after the container size correction factor was applied. Within the field measurements, the Terex foamed binder with 2.2% water content had a slightly higher $ER_{max}$ and a lower *k*-value than the Gencor foamed binder with 1.5% water content. The laboratory test results performed with the Wirtgen foamer showed that the binder was not sensitive to increasing water content, showing almost no change in $ER_{max}$ with added water. By contrast, the laboratory results obtained using the binder from the initial field trial showed increasing $ER_{max}$ with increasing water content (Figure 4-26).

Figure 4-27 illustrates the laboratory FI of the same measurements. Only the laboratory FI values are presented since the differences in container size yielded smaller field FI values that were not comparable on the same scale. Opposite to the almost constant $ER_{max}$ value observed for the laboratory measurements, the FI at 60 s did show differences, with lower water contents showing larger FI values. Binder foamed in the laboratory with 2.0%, 2.2%, and 3.0% water content had very similar FI values.

The SAI results are illustrated in Figure 4-28. As in the case of the FI at 60 s, clear differences were observed, with the binder foamed at lower water contents having higher SAI values. This indicates that the bubbles at lower water contents

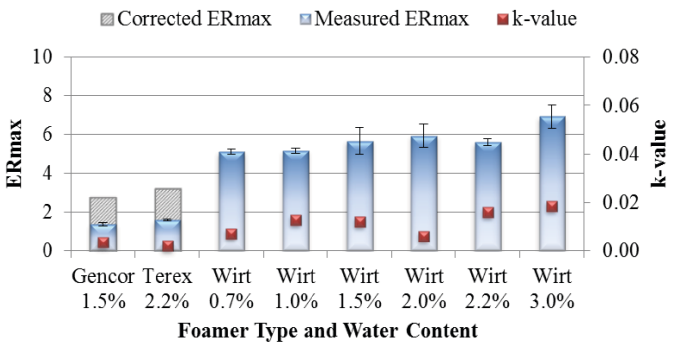


***Figure 4-26. $ER_{max}$ and k-value for the Ohio on-site and laboratory binder foam measurements.***

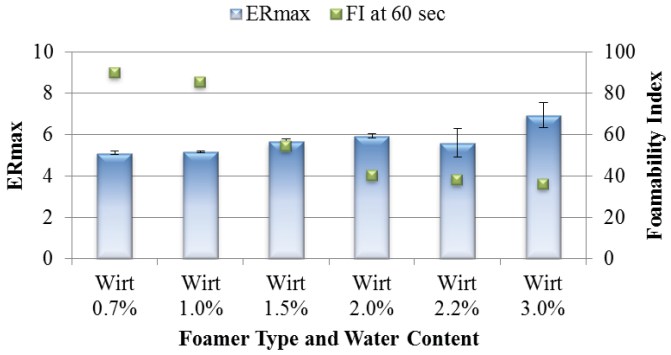


***Figure 4-27. $ER_{max}$ and FI for the Ohio laboratory binder foam measurements.***

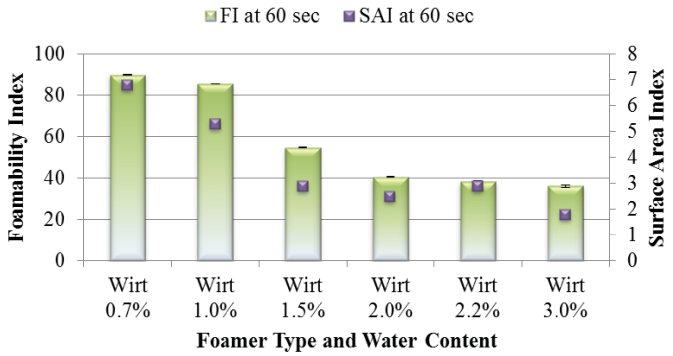


***Figure 4-28. FI and SAI for the Ohio laboratory binder foam measurements.***

were smaller and lasted longer. The SAI values decreased progressively as the water content increased.

## B.4. Mixture Workability and Coatability Measurements

The workability and coatability results for foamed PMLC and LMLC specimens fabricated at 1.0%, 2.0%, and 3.0% foaming water contents and HMA LMLC specimens are shown in Figure 4-29 and Figure 4-30, respectively. Each bar represents the average maximum shear stress value of three replicates, and the error bars in Figure 4-29 represent ±1 standard deviation from the average value.

As illustrated in Figure 4-29, a significantly lower maximum shear stress value was shown for the foamed PMLC specimens as compared to foamed LMLC specimens at different foaming water contents, which indicated that the foamed PMLC specimens had a better workability than their LMLC counterparts. The comparison in workability of LMLC specimens illustrated that an equivalent maximum shear stress value was achieved among foamed mixtures at different foaming water contents and the control HMA.

The comparison in coatability results of HMA versus foamed LMLC specimens at different foaming water contents shown

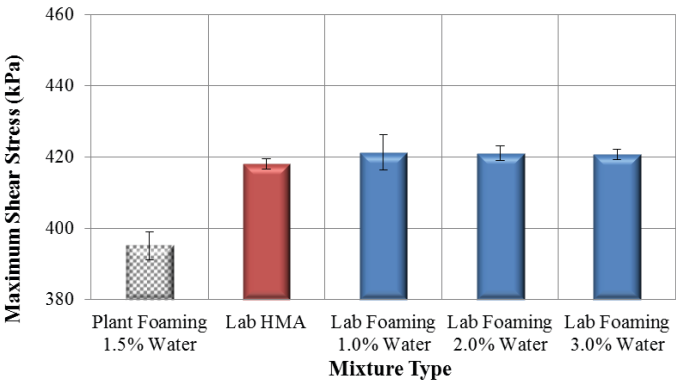


***Figure 4-29. Workability results for the Ohio Plant 1 mixtures.***

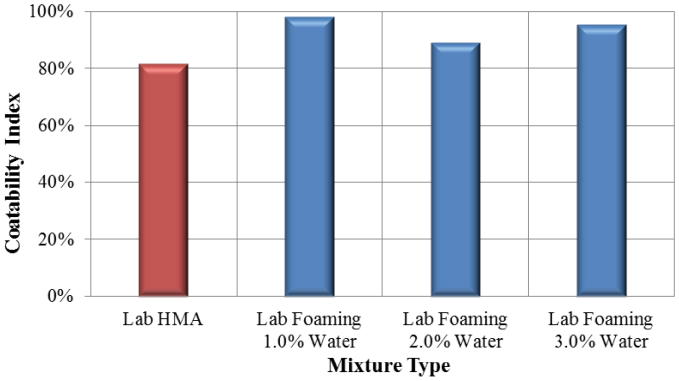


***Figure 4-30. Coatability results for the Ohio Plant 1 mixtures.***

in Figure 4-30 illustrates that all foamed specimens had higher CI values as compared to their HMA counterpart. In addition, foamed specimens at 1.0% foaming water content had the best CI as compared to those specimens prepared with higher water contents (i.e., 2.0% and 3.0%).

Therefore, according to the workability and coatability results presented in Figure 4-29 and Figure 4-30, the optimum foaming water content for this specific mixture was 1.0% and was able to produce LMLC specimens with the best workability and coatability characteristics.

## B.5. Performance Evaluation

To evaluate the performance of foamed mixtures at the optimum foaming water content, a new set of LMLC specimens was fabricated at 1.0% foaming water content using the Wirtgen foamer. In addition, another set of HMA specimens was also produced. Both the foamed mixture and the control HMA were mixed at 300°F (149°C) and then short-term aged for 2 hours at 275°F (135°C) prior to compaction. Then, the compacted specimens were tested for $M_R$, IDT strength, and HWTT. Testing parameters included $M_R$ stiffness, wet IDT strength, and TSR at 77°F (25°C). HWTT $LC_{SN}$, $LC_{ST}$, and $\Delta\varepsilon_{SN}^{vp}$ at 122°F (50°C) were used to evaluate mixture stiffness, rutting resistance, and moisture susceptibility and to compare the performance of foamed mixtures at the optimum foaming water content versus the control HMA.

### *B.5.1. Resilient Modulus Test*

The $M_R$ stiffness results for the control HMA and the foamed mixture at the optimum foaming water content (i.e., 1.0%) are shown in Figure 4-31. Each bar presents the average $M_R$ stiffness of three replicates, and the error bars represent ±1 standard deviation from the average value.

As illustrated in Figure 4-31, equivalent $M_R$ stiffness at 77°F (25°C) was achieved by the control HMA and the foamed

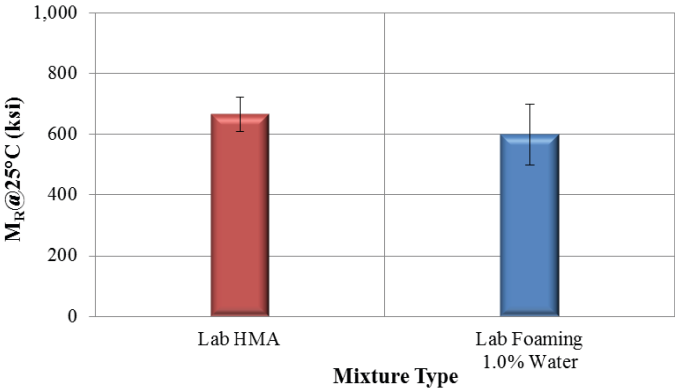


***Figure 4-31. $M_R$ test results for the Ohio Plant 1 mixtures.***

mixture at 1.0% foaming water content. Thus, the inclusion of water from the foaming process had no significant effect on the mixture stiffness.

### *B.5.2. Indirect Tensile Strength Test*

Three specimens were tested in a dry condition and three specimens after moisture conditioning following the procedure outlined by AASHTO T 283. The wet IDT strength and TSR value at 77°F (25°C) were considered as indicators of mixture moisture susceptibility. The IDT strength test results for the foamed mixture and the control HMA are shown in Figure 4-32. The solid bar and pattern-filled bar represent the average dry and wet IDT strength, respectively. The error bars represent ±1 standard deviation from the average value. In addition, the TSR values are shown above the IDT strength bars.

As illustrated in Figure 4-32, a slightly higher dry IDT strength at 77°F (25°C) was observed for the control HMA as compared to the foamed mixture at 1.0% foaming water content. However, an equivalent wet IDT strength and, subsequently, a higher TSR value were shown by the foamed mixture as compared to the control HMA. Therefore, IDT strength test results indicated that the foamed mixture fabricated at the optimum foaming water content had slightly better moisture susceptibility than the control HMA.

### *B.5.3. Hamburg Wheel Tracking Test*

The HWTT was performed at 122°F (50°C) following AASHTO T 324, and test parameters, including $LC_{SN}$, $LC_{ST}$, and $\Delta\varepsilon_{SN}^{vp}$, were used to evaluate mixture moisture susceptibility and rutting resistance. HWTT results in terms of rut depth versus load cycle for the control HMA and the foamed mixture at 1.0% foaming water content are shown in Figure 4-33.

Both mixtures passed the failure criteria of 20,000 load cycles with less than the 0.5-in. (12.5-mm) rut depth of TxDOT specifications. Figure 4-34 presents the comparison in $LC_{SN}$, $LC_{ST}$, and $\Delta\varepsilon_{SN}^{vp}$ results of the foamed mixture versus the control HMA. As illustrated in Figure 4-34(a), higher $LC_{SN}$ and $LC_{ST}$ values were shown for the control HMA as compared to the foamed mixture, indicating better moisture resistance in the HWTT. Test results presented in Figure 4-34(b) illustrate that the foamed mixture at the optimum foaming water content had a $\Delta\varepsilon_{SN}^{vp}$ value approximately 0.5 με/cycle [equivalent to rut depth of 0.0012 in. (0.03 mm) per 1,000 load cycles] higher than the control HMA did. Thus, worse moisture susceptibility and rutting resistance were exhibited by the foamed mixture at the optimum foaming water content than the control HMA in the HWTT.

## C. Field Validation of Proposed Mix Design

The field validation of the proposed foamed mix design presented in Section 2.C was done at a plant located in Huntsville, Texas. This plant consisted of an Astec Double

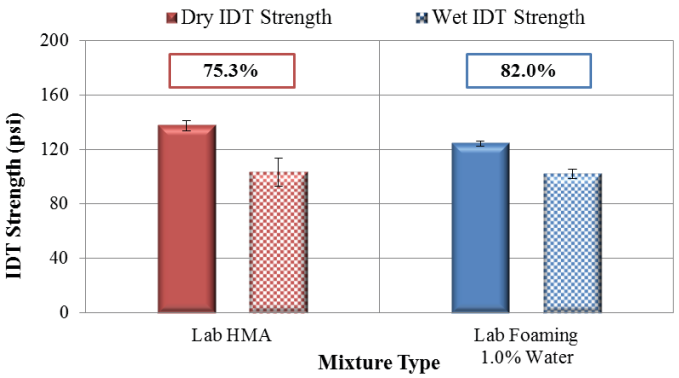


***Figure 4-32. IDT strength test results for the Ohio Plant 1 mixtures.***

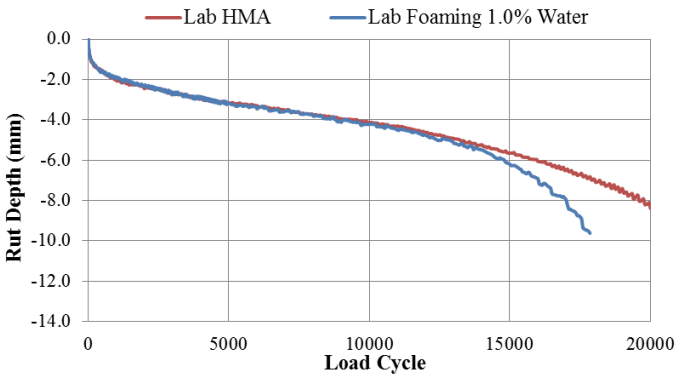


***Figure 4-33. HWTT rut depth versus load cycles at 122°F (50°C) for the Ohio Plant 1 mixtures.***

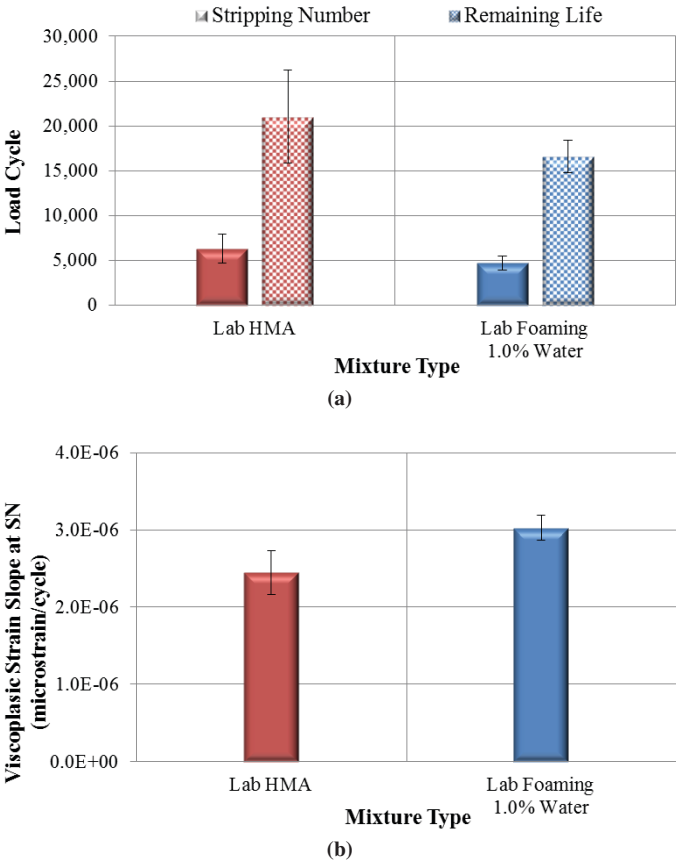


***Figure 4-34. HWTT results at 122°F (50°C) for the Ohio Plant 1 mixtures; (a) $LC_{SN}$ and $LC_{ST}$, and (b) $\Delta\varepsilon_{SN}^{vp}$.***

Barrel with a Stansteel Accushear foaming unit. The foaming unit was located on its own platform (Figure 4-35) with an approximately 15-ft run to the inlet on the drum with a 3-ft drop. The plant was capable of producing 250 tons of mix per hour; the mix design details are given later. The foam sampling port on this plant was located about 3 ft downstream from the foaming unit with a ¾-in. sampling port. Although

***Figure 4-35. Foaming unit on platform, Huntsville, Texas.***

***Figure 4-36. Heating valve prior to sampling foam, Huntsville, Texas.***

the valve needed to be heated prior to sampling the foamed binder (Figure 4-36), there were no problems taking and testing samples from this plant (Figure 4-37).

## C.1. Experimental Plan

Figure 4-38 presents the experimental design followed in this portion of the study. During the first plant visit, on November 29, 2013, the plant was producing foamed mixtures with 5.5% water content at approximately 300°F (149°C). Binder foaming characteristics produced by the plant foaming unit were measured on-site using a laser device and a digital camera on a side platform. Foamed loose mix produced at the plant was sampled from the trucks after being loaded from the silo and then transported back to the laboratory (approximately 60 miles away from the plant) for fabricating PMLC specimens and evaluated for their workability. Raw materials, including virgin asphalt binder, aggregates, and RAP, were also sampled during the visit.

In the laboratory, asphalt was foamed using a Wirtgen foamer at the following water contents: 0.7% (which was the

***Figure 4-37. Free-flowing foamed binder sample, Huntsville, Texas.***

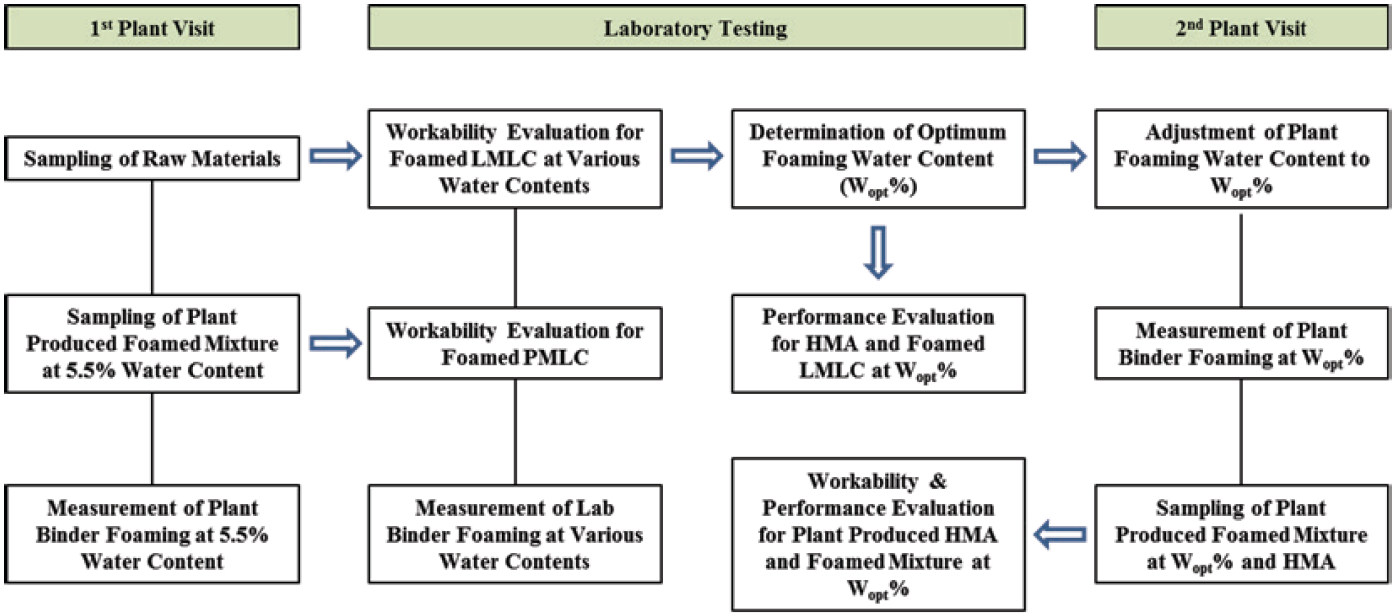


*Figure 4-38. Experimental plan for the field validation of the foamed mix design.*

minimum water content the equipment was able to output), 1.0%, 1.5%, 2.0%, 3.0%, and 5.5%. Evaluation of binder foaming characteristics and foamed mixture workability was performed to determine an optimum foaming water content, referring to the specific water content at which the laboratory-foamed mixture had the best workability. Afterward, foamed LMLC specimens were fabricated at the optimum foaming water content for performance evaluation and comparison to the performance of the HMA.

A second visit to the plant was made on December 3, 2013, adjusting the water content on-site to match the optimum value obtained via laboratory measurements. Binder foaming characteristics produced by the plant foaming unit at the adjusted water content were measured, and samples of the foamed loose mix were collected for workability and performance evaluation.

The foamed plant loose mix acquired during production was used to fabricate PMLC specimens by reheating in an oven at 275°F (135°C). The temperature of the loose mix was monitored using a digital thermometer every 15 minutes after being reheated for 1 hour. Once the temperature achieved 275°F (135°C), the foamed loose mix was compacted in the SGC. LMLC specimens were produced at a mixing temperature of 300°F (149°C) and then short-term aged for 2 hours at 275°F (135°C) prior to compaction. For mixture performance evaluation, PMLC and LMLC specimens of both plant-produced and laboratory-produced foamed mixtures were tested for $M_R$, IDT strength, and by the HWTT to evaluate mixture stiffness, rutting resistance, and moisture susceptibility, and to compare the performance versus the control HMA.

## C.2. Materials

The binder used was a Valero PG64-22. The optimum binder content per mix design was 4.5%. Limestone was the primary aggregate used in the mixture, and sandstone and fractioned RAP were also used. Details on the aggregate type, source, and gradation are presented in Table 4-7, Table 4-8, and Figure 4-39.

## C.3. Initial Measurements at Plant

### *C.3.1. Foaming*

The $ER_{max}$ and *k*-value of the on-site binder foaming measurements performed are illustrated in Figure 4-40. The bars and red squares represent the average $ER_{max}$ and *k*-value of three replicate measurements, respectively. The error bars span ±1 standard deviation from the average $ER_{max}$ value. The initial plant measurement with a water content of about 5.5% yielded an $ER_{max}$ of about 12 and a *k*-value of 0.04. The repeatability of the measurements seemed adequate. The FI at 60 s is illustrated in Figure 4-41. The FI for the initial plant measurement had a steady increase with time.

### *C.3.2. Workability*

The workability results for plant-produced HMA and laboratory-foamed mixture with 5.5% water content are shown in Figure 4-42. Each bar in Figure 4-42 represents the average value of three replicates, and the error bars represent

**Table 4-7. Aggregate source, Huntsville, Texas.**

| | Bin No. 1 | Bin No. 2 | Bin No.3 | Bin No.4 | Bin No.5 |
|---|---|---|---|---|---|
| **Aggregate Source** | Sandstone | Limestone | Limestone | Austin White Lime | Fractioned RAP |
| **Aggregate Pit** | Marble Falls | Marble Falls | Marble Falls | – | – |

**Table 4-8. Aggregate gradation, Huntsville, Texas.**

| | Sieve Analysis (Cum.% Passing) | | | | | | | | |
|---|---|---|---|---|---|---|---|---|---|
| **Aggregate Source** | **%** | **1”** | **¾”** | **⅜”** | **#4** | **#8** | **#30** | **#50** | **#200** |
| Sandstone | 28.0 | 100 | 99.0 | 12.0 | 6.0 | 4.3 | 3.9 | 3.7 | 2.5 |
| Limestone | 24.1 | 100 | 100 | 91.0 | 22.0 | 4.2 | 2.4 | 2.2 | 1.5 |
| Limestone | 27.0 | 100 | 100 | 100 | 99.0 | 80.0 | 39.0 | 25.0 | 4.2 |
| Austin White Lime | 1.0 | 100 | 100 | 100 | 100 | 100 | 100 | 100 | 100 |
| Fractioned RAP | 19.9 | 100 | 100 | 94.0 | 68.1 | 49.3 | 31.5 | 23.2 | 7.1 |
| Combined Gradation | 100 | 100 | 100 | 95.5 | 78.0 | 62.5 | 40.0 | 17.6 | 3.0 |

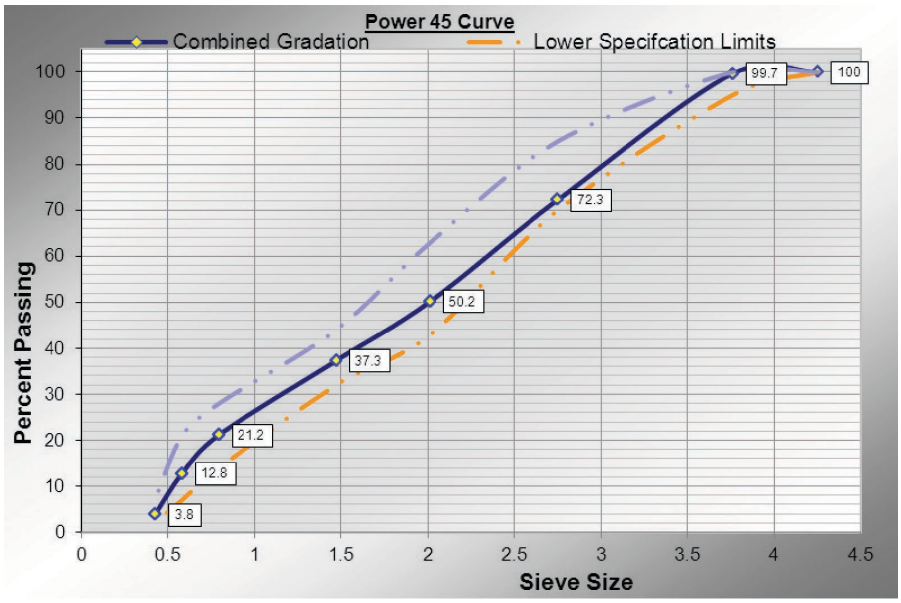


***Figure 4-39. Combined aggregate gradation, Huntsville, Texas. Note: Dashed purple line is the upper specification limit.***

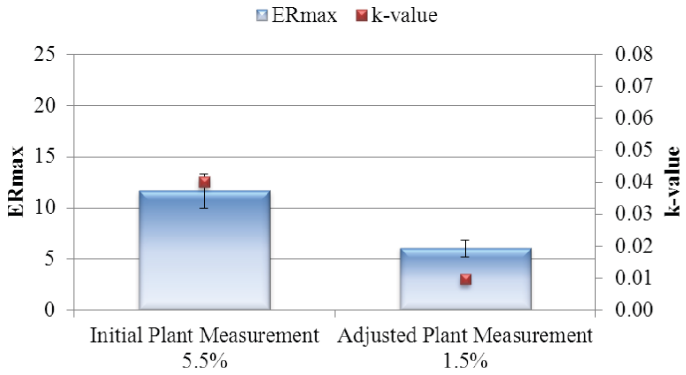


***Figure 4-40. $ER_{max}$ and k-value for the Huntsville on-site binder foam measurements.***

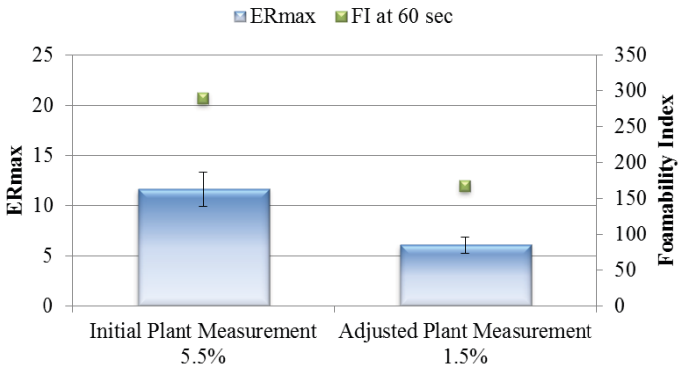


***Figure 4-41. $ER_{max}$ and FI for the Huntsville on-site binder foam measurements.***

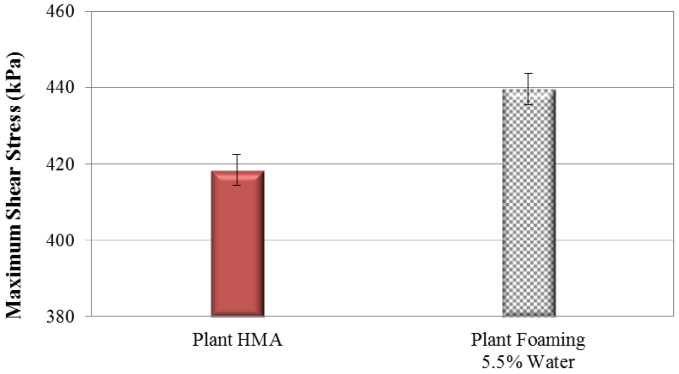


***Figure 4-42. Workability results for the Huntsville plant–produced HMA and laboratory-foamed mixture with 5.5% water content.***

±1 standard deviation from the average value. As illustrated, a lower $\tau_{max}$ value was exhibited for the control HMA versus the laboratory-foamed mixture with 5.5% water content, indicating that plant-produced HMA had a better workability than the foamed mixture.

## C.4. Laboratory Mix Design

The proposed mix design method illustrated in Figure 2-9 was applied to the materials collected at the Huntsville plant. Once the foaming ability of the binder was corroborated, the traditional HMA mix design used during production was replicated in the laboratory to estimate the optimum water content via workability and coatability measures.

### *C.4.1. Foaming Measurements*

The binder foaming measurements were performed in the laboratory using the Wirtgen foamer. The water content was varied from 0.7% (which was the minimum water level the equipment was able to output) to 3.0%. The following water contents were tested: 0.7%, 1.0%, 1.5%, 2.0%, 3.0%, and 5.5%. The $ER_{max}$ and *k*-value results are illustrated in Figure 4-43. As before, the bars represent the average $ER_{max}$ of two replicates, the dots correspond to the average *k*-value, and the error bars span ±1 standard deviation from the average value.

A direct correlation was observed between the amount of water added to the foaming process and the $ER_{max}$ value. The foam was relatively stable, with a low *k*-value for almost all samples, except for the one with 5.5% water content, which showed a very large value.

The FI results are presented in Figure 4-44. Consistent with the $ER_{max}$ and *k*-value results, the FI at 60 s also showed the lowest values for the sample foamed with 5.5% water content. The samples with lower water contents, from 0.7% through 2.0%, showed higher and equivalent FI values at 60 s. Therefore, as more water was used in the foaming process, the binder foaming achieved a higher volume expansion but also a faster foam collapse rate, which ultimately led to lower stability. However, an opposite trend was observed for plant binder foaming measurements, where foamed binder at 1.5% water content exhibited lower stability, as indicated by a lower FI value than that at a higher water content of 5.5% (Figure 4-41). In addition, the comparison between plant binder foaming versus laboratory binder foaming showed that plant binder foaming had a significantly higher FI value at 60 s than the laboratory-foamed sample at the same water contents.

The SAI values obtained from the analysis of the digital images acquired during the foaming process are illustrated in Figure 4-45. As previously mentioned, this parameter takes into consideration the total number of foaming bubbles and the bubble size distribution. As time after foaming increases, the decrease in ER and the increase in surface area of the foaming bubbles (due to the transition from larger bubbles to smaller bubbles) are competing mechanisms. Foamed binder with larger SAI values (throughout the dynamic foaming process) is expected to have better aggregate coating ability. For the results shown in Figure 4-45, SAI could not be calculated for 3.0% and 5.5% water content due to rapid bubble collapse, which also corresponds to lower values of FI.

As will be explained in more detail in the next section, the maximum shear stress also follows a decreasing trend up

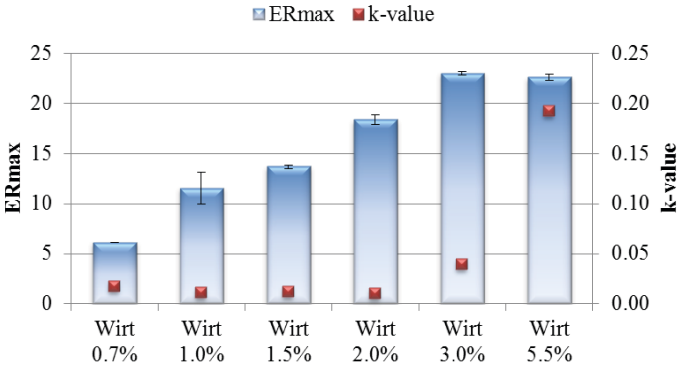


***Figure 4-43. $ER_{max}$ and k-value for the Huntsville laboratory binder foam measurements.***

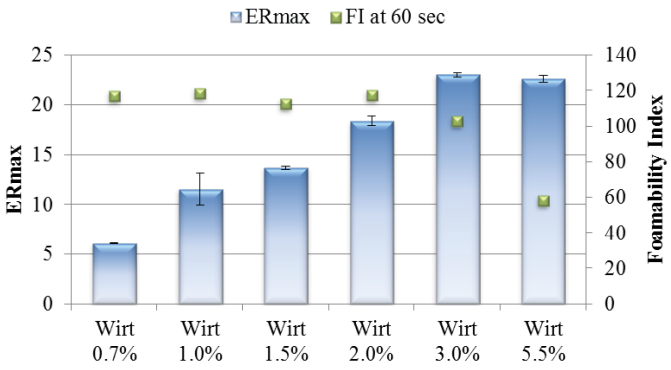


***Figure 4-44. Foamability index versus foaming time for the Huntsville laboratory binder foam measurements.***

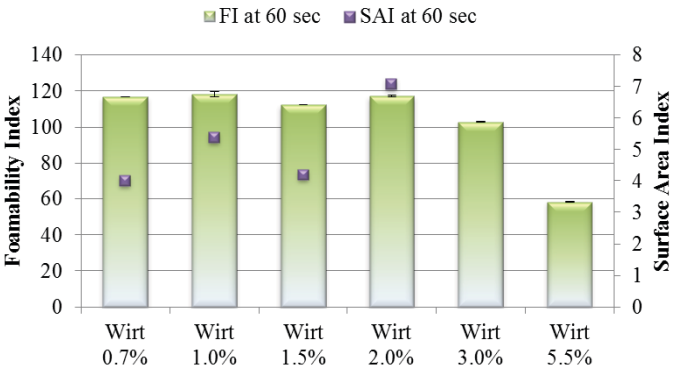


***Figure 4-45. Surface area index for the Huntsville laboratory binder foam measurements.***

to a point where the maximum shear stress increases again (Figure 4-46). These parallel observations suggest that either workability or binder foamed characteristics could be used during mix design to obtain the optimum water content.

### C.4.2. Mixture Workability Measurements

The workability results for LMLC specimens produced at 0.7%, 1.0%, 1.5%, 2.0%, 3.0%, and 5.5% foaming water contents are shown in Figure 4-46. Each bar in Figure 4-46 represents the average value of three replicates, and the error bars represent ±1 standard deviation from the average value. As illustrated, $\tau_{max}$ values of laboratory-produced foamed mixtures decreased as foaming water contents increased from 0.7% to 1.5%, while the opposite trend was shown for foaming water contents higher than 1.5%. Therefore, 1.5% was selected as the optimum foaming water content that was able to produce foamed mixture with the best workability characteristic (the lowest $\tau_{max}$ value).

## C.5. Recommended Plant Adjustments

During a second visit to the Huntsville plant, the foaming water content was modified to 1.5% to match the optimum

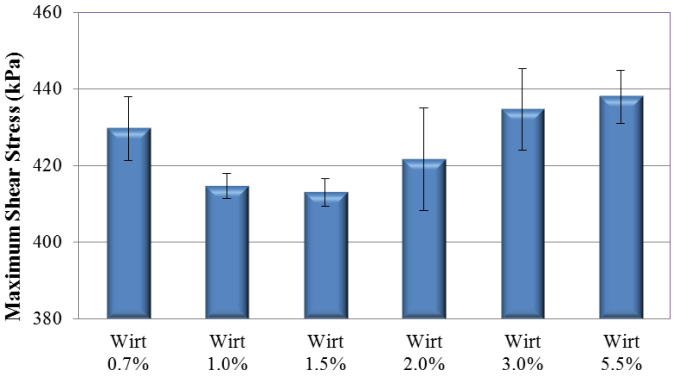


***Figure 4-46. Workability results for the Huntsville laboratory-produced foamed mixtures.***

obtained via the laboratory measurements. On-site binder foaming measurements and loose mix were collected during the second visit to the plant to compare against the values collected during the first visit.

### C.5.1. Foaming Measurements

The on-site foaming measurements are shown in Figure 4-40 and Figure 4-41. In contrast to the first visit, $ER_{max}$ and *k*-value were lower and the FI at 60 s smaller than when 5.5% water content was used. This observation is opposite to what has been observed in the laboratory measurements, where lower water contents seem to have better FI.

### C.5.2. Mixture Workability Measurements

The workability results for plant-produced foamed mixture at adjusted foaming water content (1.5%) were compared to the results of plant-produced HMA and foamed mixtures at 5.5% foaming water content and are shown in Figure 4-47. Each bar in Figure 4-47 represents the average value of three replicates, and the error bars represent ±1 standard deviation from the average value.

Plant-produced foamed mixture at 1.5% foaming water content had a better workability characteristic (indicated by a lower $\tau_{max}$ value) as compared to both the control HMA and the foamed mixture with 5.5% water content. Therefore, the optimum foaming water content of 1.5%, which was determined by laboratory foaming, was verified by plant foaming.

### C.5.3. Performance Evaluation

To fabricate PMLC specimens for performance evaluation, plant loose mix acquired during production was taken out of buckets and reheated in an oven at 275°F (135°C). The temperature of the loose mix was monitored using a digital thermometer every 15 minutes after being reheated in

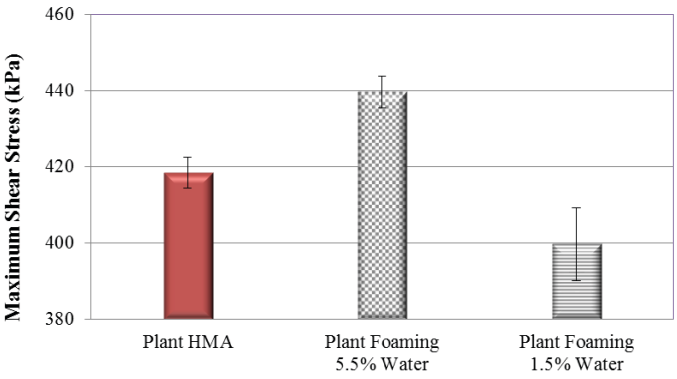


***Figure 4-47. Workability results for plant-produced HMA and foamed mixtures at 1.5% and 5.5% foaming water contents.***

the oven for 1 hour. Once the temperature achieved 275°F (135°C), plant loose mix specimens were compacted using an SGC. Then, the compacted specimens were tested for $M_R$, IDT strength, and by the HWTT to evaluate mixture stiffness, rutting resistance, and moisture susceptibility.

**C.5.3.1. Resilient Modulus Test.** The $M_R$ stiffness results for plant-produced HMA and foamed mixtures at 1.5% foaming water content are shown in Figure 4-48. Each bar in Figure 4-48 represents the average $M_R$ stiffness value at 77°F (25°C) of three replicates, and the error bars represent ±1 standard deviation from the average value. A slightly lower $M_R$ stiffness was shown by foamed mixture at 1.5% foaming water content as compared to the HMA. The larger stiffness for HMA was possibly due to additional aging experienced by the mixture in the plant versus the laboratory setting.

**C.5.3.2. Indirect Tensile Strength Test.** Three PMLC specimens were tested in a dry condition and three specimens after moisture conditioning following the procedure outlined by AASHTO T 283. The wet IDT strength and TSR value at 77°F (25°C) were considered as indicators of mixture moisture susceptibility. The IDT strength test results for plant-produced foamed mixture and control HMA are shown in Figure 4-49. The solid bar and pattern-filled bar represent the average dry and wet IDT strength, respectively. The error bars represent ±1 standard deviation from the average value. In addition, the TSR values are shown on top of the IDT strength bars.

Equivalent dry and wet IDT strength at 77°F (25°C) and, consequently, an equal TSR value were achieved by HMA and foamed mixture at 1.5% foaming water content. Therefore, plant-produced HMA and foamed mixture at the optimum foaming water content had equivalent moisture susceptibility in the IDT strength test.

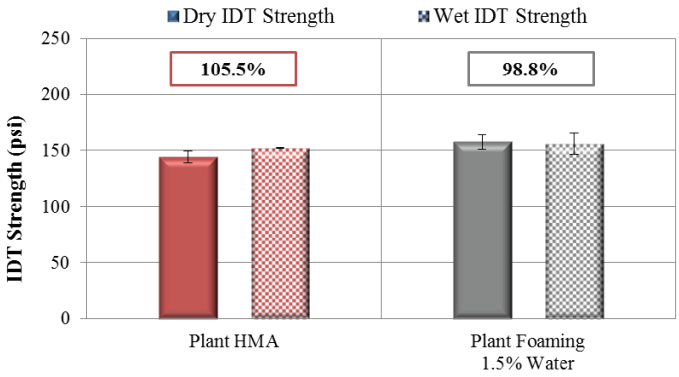


***Figure 4-49. IDT strength test results for the Huntsville plant-produced HMA versus foamed mixtures at 1.5% foaming water content.***

**C.5.3.3. Hamburg Wheel Tracking Test.** The HWTT was performed at 122°F (50°C) following AASHTO T 324, and test parameters including $LC_{SN}$, $LC_{ST}$, and $\Delta\varepsilon_{SN}^{vp}$ were used to evaluate mixture moisture susceptibility and rutting resistance. HWTT results in terms of rut depth versus load cycle for the control HMA and foamed mixture at 1.5% foaming water content are shown in Figure 4-50.

Both mixtures passed the failure criteria of 20,000 load cycles with less than 0.5-in. (12.5-mm) rut depth of TxDOT specifications. Figure 4-51 presents the comparison of plant-produced foamed mixture versus control HMA in $LC_{SN}$, $LC_{ST}$, and $\Delta\varepsilon_{SN}^{vp}$. As shown in Figure 4-51(a), the foamed mixture had a significantly higher $LC_{SN}$ value than the control HMA, indicating better moisture susceptibility before stripping occurred. A $LC_{ST}$ value of 45,627 was obtained for the plant-produced HMA. However, the determination of $LC_{ST}$ for the foamed mixture was not available since no stripping occurred within the mixture during the test (indicated by a $LC_{SN}$ value of 20,000). Test results shown in Figure 4-51(b) illustrate

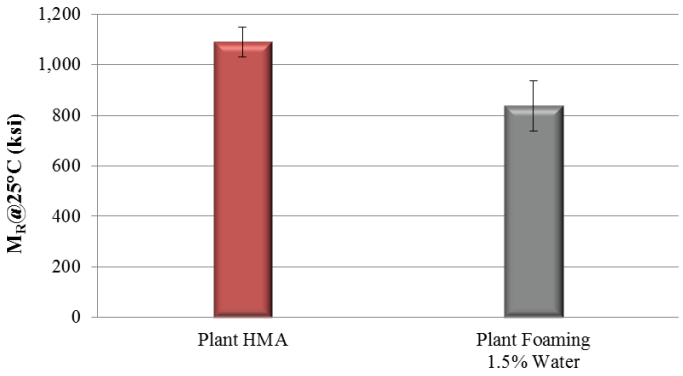


***Figure 4-48. $M_R$ test results for the Huntsville plant-produced HMA versus foamed mixtures at 1.5% foaming water content.***

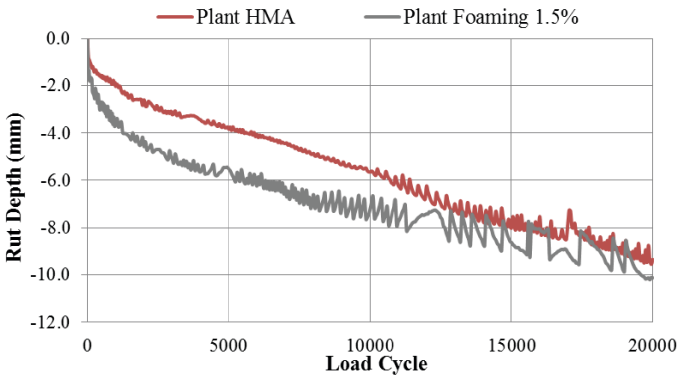


***Figure 4-50. HWTT rut depth versus load-cycle results for the Huntsville plant-produced HMA versus foamed mixtures at 1.5% foaming water content.***

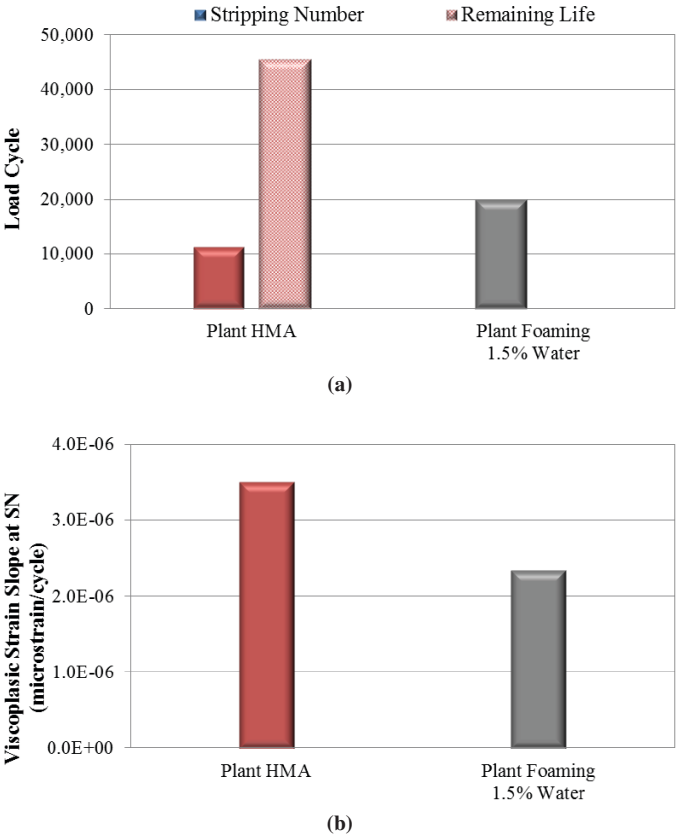


***Figure 4-51. HWTT results for the Huntsville plant-produced HMA versus foamed mixtures at 1.5% foaming water content; (a) $LC_{SN}$ and $LC_{ST}$, and (b) $\Delta\varepsilon_{SN}^{vp}$.***

that plant-produced foamed mixture at 1.5% foaming water content had a better rutting resistance than the HMA counterpart, as indicated by a lower $\Delta\varepsilon_{SN}^{vp}$ value. Thus, better moisture susceptibility and rutting resistance were exhibited by the plant-produced foamed mixture at 1.5% foaming water content than by the HMA counterpart in the HWTT.

## C.6. Performance Evaluation

To evaluate the performance of laboratory-produced foamed mixtures at the optimum foaming water content, a new set of LMLC specimens were fabricated at 1.5% foaming water content using the Wirtgen foamer. In addition, a companion set of HMA LMLC specimens were produced as well. Both the foamed mixtures and control HMA were mixed at 300°F (149°C) and then short-term aged for 2 hours at 275°F (135°C) prior to compaction. Then, the compacted specimens were tested for $M_R$, IDT strength, and by the HWTT. Testing parameters, including $M_R$ stiffness, wet IDT strength, TSR at 77°F (25°C), and HWTT $LC_{SN}$, $LC_{ST}$, and $\Delta\varepsilon_{SN}^{vp}$ at 122°F (50°C), were used to evaluate mixture stiffness, rutting resistance, and moisture susceptibility and to compare the performance of foamed mixtures versus the control HMA.

### C.6.1. Resilient Modulus Test

The $M_R$ stiffness results for plant- and laboratory-produced foamed mixtures at the optimum foaming water content of 1.5% and the control HMA are shown in Figure 4-52. Each bar in Figure 4-52 represents the average $M_R$ stiffness value at 77°F (25°C) of three replicates, and the error bars represent ±1 standard deviation from the average value. As illustrated, a slightly lower $M_R$ stiffness was shown by plant-produced foamed mixtures as compared to plant-produced HMA. Equivalent stiffness was exhibited for a laboratory-produced foamed mixture versus the HMA counterpart. Therefore, the inclusion of water as part of the foaming process did not reduce the mixture stiffness in this case.

### C.6.2. Indirect Tensile Strength Test

The IDT strength test results for plant- and laboratory-produced foamed mixtures and the control HMA are shown in Figure 4-53. The solid bar and pattern-filled bar represent the average dry and wet IDT strength, respectively, after moisture conditioning according to AASHTO T 283 with partial vacuum saturation, one freeze–thaw cycle, and soaking in warm water of three replicates. The error bars represent ±1 standard deviation from the average value. In addition, the TSR values are shown at the top of each pair of IDT strength bars.

The IDT strength test results for plant-produced mixtures indicated that equivalent dry and wet IDT strength at 77°F (25°C) and, consequently, an equal TSR value of approximately 100% were achieved by both HMA and the foamed mixture at 1.5% foaming water content. For laboratory-produced mixtures, equivalent dry IDT strength at 77°F

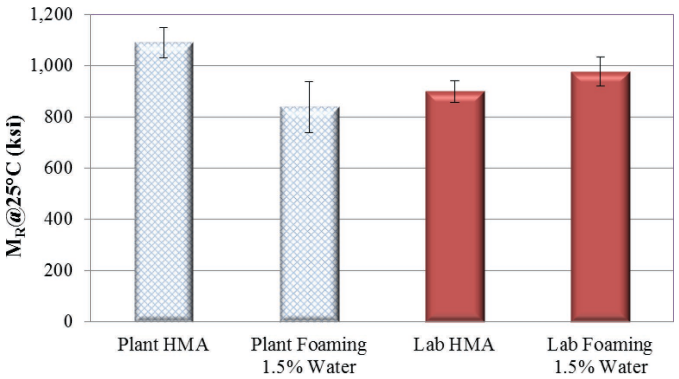


***Figure 4-52. $M_R$ test results for the Huntsville plant- and laboratory-produced HMA versus foamed mixtures at 1.5% foaming water content.***

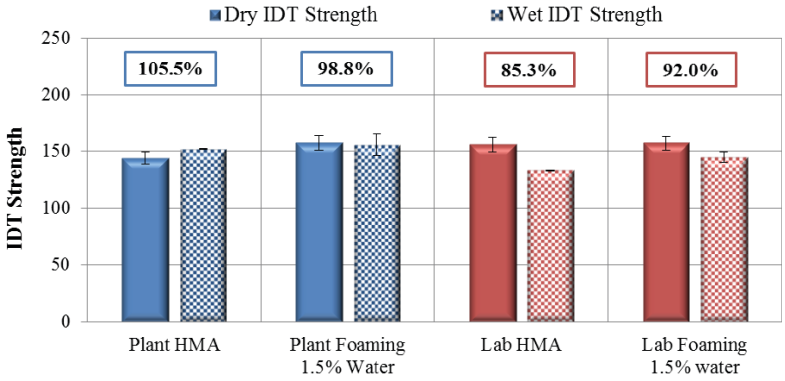


***Figure 4-53. IDT strength test results for the Huntsville plant- and laboratory-produced HMA versus foamed mixtures at 1.5% foaming water content.***

(25°C) was achieved between the foamed mixture at 1.5% foaming water content and the control HMA. However, a significantly higher wet IDT strength and, subsequently, a higher TSR value were shown for the foamed mixture as compared to its HMA counterpart, which indicated that laboratory-produced foamed mixtures produced at the optimum foaming water contents had better moisture susceptibility than the control HMA in the IDT strength test.

### *C.6.3. Hamburg Wheel Tracking Test*

HWTT results in terms of rut depth versus load cycle for laboratory-produced foamed mixture at 1.5% foaming water content and the control HMA are shown in Figure 4-54. As illustrated, both laboratory-produced mixtures passed the failure criteria of 20,000 load cycles with less than 0.5-in. (12.5-mm) rut depth. Additionally, the shape of the HWTT curve indicated no sign of stripping occurring during the test for either mixture.

Figure 4-55 presents the $LC_{SN}$, $LC_{ST}$, and $\Delta\varepsilon_{SN}^{VP}$ results of plant- and laboratory-produced foamed mixtures at 1.5% foaming water content versus the control HMA. As shown in Figure 4-55(a), a $LC_{SN}$ value of 20,000 load cycles was observed for a plant-produced foamed mixture, a laboratory-produced foamed mixture, and laboratory-produced HMA, indicating that no stripping occurred during the test for any mixtures. A significantly lower $LC_{SN}$ value was shown for plant-produced HMA as compared to the other three mixtures, indicating a higher moisture susceptibility in the HWTT. This is consistent with findings from Abbas et al. (2013) that show greater rutting susceptibility of the plant HMA than the laboratory-produced mixtures. A $LC_{ST}$ value of 45,627 load cycles was obtained for the plant-produced HMA, while the determination of $LC_{ST}$ for the other three mixtures was not available since no stripping occurred within the mixture during the test.

Test results in Figure 4-55(b) show that for both plant-produced and laboratory-produced mixtures, a better rutting

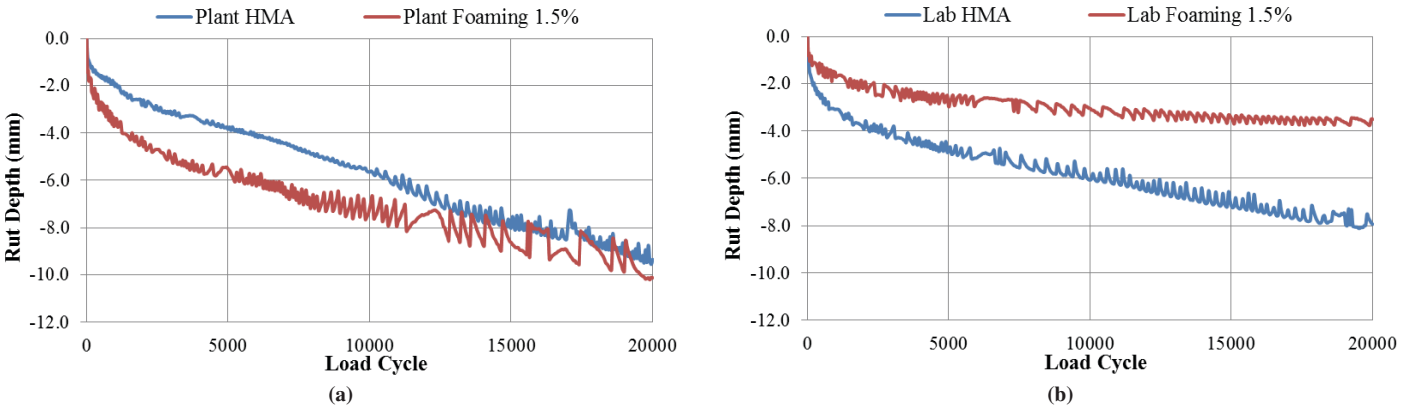


***Figure 4-54. HWTT rut depth results for the Huntsville HMA versus foamed mixtures at 1.5% foaming water content; (a) plant produced and (b) laboratory produced.***

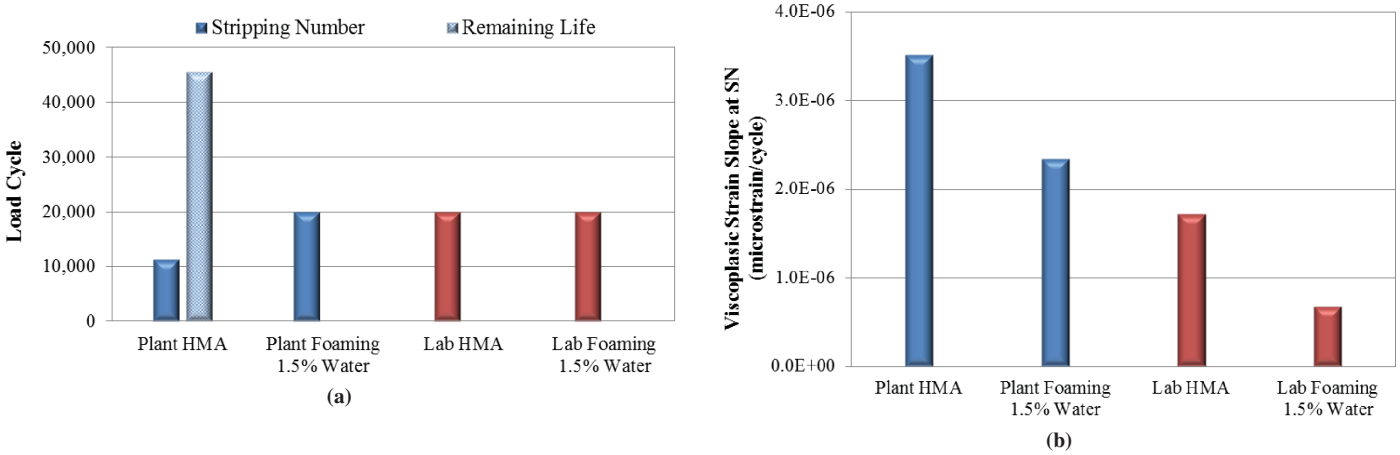


***Figure 4-55. HWTT results for the Huntsville laboratory-produced HMA versus foamed mixtures at 1.5% foaming water content; (a) $LC_{SN}$ and $LC_{ST}$, and (b) $\Delta\varepsilon_{SN}^{vp}$.***

resistance, as indicated by lower $\Delta\varepsilon_{SN}^{vp}$ values, was exhibited by foamed mixtures at the optimum foaming water content as compared to their HMA counterparts. Thus, better rutting resistance was exhibited by the mixtures produced with 1.5% foaming water content versus their HMA counterparts in the HWTT. Additionally, a better performance in the HWTT was observed for laboratory-produced mixtures than for those produced in the plant. Therefore, HWTT results presented in Figure 4-55 indicate that equivalent or better performance in terms of moisture susceptibility and rutting resistance can be achieved by foamed mixtures than by the control HMA when produced at the optimum foaming water content.

CHAPTER 5

# Conclusions

HMA is a well-established paving material with over 100 years of proven performance. High temperatures [275°F (135°C) to 325°F (162°C) and higher] are necessary to ensure complete drying of the aggregate and subsequent bonding with the binder, coating of the aggregate by the binder, and workability for adequate handling and compaction. All of these processes contribute to good pavement performance in terms of durability and resistance to permanent deformation and cracking. Economic, environmental, and possible performance benefits motivate the reduction of HMA mixing and compaction temperatures. The latest technology is WMA, where production temperatures are reduced to a range of 175°F (79°C) to 295°F (146°C). Some of the benefits of WMA are decreases in energy consumption, emissions, odors, and fumes during production, extended haul distances and pavement construction season, and improved workability and compactability of the mixtures.

WMA production in the United States has increased exponentially in recent years, from 19.2 million tons in 2009 to 86.7 million tons in 2012. The work in this research study focused on asphalt foaming because it is the largest segment of the WMA market in the United States. According to a survey done by NAPA, mechanical foaming units were responsible for about 88% of all WMA produced in 2012 (Hansen and Copeland, 2013). The changes brought about by WMA in mixture components, mix processing, and plant design have prompted many questions about the validity of current mix design methods in adequately assessing the volumetric needs of asphalt mixtures and the physical characteristics required to meet performance expectations.

This research study considered the impact of WMA foaming technology on the properties of binders and the volumetric and performance characteristics of mixtures. Accordingly, the objectives were to (1) determine the properties of foamed binders that relate to asphalt mixture performance and (2) develop laboratory foaming and mixing protocols that may be used to design asphalt mixtures.

Several test methods and metrics were explored to characterize the properties of the foamed binder, including noncontact and image-based methods. A laser-based sensor method was preferred to measure the expansion ratio and collapse of the binder foam because it required minimal hardware and software for setup and use, and allowed periodic data acquisition at 1-s intervals. In addition, digital images of the surface of the foamed binder were also acquired at 1-s intervals to quantify the number and size of the bubbles with time. The outcome of these two test methods yielded the following metrics to characterize binder foam:

1. Maximum expansion ratio – $ER_{max}$.
2. Rate of collapse of semi-stable foam – *k*-value.
3. Foamability index – FI.
4. Surface area index – SAI.

A laboratory binder study was performed to investigate the influence of binder source, water content, temperature, liquid additives, and shearing action on foamed binder characteristics. Several binders from six different producers and refinery locations were collected and used for that purpose, and the following observations were made:

- Binders of different sources/locations and PG grade had different $ER_{max}$, *k*-value, FI, and SAI at the same water content.
- Some binders were more sensitive to changes in water content than others.
- The elapsed time between measurements of the same binder source/location seemed to have an effect in $ER_{max}$, *k*-value, FI, and SAI.
- For most binders, there was a linear correlation between $ER_{max}$ and water content.
- For most binders, *k*-value increased with water content; that is, at higher water contents the foam was more unstable.

- For most binders, FI decreased with water content; that is, at higher water contents, the area under the ER versus time curve was smaller due to the instability of the binder.
- For most binders, SAI decreased with water content; that is, larger bubbles with a faster foam collapse (larger *k*-value) were observed at higher water contents. At low water contents, smaller bubbles with a slower foam collapse (smaller *k*-value) were formed.
- There was no apparent effect of temperature on the foamed binder properties when dispensing the foamed binder sample in a container kept at room temperature versus a container kept at elevated temperature inside a heating mantle.
- Liquid additives had an effect on foamed binder produced in the Accufoamer; the alkaline one (similar to Evotherm) produced a greater $ER_{max}$ and lower *k*-value, while the amine surfactant (Rediset) showed no difference with respect to the binder without additives.
- Viscosity measurements after foaming were lower than for the unfoamed binder. The difference, however, was the same regardless of the water content for foaming.
- No noticeable ER differences were observed for the binders with zeolite (Advera). However, when the binders were subjected to RTFO aging, there was a greater mass loss in the binders with zeolite, suggesting the presence and continued release of moisture from the blended binders.
- The effect of residual water was corroborated on binder samples foamed in the Accufoamer and subjected to RTFO aging, which also showed a greater mass loss than the unfoamed binder samples.

With respect to the effect of foaming on the rheological properties of the foamed binder residue after RTFO aging, there was a slight increase in the continuous high-temperature grade of the binder. The intermediate- and low-temperature performance of the foamed binder residue after PAV aging showed no change for the *S* and *m*-value bending beam BBR parameters, but a slight increase in $G^*\sin\delta$ as compared to the unfoamed binders.

The three foaming units (Wirtgen WLB 10S, InstroTek Accufoamer, and PTI foamer) showed distinct differences in the foamed binder properties. The Wirtgen foamer had the largest $ER_{max}$ values in the majority of the cases, while the PTI foamer had the lowest $ER_{max}$ values in all cases. In fact, the PTI foamer showed very small expansion compared to the other two units (in the range of 1 to 1.5). The FI was similar for the binders foamed with 1.0% water content in both the Wirtgen foamer and the Accufoamer, but was different when a larger water content (i.e., 3.0%) was used. With respect to the bubble size distribution analysis, in all three units, foamed bubbles decreased in size with elapsed time and became more homogeneous. In addition, the difference in bubble size seemed to be more pronounced at 3.0% water content versus 1.0% water content. The PTI foamer seemed to produce more stable bubbles regardless of the elapsed time after foaming. The size of the bubbles 90 s after foaming was about 0.11 in. (2.8 mm).

A laboratory mixture study was also conducted to establish the relationship between binder foam characteristics and mixture workability, coatability, and performance. Since foaming is intended to improve mixture workability and coatability, it was important to focus on the evaluation of workability and coatability of the foamed asphalt mixtures. The objectives of this portion of the research study were to (1) develop laboratory test methods to measure workability and coatability of asphalt mixtures, (2) evaluate the effect of different binder types and foaming water contents on the workability and coatability of foamed asphalt mixtures, and (3) compare the workability and coatability of foamed WMA versus HMA.

Maximum shear stress measured in the SGC was proposed as a mixture workability parameter; mixtures with lower maximum shear stress are considered more workable. For coatability, a procedure based on aggregate absorption was used. The method is based on the assumption that a completely coated aggregate submerged in water for a short period (i.e., 1 hour) cannot absorb water since water cannot penetrate through the binder film surrounding the aggregate surface. On the other hand, a partially coated aggregate is expected to have detectable water absorption since water is able to penetrate and be absorbed by the uncoated particle. The coatability index was proposed as the mixture coating parameter. A preliminary CI threshold of 70% was established based on the laboratory test results.

To verify the workability and coatability procedures, foamed WMA using three binders with three foaming water contents was produced using the Wirtgen foamer in addition to a control HMA produced using the same laboratory unit with no water. The workability and coatability of the foamed WMA mixtures were compared to the characteristics of the HMA mixtures. In addition, the effect of binder source, binder grade, and foaming water contents on mixture workability and coatability was investigated. The following observations were made based on the results:

- Significant differences in the maximum shear stress and CI for foamed WMA mixtures versus the control HMA were observed for two of the three binders.
- Two foamed WMA mixtures had better workability and coatability when 1.0% water content was used as compared to higher foaming water contents (i.e., 2.0% and 3.0%). Thus, 1.0% was considered the optimum foaming water content. However, equivalent workability and coatability were observed for the third WMA mixture as compared to the control HMA regardless of the foaming water content used.

- WMA mixtures produced at 1.0% foaming water content had better workability and coatability characteristics as compared to the control HMA, while WMA mixtures foamed at higher foaming water contents (i.e., 2.0% and 3.0%) had equivalent or worse characteristics as compared to the control HMA when mixed and compacted at the same temperatures. This finding highlights the importance of identifying the best materials and foaming conditions to maximize the workability and coatability of foamed mixtures.

A proposed foamed mix design approach was also validated, using the Wirtgen WLB 10S, InstroTek Accufoamer, and PTI foamer, as part of the mixture laboratory study. The results showed distinct workability trends from which an optimum water content was selected, although not all units produced the same binder foaming characteristics.

Finally, three field studies were conducted. An initial trial was done in Austin, Texas, to apply the laboratory test methods and metrics in a field setting as well as to compare the foamed binder measurements with the workability and coatability results. The on-site foaming measurements showed clear differences when the binder was sampled using an extension pipe versus directly from the valve outlet. In addition, the foaming metrics were different from the laboratory measurements performed with the Wirtgen foamer. The difference in sampling container size used in the laboratory and the field (i.e., 1 gallon versus 5 gallon) seemed to have an effect on the foamed binder metrics. A correction factor was determined for $ER_{max}$, but even after modifying the field values, the results were still smaller than the ones recorded in the Wirtgen foamer. With respect to workability, 1.0% was the optimum water content (lower shear stress). The performance evaluation of the mixtures showed equivalent or better performance as compared to the control HMA.

A second field study was done in two separate plants in Ohio to compare field foaming units (Terex and Gencor) against foamed binder and foamed mixture measurements. Similar to the initial trial, the on-site foaming measurements were different from the laboratory-foamed binder measurements in terms of $ER_{max}$ and *k*-value.

The third field study was done in Huntsville, Texas, with the objective of validating the proposed foamed mix design approach with plant data. An initial visit was done to measure foamed binder properties on-site and to collect loose mix and raw materials. After following the steps of the proposed mix design and finding the optimum water content, a second visit to the plant was made in order to request a change to the water content to match the optimum. During the second visit, foamed binder measurements were acquired again and loose mix collected.

With respect to the on-site foamed binder measurements, distinct differences were observed between the values obtained during the first and second visits. As expected, when the water content was reduced, the $ER_{max}$, *k*-value, and FI were reduced. The workability of the foamed mixture with the initial water content (5.5%) was worse than the control HMA. The laboratory measurements showed that the optimum water content was 1.5%, and at this water level, the workability had a dramatic improvement as compared to the control HMA. The foamed mixture at optimum water content had equivalent or better performance than the control HMA fabricated using the plant mix. The mix design was further evaluated using HMA specimens produced in the laboratory. As before, the performance of the foamed mixture with 1.5% water content was equivalent or better than that of the control HMA.

Based on the results of the laboratory and field foamed mix design validation studies, the initial approach that included determining the foaming ability of the binder was revised. This requirement was initially incorporated since the laboratory binder study showed some binders had little foaming ability. However, after following the proposed foamed mix design using various laboratory foaming units and plant data, it was clear that this step was not essential since the same binders in different foamers may or may not expand, but in all cases clear differences were observed when evaluating workability. Therefore, the revised foamed mix design recommendation, as shown in Figure 5-1, does not include this step, but it could still be performed at the discretion of the agency or organization conducting the mix design. In addition, the comparison against HMA was eliminated for practical purposes and because the comparisons performed in this study of the foamed mixtures at optimum water content versus HMA showed equivalent or better performance.

As shown in Figure 5-1, the procedure starts with materials selection for the development of a traditional AASHTO Superpave R 35 mix design procedure to determine the optimum binder content. Afterward, the optimum foaming water content is established using workability by measuring the maximum shear stress during compaction on foamed mixtures prepared at 1.0%, 2.0%, and 3.0% water content. The water content that yields the lowest maximum shear stress is considered the optimum. Then, coatability is evaluated at the optimum water content and compared against the CI threshold of 70%. The last step in the proposed mix design method is to evaluate the performance of the foamed asphalt mixtures at optimum water content via standard tests (resilient modulus per ASTM D7369, indirect tensile strength per AASHTO T 283, or HWTT per AASHTO T 324). If the selected performance parameter or parameters comply with established AASHTO or DOT specifications, the mixture is accepted. Otherwise, changes in mixture components should be considered and the mixture retested.

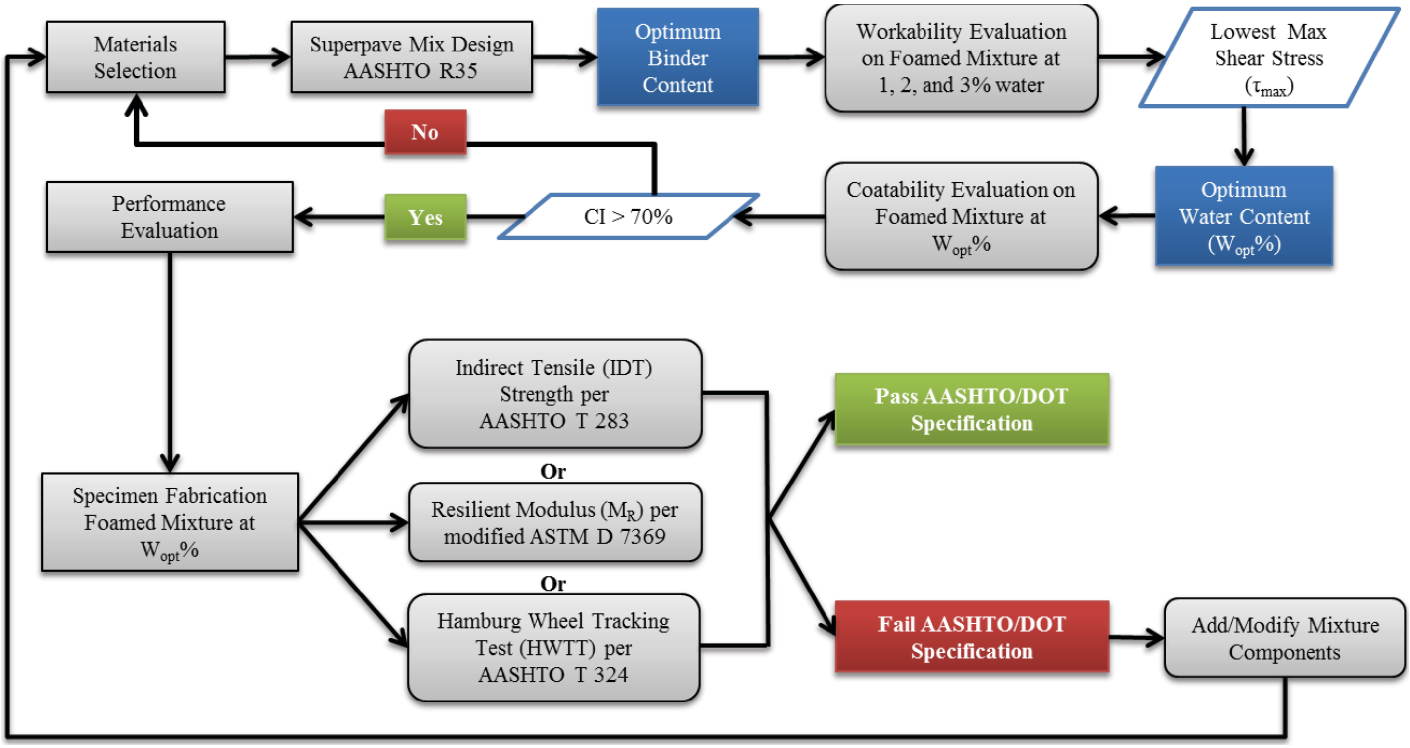


***Figure 5-1. Final recommended foamed asphalt mix design method.***

# References

Abbas, A. and A. Ali. 2011. Mechanical Properties of Warm Mix Asphalt Prepared Using Foamed Asphalt Binders. Report No. FHWA/OH-2011/6. Ohio Department of Transportation, Columbus.

Abbas, A., M. Nazzal, S. Sargand, A. Ali, A. Roy, and A. Alhasan. 2013. Determining the Limitations of Warm Mix Asphalt by Water Injection in Mix Design, Quality Control and Placement. Report No. FHWA/OH-2013/9. Ohio Department of Transportation, Columbus.

Abel, F. 1978. Foamed Asphalt Base Stabilization. Proceedings. 6th Annual Asphalt Paving Seminar. Colorado State University, Loveland.

Abel, F. and C. R. Hines. 1979. Base Stabilization with Foamed Asphalt. Interim Report, Colorado Department of Transportation, Denver, CO.

Adamson, A. W. and A. P. Gast. 1997. *Physical Chemistry of Surfaces*. John Wiley & Sons, Inc., New York.

Allosta, A. A., W. A. Zeiada, and K. Kaloush. 2011. Evaluation of Warm Mix Asphalt Versus Conventional Hot Mix Asphalt for Field And Laboratory-Compacted Specimens. Proceedings. 2nd Int'l Conf on Warm Mix Asphalt. National Asphalt Pavement Association, Lanham, MD. Accessed Oct. 22, 2011.

Andrés-Lacueva, C., E. López-Tamames, R. M. Lamuela-Raventós, S. Buxaderas, and M. del C. de la Torre-Boronat. 1996. Characteristics of Sparkling Base Wines Affecting Foam Behavior. *Journal of Agricultural and Food Chemistry*, 44(4), 989–995.

Arzhavitina, A. and H. Steckel. 2010. Foams for Pharmaceutical and Cosmetic Application. *International Journal of Pharmaceutics*, 394 (1–2), 1–17.

Berthier, J. 2008. Microdrops and Digital Microfluidics. William Andrew Publishing.

Bhasin, A., J. E., Howson, E. Masad, D. N. Little, and R. L. Lytton. 2007. Effect of Modification Processes on Bond Energy of Binders. *Transportation Research Record: Journal of the Transportation Research Board, No. 1998*, 29–37, Transportation Research Board of the National Academies, Washington, D.C.

Bistor, B. 2008. Florida Contractor Uses Warm Mix in Challenging Applications. Warm Mix Asphalt: Contractors' Experiences. IS 134. National Asphalt Pavement Association, Lanham, MD. pp. 18–19.

Bowering, R. H. and C. L. Martin. 1976. Foamed Bitumen Production and Application of Mixtures, Evaluation and Performance of Pavements. Proceedings. Association of Asphalt Paving Technologists. Vol. 45. Lino Lakes, MN. pp. 453–477.

Brennen, M., M. Tia, A. G. Altschaeffl, and L. E. Wood. 1983. Laboratory Investigation of the Use of Foamed Asphalt for Recycled Bituminous Pavements. *Transportation Research Record 911*. TRB, National Research Council, Washington, D.C. pp. 80–87.

Button, J. W., C. Estakhri, and A. Wimsatt. 2007. A Synthesis of Warm-Mix Asphalt. College Station, Texas Transportation Institute, College Station, Texas.

Castedo, F. L. H. and L. E. Wood. 1983. Stabilization with Foamed Asphalt of Aggregates Commonly Used in Low-Volume Roads. *Transportation Research Record 898*. TRB, National Research Council, Washington, D.C.

Clark, T. M. and T. M. Rorrer. 2011. Rapid Implementation of WMA in Virginia. Proceedings. 2nd Int'l Conf on Warm Mix Asphalt. National Asphalt Pavement Association, Lanham, MD. www.asphaltpavement.org. Accessed Oct. 22, 2011.

Csanyi, L. H. 1957. Foamed Asphalt in Bituminous Pavements. *Highway Research Record 160*. Highway Research Board. Washington, D.C. pp. 108–122.

D'Angelo, J., E. Harm, J. Bartoszek, G. Baumgardner, M. Corrigan, J. Cowsert, T. Harman, M. Jamshidi, W. Jones, D. Newcomb, B. Prowell, R. Sines, and B. Yeaton. 2008. Warm-Mix Asphalt: European Practice. Report No. FHWA-PL-08-007. Federal Highway Administration. Washington, D.C.

De Sombre, R., D. Newcomb, B. Chadbourn, and V. Voller. 1998. Parameters to Define the Laboratory Compaction Temperature Range of Hot-Mix Asphalt. *Paving Technology*. Vol. 67. Assn. of Asphalt Paving Technologists, Lino Lakes, MN. pp. 125–142.

Engelbrecht, D. C. 1999. Manufacturing Foam Bitumen in a Standard Drum Mixing Asphalt Plant. 7th Conference on Asphalt Pavements for Southern Africa, South Africa.

FHWA. 2008. Highway Statistics. Retrieved January 6, 2010, from http://www.fhwa.dot.gov/policyinformation/statistics/2008/.

Fort, J.-P., G. Graham, J. Farnham, S. Sinn, and G. M. Rowe. 2011. I-55/I-57 Warm Mix Project in Missouri Contractor's WMA Experience. Proceedings. 2nd Int'l Conf on Warm Mix Asphalt. National Asphalt Pavement Association, Lanham, MD. www.asphaltpavement.org. Accessed Oct. 22, 2011.

Fu, P. 2011. Foamed Asphalt 101. http://foam101.info/Science/Asphalt.html Sustainable Transportation Center. University of California Davis. Accessed December 5, 2011.

Fu, P., D. Jones, and J. T. Harvey. 2011. The Effects of Binder and Granular Material Characteristics on Foamed Asphalt Mix Strength. *Construction and Building Materials*, 25(2), 1093–1101.

Gallart, M., E. López-Tamames, and S. Buxaderas. 1997. Foam Measurements in Wines? Comparison of Parameters Obtained by Gas Sparging Method. *Journal of Agricultural and Food Chemistry*, 45(12), 4687–4690.

German, J., T. O'Neill, and J. Kinsella. 1985. Film Forming and Foaming Behavior of Food Proteins. *Journal of the American Oil Chemists' Society*, 62(9), 1358–1366.

Hajj, E. Y., C. Chia, P. E. Sebaaly, A. M. Kasozi, and S. Gibson. 2011. Properties of Foamed Warm-Mix Asphalt Incorporating Recycled Asphalt Pavement from Two Field Projects—Case Studies. Proceedings. 2nd Int'l Conf on Warm Mix Asphalt. National Asphalt Pavement Association, Lanham, MD. www.asphaltpavement.org. Accessed Oct. 22, 2011.

Hailisilassie, B., P. Schuetz, I. Jergen, A. Bieder, M. Hugener, and M. N. Partl. 2014. Evolution of Bubble Size Distribution During Foam Bitumen Formation and Decay. Presentation in Session W-1-D. International Conference on Asphalt Pavements. International Society for Asphalt Pavements, Raleigh, North Carolina.

Hansen, K. and A. Copeland. April 2013. 2nd Annual Asphalt Pavement Industry Survey on Reclaimed Asphalt Pavement, Reclaimed Asphalt Shingles, and Warm-Mix Asphalt Usage: 2009–2011. Information Series 138. National Asphalt Pavement Association, Lanham, MD.

Harder, G. A., Y. LeGoff, A. Loustou, Y. Martineau, B. Heritier, and A. Romier. 2008. Energy and Environmental Gains of Warm and Half-Warm Asphalt Mix: Quantitative Approach. *TRB 87th Annual Meeting Compendium of Papers*. DVD. Transportation Research Board of the National Academies, Washington, D.C.

He, G. and W. Wong. 2006. Decay Properties of the Foamed Bitumens. *Construction and Building Materials*, 20(10), 866–877.

Huang, X. L., G. L. Catignani, and H. E. Swaisgood. 1997. Micro-Scale Method for Determining Foaming Properties of Protein. *Journal of Food Science*, 62(5), 1028–1060.

Hurley, G. C. and B. Prowell. 2005. Evaluation of Aspha-Min Zeolite for Use in Warm Mix Asphalt. National Center for Asphalt Technology, Auburn, AL.

Jenkins, K. J. 2000. Mix Design Considerations for Cold and Half-Warm Bituminous Mixes with Emphasis on Foamed Bitumen. Doctoral Dissertation, University of Stellenbosch, South Africa.

Jenkins, K. J., A. A. A. Molenaar, J. L. A. de Groot, and M. F. C. van de Ven. 2002. Foamed Asphalt Produced Using Warmed Aggregates. *Journal of the Association of Asphalt Paving Technologists 71:* 444–478.

Jones, W. 2004. Warm Mix Asphalt Pavements: Technology of the Future? *Asphalt*. The Asphalt Institute. Lexington, KY. pp. 8–11.

Kandhal, P. S., K. Y. Foo, and R. B. Mallick. 1988. A Critical Review of VMA Requirements in Superpave. NCAT Report No. 98-1.

Kealy, T., A. Abram, B. Hunt, and R. Buchta. 2008. The Rheological Properties of Pharmaceutical Foam: Implications for Use. *International Journal of Pharmaceutics*, 355(1-2), 67–80.

Kekevi, N., H. Berber, and H. Yildirim. 2012. Synthesis and Characterization of Silicone-Based Surfactants as Anti-Foaming Agents. *J Surfact Deterg*, Springer, 15:73–81.

Kim, Y. and W. Li. 2011. Modeling of a Subcritical $CO_2$ Microcellular Extrusion Process. North American Manufacturing Research Conference, Corvallis, Oregon.

Klempner, D., V. Sendijarevic, and R. M. Aseeva. 2004. Polymeric Foams and Foam Technology. Hanser Verlag.

Koehler, S. A., H. A. Stone, M. P. Brenner, and J. Eggers. 1998. Dynamics of Foam Drainage. *Physical Review E*, 58(2), 2097–2106.

Koenders, B. G., D. A. Stoker, C. Robertus, O. Larsen, and J. Johansen. 2002. WAM-Foam, Asphalt Production at Lower Operating Temperatures. Proceedings. 9th International Conference on Asphalt Pavements, Copenhagen, Denmark, International Society for Asphalt Pavements.

Kristjansdottir, O. 2006. Warm Mix Asphalt for Cold Weather Paving. M. S. Thesis. Civil Engineering. Seattle, University of Washington.

Kuennen, T. 2004. Warm Mixes Are a Hot Topic. *Better Roads*. 74-6. James Informational Media. Des Plaines, IA.

Leibson, I., E. G. Holcomb, A. G. Cacoso, and J. J. Jacmic. 1956. Rate of Flow and Mechanics of Bubble Formation from Single Submerged Orifices. II. Mechanics of Bubble Formation. *AIChE Journal*, 2(3), 300–306.

Muthen, K. M. 1998. Foamed Asphalt Mixes—Mix Design Procedure. Report No. CR-98/077. CSIR Transportek. Pretoria.

McKenzie, P. 2006. Taking a Closer Look at Warm Mix. *Better Roads*. 74-6. James Informational Media, Des Plaines, IA.

Namutebi, M. 2011. Some Aspects of Foamed Bitumen Technology. Dissertation, KTH.

Namutebi, M., B. Birgisson, and U. Bagampadde. 2011. Foaming Effects on Binder Chemistry and Aggregate Coatability Using Foamed Bitumen. *Road Materials and Pavement Design*. 12:4. Taylor and Francis. pp. 821–847.

National Asphalt Pavement Association (NAPA). 2010. Asphalt Industry Update and Overview. Retrieved January 6, 2010, from http://www.hotmix.org/index.php?option=com_content&task=view&id=14&Itemid=33.

National Center for Asphalt Technology (NCAT). 2005. NCAT Evaluates Warm Mix Asphalt. *Asphalt Technology News*. Vol. 17, No.2. Auburn University. pp. 1–5.

Nazzal, M. D., S. Sargand, D. Powers, E. P. Morrison, and A. Al-Rawashdeh. 2011. Evaluation of Fine Graded Polymer Asphalt Mixture Produced Using Foamed Warm Mix Asphalt Technology. Proceedings. 2nd Int'l Conf on Warm Mix Asphalt. National Asphalt Pavement Association, Lanham, MD. www.asphaltpavements.org. Accessed October 6, 2011.

Newcomb, D. 2005a. Warm Mix Asphalt: Wave of the Future. HMAT. July/August. National Asphalt Pavement Association, Lanham, MD.

Newcomb, D. 2005b. Warm Mix Asphalt. Retrieved January 6, 2010, from http://cms.transportation.org/sites/construction/docs/Newcomb%20-%20Warm%20Mix%20Asphalt.pdf.

Ozturk, H. I. and M. Kutay. 2014a. Effect of Foamed Binder Characteristics on Warm Mix Asphalt (WMA) Performance. Paper No. 14-3953. TRB 93rd Annual Meeting Compendium of Papers. CD-ROM. Transportation Research Board of the National Academies, Washington, D.C.

Ozturk, H. I. and M. Kutay. 2014b. Sensitivity of Nozzle–Based Foamed Asphalt Binder Characteristics to Foaming Parameters. Paper No. 14-3961. TRB 93rd Annual Meeting Compendium of Papers. CD-ROM. Transportation Research Board of the National Academies, Washington, D.C.

Pellicer, J., V. García-Morales, and M. J. Hernández. 2000. On the Demonstration of the Young-Laplace Equation in Introductory Physics Courses. *Physics Education*, 35(2), 126.

Phillips, L. G., Z. Haque, and J. E. Kinsella. 1987. A Method for the Measurement of Foam Formation and Stability. *Journal of Food Science*, 52(4), 1074–1077.

Prowell, B., G. C. Hurley, and B. Frank. 2011a. Warm Mix Asphalt: Best Practices. QIS 125. 2nd Edition. National Asphalt Pavement Association, Lanham, MD.

Prowell, B., R. J. Schreck, and S. Sasaki. 2011b. Evaluation of the Benefits of Foamed Asphalt Mixtures at Varying Production Temperatures. Proceedings. 2nd Int'l Conf on Warm Mix Asphalt. National Asphalt Pavement Association, Lanham, MD. www.asphaltpavement.org. Accessed Oct. 22, 2011.

Pugh, R. J. 2005. Experimental Techniques for Studying the Structure of Foams and Froths. *Advances in Colloid and Interface Science*, 114–115, 239–251.

Raymundo, A., J. Empis, and I. Sousa. 1998. Method to Evaluate Foaming Performance. *Journal of Food Engineering*, 36(4), 445–452.

Romier, A., M. Audeon, J. David, Y. Martineau, and F. Olard. 2006. Low-Energy Asphalt with Performance of Hot-Mix Asphalt. *Transportation Research Record: Journal of the Transportation Research Board, No. 1962*. Transportation Research Board of the National Academies, Washington, D.C. pp. 101–112.

Sakr, H. A. and P. G. Manke. 1985. Innovations in Oklahoma Foamix Design Procedures. *Transportation Research Record 1034*. TRB, National Research Council, Washington, D.C. pp. 26–34.

Saye, R. I. and J. A. Sethian. 2013. Multiscale Modeling of Membrane Rearrangement, Drainage, and Rupture in Evolving Foams. *Science*, 340(6133), 720–724.

Schick, C. 2004. A Mathematical Analysis of Foam Films. Doctoral Dissertation, Kaiserslautern University of Technology, Kaiserslautern, Germany.

Schramm, L. L. 1994. Foam Stability in the Presence of Crude Oil. Foams: Fundamentals and Applications in the Petroleum Industry. Schramm, L. L., ed. Advances in Chemistry Series No. 242. American Chemical Society. pp. 165–197.

Stroup-Gardiner, M., C. R. Lange, and A. Carter. 2005. Quantification of Emission Potential from Binders Using Mass Loss and Opacity Measurements. *International Journal of Pavement Engineering*, 6 (3): 191–200.

Sunarjono, S. I. 2008. Influence of Foamed Bitumen Characteristics on Cold Mix Asphalt Properties. Ph.D. Dissertation. University of Nottingham. England.

Uhlig, H. H. 1937. The Solubilities of Gases and Surface Tension. *J Phys Chem* 41:1215–1225.

Ursich, C. 2008. Flexible Pavements of Ohio Helps Industry Get a Closer Look at Warm Mix. Warm Mix Asphalt: Contractors' Experiences. IS 134. National Asphalt Pavement Association, Lanham, MD. pp. 14–16.

Velasquez, R., G. Cuciniello, D. Swiertz, R. Bonaquist, and H. Bahia. 2010. Methods to Evaluate Aggregate Coating for Asphalt Mixtures Produced at WMA Temperatures. Canadian Technical Asphalt Association Proceedings.

Wang, H. and W. Li. 2008. Selective Ultrasonic Foaming of Polymer for Biomedical Applications. *ASME Transaction Journal of Manufacturing Science and Engineering*, Vol. 130, No. 2, pp. 021004-1-021004-9.

Wilde, P. J. 1996. Foam Measurement by the Microconductivity Technique: An Assessment of Its Sensitivity to Interfacial and Environmental Factors. *Journal of Colloid and Interface Science*, 178(2), pp.733–739.

Xu, J. 2010. Microcellular Injection Molding. Wiley Series on Polymer Engineering and Technology. R. F. Grossman and D. Nwabunma, ed. John Wiley and Sons, Inc.

Yin, F., E. Arambula, R. Lytton, A. Epps Martin, and L. Garcia Cucalon. 2014. Novel Method to Evaluate Moisture Susceptibility and Rutting Resistance of Asphalt Mixtures Using the Hamburg Wheel Tracking Test. *Transportation Research Record: Journal of the Transportation Research Board, No. 2446*. Transportation Research Board of the National Academies, Washington, D.C. pp. 1–7.

Zettler, R. 2006. Warm Mix Stands Up to Its Trials. *Better Roads*. 76-2. James Informational Media. Des Plaines, IA.

# Abbreviations, Acronyms, and Definitions

| | |
|---|---|
| BBR | Bending Beam Rheometer – A device for measuring the low-temperature stiffness of asphalt binder. |
| CI | Coatability Index – A measure of the binder's ability to coat aggregate particles by measuring water absorption of the coarse aggregate mixed with binder relative to the water absorption of the bare coarse aggregate. |
| CT | Computed Tomography – A method to acquire and interpret a two-dimensional x-ray image of an object to study its internal structure nondestructively. |
| $\Delta\varepsilon_{SN}^{vp}$ | Viscoplastic Strain at $LC_{SN}$ – A measure of non-recoverable deformation in the Hamburg Wheel Tracking Test. |
| DSR | Dynamic Shear Rheometer – A device to measure the shear modulus and phase angle of a substance at various temperatures and loading frequencies. |
| ER | Expansion Ratio – The volume of a foamed liquid at any point in time relative to its unfoamed volume. |
| $ER_{max}$ | Maximum Expansion Ratio – The greatest volume increase experienced by a foamed liquid. |
| FI | Foamability Index – The area under the curve defined by the expansion ratio of a liquid versus time. |
| HL | Half-Life – The period between the maximum expansion ratio and one-half of the expansion ratio. |
| HMA | Hot Mix Asphalt – An asphalt mixture produced at a temperature above 275°F (135°C). |
| HWTT | Hamburg Wheel Tracking Test – A loaded-wheel method of ascertaining the stripping and rutting susceptibility of an asphalt mixture. |
| IDT | Indirect Tensile (Strength Test) – A test method in which a cylindrical sample of material is loaded diametrically to produce a region of uniform tensile strain in the horizontal direction. |
| *k*-value | Rate of Collapse of Semi-Stable Foam – The slope of the curve defined by the expansion ratio of a liquid versus time at a specific time interval. |
| $LC_{SN}$ | Load Cycles to Stripping Number – In the Hamburg Wheel Tracking Test, it is the number of loading repetitions at which the curve of rut depth versus loading cycles changes from negative to positive curvature. |
| $LC_{ST}$ | Load Cycles to Remaining Life – Number of additional load cycles after $LC_{SN}$ needed for the rut depth accumulated by the stripping strain to reach a certain rut depth, usually 0.5 in. (12.5 mm). |

| | |
|---|---|
| LDM | Laser Distance Meter – A device employing light reflection to measure length. |
| LEA | Low-Emission Asphalt – A name given to a WMA production process in which wet sand is used to create foamed asphalt binder during mixing. |
| LMLC | Laboratory Mixed, Laboratory Compacted – A type of asphalt mixture specimen where the mixture components are combined and compacted in the laboratory. |
| $M_R$ | Resilient Modulus – A repeated load indirect tension test to obtain the stiffness of a material. |
| NAPA | National Asphalt Pavement Association – A trade association of plant asphalt mixture producers in the United States. |
| PAV | Pressure Aging Vessel – A device for rapidly oxidizing asphalt binder to simulate approximately 5 years of field aging. |
| PMLC | Plant Mix Laboratory Compacted – A type of asphalt mixture specimen where the mixture components are combined in an asphalt mixing plant and compacted in the laboratory. |
| RTFO | Rolling Thin Film Oven – A method for simulating asphalt plant aging in the laboratory. |
| SAI | Surface Area Index – The ratio of the estimated surface area of all bubbles in a foamed liquid at a given time to the surface area of the unfoamed liquid. |
| SGC | Superpave Gyratory Compactor – A type of laboratory asphalt mixture compactor designed to produce cylindrical specimens for testing. |
| $\tau_{max}$ | Maximum Shear Stress – In a Superpave gyratory compactor, it is the greatest level of stress generated in the horizontal plane during compaction. |
| TSR | Tensile Strength Ratio – The wet-conditioned indirect tensile strength divided by the dry indirect tensile strength. |
| WMA | Warm Mix Asphalt– An asphalt mixture produced at a mixing temperature of less than 275°F (135°C). |

APPENDIX A

# Influence of Binder Properties on Binder Foam Expansion

A validated physical model for binder foaming can be an extremely useful tool to understand and explain the impact of various factors on binder foaming. For example, a physical model can be used to qualitatively explain the effects of temperature, binder type, water content, additive, and foaming nozzle (through water droplet size during mixing of binder with water) on the foaming characteristics. Eventually, this knowledge can be used to (1) identify the factors that have the most significant impact on foaming characteristics and (2) optimize the water content for effective foaming of different binders. To this end, a physical model that explains expansion and foaming in binders is presented in the following section.

## Analytical Background

Foamed binder is produced through the injection of small droplets of cold water into hot binder. When a droplet of water comes in contact with hot binder, it turns into steam and expands to form a bubble. Binder that forms the skin of the bubble holds the pressurized steam within it by balancing the difference between the internal and atmospheric pressure with its surface tension. This process occurs for each droplet, resulting in a foamed binder. The relationship between external atmospheric pressure, internal pressure due to steam, and surface tension is given by the Laplace equation (Equation A-1). The internal pressure due to steam can also be calculated using the universal gas law (Equation A-2). The two equations (Laplace and universal gas law) can be combined to obtain a relationship between the bubble diameter, droplet size, temperature, and surface tension of the binder, as shown in Equation A-3. The main assumptions in these two equations are that the gas (steam) in each of the bubbles is ideal, the bubbles are spherical, and every droplet of water converts into steam and is effective in forming a bubble. The only unknown parameters to employ in these equations are the surface tension of the binder at the foaming temperature and the size distribution of the water droplets. The size distribution of water droplets diffusing within the binder is in turn dictated by factors such as the water content and design of the foaming nozzle.

$$P_{bubble} - P_{atm} = \frac{4\gamma}{D} \quad \text{(A-1)}$$

Where:

$P_{bubble}$ = pressure inside the bubble (Pa).
$P_{atm}$ = atmospheric pressure (Typical value: 101325 Pa).
$\gamma$ = surface tension of the binder (N/m).
$D$ = bubble diameter (m).

$$P_{bubble}V = nRT \quad \text{(A-2)}$$

Where:

$P_{bubble}$ = pressure inside the bubble (Pa).
$V$ = volume of the bubble ($m^3$).
$n$ = number of moles (mass/atomic mass of compound).
$R$ = the universal gas constant (8.314 J/mole. Kelvin).
$T$ = temperature (Kelvin).

$$\frac{P_{atm}\pi D^3}{6} + \frac{2\gamma\pi D^2}{3} - nRT = 0 \quad \text{(A-3)}$$

Where:

$P_{atm}$ = the atmospheric pressure (Pa).
$\gamma$ = the surface tension of the binder (N/m).
$D$ = the diameter of the bubble (m).
$n$ = number of moles (mass/atomic mass of compound).
$R$ = the universal gas constant (8.314 J/mole. Kelvin).
$T$ = foaming temperature (Kelvin).

The aforementioned physical relationships were used to (1) develop a physical model to theoretically determine $ER_{max}$ using water content, initial bubble size distribution, and surface tension of base binders as inputs, and (2) employ the theoretical analysis in conjunction with experimental data to explore the impact of water content, initial bubble size distribution, and surface tension of binders on $ER_{max}$.

## Materials and Test Method

To accomplish the aforementioned objectives, a testing program was designed to measure $ER_{max}$, bubble size distribution on the surface of the foam, and surface tension of base binders. Three binders were used for this study: N6, N7, and O7. Each binder was foamed in the laboratory using the Accufoamer foaming unit at three water contents that varied from 1% to 3% by weight of the binder. All foaming was carried out at 160°C.

Test procedures included the use of the following: a laser sensor to measure ER as a function of time, a digital camera to measure bubble size distribution on the surface of the foam, and a maximum bubble pressure device (manufactured by SensaDyne) to measure surface tension of the binders.

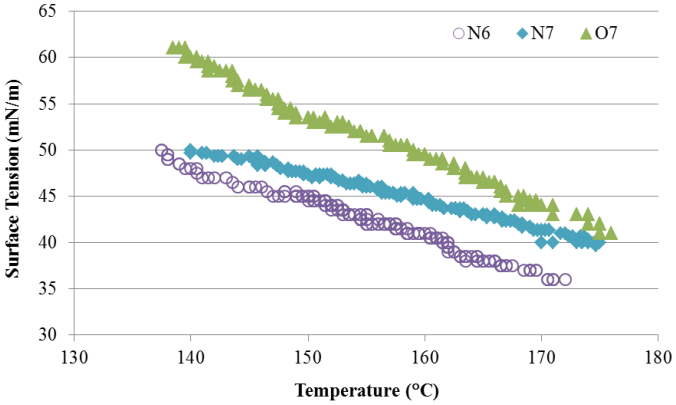


*Figure A-1. Surface tension of binders as a function of temperature.*

## Results of the Parametric Analysis

### Influence of Surface Tension on Bubble Size Distribution

The surface tensions of the three binders were measured using the differential maximum bubble pressure method. This method measures the pressure difference between two capillaries of different radii as bubbles are produced by injecting a gas through these capillaries when immersed in the binder. In this study, argon was injected through the binder via two orifices of different diameters. The pressure differential between the bubbles from the two orifices was measured using a differential pressure transducer. Water at different temperatures was used to calibrate the transducer. The maximum differential bubble pressure is directly proportional to the surface tension of the binder. The surface tension of the binder was continually measured and recorded over a range of temperatures. A bubble flow rate of 1 bubble/s was used for these tests. Figure A-1 illustrates the surface tension of the three binders as a function of temperature. The test results demonstrate that the surface tension of binders is linearly related to temperature; this is true for most liquids.

The surface tension of the binders was used with the Laplace equation to determine the internal pressure within the foam bubbles. The most important feature of the Laplace equation is that the pressure required to maintain the bubble is inversely proportional to its diameter. This means that smaller bubbles have greater internal steam pressures. The expected internal pressure within the bubbles was calculated for different bubble diameters assuming the binder surface tension to be 45 mN/m. Figure A-2 illustrates the results from this analysis.

These results show that bubble size does not significantly affect the internal bubble pressure for binder bubbles that are greater than 100 micrometers in diameter. In other words, the contribution of surface tension to internal steam pressure is negligible (for bubbles greater than 100 micrometers). A corollary to this is that **the bubble size distribution of the foamed binder is not significantly affected by the surface tension of the base binder, and internal steam pressure is approximately equal to atmospheric pressure**.

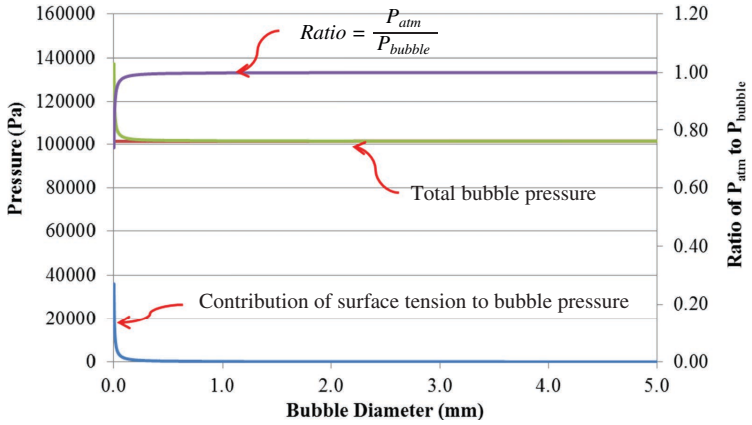


*Figure A-2. Influence of surface tension on binder foam internal pressure.*

Image analysis of the binder foam surface at different times showed that bubbles have sizes that are much higher than 100 micrometers.

## Influence of Bubble Size Distribution on $ER_{max}$

An analysis was conducted to determine whether the initial distribution of water droplets in the mixing unit of the foaming device and the subsequent initial distribution of the bubble diameters had an impact on $ER_{max}$. $ER_{max}$ was calculated for several initial water droplet/bubble size distributions for a given water content, and surface tension of the binder ($\gamma = 45$ mN/m) was kept as a constant. The methodology used for this analysis was as follows.

The mass of the binder ($m_{binder}$) used for this analysis was 200 g, which is also the mass used in the experimental measurements. The atmospheric pressure ($P_{atm}$) was taken as 101,325 N/m$^2$, and it was assumed that $m_{water}$ grams of water were added by the foaming unit by dispensing and mixing it with the binder in the form of $N$ number of water droplets. Consequently, $N$ numbers of binder foam bubbles are created. Using the Laplace equation, the following can be obtained for the internal pressure of any bubble $j$:

$$P_{bubble\ j} = P_{atm} + \frac{4\gamma}{D_j} \tag{A-4}$$

The following equation can be derived by solving Equation A-3 for $n_j$:

$$n_j = \frac{101325\pi D_j^3}{6RT_f} + \frac{2\gamma\pi D_j^2}{3RT_f} \tag{A-5}$$

The number of water droplets, $N$, can be obtained as:

$$N = \frac{m_{water}}{18n_{avg}} \tag{A-6}$$

Substituting Equation A-4 into the ideal gas law equation, individual bubble volume ($V_j$) can be calculated as follows:

$$V_j = \frac{n_j RT_f}{P_{bubble\ j}} = \frac{\frac{P_{atm}\pi D_j^3}{6} + \frac{2\gamma\pi D_j^2}{3}}{P_{atm} + \frac{4\gamma}{D_j}} \tag{A-7}$$

The cumulative volume of foam, $V_t$, for $N$ number of water droplets is the sum of the individual bubble volume and the volume of the binder:

$$V_t = \sum_{j=1}^{N} V_j + V_{binder} \tag{A-8}$$

$$ER_{max} = \frac{V_t}{V_{binder}} = \frac{\sum_{j=1}^{N} V_j + V_{binder}}{V_{binder}} \tag{A-9}$$

Volume of the binder (without foam), $V_{binder}$, can be determined using mass ($m_{binder}$) and density of the unfoamed binder, taken as 1.034 g/cm$^3$:

$$V_{binder} = \frac{m_{binder}}{1.034} = 0.967 m_{binder} \tag{A-10}$$

Where:

$T_f$ = the temperature of the foam (not the same as the foaming temperature of the binder).

When the binder at 160°C mixes with water at 25°C (room temperature), the foam will have a temperature lower than the temperature of the binder. The temperature of the foam can be determined using thermal equilibrium, assuming no heat is lost during the foaming process. If $T_f$ is the final temperature of the foam, the quantity of excess heat, $Q$, available from the binder to vaporize water can be determined as:

$$Q = m_{binder} C_{binder} (160 - T_f) \tag{A-11}$$

Where:

$C_{binder}$ = the specific heat of binder ($C_{binder} = 2.093$ J/g/°C).

The excess heat, $Q$, from the binder is equivalent to the amount of heat needed to vaporize $m_{water}$ at 25°C and raise its temperature to $T_f$, which can be determined as:

$$Q = m_{water} C_{water} (T_f - 25) + m_{water} L_v \tag{A-12}$$

Where:

$C_{water}$ = the specific heat of water ($C_{water} = 4.185$ J/g/°C).

$L_v$ = latent heat of vaporization ($L_v = 2256$ J/g).

Combining Equations A-11 and A-12 and solving for $T_f$:

$$T_f = \frac{160 * m_{binder} C_{binder} + 25 * m_{water} C_{water} - m_{water} L_v}{m_{binder} C_{binder} + m_{water} C_{water}} \tag{A-13}$$

Substituting these values for the 200 g binder foamed with 1% (2 g) water content and solving Equation A-13, $T_f = 146.8$°C.

A typical average bubble size of 4.2-mm diameter was assumed for the analysis. The number of moles, $n$, for the average bubble size was back-calculated using Equation A-5. $N$ was then determined using Equation A-6. That is, water is dispensed in the form of 101,756 droplets with each weighing 19.65 micrograms to mix with the binder and produce foam. The volume of the bubbles for each of the droplets and then the total volume of the foam were computed. For a mean of 19.65 micrograms, the total volume of the foam was

calculated as 4,147 cm$^3$. This translates into an $ER_{max}$ of 20.7 for the 200 g of binder used in these calculations.

Similarly, $ER_{max}$ was computed for several different bubble diameters and numbers of bubbles. Figure A-3 presents a summary of results from this analysis. Note that for a given water content, only one of the two parameters, initial average bubble diameter or number of bubbles, needs to be assumed, while the other can be calculated. Results of the analysis demonstrate that $ER_{max}$ remains the same irrespective of the bubble size and number of bubbles as long as the total water content turning into steam and forming the bubbles was constant. In other words, **for a given volume of binder and water content, bubble size distribution does not significantly affect the maximum expansion ratio of the foam for bubbles that are more than 100 micrometers in diameter**. The theoretical maximum expansion ratio was also computed by varying the surface tension of the binder between 40 and 60 mN/m for a fixed water content and an assumed initial bubble/water droplet size distribution. The results from this analysis show that the surface tension of the binders (in the range specified previously) does not significantly affect the maximum expansion ratio. This is consistent with the analysis shown in Figure A-2. **The bubble size distribution affects rate of foam decay because of Stokes' law**.

Hence, for large bubbles (bubbles that are more than 100 micrometers in diameter) where the surface tension of the binder does not affect the bubble volume significantly, the equation for $ER_{max}$ can be simplified as follows.

From Equation A-9, $ER_{max}$ is given by:

$$ER_{max} = \frac{V_t}{V_{binder}} = \frac{V_{bubble} + V_{binder}}{V_{binder}} \quad \text{(A-14)}$$

Total volume of the bubble, $V_{bubble}$, can be determined using the ideal gas law equation:

$$V_{bubble} = \frac{nRT_f}{P_{atm}} = \frac{\frac{m_{water}}{18}RT_f}{P_{atm}} = \frac{m_{water}RT_f}{18P_{atm}} \quad \text{(A-15)}$$

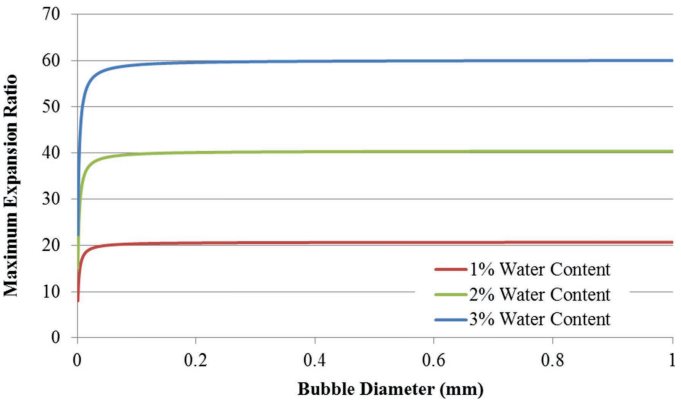


***Figure A-3. Influence of bubble size on maximum expansion ratio.***

Hence, $ER_{max}$ can be simplified to:

$$ER_{max} = \frac{V_{bubble} + V_{binder}}{V_{binder}} = \frac{\frac{m_{water}RT_f}{18P_{atm}} + 0.967m_{binder}}{0.967m_{binder}}$$

$$ER_{max} = \frac{m_{water}RT_f + 17.41m_{binder}P_{atm}}{17.41m_{binder}P_{atm}} \quad \text{(A-16)}$$

The excess heat available from the binder can also be used to determine the theoretical maximum amount of water that can be added to the binder for foaming. If water exceeding this threshold is added, a portion of the foaming water will not be converted to steam due to lack of heat to achieve this. Combining Equations A-11 and A-12, and solving for $m_{water}$:

$$m_{water} = \frac{m_{binder}C_{binder}(160 - T_f)}{C_{water}(T_f - 25) + L_v} \quad \text{(A-17)}$$

If the minimum foam temperature, $T_f$, is set to a typical WMA mixing temperature, for example, to 135°C, the maximum limit will be 3.85 g. This value translates to 1.93% water content. Also, theoretically a binder at a temperature of 160°C has enough heat to convert a maximum value of 4.89% water by weight, resulting in a foam at a temperature of 100°C (boiling point of water). In other words, if one were to mix more than approximately 5% of water at room temperature with the binder at 160°C, the temperature of the resulting foam would fall to 100°C, preventing conversion of excess water to steam.

## Effect of Foaming Water Content on Foaming Efficiency

By comparing the theoretical $ER_{max}$ to the measured $ER_{max}$, it is possible to determine the percentage of water that is effective in foaming the binder. This comparison for the three binders at 1%, 2%, and 3% water content reveals that the measured expansion ratio is consistently much lower than the theoretical maximum expansion ratio. The ratio between the measured and theoretical expansion ratios decreases as the water content increases (Figure A-4). Despite the ideal conditions assumed for the theoretical $ER_{max}$, the results clearly indicate that not all water added to the binder is effective in foaming the binder. It is also clear that as the water content is increased, the percentage of water that is effective in foaming decreases. The reduced foaming may be due to incomplete mixing of the water droplets with the binder during the production of the foam. Other factors, such as the dispensing mechanism of the foaming unit, can also affect the percentage of water that is effective in foaming.

Although results from Figure A-2 illustrate that the surface tension of the binder does not influence the size of large foamed bubbles, the surface tension of the binder may still affect the

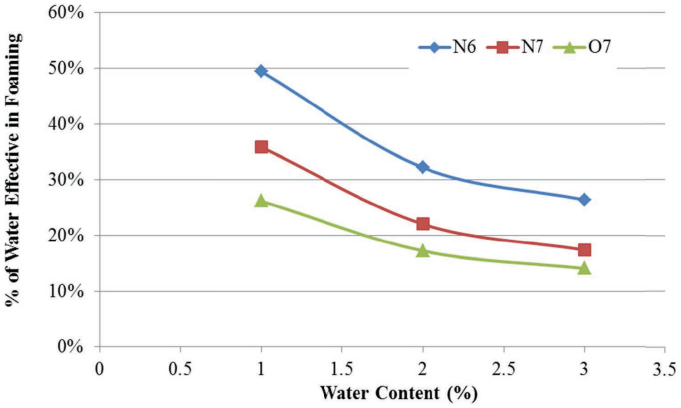


***Figure A-4. Percent of water effective in foaming as a function of water content.***

mixing characteristics of water droplets with the binder, consequently affecting the percentage of water that is effective in foaming. For example, Berthier (2008) showed that on a microscopic scale, surface tension and capillary forces dominate the fluid mechanics of micro-droplets. Surface tension and capillary forces dominate gravity or inertia forces, which are dominant on a macroscopic scale. The surface tension and capillary forces play a key role in determining the behavior of micro-droplets on different substrates and geometry in microsystems (Berthier 2008). Uhlig (1937) also investigated the relationship between surface tension and solubility of gases and developed a theory to describe the solubility of gases based on energy change in transferring a solute molecule of radius $r$ to a solvent of surface tension $\sigma$ as follows:

$$ln\gamma = \frac{-4\pi r^2\sigma + E}{kT} \quad \text{(A-18)}$$

Where:

$E$ = the interaction energy of solute and solvent.
$\gamma$ = solubility (ratio of concentration of solute in the solvent to that in the gas).
$K$ = the Boltzmann's constant.
$T$ = the absolute temperature.

Solubility is defined as the ratio of concentration of solute in the solvent to that in the gas. The equation derived by Uhlig (1937) demonstrates that solubility decreases as the surface tension of the solvent increases. Therefore, the surface tension of binders at the foaming temperature may affect the efficiency with which the binder and water mix with each other to produce foam. To investigate this, the surface tensions of three binders (N6, N7, and O7) at the foaming temperatures were compared to solubility (ratio of water effective in foaming to that of water wasted). The surface tensions of the binders determined using the differential maximum bubble pressure method are presented in Table A-1. The percent of water effective in foaming was back-calculated using the lab-measured maximum expansion ratio, $ER_{max}$. The percent effective water content and solubility values for the three binders at three water contents are presented in Table A-2.

Figure A-5 compares the surface tensions of the binders to solubility and shows a strong correlation between solubility and surface tension of binders. Figure A-6 shows a similar trend between percent of water effective in foaming to surface tension of binders. These empirical results indicate that the surface tension of the binder dictates the efficiency with which water mixes with the binder to produce foam. Once this relationship is established, the maximum expansion ratio can be theoretically estimated using the equations developed in the previous section. However, more data need to be collected for a thorough theoretical investigation of this phenomenon.

The following conclusions were drawn on the basis of the results from the theoretical analysis:

1. The surface tension of the binder affects $ER_{max}$ significantly, not by influencing the internal pressure of bubbles but by affecting mixing characteristics of binders with water.
2. The initial bubble size (or water droplet size) distribution does not affect the maximum expansion ratio of the

**Table A-1. Surface tension of base binders and final temperature of binder foams at various water contents.**

| Water Content (%) | Foam Temperature ($T_f$), °C | Surface Tension, mN/m | | |
|---|---|---|---|---|
| | | N6 | N7 | O7 |
| 1 | 146.8 | 45.8 | 48.4 | 55.9 |
| 2 | 134.1 | 50.9 | 52.2 | 62.3 |
| 3 | 121.9 | 55.8 | 55.8 | 68.5 |

**Table A-2. Effective water content and solubility of binder foams.**

| Water Content (%) | Effective Water Content (%) | | | Solubility | | |
|---|---|---|---|---|---|---|
| | N6 | N7 | O7 | N6 | N7 | O7 |
| 1 | 0.49 | 0.36 | 0.26 | 0.979 | 0.559 | 0.355 |
| 2 | 0.32 | 0.22 | 0.17 | 0.474 | 0.283 | 0.208 |
| 3 | 0.26 | 0.17 | 0.14 | 0.359 | 0.210 | 0.164 |

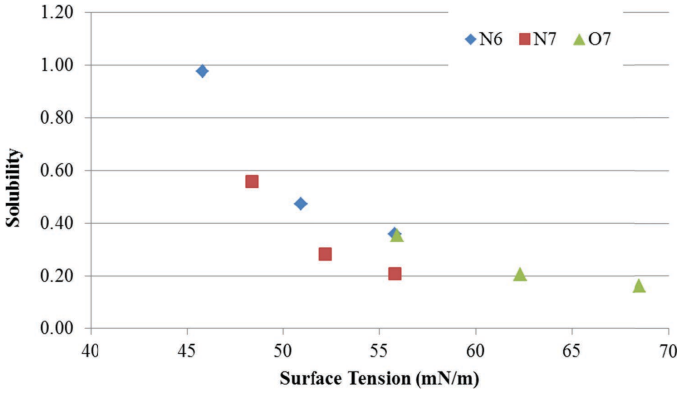


*Figure A-5. Relationship between solubility and surface tension of the binder.*

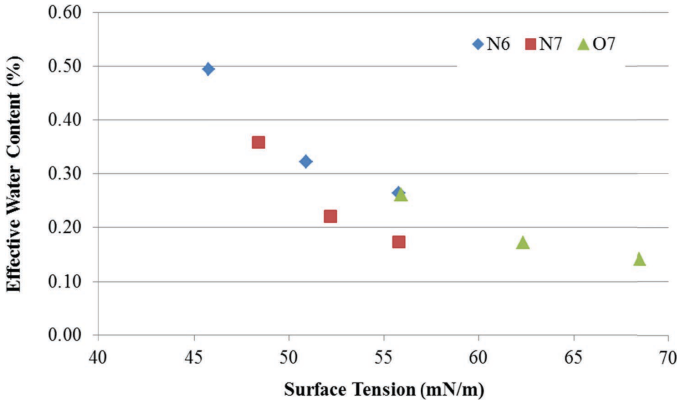


*Figure A-6. Relationship between effective water content and surface tension of the binder.*

foam as long as initial bubble diameter is more than about 100 micrometers. This corresponds to an initial water droplet size of 0.016 mm or more. Based on experimental results, it is clear that significant expansion is achieved due to bubbles that exceed this diameter.

3. A comparison of the theoretical to the measured maximum expansion ratio reveals that only a small fraction of water added to the binder is effective in foaming. This fraction of water decreases as the water content increases. The effective water content is an important consideration because it may be possible to optimize the water content used to produce foamed binder by using less water and thus reducing the risk of a higher humidity environment in the drum mix plant.
4. The physical model presented can assess the effect of water content and binder type on foam quality.

APPENDIX B

# Draft Commentary on Guidelines Proposed for Revising Appendix to AASHTO R 35

This appendix provides a commentary on the proposed revisions to the appendix to AASHTO R 35 Special Mixture Design Considerations and Methods for WMA based on the results of NCHRP Project 9-53, "Properties of Foamed Asphalt for Warm Mix Asphalt Applications." The commentary provides marked changes to the sections on additional laboratory equipment (X2.3), technology-specific specimen fabrication procedures (X2.7), WMA mixture evaluations (X2.8), a justification for proposed revisions, and the need for future research. Specifically, the changes address:

1. More detailed requirements for laboratory foaming units.
2. Two alternate methods for adding foamed asphalt to mixtures in the laboratory.
3. A special provision for mixture preparation for coatability and workability measurements.
4. An objective method for a mixture coatability evaluation test.
5. A mixture workability evaluation.
6. A method to identify the optimum amount of foaming water to be used in WMA mixtures.

## B.1. PROPOSED DRAFT REVISIONS TO APPENDIX TO AASHTO R 35

### X2. SPECIAL MIXTURE DESIGN CONSIDERATIONS AND PRACTICES FOR WARM MIX ASPHALT (WMA)

X2.2. Summary:

X2.2.1. This appendix includes separate sections addressing the following aspects of WMA mixture design:

- Equipment for Designing WMA,
- WMA Technology Selection,
- Binder Grade Selection,
- RAP in WMA,
- Technology-Specific Specimen Fabrication Procedures,
- Determining the Optimum Water Content for Plant Foaming,
- Evaluation of Workability,
- Evaluation of Coating,
- Evaluation of Compactability,
- Evaluation of Moisture Sensitivity,
- Evaluation of Rutting Resistance, and
- Adjusting the Mixture to Meet Specification Requirements.

X2.3. **Additional Laboratory Equipment:**

X2.3.3. **Plant Foaming Processes:**

*Laboratory-Foamed Asphalt Plant*—A laboratory-scale foamed asphalt plant (laboratory foaming unit) that is capable of producing consistent foamed asphalt at the water content used in field production. The unit should be capable of producing foamed asphalt for laboratory batches ranging from approximately 10 to 20 kg. The laboratory foaming unit should be capable of heating the asphalt binder to between 320°F (160°C) and 360°F (182°C). The water supply line should have a flow meter capable of regulating the water input to the foam by ±0.1 percent by weight of the unfoamed binder. The water and asphalt should be combined by a suitable means to achieve a uniform dispersion of water in the asphalt prior to discharge from the unit.

Note X6—Research has shown that the range of commercially available laboratory foaming units is capable of producing suitable foamed asphalt for mixture evaluation.

X2.7.6. **Preparation of Foamed Asphalt Mixtures:**

X2.7.6.1. The preparation of foamed asphalt mixtures requires special asphalt binder foaming equipment that can produce foamed asphalt using the amount of moisture that will be used in field production.

X2.7.6.2. Prepare the asphalt binder foaming equipment, and load it with binder per the manufacturer's instructions.

X2.7.6.3. If a liquid anti-stripping additive is required, add it to the binder in the foaming equipment according to the manufacturer's instructions.

X2.7.6.4. Heat the mixing tools, aggregate, and RAP in accordance with Section X2.7.2.

X2.7.6.5. Prepare the foamed asphalt binder according to the instructions for the foaming equipment.

X2.7.6.6. Mixing Method 1: Foam weighed into aggregate.

X2.7.6.6.1. Place the hot mixing bowl on a scale, and tare the scale.

X2.7.6.6.2. Charge the mixing bowl with the heated aggregates and RAP, and dry-mix thoroughly.

X2.7.6.6.3. Form a crater in the blended aggregate, and add the required amount of foamed asphalt into the mixture to achieve the desired batch weight.

X2.7.6.6.4 Remove the mixing bowl from the scale, and mix the materials with a mechanical mixer for ~~90~~ 60 s for workability evaluation or 90 s for volumetric and performance testing.

X2.7.6.7. Mixing Method 2: Foam discharged into aggregate.

X2.7.6.7.1. Calibrate the rate of discharge of the laboratory foaming unit into a tared, empty container. Three separate discharge times should be used to determine the amount of foamed asphalt binder being dispensed. A graph of weight versus time should be constructed, and a discharge time equal to the desired weight of binder should be found.

X2.7.6.7.2. Charge the heated bucket with the pre-weighed and heated aggregate and place under the foamed asphalt outlet on the laboratory foaming unit.

X2.7.6.7.3. Discharge the foamed binder into the mixing bowl or the bucket mixer for the desired time interval from paragraph X2.7.6.7.1.

X2.7.6.8. Mix for 90 s for volumetric or performance testing.

X2.7.6.8.1. Mix for 60 s ± 3 s for workability testing or 90 s for volumetric and performance testing.

Note X21—The laboratory foaming equipment uses a timer to control the amount of foamed asphalt produced. Ensure the batch size is large enough that the required amount of foamed asphalt is within the calibrated range of the foaming device. Depending upon the foaming equipment this operation may require producing one batch for the two gyratory specimens and the two maximum specific gravity specimens at each asphalt content then splitting the larger batch into individual samples.

Note X2X—If any binder additives have been used in the laboratory foaming unit immediately prior to mixing, clear all residue from the unit as thoroughly as possible before producing other foamed binders that do not contain the same additive. It has been found that running approximately 2 gal. (8 L) of straight asphalt through the unit is adequate to accomplish this.

Note X22—If the aggregates and RAP have been stored for an extended period of time in a humid environment, then it may be necessary to adjust the weight of binder based on the oven-dry weight of the aggregates and RAP as follows:

1. Record the oven-dry weight of the aggregates and RAP, $w_i$.
2. Determine the target total weight of the mixture as follows:

$$w_t = \frac{w_i}{\left(1 - \frac{P_{b_{new}}}{100}\right)} \qquad (X2.5)$$

Where:

$w_t$ = target total weight, g;

$w_i$ = oven-dry weight from Step 1, g; and

$P_{bnew}$ = percent by weight of total mix of new binder in the mixture.

3. Add foamed binder to the bowl to reach $w_t$.

X2.7.6.9. Place the mixture in a flat, shallow pan at an even thickness of 25 to 50 mm, and place the pan in the forced-draft oven at ~~the planned field~~ a compaction temperature of 240°F (116°C) for WMA or 275°F (135°C) for HMA for 2 hours. Stir the mixture once after 1 hour.

## X2.8. WMA Mixture Evaluations

X2.8.1. At the optimum binder content determined in accordance with R 35, prepare WMA mixtures in accordance with the appropriate procedure from Section X2.7 for the following evaluations:

- Workability
- Compactability
- Coating
- Moisture sensitivity
- Rutting resistance

~~X2.8.2. Coating~~

~~X2.8.2.1. Prepare a sufficient amount of mixture at the design binder content to perform the coating evaluation procedure in T 195 using the appropriate WMA fabrication procedure from Section X2.7. Do not short-term condition the mixture.~~

~~X2.8.2.2. Evaluate the coating in accordance with T 195.~~

~~X2.8.2.3. The recommended coating criterion is at least 95 percent of the coarse aggregate particles being fully coated.~~

X2.8.2. Workability to Determine Optimum Water Content for Foamed Mixtures per AASHTO TP XX-XX.

X2.8.2.1. Prepare a sufficient amount of mixture at the design binder content for two gyratory specimens at 1, 2, and 3 percent water using a laboratory foaming unit from Section X2.7.6 including the short-term conditioning.

X2.8.2.2. Compact the specimens at 240°F (116°C) using a gyratory compacter capable of measuring the shear force (stress) generated during compaction to a point just beyond the maximum shear force (stress).

X2.8.2.3. Record the maximum shear stress for each specimen following the procedure in TP XX-XX. Average the two results for each foaming water content.

X2.8.2.4. The optimum foaming water content is that which produces the lowest average maximum shear stress.

X2.8.2.5. In the event that an optimum water content cannot be determined, use a foaming water content of 1 percent.

Note X.X. While almost all asphalt binders will readily foam, there are a few that demonstrate insensitivity to the water content. For these it is recommended that the lowest level of water content be used as the additional water will serve no purpose.

X2.8.3. Coating: Method 1 for any WMA material.

X2.8.3.1. Prepare a sufficient amount of mixture at the design binder content and design foaming water content to perform the coating evaluation procedure in T 195 using the appropriate WMA fabrication procedure from Section X2.7. Do not short-term condition the mixture.

X2.8.3.2. Evaluate the coating in accordance with T 195.

X2.8.3.3. The recommended coating criterion is at least 95 percent of the coarse aggregate particles being fully coated.

X2.8.4. Coating: Method 2 for laboratory-foamed asphalt mixtures.

X2.8.4.1 Prepare a sufficient amount of mixture at the design binder content and design foaming water content to perform the coating evaluation procedure described in TP XX-XX using a laboratory foaming unit and a mixing time of 60 s ± 3 s. Short-term age the sample for 2 hours at 240°F (116°C).

X2.8.4.2 Evaluate the coating in accordance with TP XX-XX.

X2.8.4.3 The recommended coating criterion is a coatability index of at least 70 percent.

# B.2. COMMENTARY ON PROPOSED DRAFT REVISIONS TO THE APPENDIX TO AASHTO R 35

## Introduction

The suggested modifications to the appendix of AASHTO R 35 to optimize the foaming water content through the mix design process were presented in Chapter 1. These changes are suggested on the basis of results obtained in NCHRP Project 9-53, "Properties of Foamed Asphalt for Warm Mix Asphalt Applications." The original warm mix asphalt (WMA) modifications to the mix design process were the result of NCHRP Project 9-43. A summary of the expanded changes for foamed asphalt applications includes:

1. More detailed requirements for laboratory foaming units.
2. Two alternate methods for adding foamed asphalt to mixtures in the laboratory.
3. A special provision for mixture preparation for coatability and workability measurements.
4. A second method for a mixture coatability evaluation test.
5. A mixture workability evaluation.
6. A method to identify the optimum amount of foaming water to be used in WMA mixtures.

Figure B-1 presents the flowchart for the mixture design process developed in NHCRP Project 9-53, including foamed binder and mixture characteristics. The recommended procedure begins after the determination of the optimum asphalt content according to R35. Next, foamed asphalt mixtures are produced with 1%, 2%, and 3% foaming water. These mixtures are evaluated for workability by monitoring shear stress during compaction in a Superpave gyratory compactor (SGC). The mix producing the lowest maximum shear stress during compaction is considered to be at the optimum foaming water content. This mixture is then evaluated for coatability using a new method based on the moisture absorption of the coated aggregate relative to the uncoated aggregate. After the evaluation of coatability, the mixture undergoes the desired performance testing protocol. This appendix will present the justifications for these changes and identify future research needs.

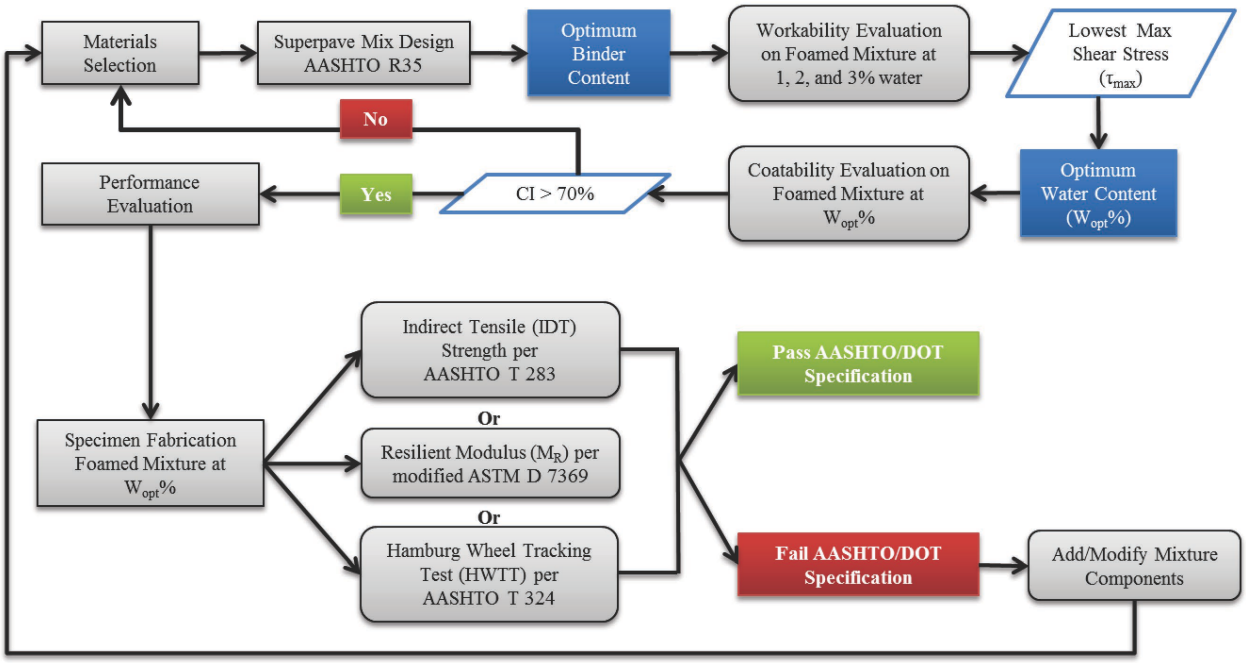


**Figure B-1. Final proposed foamed asphalt mix design method.**

## Laboratory Foamers

At the time of preparation of this report there were three commercially available laboratory foamers, and all three were evaluated during the course of the project. The general characteristics of these units are presented in Table B-1. Although the discharge rate varies from very rapid (approximately 100 g/s) to much slower (approximately 14 g/s), and the three units produced very different foamed asphalt properties (Figure B-2 and Figure B-3), all of the laboratory foamers were capable of successfully producing foamed asphalt that could be incorporated into mixtures to identify an optimum water content.

It can be seen that two of the three units produced the same workability optimum water content (1.0%), while the third produced an optimum water content of 2.0% (Figure B-3). In each case, the foamed WMA mixture was more workable than the corresponding hot mix asphalt (HMA) mixture. Furthermore, the differences in mix performance properties were not correlated to the foamed binder properties.

The laboratory foaming unit should have an adjustable positive water flow control capable of ±0.1% by weight of the unfoamed binder tolerance on water content. Two methods of binder addition to the aggregate are provided for (1) laboratory foamers capable of discharging directly into the aggregate and (2) laboratory foamers requiring discharge into a separate container for gravimetrically adding the foamed binder to the aggregate on a weigh scale.

**Table B-1. Summary of characteristics for commercially available laboratory foamers.**

| Characteristic | Wirtgen WLB 10S | InstroTek Accufoamer | PTI foamer |
|---|---|---|---|
| Air flow pressure | Min. 15 psi (100 kPa)<br>Max. 145 psi<br>(1,000 kPa) | Min. 75 psi (517 kPa),<br>Max. 150 psi<br>(1,034 kPa) | Min. 80 psi (552 kPa)<br>Max. 110 psi (758 kPa) |
| Water flow pressure | Max. 145 psi<br>(1,000 kPa) | Max. 30 psi (207 kPa) | 33 psi (230 kPa) |
| Binder flow pressure | Max. 145 psi<br>(1,000 kPa) | Max. 60 psi (413 kPa) | The binder is dispensed by gravity |
| Reaction chamber | Water and compressed air are injected into the hot binder. | Pressurized binder and water meet at a single junction. | A small amount of air is used to atomize the water to a fine droplet. |
| Binder temperature | 284°F–392°F<br>(140°C–200°C) | 320°F–390°F<br>(160°C–200°C) | Max 350°F<br>(177°C) |
| Discharge time | 100 g/s | 16–20 g/s | 14–20 g/s |
| Mass control | Mass flow control | Overhead pressure control | Scale control |
| Power requirement | Adaptable to various international supplies | 208–240 VAC, 220-volt, 30-amp circuit | 120 VAC, 20 amp |
| Binder chamber size | 5.3 gallon (20 L) | 0.3–15.0 lb<br>(150 to 6,800 g) | 14 lb (6,350 g) |
| Foaming agent dosage (water content) | 0%–5% | 0%–9% | 1%–7% |
| Foaming agent temperature | No heat | Max. 180°F (82°C) | No heat |

VAC = volts alternating current.

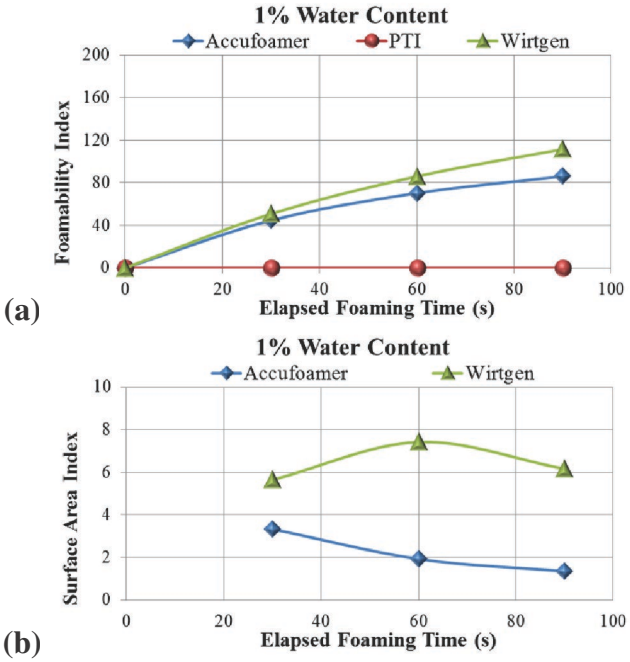


**Figure B-2. (a) Foamability index and (b) surface area index (SAI) at 1.0% water content for commercially available laboratory foamers (SAI could not be measured on the PTI foamer).**

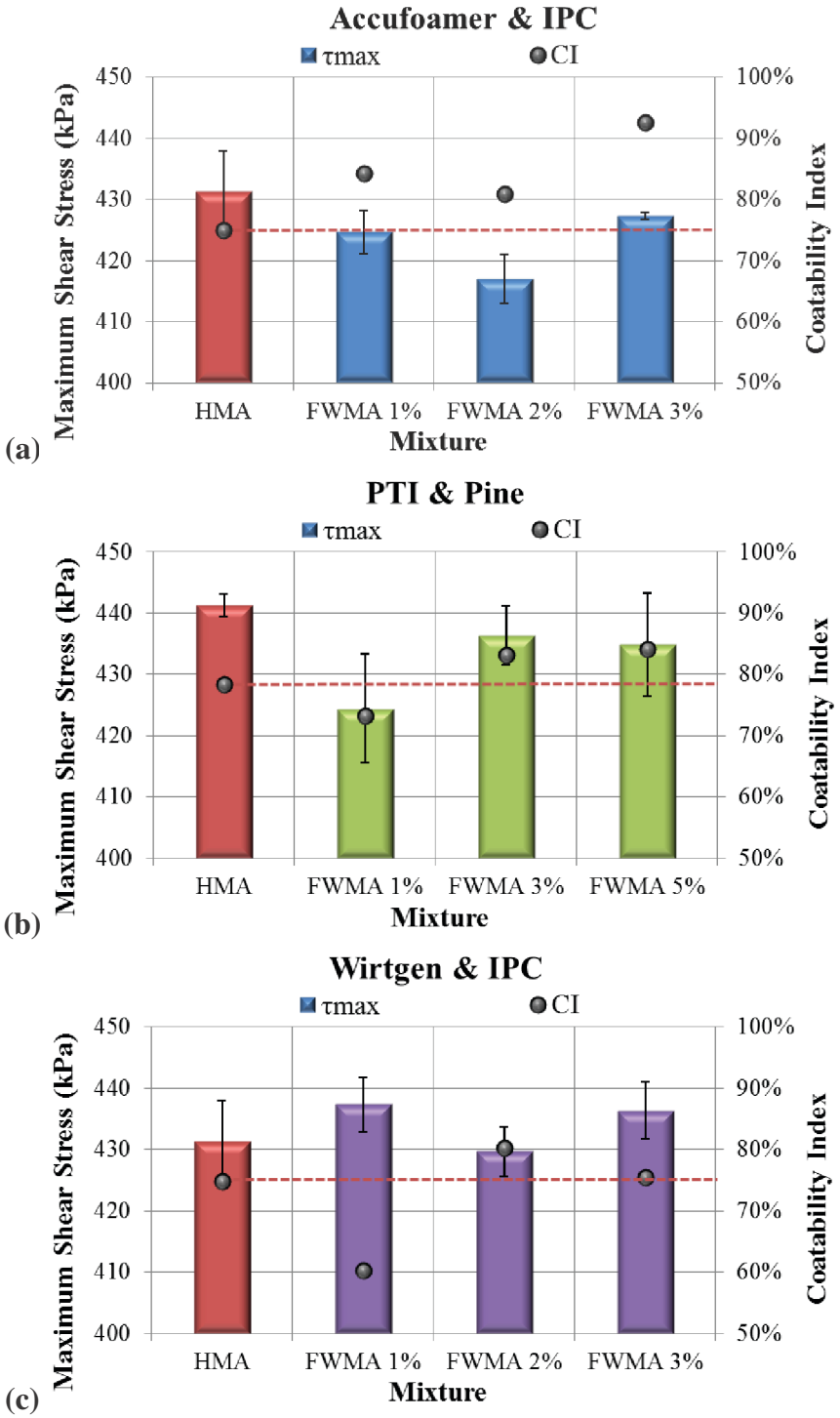


**Figure B-3. Workability and coatability results for the control HMA and foamed mixture; (a) produced in the Accufoamer, (b) produced in the PTI foamer, and (c) produced in the Wirtgen foamer.**

## Mixing Methods

Two methods for producing foamed asphalt mixtures in the laboratory are presented in the proposed appendix to AASHTO R 35 recommended practice. The design of the laboratory foamers included as part of NCHRP Project 9-53 necessitated that these two options be presented. Two of the units were able to dispense foamed asphalt directly into mixing containers at a prescribed amount, but the third unit did not have room for a mixing container below the outlet.

*Mixing Method 1* involves dispensing foamed asphalt at the desired water content into an empty container and then pouring the foamed binder into a pre-weighed amount of aggregate in the same way that unfoamed asphalt binder is added to aggregate. The foamed binder and aggregate may then be mixed in either a bucket mixer or planetary mixer. Mixing Method 1 is applicable to any laboratory foaming unit.

*Mixing Method 2* is applicable for laboratory foamers capable of discharging the foamed binder directly into a mixing bucket or bowl. An important step in this method is calibrating the discharge time for the desired amount of binder. A graph of binder weight versus binder discharge time is constructed by weighing the amount of binder dispensed from the foaming unit at three different times and determining the appropriate amount of time for the desired binder content. The bucket mixer or mixing bowl is then placed directly below the foaming nozzle, and the foamed binder is added to the aggregate according to the desired dispensing time. Method 2 is applicable only to those laboratory foamers capable of direct addition of the binder to the aggregate.

For the evaluation of asphalt mix workability and coatability, it is necessary to carefully monitor the mixing time of the heated aggregate and foamed asphalt. The time set during this research project was 60 s ± 3 s for both test methods. This provided a basis to compare foamed asphalt mixtures containing different amounts of foaming water, and allowed researchers to identify and discriminate the effects of water content on the workability and coatability of the mix.

Based on research accomplished in NCHRP Projects 9-49 and 9-52, it is recommended that the foam-produced WMA be aged at 240°F for 2 hours prior to compaction in order to simulate aging that occurs in a batch or drum mixing plant. The original recommendation from NCHRP Project 9-43 (Advanced Asphalt Technologies 2012) was that aging should be accomplished at the planned field-compaction temperature, but this is difficult to anticipate during mix design.

## Technology-Specific Specimen Fabrication Procedures

Discussions on the changes to the mixing procedure, calibration techniques for dispensing foamed asphalt, methods of adding foamed binder to the aggregate, the mixing procedure for workability and coatability testing, and the short-term oven aging of the foamed WMA were presented in the previous sections. In summary, the two methods of mixing foamed asphalt into aggregate are (1) dispensing the foamed asphalt into a container and then pouring the desired amount of foamed asphalt into the mixing bucket or bowl containing the heated aggregate and (2) discharging the binder at a calibrated rate directly into the mixing bucket or bowl containing the heated aggregate. For volumetric and performance testing specimens, the mixing time remains at 90 s, as originally proposed in NCHRP Project 9-43 (Advanced Asphalt Technologies

2012), and for workability and coatability testing, the mixing time is set at 60 s ± 3 s. Short-term oven aging for 2 hours at 240°F (116°C) should precede specimen preparation.

## WMA Mixture Evaluation

The evaluation of WMA mixtures is focused on two important interrelated aspects of mix behavior. The first of these is the production and placement of the mixture, and the second is the long-term performance. This discussion will present the recommendations from NCHRP Project 9-43 and those from NCHRP Project 9-53 with respect to WMA evaluation.

During mix production, the asphalt binder must be evenly distributed throughout the mixture so that the aggregate particles are completely covered. In NCHRP Project 9-43, recommendations were made to evaluate coating using AASHTO T 195, which is a visual inspection of the coarse coated aggregate particles. During placement, the mixture must flow sufficiently to allow compaction to a specified density. For workability, NCHRP Project 9-43 recommended a compactability evaluation as the ratio of the number of gyrations to achieve 92% of maximum density at 30°C below the planned field-compaction temperature to the number of gyrations for the same density level at the planned field-compaction temperature.

Recommendations from NCHRP Project 9-53 include an alternative method to assess coatability using the relative difference between uncoated aggregate moisture absorption and coated aggregate moisture absorption as well as a workability test in which the shear stress during gyratory compaction is monitored. The coatability and workability test methods suggested in the proposed appendix to AASHTO R 35 from NCHRP Project 9-53 do not have existing AASHTO test method designations, but they do have proposed procedures presented as deliverables for NCHRP Project 9-53.

The second aspect of the mixture's qualities is its potential long-term performance. In NCHRP Project 9-43, recommendations for performance testing included an evaluation of moisture susceptibility using AASHTO T 283 and an evaluation of rutting using AASHTO TP 79, T 320, T 324, or T 340. The suggestion for performance testing is to maintain the NCHRP Project 9-43 protocol with the addition of a stiffness test and potentially add one or more mixture cracking tests at some point based on the results of NCHRP Project 9-57 and other future projects. In NCHRP Project 9-53, the suggestions for performance testing do not differ from those made in NCHRP Project 9-43 as the goal of the asphalt community is to ensure that the performance of WMA is equal to or better than that of HMA.

Based on recommendations from NCHRP Project 9-53, the first step after determining the optimum asphalt content from AASHTO R 35 is to prepare mixtures at the optimum asphalt content and foaming water contents of 1.0%, 2.0%, and 3.0% by weight of asphalt binder. These three water contents were found to span the range of optimum water contents for mixtures that were sensitive to water content during the course of NCHRP Project 9-53. The next step is to evaluate the mixtures with the three different water contents for workability using an SGC capable of measuring shear stress generated during compaction. The mixture at the water content with the lowest maximum shear stress (i.e., greatest workability) is considered to have the optimum water content.

### *Workability*

Workability describes the ease with which the mixture can be placed, worked by hand, and compacted. It is a function of temperature, binder properties (e.g., viscosity, grade, polymer

modification), and aggregate properties (e.g., size, angularity), among other factors. Because the binder is being applied to the aggregate at a reduced temperature in WMA applications, there have been concerns as to whether the binder will flow readily enough to distribute itself among the aggregate particles and whether the mixture will flow sufficiently to compact the mixture to the specified density. The maximum shear stress during compaction with the SGC was selected as a workability metric because it is essentially the amount of effort required to shove the mix around in the SGC mold at its anticipated placement and compaction temperature.

Although not all SGCs are equipped to measure shear stress during compaction, it is becoming a common feature on a number of available models. It is suggested that a standard method of quantifying shear stress during compaction be developed under a future NCHRP research project. However, since shear stress is commonly defined in gyratory compaction, simply being able to define the minimum peak shear stress among the mixtures being evaluated should suffice for the time being as a means to determine the optimum moisture content.

The best workability is ensured by selecting the foaming water content that produces the lowest maximum shear stress during compaction. This is termed the "optimum foaming water content," and it is selected from the lowest maximum shear stress obtained at 1.0%, 2.0%, or 3.0% water. In the event that the mixture is not sensitive to water content, then the lowest (i.e., 1.0%) water content should be selected as the optimum. For instance, in Figure B-4, 1.0% water would be selected for the N6 and O6 binders as that was the water content producing the lowest shear stress. For the Y6 binder, 1.0% would also be selected, but that is because the mixture is not sensitive to changes in foaming water content and the use of greater than 1.0% moisture is not justified.

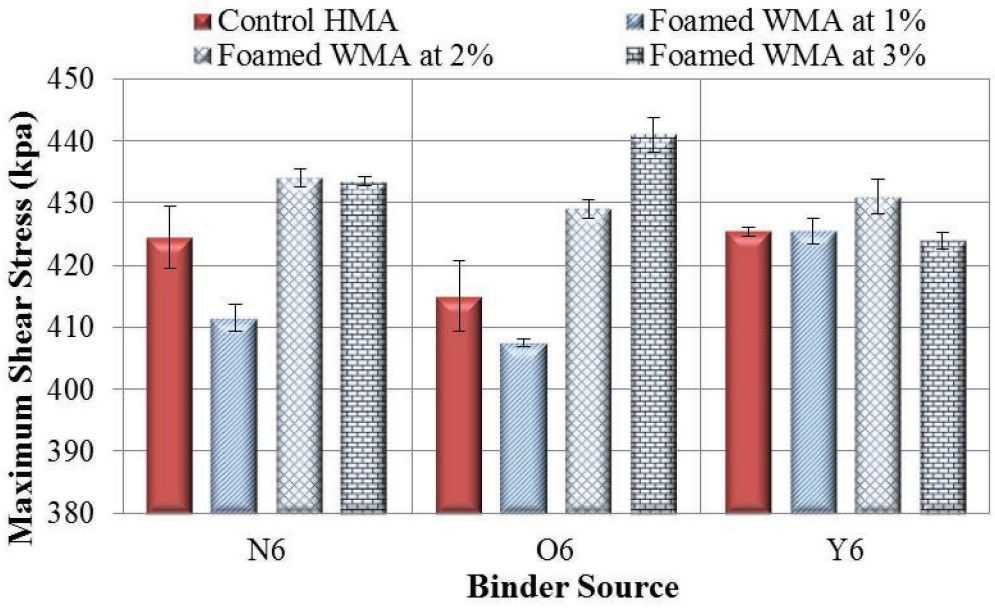


**Figure B-4. Workability test results for foamed WMA versus HMA.**

### *Coatability*

Next, the mixture with the optimum water content is evaluated to ensure that it can provide an adequate coating of binder to the aggregate. Enough of the mixture is prepared to allow the preparation of two specimens. The loose mixtures are short-term oven aged (STOA) for 2 hours at 240°F (116°C) for WMA specimens, as recommended by NCHRP Project 9-52. Coatability is a measure of the ease with which an asphalt binder distributes itself over the surface area of the aggregate.

The current method of evaluating coatability presented in the proposed appendix to AASHTO R 35 is AASHTO T 195, which is a visual rating of the uncoated coarse aggregate particles. Because it is a visual inspection, it is subjective in its determination and is somewhat dependent on (1) the skill of the technician in quantifying uncoated particles and (2) the color of the aggregate. If the aggregate is dark, then it may be difficult to determine the amount of uncoated particles.

A less subjective means to determine the coatability of foamed asphalt mixtures was developed based on work done at the University of Wisconsin (Geng et al. 2013; Velasquez et al. 2012). The procedure to determine the coatability of the mixture in the proposed changes to the proposed appendix of AASHTO R 35 is based on the relative difference in measurement of water absorption of bare coarse aggregate (adjusted for the change in surface area from the full aggregate gradation to the coarse aggregate only) and the water absorption of the coated coarse aggregate at the optimum asphalt and foaming water contents.

In this method, the coarse aggregate and foamed asphalt are mixed for 60 s and subjected to the STOA protocol of 2 hours at 240°F (116°C) for WMA. Both the coated and uncoated samples are weighed to obtain their oven-dry weights. Samples of uncoated coarse aggregate and coated coarse aggregate are soaked in water for a period of 1 hour. The samples are then brought to a saturated surface dry (SSD) condition and weighed. The relative difference in water absorption between the two samples is the coatability index (CI) and is a measure of how well the binder has coated the aggregate. A threshold value of the CI that relates to field measurements of coating needs to be established for this test from future research efforts. However, as shown in Figure B-5, a CI value of 70% is appropriate for mixtures prepared at the optimum moisture content for two of the three binders.

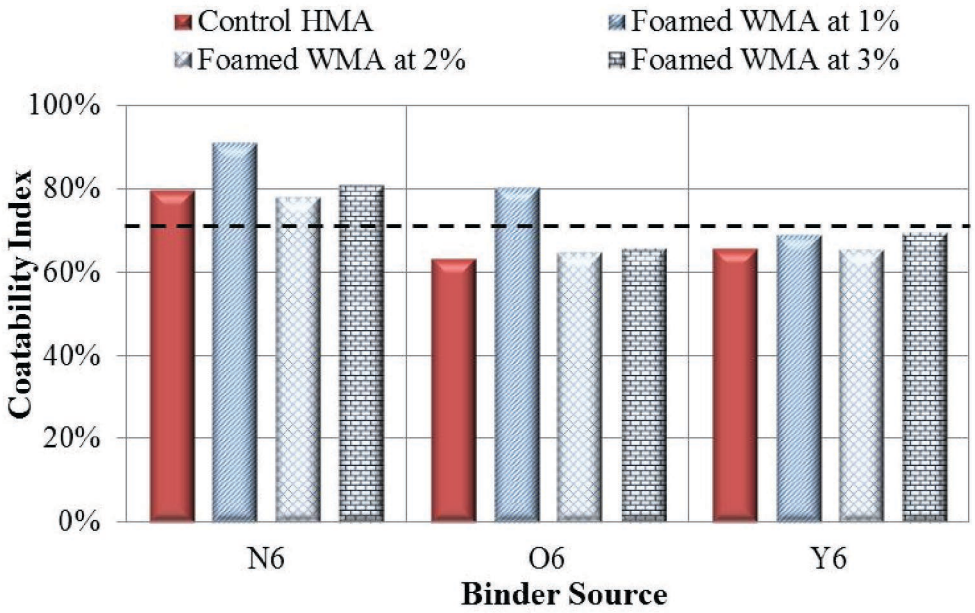


**Figure B-5. Coatability test results for foamed WMA versus HMA.**

## Conclusions

Suggested changes to Appendix X2 of AASHTO R 35 have been made accompanied by the justifications for these changes reflecting the information gathered under NCHRP Project 9-53. The important changes include:

1. More detailed requirements for laboratory foaming units.
2. Two alternate methods for adding foamed asphalt to mixtures in the laboratory.
3. A special provision for mixture preparation for coatability and workability measurements.
4. A method for a mixture coatability evaluation test.
5. A mixture workability evaluation.
6. A method to identify the optimum amount of foaming water to be used in WMA mixtures.

Provisions have been made to allow foamed asphalt production from the existing commercially available laboratory foaming units. The evaluation of workability is based on the shear stress generated in an SGC during the compaction process. It was found that this approach allowed for the determination of an optimum foaming moisture content in mixtures that were sensitive to changes in moisture content. A coatability test based on water absorption is suggested to replace AASHTO T 195. The new method is based on objective measurements rather than subjective judgments on the amount of coating of aggregate particles. This approach to determining an optimum foaming moisture content allows contractors and agencies to better use the foaming equipment at asphalt mix plants for greater mixing and placing efficiency.

## References

Advanced Asphalt Technologies, LLC. 2012. *NCHRP Report 714: Special Mixture Design Considerations and Methods for Warm Mix Asphalt: A Supplement to NCHRP Report 673: A*

*Manual for Design of Hot Mix Asphalt with Commentary*. Transportation Research Board of the National Academies, Washington, D.C.

Geng, H., C. S. Clopotel, and H. U. Bahia. 2013. Effects of High Modulus Asphalt Binders on Performance of Typical Asphalt Pavement Structures. TRB 92nd Annual Meeting Compendium of Papers, Transportation Research Board of the National Academies, Washington, D.C.

Velasquez, R., G. Cuciniello, D. Swiertz, R. Bonaquist, and H. U. Bahia. 2012. Methods to Evaluate Aggregate Coating for Asphalt Mixtures Produced at WMA Temperature. Proceeding. Canadian Technical Asphalt Association.

APPENDIX C

# AASHTO Style Standards

## Standard Method of Test for

# Determining the Expansion and Collapse of Foamed Binder by Using the Laser Distance Measurement Device

## AASHTO Designation: T xx-xx

## 1. SCOPE

1.1. This test method describes the procedure for determining the expansion and collapse of foamed binder produced by a laboratory foaming unit or sampled at a hot-mix plant using a laser distance measurement device.

1.2. While working with or handling foamed binder, lab personnel may be exposed to extreme heat and pressure, hazardous materials, and dangerous equipment operations. This standard does not address procedures and practices needed to ensure a safe and hazard-free working environment in the laboratory or at a hot-mix plant. Hence, it is the responsibility of the user of this standard to ensure safety.

1.3. *SI Units*—The values stated in SI units are to be regarded as the standard.

## 2. REFERENCED DOCUMENTS

xx

## 3. SIGNIFICANCE

3.1. The test standard is used to measure the change in height and corresponding volume of the foamed binder in real time. The laser-based sensor is comprised of an emitter and detector to measure the distance from the sensor to a reflecting surface based on the phase-shift principle. The laser sensor measures the height of the surface by reflecting light of different wavelengths over a very small circular spot of about 1 mm in diameter. The laser sensor collects data at a frequency of 1 Hz.

3.2. The test standard is used to determine the expansion and collapse characteristics of asphalt binders. The results obtained by following these procedures can be used to:

- Determine the maximum expansion ratio, $ER_{max}$, at different conditions (i.e., temperature, water content, binder type, foaming unit, and/or pressure);
- Characterize the decaying rate of the foam at different conditions (i.e., temperature, water content, binder type, foaming unit, and/or pressure);

- Use the data obtained from this test for a foam decaying model to determine asphalt foam characteristics as a function of time; and
- Investigate the influence of binder type, water content, foaming unit, temperature, and pressure on foam expansion and decay properties.

## 4. APPARATUS

4.1. Laboratory foaming unit that produces a specified amount of foamed binder or sampling port in a hot-mix plant that can be controlled to dispense a specified amount of foamed binder.

4.2. Laser distance meter (LDM) device that uses phase-shift principle to measure distances with a resolution of 0.1 mm or better, repeatability of ±0.3 mm or better, and a data collection rate of 1 data point per second or better. The device must also acquire the time at which the measurement was made with a resolution of 100 milliseconds or better.

4.3. Tripod or other suitable means to mount the laser distance meter.

4.4. Clean cylindrical metal cans for each measurement (1-gallon or 5-gallon capacity).

4.5. Personal protective equipment and other safety gear as needed.

4.6. Computer to collect data acquired by the laser distance meter.

## 5. PROCEDURE

5.1. Calibrate the laboratory foaming unit according to the manufacturer's recommendations.

5.2. Calibrate the height of the binder in the metal can with respect to the weight of the binder in the can. Although the metal may be cylindrical, the bottom of the can may be grooved in order to strengthen it. For small amounts of binder dispensed during foaming, the groove can accommodate a significant mass fraction of the binder (Figure 1). In order to avoid errors in volumetric measurement it is important to calibrate the weight of binder to the height of binder in the can. For this calibration, mount the LDM device on a tripod at a suitable location (Figure 2). The tripod and the LDM should be stable and not susceptible to vibrations. Weigh the empty metal can and place it under the LDM. Point the LDM to the bottom of the empty can. The laser should point at a flat portion of the can, preferably in the center. The distance to the bottom of the can should be recorded and the exact location of the can should be marked. Pour enough hot binder in the can so that a smooth and flat binder surface is created. Measure the mass of the binder dispensed in the previous step and measure the distance from the LDM to the surface of the binder. Subtract the last two measurements to obtain the height of the binder in the can. Repeat the procedure at least twice after adding more binder to the can and weighing it each time. The weight versus height of binder will be used for future calculations.

**Figure 1. Illustration of the bottom of a 1-gallon can.**

**Figure 2. Illustration of the LDM pointing into an empty can for calibration.**

5.3. Prepare the LDM to make measurements for the foamed binder. Mount the LDM on the tripod at a suitable location that is not susceptible to movement or vibration. Weigh the empty metal can and place it under the LDM. Point the laser from the LDM to the bottom of an empty can. The laser should point as close to the center of the can as possible. Start data acquisition to get at least 5 points that correspond to the distance between the LDM and the bottom of the can

5.4. Dispense the specified amount of foamed binder into the metal can. Depending on the foaming equipment (or location in case of a field test), it may or may not be possible to dispense the foamed binder while the LDM is pointing into the can. In situations where the can must be moved away from the LDM to collect the foamed binder sample, ensure that the location of the can is marked and that the can is placed under the LDM as soon as possible after collecting the sample. Also, in this case the time at which the sample was dispensed must be recorded using the LDM.

5.5. Record the distance between the top of the foamed binder and the LDM at regular intervals (i.e., every 1 second). Record the data for at least 90 seconds or until the change in the height of the binder sample is less than 0.1 mm, whichever comes later. Note that if the measurements are conducted at room temperature, the binder sample may cool before all the bubbles can escape. In this case, the binder may not collapse completely.

5.6. Weigh the can to obtain the actual mass of the foamed binder dispensed. Use the measured weight of the binder sample dispensed to verify the calibration of the foaming unit and to obtain the minimum height of the unfoamed binder using the binder weight-height calibration from before, $h_{final}$.

## 6. CALCULATION OF RESULTS

6.1. Obtain the distance between the top of the foamed binder and the LDM as a function of time from the computer and report it to the nearest 0.1 mm. Convert the distance measured by the LDM to height of the foamed binder at any time $t$, $h_t$, by subtracting it from the distance measured to the bottom of the container.

6.2. Determine the final height of the foamed binder, $h_{final}$, from the weight-to-height relationship established in the calibration.

6.3. Calculate the expansion ratio of the binder at any time $t$, ER($t$) as $(h_t - h_{final})/h_{final}$. For the maximum expansion ratio, the maximum height of the foamed binder measured from the marking left behind by the collapsing foam on the inside of the can is used. Note that the start time is the time when the binder sample was dispensed to the metal can.

6.4. Plot the expansion ratio versus time. The data from the LDM can be smoothened using Equation 1:

$$\mathrm{ER}(t) = 1 + (ae^{-bt}) + (\mathrm{ER}_{max} - a - 1)(e^{-ct}) \quad (1)$$

Where:
ER($t$), the expansion ratio of the foamed binder at any time $t$.
$a$, $b$, and $c$, fitting coefficients.
$\mathrm{ER}_{max}$, the maximum expansion ratio of the foamed binder.

6.5. Determine the foamability index referred as the area underneath the ER curve by Equation 2:

$$\mathrm{FI}_t = \int_0^t \mathrm{ER}_t d(t) \quad (2)$$

6.6. Use the ER data after 10 seconds of foaming to determine the rate of collapse of the semi-stable foamed binder, $k$-value. The rate of collapse of the semi-stable foam is determined as the parameter $k$ obtained by fitting the ER versus time to an exponential curve expressed as Equation 3:

$$\mathrm{ER}_t = 1 + he^{-kt} \quad (3)$$

Where:
$h$, fitting coefficient.
$k$, the rate of collapse of the semi-stable foamed binder.

## 7. REPORT

7.1. The report shall include the following:

7.1.1. Make and model of the laboratory foaming unit or plant foamer.

7.1.2. Source and grade of the binder.

7.1.3. Foaming water content in percent of dry mass of binder.

7.1.4. Type and dosage of foaming additive (if used).

7.1.5. Maximum expansion ratio of the foamed binder, $ER_{max}$.

7.1.6. Foamability index of the foamed binder, FI.

7.1.7. The rate of collapse of the semi-stable foamed binder, *k*-value.

## Standard Method of Test for

# Determining the Size Distribution and Surface Area of Binder Foam Bubbles During the Foaming Process

## AASHTO Designation: T xx-xx

## 1. SCOPE

1.1. This test method describes the procedure for evaluating the evolution of the size and amount of binder foam bubbles over time during the foaming process using a digital camera.

1.2. While working with or handling foamed binder, lab personnel may be exposed to extreme heat and pressure, hazardous materials, and dangerous equipment operations. This standard does not address procedures and practices needed to ensure a safe and hazard-free working environment in the laboratory or at a hot-mix plant. Hence, it is the responsibility of the user of this standard to ensure safety.

1.3. *SI Units*—The values stated in SI units are to be regarded as the standard.

## 2. REFERENCED DOCUMENTS

xx

## 3. SIGNIFICANCE

3.1. The test standard is used to capture the image of the surface binder foam bubbles during the foaming process using a digital camera. The digital camera collects images at a frequency of 1 Hz. The results obtained by following these procedures can be used to:

3.1.1. Determine the size distribution of binder foam bubbles at different conditions (i.e., temperature, water content, binder type, foaming unit, and/or pressure);

3.1.2. Calculate the surface area of binder foam bubbles at different conditions (i.e., temperature, water content, binder type, foaming unit, and/or pressure); and

3.1.3. Investigate the influence of binder type, water content, foaming unit, temperature, and pressure on characteristics of binder foam bubbles during the foaming process.

## 4. APPARATUS

4.1. Laboratory foaming unit that produces a specified amount of foamed binder or sampling port in a hot-mix plant that can be controlled to dispense a specified amount of foamed binder.

4.2. Digital camera with at least 12-megapixel resolution and continuous timed shutter release able to capture images every 1 second from the start of the foaming process (or the sample being placed under the tripod).

4.3. Tripod or other suitable means to mount the digital camera.

4.4. Clean cylindrical metal cans for each measurement (1-gallon or 5-gallon capacity).

4.5. Personal protective equipment and other safety gear as needed.

4.6. Computer to collect data acquired by the laser distance meter.

## 5. PROCEDURE

5.1. Calibrate the laboratory foaming unit according to the manufacturer's recommendations.

5.2. Set up a tripod on a leveled surface and use bubble levels to ensure the center post is vertical and perpendicular to the ground. Mount the digital camera on the tripod as shown in Figure 1.

**Figure 1. Camera setup for digital image capture of foamed binder sample.**

5.3. Place an empty metal can below the tripod. Adjust the location to ensure that the camera can capture the inside of the 5-gallon bucket and that the laser is pointed into the bucket and is free of obstructions. After the adjustment, use a marker to identify the position of the metal can and the tripod.

5.4. Connect the digital camera with the computer. Turn on the digital camera and run appropriate software on the computer to remotely control the digital camera.

5.5. After filling the metal can to between ⅓ and ½ of its height with the foamed binder, stop the laboratory foaming unit or turn off the sampling valve connected to the plant foamer unit. Move the metal can containing the foamed binder sample to the location under the tripod marked in Step 5.3.

5.6. Stop the digital camera when no significant changes in the foaming height can be observed. Save all digital images.

## 6. CALCULATION OF RESULTS

6.1. Download the set of images captured during the foaming experiment from the camera to a computer.

6.2. Select an original image (as shown in Figure 2) acquired at a specific desired time and label it using the a) binder source, b) binder grade, c) foaming water content, and d) time the image was acquired counting from the discharge of the foamed asphalt binder into the test container.

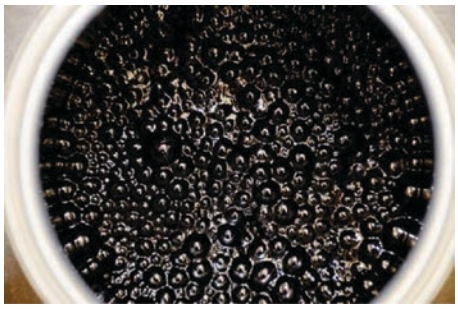

**Figure 2. Original image of binder foam bubbles.**

6.3. Adjust the contrast of the original image using *Adaptive Histogram Equalization* in Matlab® with the following code. The adjusted image is shown in Figure 3.

```
img = imread;
pic = rgb2gray(img);
fin = adapthisteq(pic);
imshow(fin)
imsave
```

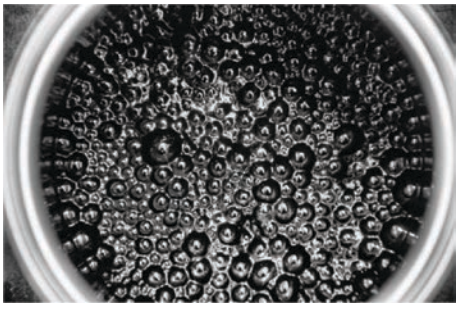

**Figure 3. Adjusted image of binder foam bubbles.**

6.4. Select the inner part of the image to avoid the reflection of the foamed binder on the surface of the metal can. Set the scale of the image using as reference the rim of the can holding the foamed binder sample (e.g., 6.5 inches for a typical 1-gallon can as show in Figure 4).

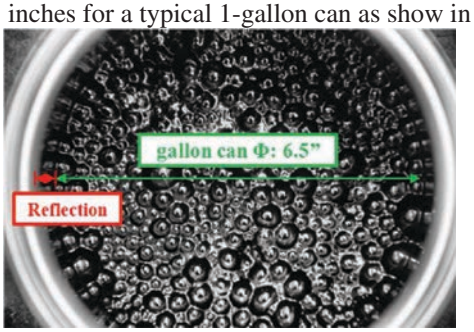


**Figure 4. Scale calibration for a 1-gallon can.**

6.5. Segment the image by drawing four lines through its center. The lines extend from side to side of the container separated by a 45-degree angle from each other as illustrated in Figure 5 (i.e., lines in the N/S, W/E, NW/SE, and SW/NE directions).

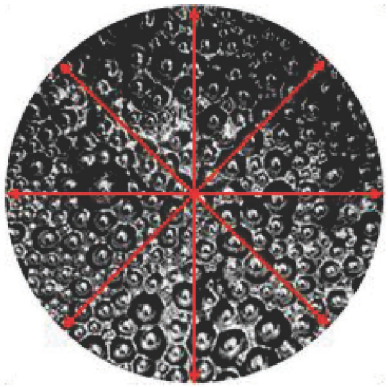

**Figure 5. Image segmentation.**

6.6. Print the image and manually detect and draw circles around all foamed bubbles that intersect the lines sketched in Step 6.5.

6.7. Count and measure the diameter (in mm) of the bubbles identified in Step 6.6 using a ruler. Record the measured diameter of each bubble and then use the scale established in Step 6.4 to adjust the measurements (i.e., adjusted diameter in Table 1).

**Table 1. Bubble count and size data.**

| Bubble # | Measured Diameter (cm) | Adjusted Diameter (mm) |
|---|---|---|
| 1 | 0.6 | 5.0 |
| 2 | 0.3 | 2.7 |
| 3 | 0.5 | 4.1 |
| 4 | 0.7 | 5.4 |
| 5 | 0.3 | 2.3 |
| 6 | 1.3 | 10.9 |
| 7 | 1.2 | 10.2 |
| 8 | 0.3 | 2.7 |
| 9 | 0.3 | 2.3 |
| 10 | 0.3 | 2.7 |
| 11 | 0.3 | 2.7 |

6.8. Generate a bubble size distribution histogram using JMP® or other similar software (Figure 6), and fit a curve to the histogram using a gamma function (Figure 7).

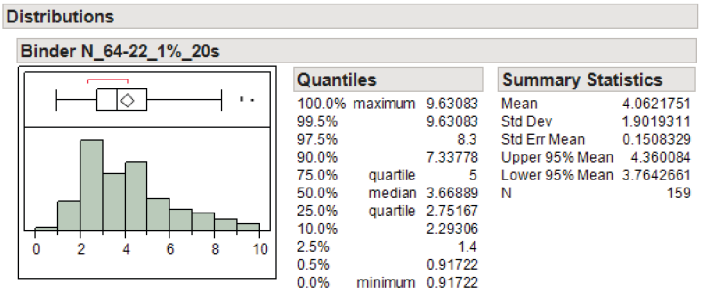


**Figure 6. Bubble size distribution histogram.**

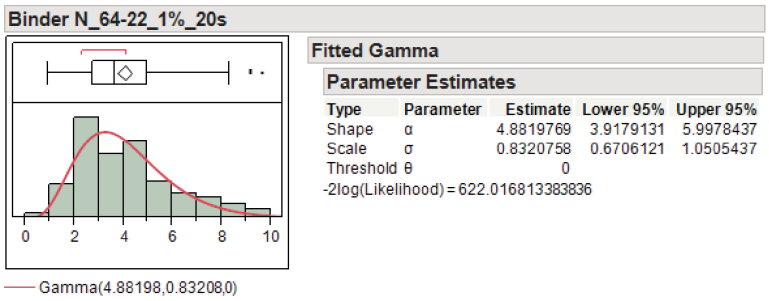


**Figure 7. Fitted gamma function to the bubble size distribution histogram.**

6.9. Report the gamma function curves at the selected time intervals to illustrate the change in bubble size distribution with time (as shown in Figure 8).

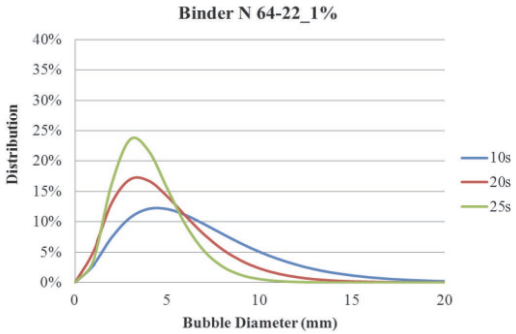


**Figure 8. Gamma function curves at selected times.**

6.10. Calculate the volume of the foamed and unfoamed binder using Equation 1 and Equation 2, respectively. The terms used in the two equations are defined in Figure 9.

6.11.
$$V_f(t) = \frac{\pi {D_0}^2 h_f(t)}{4} \quad (1)$$

$$V_{uf}(t) = \frac{\pi (D_0)^2 h_{\min}}{4} \quad (2)$$

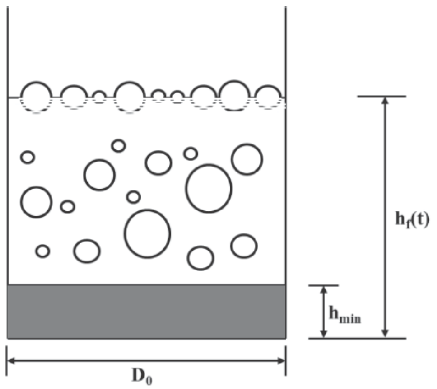


**Figure 9. Schematic of binder sample after foaming.**

The difference in volume between the foamed binder at time *t* and the unfoamed binder is the expanded volume created by foaming bubbles. Therefore, the volume of all foaming bubbles at time *t* can be calculated using Equation 3.

$$V_b(t) = V_f(t) - V_{uf}(t) = \frac{\pi(D_0)^2[h_f(t) - h_{\min}]}{4} \quad (3)$$

6.12. Knowing the total number of surface binder foam bubbles, $n_s(t)$, and the diameter of each surface binder foam bubble, $D_{s\text{-}i}(t)$, where $i$ is from 1 to $n_s(t)$, the surface binder foam bubbles at time $t$ can be expressed using Equation 4.

$$\begin{Bmatrix} D_{s-1}(t) \\ \vdots \\ D_{s-n_s}(t) \end{Bmatrix} \quad (4)$$

6.13. Assuming all surface binder foam bubbles are sphere shaped, calculate the volume of all surface binder foam bubbles at time $t$ using Equation 5.

$$V_{sb}(t) = \sum_1^{n_s(t)} \frac{\pi[D_{s-i}(t)]^3}{6} \quad (5)$$

6.14. Assuming all binder foam bubbles in the foamed binder volume have the same diameter distribution as the surface ones, estimate the total number of binder foam bubbles at time $t$ per Equation 6.

$$N_t(t) = \frac{V_b(t)}{V_{sb}(t)} n_s(t) \quad (6)$$

6.15. Determine the total surface area of all binder foam bubbles at time $t$ and the surface area of the unfoamed binder using Equation 7 and Equation 8, respectively.

$$\mathrm{SA}_t(t) = \frac{N_t(t)}{n_s(t)} \sum_1^{n_s(t)} \pi[D_{s-i}(t)]^3 \quad (7)$$

$$\mathrm{SA}_0 = \pi D_0 \left(\frac{D_0}{2} + h_{\min}\right) \quad (8)$$

6.16. Calculate the surface area index (SAI) at time $t$ as the ratio of $\mathrm{SA}_t(t)$ over $\mathrm{SA}_0$ as expressed in Equation 9.

$$\mathrm{SAI}(t) = \frac{\mathrm{SA}_t(t)}{\mathrm{SA}_0} \quad (9)$$

## 7. REPORT

7.1. The report shall include the following:

7.1.1. Make and model of the laboratory foaming unit or plant foamer.

7.1.2. Source and grade of the binder.

7.1.3. Foaming water content in percent of dry mass of binder.

7.1.4. Type and dosage of foaming additive (if used).

7.1.5. Gamma function for size distribution of binder foam bubbles at certain times.

7.1.6. Surface area index of all binder foam bubbles, SAI.

## Standard Method of Test for

# Evaluating the Workability of Foamed Warm Mix Asphalt by a Laboratory Foaming Unit Using a Superpave Gyratory Compactor

## AASHTO Designation: T xx-xx

## 1. SCOPE

1.1. This test method describes the procedure for evaluating workability of foamed warm mix asphalt (WMA) by a laboratory foaming unit using a Superpave gyratory compactor (SGC).

1.2. While working with or handling foamed binder, lab personnel may be exposed to extreme heat and pressure, hazardous materials, and dangerous equipment operations. This standard does not address procedures and practices needed to ensure a safe and hazard-free working environment in the laboratory or at a hot-mix plant. Hence, it is the responsibility of the user of this standard to ensure safety.

1.3. *SI Units*—The values stated in SI units are to be regarded as the standard.

## 2. REFERENCED DOCUMENTS

AASHTO T 312, Preparing and Determining Density of Hot Mix Asphalt (HMA) Specimens by Means of the Superpave Gyratory Compactor

## 3. SIGNIFICANCE

3.1. The test standard is used to evaluate the workability of foamed asphalt mixture produced by a laboratory foaming unit using an SGC. The standard is essential for determining the optimum foaming water content that is able to produce foamed asphalt mixture with the best workability in the laboratory.

## 4. APPARATUS

4.1. Laboratory foaming unit that produces a specified amount of foamed binder or sampling port in a hot-mix plant that can be controlled to dispense a specified amount of foamed binder.

4.2. Portable asphalt mixer to mix foamed asphalt with aggregates.

4.3. Draft dry oven to short-term age foamed asphalt loose mix prior to compaction.

4.4. SGC to compact foamed asphalt loose mix with capacity of recording shear stress during compaction.

## 5. PROCEDURE

5.1. Prepare the aggregate batch following the mix design gradation, and place the aggregate batch in a shallow rectangular metal pan in the oven at 275°F (135°C) and leave overnight. Place the mixing bucket and other mixing tools in the oven at least 1 hour prior to foaming.

5.2. Calibrate the laboratory foaming unit according to the manufacturer's recommendations.

5.3. Pour the preheated aggregate batch in the bucket mixer and make a crater in the middle of the aggregate material. Dispense the specific amount of foamed binder into the bucket mixer.

5.4. Start the bucket mixer and place the metal paddle in the support. To help achieve complete aggregate coating, while the bucket mixer is turning, push the arm down and to the side of the bucket; a flat spatula can also be introduced into the bucket to scrape the material from the sides and the bottom.

5.5. When all aggregates appear to be completely coated, empty the foamed asphalt loose mix into a shallow rectangular metal pan, uniformly spread the loose mixture, and place inside the oven. Change the temperature of the oven to 240°F (116°C). Keep the loose mix in the oven for 2 hours.

5.6. Place the SGC molds and other compaction tools in the oven one hour prior to compacting. Stir the foamed asphalt loose mix and then start preparing the loose mix in individual specimen size batches (4,700 g per batch) 30 minutes prior to compacting. Return the loose mix to the oven immediately after batching to guarantee compaction temperature.

5.7. Obtain an individual specimen size batch and a preheated compaction mold from the oven. Place a piece of paper at the bottom of the compaction mold. Pour the individual specimen batch in the compaction mold and manually level the loose mix. Place another piece of paper on top of the loose mix. Slide the compaction mold into the SGC and start the compactor.

5.8. During compaction, height of the loose mix in the SGC mold and the shear stress are continually monitored for each gyration. Compaction will cease after 300 gyrations.

5.9. After compaction, remove the mold containing the compacted specimen from the compactor and slowly extrude the specimen from the mold. Remove the pieces of paper from the top and bottom of the specimen and allow the specimen to cool undisturbed.

5.10. Place the mold and base plate back in the oven to reach compaction temperature for the next specimen. Repeat the compaction procedure for each specimen.

## 6. CALCULATION OF RESULTS

6.1. Obtain the shear stress data from the SGC. Figure 1 presents a typical plot of the shear stress versus number of SGC gyrations during compaction. As illustrated, the shear stress plot can be divided into three main phases:

- First Phase – The slope of the shear stress curve is steep, the loose mix particles are being reoriented due to compaction, and there is a significant increase in internal friction within the mix due to the stone-on-stone contact.

- Second Phase – The shear stress starts to level off. The density of the specimen is expected to be near or at target value.
- Third Phase – The shear stress starts to decrease significantly from a maximum stress level. The reduction in shear stress is attributed to the degradation of the aggregate and pore pressure.

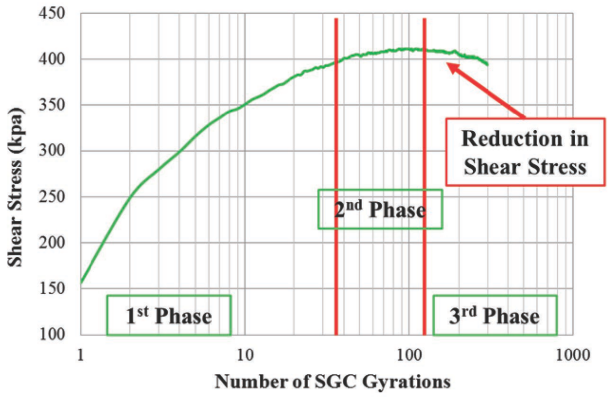


**Figure 1. Typical shear stress compaction curve.**

6.2. Evaluate the workability of foamed asphalt mixture using the maximum shear stress. Asphalt mixtures with more compaction in the first few cycles are expected to have higher shear stress afterwards due to the increased internal friction within the mix. Additionally, mixtures with better workability are expected to have a lower level of shear stress.

## 7. REPORT

7.1. The report shall include the following:

7.1.1. Make and model of the laboratory foaming unit or plant foamer.

7.1.2. Source and grade of the binder.

7.1.3. Mix design information.

7.1.4. Foaming water content in percent of dry mass of binder.

7.1.5. Type and dosage of foaming additive (if used).

7.1.6. Maximum shear stress obtained during compaction, $\tau_{max}$.

7.1.7. Number of SGC gyration where the maximum shear stress is obtained.

## Standard Method of Test for

# Evaluating the Coatability of Foamed Warm Mix Asphalt by a Laboratory Foaming Unit Using a Superpave Gyratory Compactor

## AASHTO Designation: T xx-xx

## 1. SCOPE

1.1. This test method describes the procedure for evaluating the coatability of foamed warm mix asphalt (WMA) by a laboratory foaming unit based on the aggregate absorption method.

1.2. While working with or handling foamed binder, lab personnel may be exposed to extreme heat and pressure, hazardous materials, and dangerous equipment operations. This standard does not address procedures and practices needed to ensure a safe and hazard-free working environment in the laboratory or at a hot-mix plant. Hence, it is the responsibility of the user of this standard to ensure safety.

1.3. *SI Units*—The values stated in SI units are to be regarded as the standard.

## 2. REFERENCED DOCUMENTS

AASHTO T 255, Total Evaporable Moisture Content of Aggregate by Drying

## 3. SIGNIFICANCE

3.1. The test standard is used to evaluate the coatability of foamed asphalt mixture produced by a laboratory foaming unit based on the aggregate absorption method. The standard is essential for determining the optimum foaming water content that is able to produce foamed asphalt mixture with the best coatability in the laboratory.

## 4. APPARATUS

4.1. Laboratory foaming unit that produces a specified amount of foamed binder or sampling port in a hot-mix plant that can be controlled to dispense a specified amount of foamed binder.

4.2. Portable asphalt mixer to mix foamed asphalt with aggregates.

4.3. Draft dry oven to short-term age foamed asphalt loose mix prior to compaction.

4.4. Water container to soak foamed asphalt loose mix.

4.5. Terry cloth to achieve saturated surface dry (SSD) condition for the aggregate and the foamed asphalt loose mix.

## 5. PROCEDURE

5.1. Prepare approximately 4,000 g coarse aggregate batch (retained on the 3/8-inch sieve) following the percentages specified in the mix design. Wash and dry them to constant weight per AASHTO T 255.

5.2. Separate the coarse aggregate batch into two samples and record the dry weights of each sample as $W_{\text{agg OD-1}}$ and $W_{\text{agg OD-2}}$. Place the first coarse aggregate sample in a metal pan in the oven at 275°F (135°C) and leave overnight. Store the second coarse aggregate sample at room temperature.

5.3. Calculate the amount of binder for the first coarse aggregate sample, based on the total binder content specified in the mix design and the surface area distribution of the combined aggregates. The amount of binder is calculated per Equation 1.

$$W_{b-\text{coarse}} = W_{\text{agg OD}-1} * \frac{P_b}{1-P_b} * \frac{\text{SA}_{\text{coarse}}}{\text{SST}} * \frac{1}{P_{s-\text{coarse}}} \quad (1)$$

Where:

$W_{b\text{-coarse}}$, amount of binder for the first coarse aggregates sample.

$W_{\text{agg OD-1}}$, oven-dry weight of the first coarse aggregates sample.

$P_b$, total binder content of the combined aggregates.

$\text{SA}_{\text{coarse}}$, surface area of the coarse aggregate fraction retained on the 3/8-inch sieve.

SST, total surface area of the combined aggregates.

$P_{s\text{-coarse}}$, percentage of coarse aggregates retained on 3/8-inch sieve by weight of the combined aggregates.

5.4. Place the mixing bucket and other mixing tools in the oven at least 1 hour prior to foaming. Calibrate the laboratory foaming unit according to the manufacturer's recommendations.

5.5. Pour the first coarse aggregate batch in the bucket mixer and dispense the calculated amount of foamed binder into the bucket mixer.

5.6. Start the bucket mixer and place the metal paddle in the support. To help achieve complete aggregate coating, while the bucket mixer is turning, push the arm down and to the side of the bucket; a flat spatula can also be introduced into the bucket to scrape the material from the sides and the bottom. Stop the mixer after 60 s.

5.7. Empty the foamed asphalt loose mix into a pan and place inside the oven. Change the temperature of the oven to 240°F (116°C). Keep the loose mix in the oven for 2 hours.

5.8. Take the pan with loose mix out of the oven and let it cool to room temperature in front of a fan. Separate the loose mix sample into two smaller samples of about 1000 g each and record the dry weight of each group as $W_{\text{loose OD-1}}$ and $W_{\text{loose OD-2}}$.

5.9. Submerge the second coarse aggregate sample and two loose mix samples in a water container at ambient temperature for 60 minutes.

5.10. Damp-dry the coarse aggregate sample and two loose mix samples with a terry cloth to achieve the SSD condition and record the SSD weights as $W_{\text{agg SSD-2}}$, $W_{\text{loose SSD-1}}$, and $W_{\text{loose SSD-2}}$, respectively.

## 6. CALCULATION OF RESULTS

6.1. Calculate the water absorption of the foamed asphalt loose mix samples per Equations 2–4.

$$\text{Absorption}_{\text{loose-1}} = \frac{W_{\text{loose SSD-1}} - W_{\text{loose OD-1}}}{W_{\text{loose OD-1}}} * 100\% \quad (2)$$

$$\text{Absorption}_{\text{loose-2}} = \frac{W_{\text{loose SSD-2}} - W_{\text{loose OD-2}}}{W_{\text{loose OD-2}}} * 100\% \quad (3)$$

$$\text{Absorption}_{\text{loose-average}} = \frac{\text{Absorption}_{\text{loose-1}} + \text{Absorption}_{\text{loose-2}}}{2} \quad (4)$$

6.2. Determine the mixture coatability index as the relative difference in water absorption between the aggregate sample and the foamed asphalt loose mix sample per Equation 5.

$$\text{Coatability Index} = \frac{\text{Absorption}_{\text{agg}} - \text{Absorption}_{\text{loose-average}}}{\text{Absorption}_{\text{agg}}} * 100\% \quad (5)$$

6.3. Foamed asphalt mixtures with higher coatability index values are expected to have a better coatability.

## 7. REPORT

7.1. The report shall include the following:

7.1.1. Make and model of the laboratory foaming unit or plant foamer.

7.1.2. Source and grade of the binder.

7.1.3. Mix design information.

7.1.4. Foaming water content in percent of dry mass of binder.

7.1.5. Type and dosage of foaming additive (if used).

7.1.6. Coatability index, CI.

APPENDIX D

# Field Foaming Data Acquisition Form

| | |
|---|---|
| Plant type (include drum make/model if applicable) | |
| Production rate (tons/hour) | |
| Production temperature (°F) | |
| Foamer | |
| Type/manufacturer/make/model | |
| Description of foaming pipe | |
| Foaming pipe diameter (inch) | |
| Description of sampling port | |
| Sampling pipe diameter (inch) | |
| Total length of pipe from foamer to discharge in drum (ft) | |
| Total length of pipe inside the drum (ft) | |
| Vertical length of pipe from foamer to discharge in drum (ft) | |
| Water | |
| Content (% by weight of _____) | |
| Flow rate (_____) | |
| Binder | |
| PG grade | |
| Content (% by weight of _____) | |
| Flow rate (_____) | |
| Temperature (°F) | |
| Pipe diameter (inches) | |
| Other items: mix design, pictures of foamer and plant | |

*Abbreviations and acronyms used without definitions in TRB publications:*

| | |
|---|---|
| A4A | Airlines for America |
| AAAE | American Association of Airport Executives |
| AASHO | American Association of State Highway Officials |
| AASHTO | American Association of State Highway and Transportation Officials |
| ACI–NA | Airports Council International–North America |
| ACRP | Airport Cooperative Research Program |
| ADA | Americans with Disabilities Act |
| APTA | American Public Transportation Association |
| ASCE | American Society of Civil Engineers |
| ASME | American Society of Mechanical Engineers |
| ASTM | American Society for Testing and Materials |
| ATA | American Trucking Associations |
| CTAA | Community Transportation Association of America |
| CTBSSP | Commercial Truck and Bus Safety Synthesis Program |
| DHS | Department of Homeland Security |
| DOE | Department of Energy |
| EPA | Environmental Protection Agency |
| FAA | Federal Aviation Administration |
| FHWA | Federal Highway Administration |
| FMCSA | Federal Motor Carrier Safety Administration |
| FRA | Federal Railroad Administration |
| FTA | Federal Transit Administration |
| HMCRP | Hazardous Materials Cooperative Research Program |
| IEEE | Institute of Electrical and Electronics Engineers |
| ISTEA | Intermodal Surface Transportation Efficiency Act of 1991 |
| ITE | Institute of Transportation Engineers |
| MAP-21 | Moving Ahead for Progress in the 21st Century Act (2012) |
| NASA | National Aeronautics and Space Administration |
| NASAO | National Association of State Aviation Officials |
| NCFRP | National Cooperative Freight Research Program |
| NCHRP | National Cooperative Highway Research Program |
| NHTSA | National Highway Traffic Safety Administration |
| NTSB | National Transportation Safety Board |
| PHMSA | Pipeline and Hazardous Materials Safety Administration |
| RITA | Research and Innovative Technology Administration |
| SAE | Society of Automotive Engineers |
| SAFETEA-LU | Safe, Accountable, Flexible, Efficient Transportation Equity Act: A Legacy for Users (2005) |
| TCRP | Transit Cooperative Research Program |
| TEA-21 | Transportation Equity Act for the 21st Century (1998) |
| TRB | Transportation Research Board |
| TSA | Transportation Security Administration |
| U.S.DOT | United States Department of Transportation |